



SEISMIC EVALUATION OF THE OHIO RIVER BRIDGE ON US51 AT WICKLIFFE, KENTUCKY (KYSPR 96-173)

by

Issam E. Harik

Professor of Civil Engineering and Head, Structures Section,
Kentucky Transportation Center

Chelliah Madasamy

Visiting Professor, Kentucky Transportation Center

Denglin Chen

Research Assistant, Dept. of Civil Engineering

Leonong Zhou

Formerly Visiting Professor, Kentucky Transportation Center

Kevin Sutterer

Assistant Professor, Department of Civil Engineering

Ron Street

Assistant Professor, Department of Geological Sciences

and

David L. Allen

Transportation Engineer V, Kentucky Transportation Center

Kentucky Transportation Center
College of Engineering, University of Kentucky

in cooperation with

Transportation Cabinet
Commonwealth of Kentucky

and

Federal Highway Administration
U.S. Department of Transportation

The contents of this report reflect the views of the authors who are responsible for the facts and accuracy of the data presented herein. The contents do not necessarily reflect the official views or policies of the University of Kentucky, the Kentucky Transportation Cabinet, nor the Federal Highway Administration. This report does not constitute a standard, specification or regulation. The inclusion of manufacturer names or trade names are for identification purposes and are not to be considered as endorsement.

December 1998

1. Report No. KTC-98-20	2. Government Accession No.	3. Recipient's Catalog No.	
4. Title and Subtitle SEISMIC EVALUATION OF THE OHIO RIVER BRIDGE ON US51 AT WICKLIFFE, KENTUCKY (KYSR 96-173)		5. Report Date December 1998	6. Performing Organization Code
7. Author(s): I.E. Harik, C.M. Madasamy, D. Chen, L. Zhou, K. Sutterer, R. Street and D. Allen		8. Performing Organization Report No. KTC-98-20	
9. Performing Organization Name and Address Kentucky Transportation Center College of Engineering University of Kentucky Lexington, Kentucky 40506-0281		10. Work Unit No. (TRAI5)	11. Contract or Grant No. KYSPR 96-173
12. Sponsoring Agency Name and Address Kentucky Transportation Cabinet State Office Building Frankfort, Kentucky 40622		13. Type of Report and Period Covered Final	
15. Supplementary Notes Prepared in cooperation with the Kentucky Department of Transportation and the U.S. Department of Transportation, Federal Highway Administration.		14. Sponsoring Agency Code	
16. Abstract <p>This report presents the of seismic evaluation of the Ohio river bridge on US51 at Wickliffe, Kentucky. The main bridge is a five-span single-deck cantilever through-truss type. The approach bridge has 21 spans on the Kentucky side and 6 spans on the Illinois side. Although this bridge has not yet been subjected to a moderate or major earthquake, it is situated within the influence of the New Madrid seismic zone.</p> <p>The seismic evaluation program consists of field testing and seismic response analysis. The modal properties of the main bridge are determined through field testing, and are used to calibrate the three dimensional finite element model. The finite element model is then subjected to time histories of the 50-year earthquake event. Stresses and displacements obtained are within the acceptable limits. Analytical results indicate that the main bridge will survive the projected 50-year earthquake without significant damage and no loss-of-span. Hence, it is not recommended to retrofit the main bridge.</p> <p>The approach spans are analyzed using response spectrum method with simplified single-degree-of-freedom models. Most of the Kentucky and Illinois approach spans require additional anchor bolts at the bearings.</p>			
17. Key Words Seismic Evaluation, Time-History, Response Spectra, US51 Bridge, Field Testing, Finite Element Model		18. Distribution Statement Unlimited with approval of Kentucky Transportation Cabinet	
19. Security Classif. (of this report) Unclassified	20. Security Classif. (of this page) Unclassified	21. No. of Pages 170	22. Price

EXECUTIVE SUMMARY

Research Objectives

The main objective of this investigation is to assess the structural integrity of the Ohio river bridge (Fig. E-1) on US51 at Wickliffe, Kentucky, when subjected to a 50-year earthquake. The investigation includes both the main and approach bridges. To achieve this objective, the scope of the work was divided into the following tasks: 1) Field testing of the main bridge; 2) Finite element modeling and calibration; 3) Time-history seismic response analysis; and 4) Seismic response of the approach bridges using response spectrum method.

Background

The need for evaluating the seismic adequacy of the existing infrastructure has come into focus following the damage and collapse of numerous structures during the recent earthquakes. The 1989 Loma Prieta earthquake and 1994 Northridge earthquake brought to the attention of the public about the seismic risk to bridges and elevated freeway structures. In particular, the seismic rehabilitation of older bridges in regions of high seismicity which are designed prior to the advent of modern seismic design codes is a matter of growing concern. Many bridges in Kentucky were built as per old code requirements that had minimal provisions for earthquake loading.

Field Testing

The ambient vibration properties of the main bridge were determined through field testing under traffic and wind induced excitation. The purpose of measuring the ambient vibration properties was to determine the natural frequencies and their associated mode shapes. These vibration properties were subsequently used as the basis for calibrating the finite element model for seismic response analysis.

Finite Element Modeling

A three dimensional finite element model of the main bridge was used for free vibration and seismic response analyzes. The model was calibrated by comparing the free vibration analysis results with the ambient vibration properties obtained from field testing. After calibration, the model was used for seismic response analysis. The three dimensional model of the main bridge was subjected to the time histories of the

50-year earthquake to determine the maximum displacements, stresses and forces on the bearings.

Approach Spans

The approach spans were modeled using simplified single-degree-of-freedom systems. Seismic response was analyzed in the longitudinal direction using response spectrum method. For the approach spans, the seismic analysis dealt with the potential for loss-of-span due to excessive longitudinal displacement and bearing forces along the highway main line. From the seismic response analysis, it was found that the anchor bolt shear force demands are higher than the available capacity whereas the longitudinal bearing displacements at the bearings are less than the available support width.

Conclusions and Recommendations

The seismic analysis indicates that the main bridge can resist the 50-year earthquake event without yielding or buckling of truss members or loss-of-span at supports. Consequently, retrofitting is not required for the main bridge truss members and bearings.

The approach spans have the potential for anchor bolt shear failure due to longitudinal seismic force. Therefore, retrofitting of the fixed bearings on the approach span piers is recommended. It is also suggested that proper arrangement of additional anchor bolts or cable restrainer system can prevent from loss-of-span. A typical arrangement of additional anchor bolts is shown in Fig. E.2. The details of recommended retrofits are presented in section 6.5 and in Figures 6.11 to 6.31.

**PROTECTED UNDER INTERNATIONAL COPYRIGHT
ALL RIGHTS RESERVED
NATIONAL TECHNICAL INFORMATION SERVICE
U.S. DEPARTMENT OF COMMERCE**

Reproduced from
best available copy. 



Figure E.1 The Ohio River Bridge on US51 at Wickliffe, Kentucky

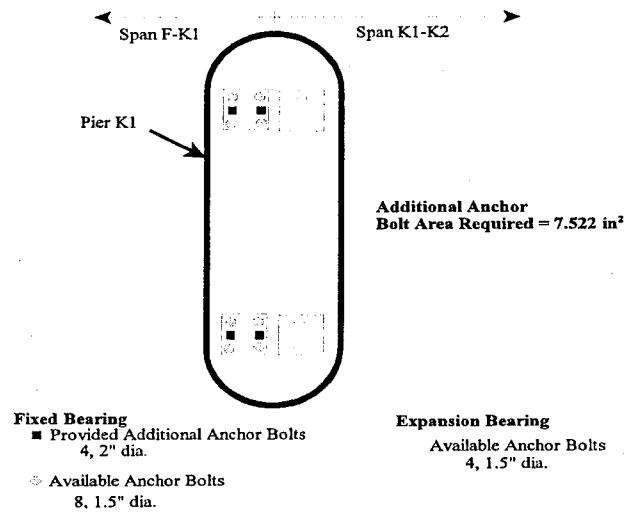


Figure E.2 Arrangement of Additional Anchor Bolts on Pier K1

ACKNOWLEDGEMENTS

The financial support for this project was provided by the Kentucky Transportation Cabinet and Federal Highway Administration. The help of John Flekenstein and Clark Graves in coordinating and conducting the bridge testing is especially noteworthy. The authors would like to acknowledge the cooperation, suggestions, and advise of the members of the study advisory committee: Donald Herd (committee chairperson), Glenn Givan, Ray Greer, David Moses, Ted Noe, N.B. Shah, and David Steele.

TABLE OF CONTENTS

DESCRIPTION	PAGE
Implementation Letter.....	i
Technical Report Documentation Page.....	ii
EXECUTIVE SUMMARY.....	ii
ACKNOWLEDGMENTS.....	vi
LIST OF TABLES.....	ix
LIST OF FIGURES.....	xi
1. INTRODUCTION.....	1
1.1 General	1
1.2 Field Testing	2
1.3 Earthquake Background	2
1.4 Scope of the work	3
2. OHIO RIVER BRIDGE ON US51 AT WICKLIFFE, KENTUCKY.....	5
2.1 General.....	5
2.2 Bridge Superstructure.....	5
2.3 Fixed and Expansion Bearings.....	6
2.4 Bridge Substructure.....	6
3. FIELD TESTING.....	8
3.1 General.....	8
3.2 Instrumentation.....	8
3.3 Testing Procedure.....	9
3.4 Data Analysis.....	9
3.5 Finite Element Model Calibration.....	11
4. FINITE ELEMENT MODELING AND FREE VIBRATION ANALYSIS.....	15
4.1 General.....	15
4.2 Finite Element Model.....	15
4.3 Free Vibration Analysis.....	16
5. SEISMIC RESPONSE ANALYSIS.....	21
5.1 General.....	21

5.2	Seismic Response.....	22
5.3	Capacity/Demand Ratios.....	26
6.	APPROACH BRIDGE.....	28
6.1	General.....	28
6.2	Structural Modeling.....	28
6.3	Seismic Response Analysis.....	29
6.4	Capacity/Demand Ratios.....	30
6.5	Retrofit for the Approach Bridge.....	31
7.	CONCLUSIONS AND RECOMMENDATIONS.....	32
7.1	General.....	32
7.2	Main Bridge.....	32
7.3	Approach Bridge.....	33
	REFERENCES.....	34

LIST OF TABLES

Table No.	Description	Page No.
3.1a	US51 Bridge testing details - Moving station on Northbound lanes	37
3.1b	US51 Bridge testing details - Base station on Northbound lanes	38
3.2a	US51 Bridge testing details - Moving station on Southbound lanes	39
3.2b	US51 Bridge testing details - Base station on Southbound lanes	40
3.3	Frequency identification from the field test data	41
4.1	Natural frequencies and mass participation of the main bridge (Exact eigen system)	45
4.2	Natural frequencies and mass participation of the main bridge (Ritz vector based)	46
5.1	Description of seismic excitation cases	47
5.2	Cross sectional properties of members for stress calculation	48
5.3	Stresses (ksi) in members due to seismic excitation case L1T2V3, dead load and temperature	49
5.4	Stresses (ksi) in members due to seismic excitation case L2T1V3, dead load and temperature	50
5.5	Stresses (ksi) in members due to seismic excitation case LL11	51
5.6	Stresses (ksi) in members due to seismic excitation case LL22	52
5.7	Stresses (ksi) in members due to seismic excitation case TT11	53
5.8	Stresses (ksi) in members due to seismic excitation case TT22	54
5.9	Stresses (ksi) in members due to temperature of 90°F	55
5.10	Self-weight induced stresses (ksi)	56
5.11	Stress requirement based on AASHTO Equations for L1T2V3 earthquake	57
5.12	Stress requirement based on AASHTO Equations for L2T1V3 earthquake	58
5.13	Displacements (in) due to seismic excitation of the 50-year earthquake event	59
5.14	Displacements (in) due to self-weight and temperature	60
5.15	Maximum and minimum base shears from modal time-history for the 50-year earthquake	61
5.16	Bearing force capacity/demand ratios of the main bridge without site soil coefficients for the 50-year earthquake	62
5.17	Bearing displacement capacity/demand ratio for the 50-year earthquake	62
6.1	Dimensions and stiffnesses of the approach span piers	63

6.2	Weight of the superstructure of the Illinois approach spans (Girder spans)	64
6.3	Weight of the superstructure of the Illinois approach spans (Deck-truss spans)	64
6.4	Weight of the superstructure of the Kentucky approach spans (From pier F to Pier K9)	65
6.5	Weight of the superstructure of the Kentucky approach spans (From Pier K9 to K20)	65
6.6	Natural frequencies of the approach spans - Flexible system	66
6.7	Natural frequencies of the approach spans - Stiff system	67
6.8	Seismic response using response spectrum method - Flexible system	68
6.9	Seismic response using response spectrum method - Stiff system	69
6.10	Bearing force capacity/demand ratios and retrofiting recommendations - Flexible system	70
6.11	Bearing force capacity/demand ratios and retrofiting recommendations - Stiff system	71
6.12	Bearing displacement capacity/demand ratio for the flexible system	72

LIST OF FIGURES

Fig. No.	Description	Page No.
2.1a	View showing Illinois approach and US51 main bridge	73
2.1b	US51 main bridge across the Ohio river	73
2.1c	Illinois approach and end view of the main bridge	74
2.1d	End portal of the main bridge	74
2.1e	Bottom view of the main bridge	75
2.2	Plan and elevation views of the US51 bridge over the Ohio river	76
2.3	Elevation view of the first span A-B	77
2.4	Elevation view of the second span B-C	78
2.5	Elevation view of the third span C-D	79
2.6	Elevation view of the fourth span D-E	80
2.7	Elevation view of the fifth span E-F	81
2.8	Transverse cross section of the US51 main bridge	82
2.9	Elevation and sectional views of pier A	83
2.10a	Plan view of piers B, C, D and E	84
2.10b	Elevation and sectional views of piers B, C, D and E	84
2.11a	Plan view of pier F	85
2.11b	Elevation and sectional views of pier F	85
3.1a	Triaxial accelerometer block	86
3.1b	Accelerometer locations (moving and base stations) on one side of the bridge	86
3.1c	Accelerometer placement on the deck	87
3.2a	Transverse acceleration time-history obtained from field testing at moving station 6	88
3.2b	FFT of transverse acceleration time-history at moving station 6	88
3.2c	Vertical acceleration time-history obtained from field testing at moving station 6	89
3.2d	FFT of vertical acceleration time-history at moving station 6	89
3.2e	Longitudinal acceleration time-history obtained from field testing at moving station 6	90
3.2f	FFT of longitudinal acceleration time-history at moving station 6	90
3.3a	First transverse mode	91
3.3b	Peak comparison for the first transverse mode	91
3.4a	First vertical mode	92
3.4b	Peak comparison for the first vertical mode	92
3.5a	First longitudinal mode	93
3.5b	Peak comparison for the first longitudinal mode	93
3.6a	Second transverse mode	94

3.6b	Peak comparison for the second transverse mode	94
3.7a	Second vertical mode	95
3.7b	Peak comparison for the second vertical mode	95
3.8a	Third transverse mode	96
3.8b	Peak comparison for the third transverse mode	96
3.9a	Third vertical mode	97
3.9b	Peak comparison for the third vertical mode	97
3.10a	Fourth transverse mode	98
3.10b	Peak comparison for the fourth transverse mode	98
3.11a	Fourth vertical mode	99
3.11b	Peak comparison for the fourth vertical mode	99
3.12a	Fifth vertical mode	100
3.12b	Peak comparison for the fifth vertical mode	100
3.13a	Sixth vertical mode	101
3.13b	Peak comparison for the sixth vertical mode	101
4.1	3D finite element model of the Ohio river bridge on US51	102
4.2	Mode shape of the fundamental natural frequency (0.3831 Hz) (a) isometric view, (b) elevation view, and (c) plan view	103
4.3	Mode shape of the second natural frequency (0.5017 Hz) (a) isometric view, (b) elevation view, and (c) plan view	104
4.4	Mode shape of the third natural frequency (0.6206 Hz) (a) isometric view, (b) elevation view, and (c) plan view	105
4.5	Mode shape of the fourth natural frequency (0.7578 Hz) (a) isometric view, (b) elevation view, and (c) plan view	106
4.6	Mode shape of the fifth natural frequency (0.9147 Hz) (a) isometric view, (b) elevation view, and (c) plan view	107
4.7	Mode shape of the sixth natural frequency (0.9725 Hz) (a) isometric view, (b) elevation view, and (c) plan view	108
4.8	Mode shape of the seventh natural frequency (0.9933 Hz) (a) isometric view, (b) elevation view, and (c) plan view	109
4.9	Mode shape of the eighth natural frequency (1.072 Hz) (a) isometric view, (b) elevation view, and (c) plan view	110
4.10	Mode shape of the ninth natural frequency (1.1318 Hz) (a) isometric view, (b) elevation view, and (c) plan view	111
4.11	Mode shape of the tenth natural frequency (1.1435 Hz) (a) isometric view, (b) elevation view, and (c) plan view	112
4.12	Mode shape of the eleventh natural frequency (1.2812 Hz) (a) isometric view, (b) elevation view, and (c) plan view	113
4.13	Mode shape of the twelfth natural frequency (1.2866 Hz) (a) isometric view, (b) elevation view, and (c) plan view	114
4.14	Mode shape of the thirteenth natural frequency (1.3279 Hz) (a) isometric view, (b) elevation view, and (c) plan view	115

4.15	Mode shape of the fourteenth natural frequency (1.3849 Hz) (a) isometric view, (b) elevation view, and (c) plan view	116
4.16	Mode shape of the fifteenth natural frequency (1.3978 Hz) (a) isometric view, (b) elevation view, and (c) plan view	117
4.17	Mode shape of the 21 st natural frequency (1.8848 Hz) (a) isometric view, (b) elevation view, and (c) plan view	118
4.18	Mode shape of the 22 nd natural frequency (1.9348 Hz) (a) isometric view, (b) elevation view, and (c) plan view	119
4.19	Mode shape of the 27 th natural frequency (2.2327 Hz) (a) isometric view, (b) elevation view, and (c) plan view	120
5.1	Time-history and response spectra identification map for the Commonwealth of Kentucky	121
5.2	Acceleration-time history in the horizontal direction (Direction 1) for the 50-year earthquake	122
5.3	Acceleration-time history in the transverse direction (Direction 2) for the 50-year earthquake	122
5.4	Acceleration-time history in the vertical direction (Direction 3) for the 50-year earthquake	123
5.5	Displacement-time history in the transverse direction at node 44 for L1T2V3 excitation case	123
5.6	Displacement-time history in the vertical direction at node 44 for L1T2V3 excitation case	124
5.7	Axial force-time history for the element 294 under L1T2V3 excitation case	124
6.1a-b	Different views of the Illinois approach	125
6.2a-d	Different views of the Kentucky approach	125
6.3	Elevation and plan views of the Kentucky approach	126
6.4	Elevation and plan views of the Illinois approach	127
6.5	Cross section of the deck-truss type approach span	128
6.6	Cross section of the girder and suspended spans	128
6.7	Details of the deck-truss span (K10-K13)	129
6.8	Structural components for the SDOF models of the Illinois approach spans	130
6.9	Structural components for the SDOF models of the Kentucky approach spans	131
6.10	Response spectra for the 50-year event for Ballard Co. (0.30g-1 from fig. 5.1) Damping ratio = 0.05	135
6.11	Arrangement of additional anchor bolts on pier K1	136
6.12	Arrangement of additional anchor bolts on pier K2	137
6.13	Arrangement of additional anchor bolts on pier K3	138
6.14	Arrangement of additional anchor bolts on pier K4	139
6.15	Arrangement of additional anchor bolts on pier K5	140
6.16	Arrangement of additional anchor bolts on pier K6	141

6.17	Arrangement of additional anchor bolts on pier K7	142
6.18	Arrangement of additional anchor bolts on pier K8	143
6.19	Arrangement of additional anchor bolts on pier K9	144
6.20	Arrangement of additional anchor bolts on pier K10	145
6.21	Arrangement of additional anchor bolts on pier K11	146
6.22	Arrangement of additional anchor bolts on pier K12	147
6.23	Arrangement of additional anchor bolts on pier K13	148
6.24	Arrangement of additional anchor bolts on pier K15	149
6.25	Arrangement of additional anchor bolts on pier K17	150
6.26	Arrangement of additional anchor bolts on pier K19	151
6.27	Arrangement of additional anchor bolts on KY abutment	152
6.28	Arrangement of additional anchor bolts on IL abutment	153
6.29	Arrangement of additional anchor bolts on pier I4	154
6.30	Arrangement of additional anchor bolts on pier I2	155
6.31	Arrangement of additional anchor bolts on pier I1	156

1. INTRODUCTION

1.1 General

The need for evaluating the seismic adequacy of existing infrastructure has come into focus following the damage and collapse of numerous structures during recent earthquakes. In particular, the seismic rehabilitation of older bridges in regions of high seismicity which were designed prior to the advent of modern seismic design codes is a matter of growing concern. Bridge failures from earthquakes have so far only occurred in California and Alaska. The 1989 Loma Prieta earthquake [EERI 1990] and 1994 Northridge earthquake [EERI 1995], brought to the attention of the public the seismic risk to bridges and elevated freeway structures. The partial collapse of the San Francisco - Oakland Bay Bridge and the Cypress Viaduct portion of Interstate 880 not only caused the loss of life, but created considerable problems to the transportation infrastructure. The Bay bridge had been unusable for a month and transbay commuters were forced to commute on ferries or the crowded Bay Area Rapid Transit System. Following the Loma Prieta earthquake, the Federal Highway Administration commissioned the seismic evaluation of bridges located in the seismically active regions.

After the seismic evaluation, if the bridge is found to be deficient, not all bridges in highways system has to be retrofitted simultaneously; instead, only those bridges with the highest priority should be retrofitted first. It should always be remembered that the seismic retrofitting is one of several possible courses of action. Others are closing the bridge, replacing the bridge, taking no action at all, and accepting the risk of seismic damage.

Seismic design of bridges throughout most of the United States is governed by AASHTO's Standard Specifications for Highway Bridges, Division I-A (1996). Use of the AASHTO specifications is intended: (1) to allow the structure to yield during a major earthquake, (2) to produce damage (yielding) only in areas that are accessible (visible) and repairable, and (3) to prevent collapse even during very large earthquakes (NHI 1996). There are many bridges in the Commonwealth of Kentucky which have been designed before the seismic provisions are introduced into the AASHTO Code. Recently, the Brent-Spence bridge on Interstate 75 connecting Covington, Kentucky to Cincinnati, Ohio, a double-deck through-truss bridge, was evaluated for seismic excitation [Harik et al.(1997a,b)]. There are many long-span through-truss bridges in Kentucky which require seismic evaluation. The present work concentrates on the seismic evaluation of the US51 Bridge over the Ohio river. This bridge connects US51 across the Ohio river between Ballard County, Kentucky and Alexander County, Illinois.

1.2 Field Testing

Nowadays, field testing of bridges has become an integral part of the seismic evaluation process in order to eliminate the uncertainties and assumptions involved in analytical modeling. Full-scale dynamic tests on structures can be performed in a number of ways. Hudson (1977) describes the different types of testing as: (1) free vibration tests, including (i) initial displacement as in the pullback, quick-release test, and (ii) initial velocity from impacts; (2) forced vibration tests, including (i) steady-state resonance testing, (ii) variable frequency excitation including sweep, rundown, random and pulse sequences, and (iii) transient excitations including earthquakes, wind, traffic, and explosions. Shelley (1995b) provides a very informative discussion of the advantages and disadvantages of the various test methods used on highway bridges.

An alternative technique used to dynamically test bridges is through measurement of the bridges response under normal traffic and wind. In this method no equipment is required to excite the structure, instead equipment is required only to record the vibrations. This technique has been used by a number of researchers (Abdel-ghaffer and Scanlan, 1985a,b, Alampalli and Fu 1994, Buckland et al. 1979, Doll 1994, Farrar et al. 1995, Harik et al. 1993, Paultre et al. 1995, Saiidi et al. 1994, Shahawy 1995, Ventura et al. 1994,1996, Wendichansky et al. 1995). Harik et. al. (1993) used this method with success to identify the vibration mode shapes and frequencies of the Brent-Spence Bridge crossing the Ohio River in Cincinnati, Ohio.

1.3 Earthquake Background

The test bridge is located in Ballard County, Kentucky. This positions the bridge in the New Madrid Seismic Zone, site of three of the largest earthquakes known to have occurred in North America (Johnston 1982, 1985, Johnston and Nava 1985, Street et al. 1996). The zone is named for the town of New Madrid, Missouri, epicenter of the third of the great earthquakes. Each of the massive earthquakes is estimated to have had a Richter magnitude above 8.0 and each of the main shocks was followed by a protracted series of strong aftershocks. The main shocks were felt throughout all of the Central United States, most of the Eastern United States, as well as parts of Canada and dramatically altered the region's landscape.

December 16, 1811 saw the first of the great earthquakes; the second of the huge quakes followed on January 23, 1812. Inhabitants reported the earth to be rolling in waves a few feet in height during the main shocks. On February 7, 1812 the third and strongest of the main shocks occurred. Denoted the "hard shock", this temblor created waterfalls on the Mississippi and caused it to flow backward, locally, for several hours. Several islands in the Mississippi disappeared altogether. Present-day Reelfoot Lake, in Kentucky and Tennessee, was created during the February hard shock. It is

estimated to have had a Richter magnitude of up to 8.8 (Johnston 1985b).

More recently, more than 2000 earthquakes had been instrumentally detected in the New Madrid Seismic Zone during the first 9 years of deployment of seismographs which began in 1974 (Johnston 1985). Although 97% of these are too small to be felt, roughly a Richter magnitude of 2.5, an earthquake occurs in the region, on average, every 48 hours (Johnston 1982). This activity makes the New Madrid Seismic Zone the most hazardous zone east of the Rocky Mountains (Johnston 1985).

With increasing recognition of potential damage from a large New Madrid earthquake, or other less severe quake, the Kentucky Transportation Cabinet funded the research project *Evaluation and Analysis of Innovative Concepts for Bridge Seismic Retrofit*. Research was conducted by the Kentucky Transportation Center at the University of Kentucky. Fundamental to this research project was the characterization of the seismic potential affecting Kentucky from known seismic zones as well as unknown "local" events. Results from this seismological assessment of Kentucky were published in *Source Zones, Recurrence Rates, and Time Histories for Earthquakes Affecting Kentucky* (Street et al., 1996). In this report, three main tasks were covered: (1) definition and evaluation of earthquakes in seismic zones that have the potential to generate damaging ground motions in Kentucky, (2) specification of the source characteristics, accounting for the spreading and attenuation of the ground motions to top-of-bedrock at sites in Kentucky, and (3) determination of seismic zoning maps for the Commonwealth based on peak-particle accelerations, response spectra, and time-histories.

Time-histories generated in the aforementioned report were used in the seismic evaluation of the US51 bridge. Effects of these artificial earthquakes were calculated for bedrock elevation at the county seat of each Kentucky county. These acceleration time-histories were derived through the use of random vibration analysis and take into consideration the probability of earthquakes from nearby seismic zones, the attenuation of ground motions with distance in the Central United States, and the possibility of a random event occurring outside of the generally recognized seismic zones (Street et al., 1996).

1.4 Scope of the Work

The primary aim of this study is to assess the structural integrity of the US51 bridge when subjected to a 50-year earthquake event at Ballard Co., Kentucky. To achieve this the scope of work was divided into four tasks as: 1) Field testing of the main bridge, 2) finite element modeling, 3) time history seismic response analysis of the main bridge, and 4) seismic response of the approach bridge

The ambient vibration properties of the main bridge are determined through field testing under traffic and wind induced excitation. The purpose of measuring the ambient vibration properties is to determine the mode shapes and the associated natural frequencies. Full scale ambient or forced vibration tests have been used extensively in the past to determine the dynamic characteristics of highway bridges (Abdel-ghaffer and Scanlan, 1985a,b).

A three dimensional finite element model of the main bridge is used for free vibration and seismic response analyzes. The model is first calibrated by comparing the free vibration analysis results with ambient vibration properties from field testing. After the calibration, the model is used for seismic response analysis to determine the maximum displacements, stresses in truss members and forces on bearings.

The approach spans are modeled using simplified single-degree-of-freedom (SDOF) systems. The superstructure mass is lumped at the top of the piers. For the approach spans the seismic analysis dealt only with the potential for loss-of-span due to longitudinal displacement and forces on the bearings. Seismic response is analyzed in the longitudinal direction only using response spectrum method to determine the maximum displacements and forces.

2. OHIO RIVER BRIDGE ON US51 AT WICKLIFFE, KENTUCKY

2.1 General

The Ohio river bridge on US51 shown in figures 2.1(a)-(e) is a cantilever through-truss bridge, a bridge type commonly employed for spans of 600' (183 m) to 1500' (457 m) through the mid 1970's. This bridge was originally designed by Modjeski, Masters and Case Consulting Engineers in 1936. Figures 2.1(a)-(e) show the different views of the main bridge. The total length of this bridge including the approach spans is 5865' $\frac{3}{8}$ ". The length of the five-span main bridge is 2830' $\frac{3}{8}$ ". The plan and elevation views of the main bridge is shown in figure 2.2. The details of approach bridge and their seismic evaluation are discussed in separate Chapter 6.

2.2 Bridge Superstructure

The superstructure is described in terms of the vertical truss system, the lateral truss system and the floor system. The lateral truss is a combination of lateral bracing, sway and portal bracings. The bridge is a through-truss type with anchor arms and cantilever arms.

As seen from Figure 2.2, the height of vertical trusses near the midspans is 60' whereas at the supports, the height is 105.5'.

The vertical truss system shown in Figure 2.2 consists of anchor arm 'A-B', having a span of 363' $4\frac{5}{8}$ ", which is supported over piers A and B as shown in Figure 2.3. The cantilever arms, spanning 145' $5\frac{7}{16}$ " each, 'B' and 'C' supports the suspended span of 436' $4\frac{3}{8}$ " as shown in Figure 2.4. Anchor arm 'C' with a span of 458' $9\frac{7}{8}$ " is placed between piers C and D, and it is connected to the cantilever arm 'D' having a span of 191' $2\frac{1}{8}$ " as shown in Figure 2.5. Anchor arm 'D' with a span of 458' $9\frac{7}{8}$ " is placed between piers D and E, and connected to the cantilever arm 'E' having span of 191' $2\frac{1}{8}$ " as shown in Figure 2.6. The span between piers E and F is provided with anchor arm 'E-F' with a span of 363' $7\frac{5}{8}$ " as shown in Figure 2.7. The maximum span length between piers B and C is about 800'. The spans of C-D and D-E are 650' each. The end spans A-B and E-F are 363' $4\frac{5}{8}$ " and 365' $1\frac{1}{2}$ ", respectively. The length of spans A-B, B-C, C-D, D-E and E-F are 363' $4\frac{5}{8}$ ", 800', 650', 650' and 365' $1\frac{1}{2}$ ", respectively.

The lateral truss system consists of lateral bracing members in the top and bottom chord planes combined with portals and sway bracing between the two vertical trusses as shown in Figure 2.1. At the hinge locations, longitudinal sliding joints in both the top and bottom chords are designed for free thermal expansion.

The floor system consists of a 7" thick concrete slab supported by longitudinal WF stringers which are carried by transverse built-up floor beams as shown in Figure 2.8. The width of the two-lane roadway is 20'. The stringers are spaced at 4' 9(3/4)". The floor beams span 27' 6" between the vertical trusses and are attached to the truss verticals.

2.3 Fixed and Expansion Bearings

The superstructure is supported by expansion bearings at piers A and F, and fixed bearings at piers B, C and D and E. The expansion bearings permit longitudinal translation and longitudinal rotation. The fixed bearings only allows longitudinal rotation.

The fixed bearings are of standard pinned bearing design consisting of a cast steel upper shoe supported on a 6" diameter steel pin which bears on a cast steel bottom shoe. The upper shoe is bolted to the bottom chord of the truss and the bottom shoe is rigidly attached to the pier via anchor bolts. The anchor bolts are of 2" diameter and it extends 4' into the pier concrete.

The expansion bearings consist of a bottom shoe assembly with a pin. The top shoe is connected to the bottom chord of the main truss, which is then connected to the pin. The slots in the bottom chord of the main truss allows longitudinal translation. The bottom shoe is rigidly attached to the pier via anchor bolts.

2.4 Bridge Substructure

The main bridge is supported on piers A, B, C, D, E and F, which are of tapered wall type piers up to a certain height from the foundation. All the piers are supported on caisson foundation except pier A which is supported on pile foundation. The side elevations and pile arrangements of the pier A are shown in figure 2.9. The cross section of this tapered wall pier changes after a certain height from the bottom of the pier. This change in cross section is mainly to accommodate the deck-truss type approach span on the Illinois side. Side elevation and plan view of the piers B, C, D and E are shown in Figures 2.10(a) and (b). The tapered wall type piers have opening in the upper half of the pier. The side elevations and plan of the pier F are shown in Figure 2.11(a-b). It has two pairs of bearings, one pair for the main bridge and the

other for the approach bridge. All the piers are constructed with reinforced concrete of grade AA.

3. FIELD TESTING

3.1 General

Field testing a bridge provides an accurate and reliable description of its actual dynamic characteristics. Field testing was conducted on the US51 main bridge over the Ohio river on May 20, 1997. The bridge is having two lanes of traffic, namely the northbound and southbound lanes. Testing was conducted on both the northbound and southbound lanes. Since there is no symmetry in the longitudinal direction of the bridge, the full bridge was tested. All measurements were taken by placing the instruments on the pavement. Instruments were placed on the pavement due to the limited access to the actual floor beams and the time constraints involved. Each instrument was placed with its longitudinal axis aligned parallel to the longitudinal direction of the bridge. Ambient vibration measurements under traffic and wind induced excitations were recorded at 29 locations beginning from pier A to pier F.

3.2 Instrumentation

The equipment used to measure the acceleration-time histories consisted of triaxial accelerometer (Figure 3.1a) in conjunction with its own data acquisition system. The system which was used consisted of Kinematics SSA-2 digital recording strong motion accelerograph. Two of the units contained internal accelerometers and the remaining two were connected to Kinematics FBA-23 force balance accelerometers. Each of the accelerometers is capable of measuring accelerations of +/- 2g's with a frequency response of DC-50 Hz. All data were sampled using a 1002 Hz sampling rate and stored internally on the SSA-2, then downloaded to a personal computer. Each of these units were triggered simultaneously using laptop personal computers connected to each SSA-2. A nominal 60 sec record was obtained at each location. Accelerometers were mounted in order to measure vibrations in three orthogonal directions. To ensure the blocks were placed in level, adjustable feet and carpenters level were attached to each block. Accelerometers were connected to the data acquisition system by shielded cables.

Sets of three accelerometers were mounted to aluminum blocks in orthogonal directions. A block was positioned at each location with the accelerometers oriented in the vertical, transverse and longitudinal directions. To prevent any shifting of the accelerometers during testing, 25-pound bags of lead shot were laid on top of the accelerometer blocks once in position. During ambient vibration tests, traffic was allowed to cross at normal highway speed.

3.3 Testing Procedure

A reference location, hereinafter referred as the base station, was selected based on the mode shapes from the preliminary finite element model at location 6 as shown in Figure 3.1b. Two of the accelerometers, one at each side of roadway width (Figure 3.1c), remained at the base station 6 throughout the testing sequence. Five triaxial accelerometers were used at moving station locations. From the preliminary finite element analysis, 29 locations were identified to be measured to represent the dynamic behavior of the bridge. Totally there were six sets of moving station data with each set having 5 moving station locations. Tables 3.1a and 3.1b describes the designations of moving and base station accelerometer on northbound lane. Tables 3.2a and 3.2b details the designations of moving and base station accelerometers on southbound lane. First five stations 1 (two accelerometers at this location in order to get 5 in each set), 2, 3 and 4 were placed in span-1, stations 5-12 were placed in span 2, stations 14-18 were placed in span-3, stations 20 -24 were placed in span-4, and stations 26 to 28 were placed in span-5. Data collection began from pier A to pier F on the northbound lane. Same procedure was repeated for the southbound lane also without altering the base station. Station locations 1, 5, 13, 19, 25 and 29 indicate that they are just above the piers A, B, C, D, E and F, respectively.

One set of measurements consisted of recording acceleration-time history on two base stations and five moving stations simultaneously. Once the data was collected, the moveable stations were moved to the next locations while the base stations remained stationary. This sequence was repeated six times to get measurements on all stations on the northbound lane.

3.4 Data Analysis

Once the data have been downloaded from the field test, a Fast Fourier Transform (FFT) was performed on each acceleration-time history using the DADiSP software. The program DADiSP (Data Analysis and Display Software) by DSP Development Corporation, Cambridge, Massachusetts, (DADiSP 1995) was used to view and analyze the large amount of data. The program has the ability to quickly access and display the large records of 30,000 data points. Also, the program has an extensive data handling and analysis library which was needed for this research. Fast Fourier transforms of the acceleration histories were possible in few seconds. The speed of the program made analyzing and viewing such a huge amount of data manageable.

Acceleration records were transformed from the time domain to the frequency domain through the use of the Fourier transform. Equations 3.1 and 3.2 are the mathematical definitions of the Fourier transform pair. Equation 3.1 is referred to as the Fourier transform of $f(t)$ and the equation 3.2 as the inverse Fourier transform

(Press et al. 1992, Chapra and Canale 1988).

$$F(\omega) = \int_{-\infty}^{\infty} f(t) e^{i\omega t} dt \quad (3.1)$$

$$f(t) = \frac{1}{2\pi} \int_{-\infty}^{\infty} F(\omega) e^{-i\omega t} d\omega \quad (3.2)$$

where $f(t)$ = a function of time, $F(\omega)$ = amplitude as a function of frequency, and ω = circular frequency (radians per second).

From equations 3.1 and 3.2, a time function can be derived from a frequency function or vice versa. The problem with using equations 3.1 and 3.2 lies in the fact that a continuous function is required. For discretely sampled data, such as a dynamic bridge test, a different form of the Fourier transform is needed. A form of equation 3.1, known as the Discrete Fourier Transform (DFT), is used when points of data are known at evenly spaced intervals. Equations 3.3 and 3.4 are the Discrete forms of the Fourier transform pair.

$$F_n = \sum_{k=0}^{N-1} f_k e^{2\pi i kn/N} \quad (\text{for } n=0 \text{ to } N-1) \quad (3.3)$$

$$f_k = \frac{1}{N} \sum_{n=0}^{N-1} F_n e^{-2\pi i kn/N} \quad (\text{for } k=0 \text{ to } N-1) \quad (3.4)$$

where N = number of sampled points and f_k = set of N sampled points.

The DFT as expressed in equation 3.3 is usually the most useful in civil engineering applications where frequency components are sought from discretely sampled (digitized) data. However, the direct application of equation 3.3 requires N^2 complex mathematical operations. This becomes prohibitively time-consuming even for modest length data records. Fortunately, there is a numerical operation that reduces computing time for the DFT substantially.

The method is called the fast Fourier transform (FFT) and owes its efficiency to exploitation of the periodicity and symmetry of trigonometric functions. An FFT can be computed in approximately $N \log_2 N$ operations. For a set of 1000 data points, the FFT is approximately 100 times faster than the DFT. The first FFT is attributed to

Gauss in 1805 but did not become widely known until the mid 1960's with the advent of the Cooley-Tukey algorithm. A more complete mathematical and numerical treatment of the FFT can be found in Press et al. (1992) and Chapra and Canale (1988). Using the Fast Fourier Transform (FFT), natural frequencies in three orthogonal directions were determined. Additional processing into a Power Spectral Density (PSD) plot, which squares the FFT amplitudes and divides out the record length, was sometimes helpful in identifying natural frequencies.

Mode shapes were determined by plotting the ratios of accelerometer FFT magnitude to base station FFT magnitude at their respective locations along the bridge. Comparing the phase angle of an FFT frequency to the base-station FFT phase angle determined the sign of the magnitude to be plotted (in-phase or out-of-phase with the base station).

A typical ambient vibration acceleration-time history obtained in the transverse direction at the moving station 6 is shown in Figure 3.2a. Similar time histories are shown for the vertical (figure 3.2c) and longitudinal (figure 3.2e) directions at moving station 6. For the transverse direction, the FFT of the acceleration time-history of moving station 6 is shown in Figure 3.2b. Similar FFTs for vertical and longitudinal direction time-histories are shown in figures 3.2d and 3.2f. By observing the peaks of all the stations, the natural frequencies were identified. These peaks do not always occur at exactly the same frequency at all locations. Therefore, the number of peaks of adjacent natural frequencies were calculated. Table 3.3 lists the distribution of frequencies from acceleration record obtained on longitudinal, transverse and vertical direction accelerometers. Then, the bridge natural frequency was identified as the one which has maximum number of peaks and also based on the mode shape that follows closer to the preliminary finite element model results.

Table 3.3 also lists the comparison between the field tested natural frequency with that of the calibrated finite element model. They are discussed in the following section.

3.5 Finite Element Model Calibration

A logical next step to field testing in bridge evaluation is to create an analytical model which will correlate well to the measured dynamic properties. Many assumptions and modeling approximations must be made when creating a practical model of a bridge. For example, a finite element model requires input of the material properties which are inherently variable. This is one input where the analyst can only make a best estimate and later adjust to match the experimental results.

Using results from the eigenvalue analysis, the bridge model has to be calibrated to experimentally determined mode shapes and frequencies. A perfectly calibrated model would match all experimentally determined mode shapes and frequencies exactly. To hope for such a perfect calibration is not realistic. Therefore, only the most structurally significant modes and frequencies are used in the model calibration process. Namely, the first four transverse modes, first six vertical modes and the first longitudinal mode from field testing are selected as calibration targets.

Parameters which were used to correlate with the field test are: modulus of elasticity (E) of the frame elements, the bearing spring stiffness, and spring stiffnesses for the piers. Initial parameter estimates were made based on design information. Initial estimates do not account for: (1) construction tolerances or errors that can make as-built dimensions different from design dimensions, or (2) actual strengths of materials such as the actual compressive strength of concrete, which affects its modulus of elasticity. Calibration is performed by adjusting the stiffnesses and masses of the bridge members until an acceptable match is observed in the natural frequency and mode shape.

Since the bridge does not have a symmetry along the vertical direction, it is not possible to observe pure transverse modes. Instead, transverse flexural-torsional modes are obtained. But pure vertical mode are obtained, because the bridge is symmetric in the transverse direction. Longitudinal modes are accompanied with little vertical bending mainly because of the unequal pier stiffnesses. For comparison purposes, only the transverse components from field testing are taken into consideration for the transverse flexural-torsional modes. All the transverse flexural-torsional modes are hereinafter referred as transverse modes, because they have major mass participation in the transverse direction.

The finite element results for the mode shapes are generated at the end nodes in the floor beams. On the other hand, due to the limited access to the actual floor beams, all measurements were taken by placing the instruments on the pavement just above the floor stringers. Furthermore, the expansion joints in the decks were not accounted for in the 3-D model.

Figure 3.3a shows the comparison of the mode shape obtained from the test and finite element model. Although this mode is not a pure transverse mode, Figure 3.3a compares only the transverse components. This mode has five half-waves along the length of the bridge. The distribution of fundamental natural frequency is given in Figure 3.3b. It can be seen from this figure that the peak in the magnitude varied from 0.3674 Hz to 0.4342 Hz, with a maximum number of peaks occurring at 0.3871 Hz. Therefore, 0.3871 Hz is identified as the fundamental frequency from the field test. The natural frequency from the finite element model is 0.3831 Hz, and the difference is only about 1.7%.

Figure 3.4a shows the first vertical mode with a natural frequency of 0.7515 Hz from the test. The distribution of natural frequency is shown in Figure 3.4b. Although the maximum of number of peaks appears to be at 0.7849 Hz, the mode shape corresponding to 0.7515 Hz matched better with the finite element model, and hence 0.7515 Hz is identified as the natural frequency from field testing. The finite element model frequency is 0.7578 and the difference is only about 0.8%. This mode is a pure vertical mode with 5 half-waves along the length of the bridge.

The traffic induced excitation can produce clear acceleration records in the vertical direction, and the traffic combined with wind excitations can produce in the transverse direction. Since there was no excitation along the longitudinal direction, clear acceleration records in the longitudinal direction was not obtained. Therefore, the matching of the frequencies is difficult for this mode. The first longitudinal mode shape is shown in Figure 3.5a. The natural frequency from the field test according to Figure 3.5b is 1.2859 Hz. The FE model frequency is 1.2812 Hz and the difference is only about 0.36 %. Due to the difference in stiffness of the piers, pure longitudinal modes are not obtained. Therefore, longitudinal mode is accompanied with small vertical modal deformation, however, the mass participation in this mode is mainly due to the longitudinal deformation of the piers.

Figure 3.6a shows the mode shape of the second transverse mode. The distribution of natural frequency is shown in Figure 3.6b and the natural frequency is identified as 0.501 Hz. The natural frequency from the FE model is 0.502 Hz and the difference with the test is only 0.13%. This is not a pure transverse mode. It is a transverse flexural-torsional mode with five half-waves.

The mode shape of second vertical mode is shown in Figure 3.7a. The natural frequency from the test is 1.052 Hz whereas from the FE model is 1.072 Hz and the difference with the test is 1.9%. Figure 3.7b shows the distribution of natural frequency of this mode and it is seen that maximum number of peaks occur at 1.0521 Hz. The mode shape consists of five half-waves along the length of the bridge.

Figure 3.8a shows the mode shape of the third transverse mode. This is a transverse flexural-torsional mode with the frequency of 0.6346 Hz from field testing and 0.6206 from FE model. The difference of FE model natural frequency with test is only 2.2%. There are six half-waves in the mode shape along the length of the bridge. Figure 3.8b shows the distribution of the natural frequency and 0.6346 Hz is observed at 22 stations out of the total 29 stations.

Figure 3.9a shows the mode shape of the third vertical mode. The natural frequency of 1.336 Hz is identified from the test and 1.3978 from the FE model. The difference of FE model frequency with the test is 4.6%. The mode shape consists of six half-waves along the length of the bridge. From Figure 3.9b it is seen that the

maximum of number of peaks occur at 1.3026 Hz and at 1.336 Hz. The frequency 1.336 is identified as the natural frequency, since the mode shape corresponding to this frequency matches better with finite element model.

The mode shape of the fourth transverse mode is shown in Figure 3.10a. The natural frequency from the finite element model is 0.9147 Hz, whereas the field tested natural frequency is identified as 0.9352 Hz. The difference of FE model frequency with the test is 2.2%. There are seven half-waves in the mode shape along the length of the bridge. Figure 3.10b shows the distribution of natural frequency and it is seen that the maximum number of peaks occur at 0.9352 Hz. This frequency is observed at 18 stations out of the total 29 stations.

Figure 3.11a shows the fourth vertical mode. The natural frequency from the test is identified as 1.837 Hz and 1.8848 Hz from the FE model. The difference of FE model frequency with the test is 2.6%. The mode shape consists of eight half-waves along the length of the bridge. The distribution of the natural frequency is shown in Figure 3.11b and test frequency of 1.837 Hz is identified at 18 stations out of 29 stations.

The mode shape of the fifth vertical mode is shown in Figure 3.12a. The natural frequency from the test is 1.9038 Hz whereas from the FE model the frequency is 1.9348 Hz. The difference of FE model frequency with the test is 1.63%. This mode consists of eight half-waves along the length of bridge. From Figure 3.12b, it is seen that the maximum number of peaks occur at 1.9038 Hz and hence it is identified as the frequency from the test. This frequency is found to occur at 15 out of 29 stations.

Figure 3.13a shows the mode shape of the sixth vertical mode. The natural frequency of 2.2044 Hz is obtained from the test and 2.2327 Hz from the FE model. The difference of FE model frequency with the test is 1.28%. The mode shape consists of 8 half-waves along the length of the bridge. The distribution of the natural frequency is shown in Figure 3.13b and it is seen that the maximum number of peaks occur at 2.2712 Hz. This frequency is observed at 16 out of 29 stations.

4. FINITE ELEMENT MODELING AND FREE VIBRATION ANALYSIS

4.1 General

Based on the general dynamic characteristics of cantilever truss bridges and the proximity and activity of the seismic zones, the main bridge model was expected to remain elastic and displacements were anticipated to be small enough to neglect the material and geometric nonlinear effects. Hence, the consideration of linear elastic small displacement analysis is considered to be appropriate.

Free vibration analysis is a key process in the dynamic analysis of a structure; the resulting natural frequency and mode shapes succinctly describe the dynamic characteristics of a complex structure. The analytical model is calibrated by comparing free vibration analysis results with ambient vibration measurements.

4.2 Finite Element Model

A three dimensional linear elastic finite element model (Figure 4.1) of the main bridge was developed in SAP90 finite element analysis software (Wilson and Habibullah, 1994). Developed for both the free vibration analysis and earthquake response analysis, the model represents the structure in its current as-built configuration. All truss members of the superstructure are modeled using two noded frame elements which has three translational DOF and three rotational DOF at each node. Rotational degrees of freedom (DOF) of members are included in this bridge because the connections are of riveted type that could create bending stresses in addition axial stresses. Based on the connection between the concrete deck and stringers, it is assumed that the deck and stringers will not contribute to the stiffness of the bridge. Wall type piers are idealized as frame elements with gross cross-sectional properties. The full 3D model has a total of 1816 frame elements and 818 nodes. The number of material and geometric property groups are 126. The total number of active degrees of freedom (DOF) is about 3120.

The bearings at the end piers are "expansion" type and those at the interior piers are "fixed" type. The "fixed" bearings at the interior piers were modeled by simply releasing the rotational DOF in the vertical direction only. Pier and bearings are connected through a set of rigid elements that simulate the actual behavior.

The "expansion" bearings at the end piers were modeled by establishing nodes in the bottom chord of the truss and the top of the pier at the bearing centers and coupling all DOF except the longitudinal translation and the vertical bending rotation (the θ_x and u_z DOF). The coupled nodes provide direct output of the relative displacement between the top and bottom shoes of the bearings and thus indicate if the translation has exceeded the expansion capacity.

While conducting free vibration analysis, it was found that the modeling of piers using frame elements resulted into less mass participation. This may be due to large differences in stiffness and masses of members in superstructure and piers of substructure. Therefore, the piers were replaced by springs at the bottom of bearings. The spring stiffnesses were obtained by applying unit displacement along the appropriate DOF.

4.3 Free vibration Analysis

An eigenvalue analysis is used to determine the undamped, free vibrations of the structure. The eigensolution results in the "natural" mode shapes and frequencies of the structure. Free vibration analysis is required first to calibrate the finite element model with the field ambient vibration test measurements. Secondly, to perform seismic response analysis using modal time-history method, the natural frequencies and their associated mode shapes are required from free vibration. Free vibration analysis involves the solution of the following eigenvalue problem:

$$[M - \omega^2 K] u = 0 \quad (4.1)$$

where M and K are system mass and stiffness matrices and u is modal displacement vector. The eigenvalue of a mode (ω^2) is the square of the circular frequency of that mode (ω) and relates to the cyclical frequency (f) by the relation $f = \omega/2\pi$, and relates to the period of vibration (T) by the equation $T = 1/f$.

SAP90 uses an "accelerated subspace iteration" algorithm to solve the eigenvalue problem. The subspace iteration method was developed by Bathe in 1971 and a detailed discussion of the method and its fundamentals can be found in Bathe (1982). Various techniques have been used to "accelerate" the basic subspace iteration method and the particular algorithm used in the SAP90/SAP2000 programs can be found in Wilson and Tetsuji (1983).

Traditionally, mode-superposition analysis was performed using a structure's eigenvectors as the basis for the analysis. Research (Wilson, Yuan, and Dickens, 1982) indicates that this is not the best starting point for a mode-superposition time-history analysis. Instead, a special set of load-dependent, orthogonal Ritz vectors yields more

accurate results than the same number of natural mode shapes. Ritz vector analysis significantly reduces computing time and automatically includes the proven numerical techniques of static condensation, Guyan reduction, and static correction due to higher mode truncation.

The reason that Ritz vector analysis yields better results than an equal number of eigenvectors is because the Ritz vectors take into account the spatial distribution of dynamic loading. In fact, the spatial distribution of loading serves as a starting load vector to begin the process of finding appropriate Ritz vectors. Subsequent Ritz vectors are formed based on the preceding Ritz vector and the neglected inertial effects. In contrast, the eigenvectors are computed from the stiffness and mass matrices only and, therefore, can not account for the spatial distribution of loading. Eigenvectors that are orthogonal to loading do not participate in the structural response even if they are at or near the forcing frequency.

For model calibration, the natural frequencies and their mode shapes has to be accurate, therefore exact eigenvalues(natural frequencies) have been extracted. All the frequencies may not participate in calculating the response under seismic excitation kind of loading. In order to get full participation, many modes have to be extracted. In this work, around 450 modes were tried to improve the mass participation. But there was no increase in the mass participation. Therefore, Ritz-vector based (which are load dependent) extraction of eigenvalues has been carried out. This method gives more than 90% participation in all the three directions.

The natural frequencies and mass participation for the lowest 45 modes are presented in Table 4.1. Some of the frequencies and their mode shapes have been compared with the field testing in the earlier chapter. The natural frequency of the bridge ranges from 0.3831 Hz to 2.75 Hz for the first 45 modes, and the period ranges from 2.61 sec to 0.36 sec. The natural frequencies listed in Table 4.1 and their mode shapes are used only to calibrate the finite element model. They are not used for the seismic response analysis. It is seen from Table 4.1 that the mass participation of the first three modes are only in the transverse direction. Therefore, these three modes are treated as transverse modes based on the mass participation point of view, although there is some torsional and vertical displacement component as seen from Figure 4.2b.

Figures 4.2(a), (b) and (c) shows the first mode shape in isometric, elevation and plan views, respectively. The natural frequency of this mode is 0.3831 Hz. The percentage of mass participation of this mode is about 6.8. This mode has antisymmetric shape in the second and third spans. Based on mass participation, this mode is identified as the transverse mode.

Figures 4.3(a), (b) and (c) shows the second mode shape with a frequency of 0.5017 Hz in isometric, elevation and plan views, respectively. As in the first mode,

two major half-waves present in the same direction, and one major half-wave in the opposite direction. The mass participation for this mode is 2.3% . Based on mass participation, the second mode is also observed as the transverse mode.

Figure 4.4(a), (b) and (c) shows the third mode shape with a frequency of 0.6206 Hz in isometric, elevation and plan views, respectively. Since three major half-waves are falling in the same direction, the mass participation for this mode is 32.5%. Based on mass participation, this mode is noted as the transverse mode. Therefore this is one of the very important mode that significantly contribute for the transverse seismic motion.

The fourth mode shape in isometric, elevation and plan views is shown in Figures 4.5(a), (b) and (c), respectively. The natural frequency of this mode is 0.7578 Hz. Based on mass participation and from Figures 4.5(b) and (c), it is seen that this mode is the first vertical mode. The mass participation in the vertical direction is only 3%.

Figures 4.6(a), (b) and (c) show the fifth mode shape with a frequency of 0.9147 Hz, in the isometric, elevation and plan views respectively. The mass participation for this mode is 3%. Based on mass participation, this mode is observed as the transverse mode.

The sixth mode shape in isometric, elevation and plan views is shown in Figures 4.7(a), (b) and (c), respectively. The natural frequency of this mode is 0.9725 Hz and the mass participation is 1.61%. Based on mass participation, this mode is treated as transverse mode. Figures 4.8(a), (b) and (c) show the seventh mode shape with a frequency of 0.993 Hz. The mass participation is only 0.5%. Based on Figures 4.8(b) and (c), this mode is mainly a torsional mode with little transverse bending.

Figures 4.9(a), (b) and (c) show the eighth mode shape with a frequency of 1.0722 Hz. Major mass participation 2.1% is in the vertical direction with a little participation of 0.17% in the longitudinal direction. Therefore, this mode is observed as the vertical mode. The ninth mode shape with a frequency of 1.1318 Hz is shown in Figures 4.10(a), (b) and (c). The mass participation is only 2.1% in the transverse direction. This mode is identified as a transverse mode with little torsion.

The tenth mode with a frequency of 1.1435 Hz is shown in Figures 4.11(a), (b) and (c). The mass participation for this mode is 4.95%. It is observed that this mode is a transverse mode with little torsion in first two spans.

Figures 4.12(a), (b) and (c) shows the eleventh mode shape with a frequency of 1.2812 Hz. From mass participation and mode shape, it is seen that this mode is the first longitudinal mode. Mass participation for this mode is 95% in the longitudinal

direction.

The twelfth mode shape with a frequency of 1.2866 Hz is shown in Figure 4.13(a), (b) and (c). The mass participation for this mode is 2.6%. Based on the mode shape and mass participation, this mode is identified as a transverse mode with many half-waves. Figures 4.14(a), (b) and (c) show the thirteenth mode shape with a frequency of 1.3279 Hz. The mass participation for this mode is 11.27%. Based on the mode shape and mass participation, it is observed that this mode is the second dominant mode to contribute significantly in the transverse direction.

Figures 4.15(a), (b) and (c) show the fourteenth mode shape with a frequency of 1.3849 Hz. The mass participation for this mode is less than 0.025%. Therefore, this mode is observed as a torsional mode with little vertical and transverse bending. The fifteenth mode shape with a frequency of 1.3978 Hz is shown in Figures 4.16(a), (b) and (c). The mass participation for this mode in the vertical direction is 18.8% and in the longitudinal direction is 2%. Therefore, this mode is the first dominant mode to contribute significantly in the vertical direction.

Similar observations can be made for other modes from Table 4.1. However, the modes 21, 22 and 27 are explained in the following, since these modes are compared with the field test in the earlier Chapter.

The 21st mode shape with a frequency of 1.8848 Hz is shown in Figures 4.17(a), (b) and (c). This mode has mass participation in both the vertical and longitudinal directions but the value is less than 0.735%. Based on Figure 4.17b and mass participation, it is observed that this mode is a combined vertical and longitudinal mode.

Figures 4.18(a), (b) and (c) shows the 22nd mode with a frequency of 1.9348 Hz. This mode has mass participation of 6.5% in the vertical direction with a small mass participation of 0.9% in the longitudinal direction. This mode can be visualized as a vertical mode. The 27th mode shape with a frequency of 2.2327 Hz is shown in Figures 4.19(a), (b) and (c). The mass participation for this mode is 21.8% which is mainly in the vertical direction. Therefore, this is one of the pure vertical mode which is very important to contribute significantly for the vertical seismic motion.

From Table 4.1, it is seen that there is a very good mass participation in the longitudinal and transverse directions. But the mass participation in the vertical direction is only 54%. By increasing the number of modes beyond 45 modes did not improve the mass participation in the vertical direction.

The mode shapes and natural frequencies discussed above consisted of all the system frequencies. For earthquake response analysis, all these frequencies and modes

may not be excited and hence all the frequencies are not required. The Ritz-vector based method yields frequencies and mode shapes that provides significant participation in all directions. These frequencies and their mass participation are presented in Table 4.2. By comparing Tables 4.1 and 4.2, it is seen that the modes with very less mass participation in all the three directions are omitted by Ritz vector based eigenvalue extraction method. From Table 4.2, it is seen that the mass participation in all the three directions are more than 90% and this indicates that model will give reasonable response under earthquake type of loading.

5. SEISMIC RESPONSE ANALYSIS

5.1 General

A number of different analytical methods have been developed for assessing the seismic vulnerability of existing bridges including elastic analysis, inelastic pushover analysis, capacity spectrum analysis and nonlinear dynamic analysis (Priestly et al. 1996). Each approach incorporates different assumptions and varies in complexity of application. The problem of an engineer assessing the seismic vulnerability of a bridge structure is to select the most appropriate and cost-effective method for performing the assessment. Under minor ground motions, a bridge will experience little inelastic behavior and thus the linear elastic analysis is convenient and reasonable for bridge design and assessment for minor earthquakes. A limitation of the elastic analysis method is that the linear analysis offers little information regarding the inelastic response of the structure. Disadvantages of nonlinear dynamic time-history analysis are that the structural elements of nonlinear models are considerably more complex than those of their linear elastic counterparts, the numerical algorithms do not always ensure convergence to a physically valid solution, processing and evaluation of the output often requires considerable effort, and the results can be extremely sensitive to input parameters and structural models.

In this work, modal time-history analysis is used because the bridge is assumed to behave linearly elastic with small displacements under the expected earthquake loading. Modal time-history method was used instead of response spectrum method for the main bridge due to the importance of the bridge and also due to the lack of seismic considerations in its initial design. Time-history analysis is the most sophisticated analysis technique available to the structural analyst. Using this level of analysis affords the engineer a complete description of the behavior of a structure at all times throughout an earthquake. Since no strong earthquake records are available for the Eastern U.S., time-history analyses for Kentucky bridges were performed using artificial earthquake records characteristic of the New Madrid and other nearby seismic zones.

Modal time-history method for the earthquake analysis involves the solution of the following equation of motion:

$$M \ddot{u} + C \dot{u} + K u = -M \ddot{u}_g \quad (5.1)$$

where M , C and K are the system mass, damping and stiffness matrices, respectively. \ddot{u}_g , \dot{u} and u are the system nodal acceleration, velocity and displacement vectors. u_g is the

earthquake motion for which the bridge's response has to be calculated. The SAP90 software performs exact integration of the modal-response equations for a linear variation of the time-function between the input data time points. Therefore, the results are not dependent on the selection of a "time-integration interval" as in some other methods [Wislon and Habibullah, 1992]. Damping for all the modes are assumed to be 5%.

Time-histories representing the 50-year event and the 500-year event were generated for the vertical and two orthogonal horizontal directions in the report by Street et al. (1996). The definition of the 50-year event is: the peak horizontal particle acceleration, at the top of rock, that has a 90% probability of not being exceeded in 50 years (i.e. 10% probability of exceedance). Likewise, the 500-year event has a 90% probability of not being exceeded in 500 years. A recurrence rate (return period) can be calculated for the earthquakes which would produce the 50- and 500-year events.

The 50-year event that has a 10% probability of exceedance corresponds to AASHTO's (1996) design earthquake for highway bridges. For low probability of exceedance, the recurrence rate is approximately (National Highway Institute, 1996) the ratio of time and return period. Actual return period for the 50-year event is 475 years (Mayes et al. 1992). Some states require even longer return periods for their design earthquake. For example, California's Department of Transportation (Caltrans) uses a 2400-year return period, which has a 10% probability of exceedance every 250 years.

For the seismic zones affecting Kentucky, the 50-year and 500-year events defined in Street et al. (1996) correspond to the AASHTO design earthquake and near the maximum credible earthquake, respectively. For the bridge location in this study, Ballard County, Kentucky, a time-history with peak horizontal acceleration of 30% gravity represents the AASHTO design earthquake. The time-history for the "near maximum credible earthquake" (500-year event) has a peak horizontal acceleration of 60% gravity in Ballard County.

5.2 Seismic Response

The seismic response of the US51 bridge is calculated for the 50-year earthquake. For the Ballard County bridge site, peak horizontal bedrock acceleration for this artificial earthquake is 30% gravity (figure 5.1). For comparison, AASHTO's map (1996) of peak horizontal acceleration places the Ballard County bridge site in, approximately, the 25% gravity contour for the same probability event. Earthquake duration is 10.24 seconds consisting of 2049 data points at 0.005 second intervals. The input motion along longitudinal, transverse and vertical directions are presented in figures 5.2-5.4, respectively. The peak ground accelerations along longitudinal, transverse and vertical directions are 115, 70.5 and 114.6 in/sec², respectively. Since the longitudinal direction of the earthquake may not coincide with the longitudinal direction of bridge, it is necessary

to analyze the bridge under different excitation cases as described in Table 5.1. Under LL11 excitation case, as mentioned in Table 5.1, the longitudinal earthquake is applied along longitudinal direction of the bridge and vertical earthquake is applied along the vertical direction of the bridge. Similarly for other excitation cases, vertical earthquake is considered acting in the vertical direction of the bridge. Only the longitudinal and transverse earthquakes are reversed. On some excitation cases, all the three direction earthquakes are applied simultaneously.

Time-history analysis produces a very large quantity of output. It is difficult to monitor the maximum forces for all the members and maximum displacements at all the joints in a modal time-history analysis for seismic excitation kind of loading. Therefore, members and joints are selected based on their proximity to critical locations. From SAP90 software, forces and moments are obtained for selected members. Stresses are calculated externally using simple computer programs/spreadsheets. Table 5.2 presents the cross-sectional properties of members that are selected for stress calculation.

As an example, for the L1T2V3 (Table 5.1) earthquake, the time history plots of transverse and vertical displacements at joint 44 (Fig. 2.5) are presented in Figures 5.5 and 5.6. It is observed that the maximum transverse displacement of 1.61" occurs at 4.245 secs, and maximum vertical displacement of 1.77" occurs at 2.86 secs. The axial force time history for member 294 (Fig. 2.6) is presented in Figure 5.7. The maximum axial force of 58.61 kips occurs at 3.645 secs.

For stress calculations, the axial stresses are calculated from P/A and bending stresses are calculated from M_{12}/Z_{13} and M_{13}/Z_{12} . M_{12} and M_{13} are the bending moments in the local 1-2 and 1-3 planes respectively. Z_{12} and Z_{13} are the section modulus about the 1-2 and 1-3 planes, respectively. Combined stresses are calculated as the sum of P/A, M_{12}/Z_{13} , M_{13}/Z_{12} with appropriate signs to get the maximum stresses.

Axial stress = σ_a = Axial force/Area

Bending stress in 1-2 plane at Ith joint = σ_{b12i} = Absolute(M_{12} at Node I / Z_{13})

Bending stress in 1-2 plane at Jth joint = σ_{b12j} = Absolute(M_{12} at Node J / Z_{13})

Bending stress in 1-3 plane at Ith joint = σ_{b13i} = Absolute(M_{13} at Node I / Z_{12})

Bending stress in 1-3 plane at Jth joint = σ_{b13j} = Absolute(M_{13} at Node J / Z_{12})

Combined axial and bending stress:

Stress at node I = $\sigma_a + \sigma_{b12i} + \sigma_{b13i}$

Stress at node J = $\sigma_a + \sigma_{b12j} + \sigma_{b13j}$

Shear stress is calculated from the shear forces in 1-2 and 1-3 plane, i.e.,

Shear stress = $\tau = \{ \text{Square root of } [(SF_{12})^2 + (SF_{13})^2] \} / \text{Area}$

The absolute maximum of stresses obtained from the maximum and minimum responses from time-history analysis are presented in tabular form and are discussed in the following. Table 5.3 lists the stresses at selected members (Figs. 2.3-2.7) due to seismic excitation case L1T2V3 (Table 5.1). Due to earthquake motion alone, the axial stresses are found to be larger than the bending stresses with a maximum of 4.3 ksi in member 297. Bending stresses are calculated and presented at nodes I and J of the member. Table 5.3 also presents the maximum of the combined stresses from the Dead load \pm Earthquake load (EQ) \pm Thermal load (90° F). Shear stress is found to be very less with a maximum of 2.4 ksi in member 182. The maximum of combined axial and bending stress is found to be 20.2 ksi in member 294, which is less than the yield strength of steel (36 ksi).

Table 5.4 lists the stresses at selected members (Figs. 2.3-2.7) when two of the excitation directions are reversed, i.e. under L2T1V3 (Table 5.1) case. Axial stresses due to seismic forces alone are found to have a maximum of 6.1 ksi in member 288. This Table 5.4 also presents the maximum of the combined stresses from the Dead load \pm Earthquake load (EQ) \pm Thermal load (90° F). Shear stresses are very less with a maximum of 0.2 ksi in member 244. Maximum of the combined stresses is found to be 7.3 ksi in member 288, which is less than the yield strength of steel.

Under the seismic excitation case LL11, the stresses calculated for selected members (Figs. 2.3-2.7) are presented in Table 5.5. The maximum axial stress is found to be 4.25 ksi in member 294. Maximum of the combined axial and bending stress is found to be 5.0 ksi in member 294, which is less than the yield strength. Shear stress is found to have a maximum of 0.16 ksi in member 243.

Table 5.6 lists the stresses at selected members (Figs. 2.3-2.7) when the seismic excitation LL22 is applied. The maximum axial stress is found to be 4.2 ksi in member 288. Maximum of the combined axial and bending stress is 4.98 ksi in member 288, which is far less than the yield stress of steel. Shear stress is found to have a maximum of 0.15 ksi in member 243.

For the seismic excitation case TT11, the stresses at selected members (Figs. 2.3-2.7) are presented in Table 5.7. The maximum axial stress is found to be 6.12 ksi in member 294. Maximum of the combined axial and bending stress is 7.32 ksi in member 288, which is less than the yield strength of steel. Shear stress is found to have a maximum of 0.17 ksi in member 294.

Table 5.8 lists the stresses at selected members (Figs. 2.3-2.7) when the seismic excitation TT22 is applied. The maximum axial stress is found to be 4.25 ksi in member 291. Maximum of the combined axial and bending stresses is 5.1 ksi in member 291 which is less than the yield stress of steel. The shear stress is found to have a maximum of 0.15 ksi in member 243.

The stresses at selected members (Figs. 2.3-2.7) due to a differential temperature of 90°F are presented in Table 5.9. The coefficient of thermal expansion for steel is taken as $6.5 \times 10^{-6}/^\circ\text{F}$. Maximum axial stress is found to be 9.2 ksi in member 1. Maximum shear stress is obtained as 0.13 ksi. Combined stresses from axial and bending is 11.325 ksi in member 1.

Table 5.10 lists the stresses at selected members (Figs. 2.3-2.7) due to the self-weight of the bridge. Maximum axial stress is found to be 10 ksi in member 294. Maximum shear stress is obtained as 2.22 ksi in member 182. Combined stresses from axial and bending stresses have a maximum of 11.6 ksi in member 243.

In previous calculations, the stresses produced were checked purely from the material yield point of view. Under earthquake loading, truss members may experience tensile force at one time interval and compressive force at some other time interval. Therefore, it is necessary to check for the buckling of truss members. Since the bridge truss members are subjected to axial forces and bending moments, the equations (10-42) to (10-44) from AASHTO is used to check whether they satisfy the inequality condition.

AASHTO Eq. (10.42):

$$\frac{C_{mx} f_{bx}}{\left(1 - \frac{f_a}{F_{rx}}\right) F_{bx}} + \frac{C_{my} f_{by}}{\left(1 - \frac{f_a}{F_{ry}}\right) F_{by}} \leq 1.0 \quad (5.2)$$

AASHTO Eq. (10-43): At points of support

$$\frac{f_a}{F_y} + \frac{f_{bx}}{F_{bx}} + \frac{f_{by}}{F_{by}} \leq 1.0 \quad (5.3)$$

AASHTO Eq. (10-44): Euler Buckling Stress:

$$F_{rx} = \frac{\pi^2 E}{(0.75 L/r)^2} \quad (5.4)$$

$$F_{ry} = \frac{\pi^2 E}{(0.75 L/r_y)^2} \quad (5.5)$$

In Table 5.11 and 5.12, the stresses are checked by also considering the buckling of the member for the earthquake excitation cases L1T2V3 and L2T1V3, respectively. It is seen that the inequalities given in equations 10-42 and 10-43 are satisfied and hence there will not be any member failure due to combined axial and bending stresses.

The displacements at selected nodes (Figs. 2.3-2.7) are presented in Table 5.13 for the different excitation cases (Table 5.1). Maximum displacement in the longitudinal direction is 1.2" at joint 29 under L1T2V3 case. Maximum displacement in the transverse direction is 5" at joint 44 under L2T1V3 case. Maximum displacement in the vertical direction is 1.93" at joint 44 under TT22 case.

Under static dead load and temperature, the displacements at selected joints (Figs. 2.3-2.7) are listed in Table 5.14. Due to a temperature of 90°F, maximum displacements in the longitudinal direction is 4.8" at the joints 89 and 818. The transverse displacement is maximum at joint 29 is 0.16". Maximum vertical displacement is 0.97" at joint 29. Due to dead load, maximum longitudinal displacement is 0.8" at joint 118. Transverse displacement are very less, i.e. with a maximum of 0.04". The maximum vertical displacement is 8.9" at joint 23.

Maximum and minimum base shears obtained for the bridge are listed in Table 5.15. These values are presented for different excitation cases listed in Table 5.1. The maximum in each direction for all excitation cases is obtained and load combination is applied. Then, based on the translational stiffnesses of the piers, shear forces on top of the pier is calculated and presented in Table 5.16.

5.3 Capacity/Demand Ratios

Since the superstructure of the bridge is connected to the substructure through bearings, it is necessary to check these bearings against loss-of-span and anchor bolt shear failure. Table 5.16 lists the available anchor bolt shear capacity (V_c) and base shears at each pier. The anchor bolt capacity V_c is calculated by assuming the shear strength of the bolt as 26.97 ksi. The resultant of base shear is calculated as the square of the sum of squares of the longitudinal and transverse base shears. Then the seismic demand (V_b) is calculated by multiplying by 1.25 as per *FHWA Retrofitting manual*. The pier A has force C/D ratios $r_{bf}=0.84$ and for all the other piers r_{bf} are greater than 1.0.

The bearings at piers A and F are of expansion type having a slotted bottom chord member attached to the bottom shoe of the bearing. Therefore expansion is allowed to a limited extent. However in this work displacement capacity/demand (C/D) ratios $r_{bf} = (\Delta_s(c) - \Delta_i(d)) / \Delta_{eq}(d)$ [Section A.4.2, *FHWA Retrofitting Manual*] are calculated for these bearings and presented in Table 5.17. $\Delta_s(c)$ is the available seat width, $\Delta_i(d)$ is the displacement due

to temperature effects and $\Delta_{eq}(d)$ is the seismic displacement. The C/D ratios are greater than 1.0 and hence loss-of-span cannot occur due to displacement consideration.

6. APPROACH BRIDGE

6.1 General

The US51 bridge over the Ohio river consists of Kentucky and Illinois approach spans as shown in figures 6.1 and 6.2, respectively. The plan and elevation views of the Kentucky and Illinois approaches are shown in figures 6.3 and 6.4, respectively. The Kentucky approach has 21 spans whereas the Illinois approach has 6 spans. All the spans in the Illinois approach are simply supported with expansion bearings on one support and fixed bearings on the other. The total length of the Illinois and Kentucky approaches are 570.52' and 2464.4', respectively. The pier I1 on Illinois approach and piers K7, K8 and K9 on Kentucky approach are supported on caisson foundations, and all the other piers are supported on pile foundations.

The Illinois approach consist of 5 girder spans and one deck-truss span, whereas the Kentucky approach consists of nine deck-truss type spans, 2 suspended spans and the remaining 10 are girder spans. The span length of deck-truss type spans are about 182', whereas the girder spans ranges from 60' to 90' and the suspended spans are of 40' length. The cross section of superstructure for different type of spans are shown in figures 6.5-6.7. The cross section of the bridge piers have taper along the height with a batter of 1/2" per foot. The approach bridge piers are made of reinforced concrete with class AA grade concrete.

6.2 Structural Modeling

Although the approach spans are large in number, 5 on Illinois side and 20 on Kentucky side, these spans are idealized as simple structural systems based on the type of bearings provided at the top of the pier. The models are designated as Ia, Ib, Ic and Id for Illinois approach, and Ka, Kb, Kc, ... Kp for Kentucky approach. The simplified systems for the Illinois and Kentucky approach are shown in figures 6.8 and 6.9, respectively. These simplified systems are treated as single-degree-of-freedom (SDOF) system for mathematical modeling of the bridge in longitudinal direction. The mass of the SDOF consists of mass of the superstructure and one-third mass of the pier. The longitudinal translational stiffnesses of the piers are calculated using $3EI/L^3$. Modulus of elasticity of concrete is assumed as 3625 ksi for class AA grade of concrete. Average moment of inertia is used for calculating the stiffness of battered piers. Due to the unavailability of detailed site soil investigations, stiff and flexible models are adopted to get the maximum forces and displacement. In the stiff model, the pier is assumed to be fixed at the bottom of the pier, and in the flexible model the length of the pier is extended upto the half length of pile,

i.e. 17.5'. The extended length is assumed to have the same flexural properties as that of the pier.

The dimensions, gross cross sectional properties and stiffnesses of all the piers are listed in Table 6.1. The moment of inertia of piers K1 to K6 are calculated as an average of moment of inertia of the upper and lower middle portions. This is to account for the variation of shape of the cross section at the lower and upper portions of the pier. For all other piers, the moment of inertia is calculated as an average of the top and bottom moment of inertia. Table 6.2 and 6.3 list the weight of the superstructure of the girder spans and deck-truss spans of the Illinois approach. Table 6.4 and 6.5 list the weight of the superstructure of deck-truss spans and girder spans of the Kentucky approach.

6.3 Seismic Response Analysis

The approach spans are analyzed under seismic motion corresponding to 0.3g earthquake of the 50-year event. The study of damage to multi-span simple bridges reveals that longitudinal seismic waves have caused more damage than transverse (Zimmerman and Brittain, 1979). In this work, seismic analysis is performed to determine any loss-of-span due to excessive longitudinal displacement or shear failure of the bearings. In this work, seismic analysis of the simplified SDOF models for the approach spans is carried out using the response spectrum method.

The response spectrum method is a technique for obtaining the solution of the coupled, second-order, linear, differential equations of motion that govern the forced vibration of a bridge. This method involves an initial eigenvalue analysis to determine the natural frequencies and mode shapes of the bridge. The orthogonality of the mode shapes with respect to the mass, stiffness and damping matrices is then used to uncouple the equations of motion. The peak response associated with the single-degree-of-freedom system represented by each of the uncoupled equations of motion is obtained through the use of an elastic earthquake response spectrum. An estimate of the maximum response of the structure is determined by combining the peak responses of the individual modes based on statistical procedures.

The natural frequencies and periods of the models based on flexible system are presented in Table 6.6 with their stiffness and mass. These frequencies range from 0.75 hz to 5.58 Hz for the Kentucky approach whereas for the Illinois approach it ranges from 1.47 to 14.54 Hz. Table 6.6 also lists the minimum force demand on bearings which is 20% of the dead load [*FHWA retrofitting manual (1995)*]. This minimum force demand should be considered to check the bearings if the seismic force demand is less. The natural frequencies and periods of the models based on stiff system are given in Table 6.7. The natural frequency ranges from 1.26 to 22 Hz for the Kentucky approach, and 3.32 to 22.4 Hz for the Illinois approach. As expected the frequencies are high in the stiff system.

The response spectra for the Ballard County is shown in figure 6.10 for 50-year earthquake event with a peak acceleration of 0.30g (Harik et al. 1997). The damping is assumed to be 5%. The site soil coefficient is conservatively taken as 2.0 for both the flexible and stiff system. Table 6.8 lists the longitudinal displacements and forces for the different models of flexible system. The maximum longitudinal seismic displacement of 10" is found for one of the spans of Kentucky approach, and for the Illinois approach the maximum displacement was found to be 2.7". The seismic force for the Kentucky approach ranges from 163 to 471 kips, whereas for the Illinois approach it ranges from 170 to 396 kips.

Table 6.9 presents the displacement and forces in the longitudinal direction for the stiff system. The maximum displacement is 3.71" for the Kentucky approach and 0.53" for the Illinois approach. The seismic force for the Kentucky approach ranges from 163 kips to 467 kips, whereas for the Illinois approach it ranges from 170 to 397 kips. It is seen that, in most of the models of the flexible and stiff systems, the response is controlled by the $C_s \leq 2 A$ criterion.

6.4 Capacity/Demand Ratios

Table 6.10 lists, for the flexible system, the bearing force capacity (V_c)/demand (V_d) ratios, $r_{bf} = V_c/V_d$, and also gives information about the additional number of bolts required at each bearing. The anchor bolt capacity V_c is calculated by assuming the shear strength of the bolt as 26.97 ksi. Seismic demand V_d is calculated by multiplying the seismic force by 1.25 [FHWA Retrofitting manual]. The force capacity/demand ratios are less than 1.0 for all the piers with fixed bearings. The additional anchor bolts required at each pier are listed in Table 6.10.

Table 6.11 presents the capacity/demand ratios and additional anchor bolts at each pier for the stiff system. The capacity/demand ratios and additional anchor bolt requirements are same as in flexible system. Figures 6.11 to 6.31 show the arrangement of additional anchor bolts at the bearings as suggested in Table 6.11.

Table 6.12 lists the bearing displacement capacity/demand ratios $r_{bi} = (\Delta_s(c) - \Delta_i(d))/\Delta_{eq}(d)$ [Section A.4.2, FHWA Retrofitting Manual] of the flexible system. $\Delta_s(c)$ is the available seat width, $\Delta_i(d)$ is the displacement due to temperature effects, and $\Delta_{eq}(d)$ is the seismic displacement. Since the expansion bearings at the piers have anchor bolts that can slide horizontally may limit the horizontal displacement during earthquake, therefore, the method 2 in Section A.4.2 of the FHWA retrofitting manual is used for calculating the displacement capacity/demand ratios. These ratios are greater than 1 for all the spans, and hence loss-of-span can not occur from the consideration of displacement capacity/demand ratios.

6.5 Retrofit for the Approach Bridge

From the seismic analysis of the approach spans, it is found that the fixed bearings at some of the piers need additional anchor bolts to resist the 0.3g earthquake corresponding to 50-year event at the Ballard County. Additional anchor bolts may be provided according to Table 6.11 and as shown in Figures 6.11 to 6.31.

7. CONCLUSIONS AND RECOMMENDATIONS

7.1 General

The US51 bridge over the Ohio river may be subjected to future earthquakes. Therefore, it is important to evaluate the bridge under the projected seismic motion. In this work, since the bridge is located in Ballard Co. of Kentucky, 0.3g earthquake for the 50-year event is applied. Depending upon the importance of the bridge, it has been decided to use more rigorous methods for the evaluation of the main bridge and simplified methods for the approach spans.

7.2 Main Bridge

The seismic evaluation of the main bridge consisted of field ambient vibration testing, finite element modeling and seismic response analysis using modal time-history method. Field testing was mainly carried out to identify the natural frequencies and their mode shapes. These frequencies and mode shapes have been compared with the results from the finite element model. Comparisons have been performed for four transverse modes, six vertical modes and one longitudinal mode.

Three dimensional finite element model was developed with frame elements and spring elements. This model has been calibrated with the field test for natural frequencies and mode shapes. Frequencies from the field test for the first modes in the transverse, vertical and longitudinal directions are 0.3871, 0.7515 and 1.2859 Hz, respectively. Frequencies from the finite element model for the first modes in the transverse, vertical and longitudinal directions are 0.3831, 0.7578 and 1.2812 Hz, respectively. Reasonable agreement between the field test and finite element model has been obtained.

Seismic response analyses have been carried using modal time-history method. Displacements of selected joints and stresses for selected members have been calculated. The results are presented also for different seismic excitation cases by reversing the seismic excitation directions. Stresses for selected members are also presented for combined earthquake, dead load and thermal loads. For the selected joints, the maximum displacement in the transverse, vertical and longitudinal direction was found to be 5", 1.9" and 1.2", respectively. Maximum combined axial and bending stresses in the members is found to be 20 ksi. These stresses are less than the yield stress of steel and hence material yielding may not occur. Bending stresses have been combined with axial stresses by considering the buckling of members. It was found that for the selected members buckling failure may not occur.

Capacity/demand (C/D) ratios have been calculated for bearing displacements at pier A and F, and these C/D ratios are greater than 1.0. Hence loss-of-span may not occur from the displacement consideration. Bearing force C/D ratios have been calculated for the bearings at all the piers. Except at pier A, all the other piers have C/D ratios greater than 1.0 and hence retrofit is not required for the piers B to F. Pier A has a C/D ratio of 0.84. Therefore, the available number of anchor bolts may be increased by 16%.

7.3 Approach Bridge

The US51 bridge has approach spans on Kentucky and Illinois sides. Most of the approach spans are single-span with expansion bearing at one support and fixed bearing at the other. Therefore, single-degree-of-freedom models were used along with response spectrum method for the seismic response analysis. Response analysis has been carried out only in the longitudinal direction of the bridge, and maximum displacement and force responses have been calculated.

Displacement and force capacity/demand ratios have been calculated. Displacement C/D ratios are greater than 1.0, hence loss-of-span may not occur from the displacement considerations. At many piers, force C/D ratios were less than 1.0, therefore, retrofit in the form of additional anchor bolts is recommended. Alternatively, retrofit in the form of cable restrainers, isolation bearings and/or connection of bottom chord members of all the spans may be provided.

REFERENCES

AASHTO, (1996), *Standard Specifications for Highway Bridges*, 16th Edition, American Association of State Highway and Transportation Officials, Washington D.C.

Abdel-ghaffer, A.M. and R. H. Scanlan (1985a), Ambient Vibration Studies of Golden Gate Bridge: I. Suspended Structure, *ASCE J. of Engrg. Mech.*, 111(4), 463-482.

Abdel-ghaffer, A.M. and R. H. Scanlan (1985b), Ambient Vibration Studies of Golden Gate Bridge: II. *ASCE J. of Engrg. Mech.*, 111(4).

Alampalli, S., and Fu, G., (1994), "Instrumentation for Remote and Continuous Monitoring of Structural Condition," Paper No. 940261 Presented at the Transportation Research Board's 73rd Annual Meeting, Washington D.C., January, 1994.

Bathe, K.J., (1982), *Finite Element Procedures in Engineering Analysis*, Prentice-Hall, Inc., Englewood Cliffs, New Jersey, chapter 12.

Buckland, P.G., et al., (1979), "Suspension Bridge Vibrations: Computed and Measured," *Journal of the Structural Division*, Vol. 105, No. ST5, pp. 859-874.

Buckle, I.G. and I. M. Friedland (editors), *Seismic Retrofitting Manual for Highway Bridges*, Report No. FHWA-RD-94-052, Federal Highway Administration, May 1995.

Chapra, S.C., and Canale, R.P., (1988), *Numerical Methods for Engineers*, 2nd Edition, McGraw-Hill, Inc., New York, New York, Chapter 13.

DADiSP 4.0 User Manual, (1995), DSP Development Corporation, Cambridge, Massachusetts.

Doll, H., (1994), "Eigenfrequencies and Normal Modes of the Norderelb Bridge Near Hamburg: Numerical and Measuring Investigations," *Proceedings of the 12th International Modal Analysis Conference*, Honolulu, Hawaii, pp. 449-455.

EERI, Loma Prieta earthquake renaissance report, Earthquake spectra, Special supplement to Vol.6, 448pp, May 1990.

EERI, Northridge earthquake renaissance report, Earthquake spectra, Special supplement to Vol.11, 116pp, Feb.95.

Farrar, C., White, K., and Mayes, R., (1995), "Vibration Testing of the I-40 Bridge Before and After the Introduction of Damage," Presented at the North-American Workshop on Instrumentation and Vibration Analysis of Highway Bridges, Cincinnati, Ohio, July, 1995.

Harik, I.E., D. Dietz, C. Hill and M.W. Guo, Seismic Evaluation and Retrofit of Bridges, Research Report KTC-96-5, Kentucky Transportation Center, University of Kentucky, 1997.

Harik, I.E., D. L. Allen, R. L. Street, M.W. Guo, R.C. Graves, J. Harrison and M. J. Gawry (1997a), Free and Ambient Vibration of Brent-Spence Bridge, ASCE J. of Struct. Engrg., 123(9), 1262-1268.

Harik, I.E., D. L. Allen, R. L. Street, M. W. Guo, R.C. Graves, J. Harrison, and M. J. Gawry(1997b), Seismic Evaluation of Brent-Spence Bridge, ASCE J. of Struct. Engrg., 123(9), 1269-1275.

Harik, I.E. and C. Madasamy (1998), Field Testing and Seismic Evaluation of Highway Bridges, Proc. 12th Engrg. Mech. Conference at La Jolla, California.

Hudson, D.E., (1977), "Dynamic Tests of Full-Scale Structures," Journal of the Engineering Mechanics Division, Vol. 103, No. EM6, pp. 1141-1157.

Jacob, K., (1995), "Geotechnical and Seismological Aspects of New York Seismic Code Provisions," *National Center for Earthquake Engineering Research Bulletin*, Vol. 9, No. 3, July, 1995.

Johnston, A.C., (1982), "A Major Earthquake Zone on the Mississippi," *Scientific American*, Vol. 246, No. 4, pp. 60-68.

Johnston, A.C., (1985), "A Brief Overview of the Geology, Seismicity and Seismic Hazard of the Central Mississippi Valley Area," Presented at A Regional Seminar on Earthquake Fundamentals for the Mississippi Valley, Memphis, Tennessee, October, 1985.

Johnston, A.C., and Nava, S.J., (1985), "Recurrence Rates and Probability Estimates for the New Madrid Seismic Zone," *Journal of Geophysical Research*, Vol. 90, No. B8, pp. 6737-6753.

Mayes, R.L., et al., (1992), "AASHTO Seismic Isolation Design Requirements for Highway Bridges," *Journal of Structural Engineering*, Vol. 118, No. 1, pp. 284-304.

National Highway Institute (NHI) Course No. 13063, (1996), "Seismic Bridge Design Applications," Notes from Sessions 1 & 2.

Paultre, P., Proulx, J., and Talbot, M., (1995), "Dynamic Testing Procedures for Highway Bridges Using Traffic Loads," *Journal of Structural Engineering*, Vol. 121, No. 2, pp. 362-376.

Press, W.H., et al., (1992), *Numerical Recipes in FORTRAN: The Art of Scientific Computing*, 2nd Edition, Cambridge University Press, New York, New York, chapter 12.

Priestly, M.J.N., F. Seible and G. M. Calvi, *Seismic Design and Retrofit of Bridges*, John-Wiley & Sons, Inc., 1996.

Saiidi, M., Douglas, B., and Feng, S., (1994), "Prestress Force Effect on vibration Frequency of Concrete Bridges," *Journal of Structural Engineering*, Vol. 120, No. 7, pp. 2233-2241.

Shahawy, M.A., (1995), "Non Destructive Strength Evaluation of Florida Bridges," Proceedings of SPIE Nondestructive Evaluation of Aging Infrastructure Conference, Oakland, California, June, 1995.

Shelley, S.J., et al., (1995), "Dynamic Testing (Vibration Analysis) of Highway Bridges," Notes Presented at the *North-American Workshop on Instrumentation and Vibration Analysis of Highway Bridges*, Cincinnati, Ohio, July, 1995.

Street, R., Z. Wang, I. E. Harik, D. L. Allen and J. J. Griffin, *Source Zones, Recurrence Rates, and Time Histories for Earthquakes Affecting Kentucky*, Report No. KTC-96-4, Kentucky Transportation Center, University of Kentucky, 1996.

Ventura, C.E., Felber, A.J., and Prion, G.L., (1994), "Seismic Evaluation of a Long Span Bridge by Modal Testing," Proceedings of the *12th International Modal Analysis Conference*, Honolulu, Hawaii, pp. 1309-1315.

Wendichansky, D.A., Chen, S.S., and Mander, J.B., (1995), "In-Situ Performance of Rubber Bearing Retrofits," Presented at National Seismic Conference on Bridges and Highways, San Diego, California, December, 1995.

Wilson, E.L. and A. Habibullah, *SAP90 - Structural Analysis Users Manual*, Computers and Structures, Inc, May 1992.

Wilson, E.L., M.W. Yuvan, and J.M. Dickens (1982), *Dynamic Analysis by Direct Superposition of Ritz Vectors*, *Earthquake Engineering and Structural Dynamics*, 10, 813-823.

Wilson, E.L., and Tetsuji, I.J., (1983), "An Eigensolution Strategy for Large Systems," *Computers and Structures*, Vol. 16, pp. 259-265.

Zimmerman, R. M. and Brittain, R. D. (1979), *Seismic response of multi-simple span highway bridges*, In: proceedings of the 3rd Canadian Conference on Earthquake Engg., Montreal, pp1091-1120.

Table 3.1a US51 Bridge Testing Details - Moving Station on Northbound Lanes

Station	Filename	Accelerometer Block	Channel Number (xx)	Orientation
29	N1chXX.dat (NB Traffic)	Yellow	20	Horizontal
			21	Transverse
			22	Vertical
28		White	17	Horizontal
			18	Transverse
27		19	Vertical	
	Red	14	Horizontal	
		15	Transverse	
26		16	Vertical	
	Orange	11	Horizontal	
		12	Transverse	
		13	Vertical	
25	Green	8	Horizontal	
		9	Transverse	
		10	Vertical	
24	N2chXX.dat (NB Traffic)	Yellow	20	Horizontal
			21	Transverse
			22	Vertical
23	N3chXX.dat (SB Traffic)	White	17	Horizontal
			18	Transverse
			19	Vertical
22	Red	14	Horizontal	
		15	Transverse	
		16	Vertical	
21	Orange	11	Horizontal	
		12	Transverse	
		13	Vertical	
20	Green	8	Horizontal	
		9	Transverse	
		10	Vertical	
19	N4chXX.dat (NB Traffic)	Yellow	20	Horizontal
			21	Transverse
			22	Vertical
18		White	17	Horizontal
			18	Transverse
17		19	Vertical	
	Red	14	Horizontal	
		15	Transverse	
		16	Vertical	
16	Orange	11	Horizontal	
		12	Transverse	
		13	Vertical	
15	Green	8	Horizontal	
		9	Transverse	
		10	Vertical	
14	N5chXX.dat (NB Traffic)	Yellow	20	Horizontal
			21	Transverse
			22	Vertical
13		White	17	Horizontal
			18	Transverse
12		19	Vertical	
	Red	14	Horizontal	
		15	Transverse	
		16	Vertical	
11	Orange	11	Horizontal	
		12	Transverse	
		13	Vertical	
10	Green	8	Horizontal	
		9	Transverse	
		10	Vertical	
9	N6chXX.dat (NB Traffic)	Yellow	20	Horizontal
			21	Transverse
			22	Vertical
8		White	17	Horizontal
			18	Transverse
7		19	Vertical	
	Red	14	Horizontal	
		15	Transverse	
		16	Vertical	
6	Orange	11	Horizontal	
		12	Transverse	
		13	Vertical	
5	Green	8	Horizontal	
		9	Transverse	
		10	Vertical	
4	N7chXX.dat (NB Traffic)	Yellow	20	Horizontal
			21	Transverse
			22	Vertical
3		White	17	Horizontal
			18	Transverse
2		19	Vertical	
	Red	14	Horizontal	
		15	Transverse	
		16	Vertical	
1	Orange	11	Horizontal	
		12	Transverse	
		13	Vertical	
1	Green	8	Horizontal	
		9	Transverse	
		10	Vertical	

Table 3.1b US51 Bridge Testing Details - Base Station on Northbound Lanes

Moveable Station Locations	Filename	Accelerometer Block	Channel Number (XX)	Orientation
29	M1chXX.dat (NB Traffic)	Black	0	Horizontal Transverse Vertical
28			1	
27			2	
26		Blue	3	Horizontal Transverse Vertical
25			4	
			5	
24	M2chXX.dat (NB Traffic)	Black	0	Horizontal Transverse Vertical
23			1	
22			2	
21	M3chXX.dat (SB Traffic)	Blue	3	Horizontal Transverse Vertical
			4	
20			5	
19	M4chXX.dat (NB Traffic)	Black	0	Horizontal Transverse Vertical
18			1	
17			2	
16		Blue	3	Horizontal Transverse Vertical
15			4	
			5	
14	M5chXX.dat (NB Traffic)	Black	0	Horizontal Transverse Vertical
13			1	
12			2	
11		Blue	3	Horizontal Transverse Vertical
10			4	
			5	
9	M6chXX.dat (NB Traffic)	Black	0	Horizontal Transverse Vertical
8			1	
7			2	
6		Blue	3	Horizontal Transverse Vertical
5			4	
			5	
4	M7chXX.dat (NB Traffic)	Black	0	Horizontal Transverse Vertical
3			1	
2			2	
		Blue	3	Horizontal Transverse Vertical
1			4	
			5	

Black Accelerometer: Upstream NB side of Bridge
 Blue Accelerometer: Downstream SB side of Bridge

All data saved in g's
 Sampling rate is 1002 Hz

Table 3.2a US51 Bridge Testing Details - Moving Station on Southbound Lane

Station	Filename	Accelerometer Block	Channel Number (xx)	Orientation
1	P1chXX.dat (NB Traffic)	Yellow	20	Horizontal
			21	Transverse
			22	Vertical
2		White	17	Horizontal
			18	Transverse
3		19	Vertical	
	Red	14	Horizontal	
		15	Transverse	
4		16	Vertical	
	Orange	11	Horizontal	
		12	Transverse	
		13	Vertical	
5	Green	8	Horizontal	
		9	Transverse	
		10	Vertical	
6	P2chXX.dat (NB Traffic)	Yellow	20	Horizontal
			21	Transverse
			22	Vertical
7		White	17	Horizontal
			18	Transverse
8		19	Vertical	
	Red	14	Horizontal	
		15	Transverse	
9		16	Vertical	
	Orange	11	Horizontal	
		12	Transverse	
		13	Vertical	
10	Green	8	Horizontal	
		9	Transverse	
		10	Vertical	
11	P3chXX.dat (NB Traffic)	Yellow	20	Horizontal
			21	Transverse
			22	Vertical
12		White	17	Horizontal
			18	Transverse
13		19	Vertical	
	Red	14	Horizontal	
		15	Transverse	
14		16	Vertical	
	Orange	11	Horizontal	
		12	Transverse	
		13	Vertical	
15	Green	8	Horizontal	
		9	Transverse	
		10	Vertical	
16	P4chXX.dat (NB Traffic)	Yellow	20	Horizontal
			21	Transverse
			22	Vertical
17		White	17	Horizontal
			18	Transverse
18		19	Vertical	
	Red	14	Horizontal	
		15	Transverse	
19		16	Vertical	
	Orange	11	Horizontal	
		12	Transverse	
		13	Vertical	
20	Green	8	Horizontal	
		9	Transverse	
		10	Vertical	
21	P5chXX.dat (SB Traffic)	Yellow	20	Horizontal
			21	Transverse
			22	Vertical
22		White	17	Horizontal
			18	Transverse
23		19	Vertical	
	Red	14	Horizontal	
		15	Transverse	
24	P6chXX.dat (NB Traffic)	16	Vertical	
	Orange	11	Horizontal	
		12	Transverse	
		13	Vertical	
25	Green	8	Horizontal	
		9	Transverse	
		10	Vertical	
26	P8chXX.dat (NB Traffic)	Yellow	20	Horizontal
			21	Transverse
			22	Vertical
27		White	17	Horizontal
			18	Transverse
28		19	Vertical	
	Red	14	Horizontal	
		15	Transverse	
29		16	Vertical	
	Orange	11	Horizontal	
		12	Transverse	
		13	Vertical	
29	Green	8	Horizontal	
		9	Transverse	
		10	Vertical	

Table 3.2b US51 Bridge Testing Details - Base Station on Southbound Lane

Moveable Station Locations	Filename	Accelerometer Block	Channel Number (XX)	Orientation	
1 2 3 4 5	O1chXX.dat (NB Traffic)	Black	0	Horizontal	
			1	Transverse	
			2	Vertical	
		Blue	3	Horizontal	
			4	Transverse	
5	Vertical				
6 7 8 9 10	O2chXX.dat (NB Traffic)	Black	0	Horizontal	
			1	Transverse	
			2	Vertical	
		Blue	3	Horizontal	
			4	Transverse	
5	Vertical				
11 12 13 14 15	O3chXX.dat (NB Traffic)	Black	0	Horizontal	
			1	Transverse	
			2	Vertical	
		Blue	3	Horizontal	
			4	Transverse	
5	Vertical				
16 17 18 19 20	O4chXX.dat (NB Traffic)	Black	0	Horizontal	
			1	Transverse	
			2	Vertical	
		Blue	3	Horizontal	
			4	Transverse	
5	Vertical				
21 22 23 24 25	O5chXX.dat (SB Traffic)	Black	0	Horizontal	
			1	Transverse	
			2	Vertical	
	O6chXX.dat (NB Traffic)	Blue	3	Horizontal	
			4	Transverse	
5			Vertical		
26 27 28 29	O8chXX.dat (NB Traffic)	Black	0	Horizontal	
			1	Transverse	
			2	Vertical	
		Blue	3	4	Horizontal
				4	Transverse
5	Vertical				

Black Accelerometer: Upstream NB side of Bridge

Blue Accelerometer: Downstream SB side of Bridge

All data saved in g's

Sampling rate is 1002 Hz

Table 3.3 Frequency Identification from the Field Test Data

Field Tested Frequency, f_i (Hz)	Number of Peaks			Mode Description	Finite Element Frequency, f_{em} (Hz)	Relative Error $100*(f_i - f_{em})/f_i$
	Transverse Direction	Vertical Direction	Longitudinal Direction			
0.0835	22	20	23			
0.1002	4	8	7			
0.1169	10	11	7			
0.1336	13	7	12			
0.1503	9	10	11			
0.167	13	10	9			
0.1837	8	9	11			
0.2004	9	7	8			
0.2171	14	16	10			
0.2338	9	5	13			
0.2505	13	13	9			
0.2672	6	12	10			
0.2839	12	9	9			
0.3006	10	5	8			
0.3173	10	13	8			
0.334	7	12	13			
0.3507	15	8	7			
0.3674	9	9	13			
0.3841	4	12	8			
0.3871	20	10	11	First Transverse	0.3831	1.7326
0.4175	4	7	10			
0.4342	3	14	15			
0.4509	16	7	9			
0.4676	4	14	9			
0.4843	9	5	7			
0.501	19	12	17	Second Transverse	0.5017	0.1315
0.5177	8	11	8			
0.5344	6	6	5			
0.5511	8	8	14			
0.5678	12	7	10			
0.5845	8	18	9			
0.6012	15	8	14			

Table 3.3 (Cont'd) Frequency Identification from Field Test Data

Frequencies from Test Data (Hz)	Number of Peaks in all Stations				Mode Type	Finite Element Frequencies (Hz)	Relative Error 100*(f1-f2)/f1	
	Transverse Direction		Vertical Direction					Longitudinal Direction
	Transverse Direction	Vertical Direction	Transverse Direction	Vertical Direction				
0.6179	2	9	9	9				
0.6346	22	8	8	9	Third Transverse	0.6206	2.1992	
0.6513	3	7	7	11				
0.668	18	11	11	9				
0.6847	5	11	11	13				
0.7014	13	8	8	6				
0.7181	5	7	7	12				
0.7348	13	10	10	11				
0.7515	10	16	16	10	First Vertical	0.7578	0.8321	
0.7682	10	9	9	5				
0.7849	10	17	17	13				
0.8016	17	7	7	9				
0.8183	9	10	10	5				
0.835	14	9	9	11				
0.8517	5	13	13	14				
0.8684	14	9	9	3				
0.8851	13	10	10	14				
0.9018	8	7	7	4				
0.9185	4	13	13	13				
0.9352	18	5	5	9	Fourth Transverse	0.9147	2.1901	
0.9519	7	15	15	8				
0.9686	10	8	8	15				
0.9853	7	15	15	1				
1.002	12	7	7	21				
1.0187	11	8	8	5				
1.0354	5	7	7	10				
1.0521	15	15	15	13	Second Vertical	1.0722	1.9146	
1.0688	3	9	9	7				
1.0855	16	10	10	12				
1.1022	9	6	6	12				
1.1189	2	11	11	3				
1.1356	12	17	17	14				
1.1523	11	6	6	3				

Table 3.3 (Cont'd) Frequency Identification from Field Test Data

Field Tested Frequency, f_i (Hz)	Number of Peaks			Mode Description	Finite Element Frequency, f_{lem} (Hz)	Relative Error $100 \cdot (f_i - f_{lem}) / f_i$
	Transverse Direction	Vertical Direction	Longitudinal Direction			
1.169	6	14	10			
1.1857	12	8	4			
1.2024	4	5	9			
1.2191	4	12	13			
1.2358	14	9	9			
1.2525	4	6	9			
1.2692	19	14	3			
1.2859	4	10	12	First Longitudinal	1.2812	0.3641
1.3026	16	13	9			
1.3193	5	5	5			
1.336	13	13	14	Third Vertical	1.3978	4.6237
1.3527	7	9	12			
1.3694	11	9	5			
1.3861	5	9	11			
1.4028	15	10	5			
1.4195	6	5	20			
1.4362	9	13	3			
1.4529	10	12	13			
1.4696	8	11	12			
1.4863	5	7	5			
1.503	9	12	14			
1.5197	5	11	6			
1.5364	15	12	15			
1.5531	10	5	4			
1.5698	4	9	14			
1.5865	16	9	11			
1.6032	5	12	10			
1.6199	14	3	12			
1.6366	10	7	5			
1.6533	11	9	16			
1.67	11	13	4			
1.6867	2	9	12			
1.7034	19	10	8			

Table 3.3 (Cont'd) Frequency Identification from Field Test Data

Field Tested Frequency, ft (Hz)	Number of Peaks			Mode Type	Finite Element Frequencies (Hz)	Relative Error $100 \cdot (f1 - f2) / f1$
	Transverse Direction	Vertical Direction	Longitudinal Direction			
1.7201	5	10	13			
1.7368	11	12	5			
1.7535	8	7	14			
1.7702	13	9	9			
1.7869	3	11	5			
1.8036	12	13	15			
1.8203	14	6	6			
1.837	4	18	10	Fourth Vertical	1.8848	2.6036
1.8537	15	6	16			
1.8704	8	13	14			
1.8871	9	8	3			
1.9038	15	15	7	Fifth Vertical	1.9348	1.6283
1.9205	8	8	17			
1.9372	10	8	5			
1.9539	9	14	18			
1.9706	9	12	0			
1.9873	9	8	21			
2.004	4	12	6			
2.0207	19	10	18			
2.0374	4	10	4			
2.0541	13	5	23			
2.0708	6	14	2			
2.0875	12	9	18			
2.1042	2	12	6			
2.1209	15	6	7			
2.1376	6	9	13			
2.1543	19	19	16			
2.171	2	2	10			
2.1877	17	6	14			
2.2044	10	15	5	Sixth Vertical	2.2327	1.2829
2.2211	10	9	13			

**Table 4.1 Natural Frequencies and Mass Participation of the Main Bridge
(Exact Eigen System)**

Mode No.	Angular Frequency (rad/sec)	Circular Frequency (Hz)	Period (Sec)	Mass Participation			Cumulative Mass Participation		
				Longit.	Transverse	Vertical	Longit.	Transverse	Vertical
1	2.41	0.3831	2.6103	0	6.834	0	0	6.834	0
2	3.15	0.5017	1.9934	0	2.321	0	0	9.155	0
3	3.90	0.6206	1.6112	0	32.477	0	0	41.632	0
4	4.76	0.7578	1.3197	0.024	0	2.999	0.024	41.632	2.999
5	5.75	0.9147	1.0932	0	3.117	0	0.024	44.749	2.999
6	6.11	0.9725	1.0282	0	1.606	0	0.024	46.355	2.999
7	6.24	0.9930	1.0071	0	0.527	0	0.024	46.882	2.999
8	6.74	1.0722	0.9326	0.172	0	2.106	0.197	46.882	5.105
9	7.11	1.1318	0.8836	0	2.069	0	0.197	48.951	5.105
10	7.18	1.1435	0.8745	0	4.954	0	0.197	53.905	5.105
11	8.05	1.2812	0.7805	95.333	0.001	0.239	95.53	53.906	5.344
12	8.08	1.2866	0.7773	0.026	2.641	0	95.557	56.547	5.344
13	8.34	1.3279	0.7531	0	11.273	0	95.557	67.819	5.344
14	8.70	1.3849	0.7221	0.003	0.004	0.025	95.56	67.824	5.37
15	8.78	1.3978	0.7154	2.052	0.001	18.765	97.612	67.825	24.135
16	10.00	1.5986	0.6256	0	0.193	0	97.613	68.018	24.135
17	10.20	1.6202	0.6172	0	7.909	0.005	97.613	75.927	24.14
18	10.50	1.6681	0.5995	0	0.273	0	97.613	76.2	24.14
19	10.70	1.6957	0.5897	0	0.625	0.002	97.613	76.825	24.142
20	11.60	1.8472	0.5414	0.002	0.092	0.001	97.614	76.917	24.143
21	11.80	1.8848	0.5306	0.208	0	0.735	97.822	76.917	24.878
22	12.20	1.9348	0.5168	0.85	0	6.475	98.672	76.917	31.353
23	12.80	2.0335	0.4918	0	0.235	0	98.672	77.152	31.354
24	13.20	2.1057	0.4749	0	0.009	0.001	98.672	77.161	31.354
25	13.40	2.1405	0.4672	0	5.845	0	98.672	83.006	31.354
26	14.00	2.2292	0.4486	0.006	0.081	0.254	98.678	83.087	31.609
27	14.00	2.2327	0.4479	0.288	0.001	21.811	98.966	83.088	53.42
28	14.50	2.2999	0.4348	0	0.281	0.005	98.966	83.369	53.425
29	15.10	2.4031	0.4161	0	0.012	0.006	98.966	83.38	53.432
30	15.30	2.4311	0.4113	0	0.112	0.001	98.966	83.492	53.432
31	15.60	2.4812	0.4030	0	0.219	0.002	98.966	83.711	53.434
32	15.70	2.4913	0.4014	0.002	0	0.021	98.968	83.712	53.455
33	15.80	2.5104	0.3984	0	0	0.005	98.968	83.712	53.46
34	15.90	2.5272	0.3957	0	0	0.001	98.968	83.712	53.462
35	15.90	2.5345	0.3946	0	0	0	98.968	83.712	53.462
36	16.00	2.5497	0.3922	0	0.923	0.001	98.968	84.635	53.462
37	16.10	2.5574	0.3910	0	0	0	98.968	84.635	53.462
38	16.40	2.6088	0.3833	0	0	0	98.969	84.635	53.462
39	16.40	2.6110	0.3830	0	0	0	98.969	84.635	53.463
40	16.50	2.6217	0.3814	0	0.059	0	98.969	84.695	53.463
41	16.60	2.6401	0.3788	0	0.006	0.003	98.969	84.7	53.466
42	16.70	2.6647	0.3753	0	0	0	98.969	84.7	53.466
43	17.00	2.6978	0.3707	0.001	0.186	0.004	98.97	84.886	53.47
44	17.30	2.7476	0.3640	0	0.066	0.076	98.97	84.952	53.546
45	17.30	2.7593	0.3624	0.001	0.144	0.109	98.971	85.096	53.655

Table 4.2 Natural Frequencies and Mass Participation of the Main Bridge
(Ritz vector based)

Mode No.	Angular frequency (rad/sec)	Circular Frequency (Hz)	Period (sec)	Mass Participation			Cumulative Mass Participation		
				Longit.	Transverse	Vertical	Longit.	Transverse	Vertical
1	2.4070	0.3831	2.6103	0.000	6.834	0.000	0.000	6.834	0.000
2	3.1520	0.5017	1.9934	0.000	2.321	0.000	0.000	9.155	0.000
3	3.8996	0.6206	1.6112	0.000	32.471	0.000	0.000	41.625	0.000
4	4.7611	0.7578	1.3197	0.024	0.000	2.998	0.024	41.626	2.998
5	5.7473	0.9147	1.0932	0.000	3.115	0.000	0.024	44.740	2.998
6	6.1107	0.9725	1.0282	0.000	1.609	0.000	0.024	46.349	2.998
7	6.2389	0.9930	1.0071	0.000	0.526	0.000	0.024	46.876	2.998
8	6.7371	1.0722	0.9326	0.172	0.000	2.106	0.196	46.876	5.104
9	7.1110	1.1318	0.8836	0.000	2.062	0.000	0.196	48.938	5.104
10	7.1849	1.1435	0.8745	0.000	4.960	0.000	0.196	53.898	5.104
11	8.0501	1.2812	0.7805	95.351	0.001	0.241	95.547	53.899	5.346
12	8.0837	1.2866	0.7773	0.027	2.644	0.000	95.574	56.542	5.346
13	8.3431	1.3279	0.7531	0.000	11.264	0.000	95.574	67.806	5.346
14	8.7018	1.3849	0.7221	0.003	0.004	0.025	95.577	67.811	5.371
15	8.7824	1.3978	0.7154	2.052	0.001	18.785	97.630	67.811	24.156
16	10.0441	1.5986	0.6256	0.000	0.200	0.000	97.630	68.011	24.156
17	10.1800	1.6202	0.6172	0.000	7.890	0.005	97.630	75.901	24.162
18	10.4811	1.6681	0.5995	0.000	0.271	0.000	97.630	76.172	24.162
19	10.6543	1.6957	0.5897	0.000	0.621	0.002	97.630	76.793	24.164
20	11.6071	1.8473	0.5413	0.000	0.080	0.001	97.630	76.872	24.165
21	11.8426	1.8848	0.5306	0.202	0.000	0.725	97.832	76.872	24.890
22	12.1566	1.9348	0.5169	0.814	0.000	6.455	98.646	76.873	31.345
23	12.8128	2.0392	0.4904	0.000	0.291	0.000	98.646	77.164	31.345
24	13.4594	2.1421	0.4668	0.000	6.017	0.000	98.646	83.181	31.345
25	14.0275	2.2325	0.4479	0.287	0.000	22.127	98.933	83.181	53.472
26	14.2838	2.2733	0.4399	0.000	0.041	0.009	98.933	83.222	53.481
27	15.0217	2.3908	0.4183	0.000	0.608	0.007	98.933	83.830	53.488
28	15.7916	2.5133	0.3979	0.003	0.028	0.019	98.936	83.857	53.508
29	16.2156	2.5808	0.3875	0.000	0.242	0.034	98.936	84.099	53.542
30	16.4573	2.6193	0.3818	0.000	1.112	0.018	98.937	85.212	53.560
31	17.3729	2.7650	0.3617	0.140	0.001	7.062	99.076	85.213	60.621
32	17.5022	2.7856	0.3590	0.705	0.000	0.079	99.782	85.213	60.700
33	20.2316	3.2200	0.3106	0.000	0.220	0.756	99.782	85.433	61.456
34	20.5558	3.2716	0.3057	0.002	0.531	1.244	99.785	85.964	62.700
35	20.8920	3.3251	0.3007	0.006	0.363	0.489	99.791	86.327	63.189
36	22.9109	3.6464	0.2742	0.007	0.000	6.742	99.798	86.327	69.931
37	25.4467	4.0500	0.2469	0.015	0.385	0.000	99.813	86.712	69.931
38	26.4675	4.2124	0.2374	0.005	1.661	0.005	99.818	88.372	69.936
39	28.2462	4.4955	0.2224	0.002	0.002	11.383	99.820	88.375	81.319
40	31.4151	4.9999	0.2000	0.123	0.896	0.020	99.943	89.271	81.339
41	31.7474	5.0528	0.1979	0.028	3.292	0.050	99.972	92.563	81.389
42	35.5245	5.6539	0.1769	0.000	0.008	7.986	99.972	92.571	89.375
43	50.4892	8.0356	0.1244	0.000	3.341	0.014	99.972	95.911	89.389
44	53.0473	8.4427	0.1184	0.000	0.008	4.585	99.972	95.919	93.974
45	57.4253	9.1395	0.1094	0.020	0.022	0.011	99.992	95.941	93.984

Table 5.1 Description of Seismic Excitation Cases

Seismic Excitation Cases	Description
LL11	Direction-1 of 50-year Earthquake Applied Along Longitudinal Direction of the Bridge.
LL22	Direction-2 of 50-year Earthquake Applied Along Longitudinal Direction of the Bridge.
TT11	Direction-1 of 50-year Earthquake Applied Along Transverse Direction of the Bridge.
TT22	Direction-2 of 50-year Earthquake Applied Along Transverse Direction of the Bridge.
L1T2V3	Direction 1, 2 and 3 of 50-year Earthquakes are Applied Along Longitudinal, Transverse and Vertical Directions respectively.
L2T1V3	Direction 1, 2 and 3 of 50-year Earthquakes are Applied Along Transverse, Longitudinal and Vertical Directions respectively.

Table 5.2 Cross Sectional Properties of Members for Stress Calculation

Member No.	Area (in ²) (A)	Moment of Inertia (in ⁴) I ₁₁	Section Modulus (in ³) Z ₁₁	Distance from centroid to extreme fiber (in), y	Moment of Inertia (in ⁴), I ₁₂	Section Modulus (in ³) Z ₁₂	Distance from centroid to extreme fiber (in), x
1	55.23	5160	415	12.4375	3450	365.3687	9.4375
10	159.92	10800	851.99	12.625	13300	1198.2	11.0625
11	141.42	10400	743.63	13.9375	11600	1059.23	10.9375
34	141.42	10400	743.63	13.9375	11600	1059.23	10.9375
35	157.42	10700	766.83	14	13100	1327.625	9.85
51	132.42	9930	786.72	12.625	10500	979.25	10.75
52	144.94	10000	794.98	12.625	11500	1067.18	10.75
68	138.42	10200	809.53	12.625	11200	1032.499	10.875
69	159.92	10800	851.99	12.625	13300	1198.2	11.0625
78	55.23	5160	415	12.4375	3450	365.4	9.4375
89	112.2	6760	552.05	12.247	9670	894.29	10.8125
90	112.2	6760	552.05	12.247	9670	894.3	10.8125
113	112.2	6760	552.05	12.247	9670	894.3	10.8125
114	112.2	6760	552.05	12.247	9670	894.3	10.8125
130	112.2	6760	552.05	12.247	9670	894.3	10.8125
131	91.2	5750	467.48	12.303	7310	704.8	10.375
147	103.2	6330	515.51	12.276	8640	858.18	10.0625
148	103.2	6330	515.51	12.276	8640	858.18	10.0625
161	55.2	4020	321.41	12.501	3710	385.53	9.625
182	14.64	287	47.833	6	1020	113.6	9
184	58.2	4160	361.18	11.525	3990	411.91	9.6875
185	92.67	12000	777.31	15.5	6510	663.3	9.8125
186	92.67	12000	777.31	15.5	6510	663.3	9.8125
187	67.2	4600	370.32	12.412	4850	491.3	9.875
189	14.64	287	47.833	6	1020	113.6	9
240	67.2	4600	370.32	12.412	4850	491.3	9.875
243	14.64	287	47.833	6	1020	113.6	9
244	88.92	11800	932.04	12.625	6150	555.92	11.0625
245	88.92	11800	932.04	12.625	6150	555.92	11.0625
246	14.64	287	47.833	6	1020	113.6	9
249	64.2	4450	358.13	12.431	4560	464.79	9.8125
285	61.2	4310	345.91	12.452	4270	438.333	9.75
288	14.64	287	47.833	6	1020	113.6	9
289	77.73	10300	665.39	15.5	5330	549.87	9.6875
290	77.73	10300	665.39	15.5	5330	549.87	9.6875
291	67.2	4600	370.32	12.412	4850	491.3	9.875
294	14.64	287	47.833	6	1020	113.6	9
330	67.2	4600	370.32	12.412	4850	491.3	9.875
333	14.64	287	47.833	6	1020	113.6	9
334	85.17	11500	741.02	15.5	5800	598.265	9.6875
335	85.17	11500	741.02	15.5	5800	598.265	9.6875
336	58.2	4160	333.67	12.475	3990	411.91	9.6875
339	14.64	287	47.833	6	1020	113.6	9
359	55.2	4020	321.41	12.501	3710	385.52	9.625

Table 5.3 Stresses (ksi) in Members due to Seismic Excitation Case L1T2V3^a, Dead Load and Temperature

Member No.	Stresses due to L1T2V3 Earthquake								Maximum Stresses from (DL ± EQ ± Temperature)		
	Axial Stress	Bending Stress in 1-2 plane		Bending Stress in 1-3 plane		Combined Stress		Shear stress	Combined Stress at Node I	Combined Stress at Node J	Shear
		Node I	Node J	Node I	Node J	Node I	Node J				
1	1.845	0.733	0.439	0.742	0.586	3.234	2.801	0.024	16.717	18.656	0.649
10	1.354	0.597	0.772	0.421	0.787	2.264	2.866	0.025	6.78	5.879	0.298
11	2.722	0.757	0.582	0.662	0.418	4.075	3.483	0.024	12.181	12.546	0.317
34	2.309	0.494	0.884	0.258	0.453	3.023	3.581	0.009	13.025	10.975	0.25
35	1.45	0.934	0.652	0.559	0.369	2.791	2.436	0.007	11.043	11.826	0.222
51	2.63	0.568	0.977	0.347	0.677	3.545	4.284	0.007	12.354	13.482	0.262
52	1.552	1.208	0.774	0.894	0.487	3.631	2.812	0.009	11.825	9.152	0.244
68	2.224	0.668	0.798	0.369	0.74	3.176	3.613	0.02	10.188	12.401	0.322
69	1.371	0.931	0.594	0.686	0.467	2.836	2.431	0.022	6.533	4.465	0.295
78	2.388	0.446	0.446	0.487	0.605	3.275	3.439	0.013	16.664	14.032	0.623
89	1.274	0.857	1	0.098	0.17	2.229	2.358	0.008	16.035	14.948	0.308
90	1.234	0.676	0.616	0.131	0.095	2.04	1.931	0.009	14.332	15.438	0.308
113	1.946	0.993	0.917	0.089	0.174	2.899	3.037	0.029	17.055	16.015	0.401
114	1.954	0.897	0.788	0.192	0.123	2.889	2.865	0.042	15.616	16.608	0.428
130	2.179	0.866	0.88	0.092	0.176	3.095	3.235	0.009	15.01	14.591	0.318
131	2.718	0.937	0.757	0.233	0.132	3.888	3.411	0.01	18.276	17.407	0.384
147	1.643	0.949	0.983	0.12	0.153	2.695	2.723	0.009	14.053	14.254	0.338
148	1.763	0.939	0.854	0.157	0.103	2.839	2.617	0.031	14.621	14.491	0.444
161	2.405	0.333	0.249	0.503	0.418	3.213	3.003	0.077	6.493	6.007	0.881
182	2.913	0.734	0.792	0.258	0.188	3.742	3.887	0.076	17.871	17.598	2.398
184	2.772	0.327	0.371	0.41	0.151	3.451	3.214	0.039	9.391	9.893	0.188
185	1.097	0.165	0.422	0.268	0.115	1.52	1.634	0.017	11.583	12.163	0.104
186	0.98	0.497	0.724	0.126	0.205	1.597	1.858	0.003	11.043	10.928	0.056
187	1.759	0.34	0.381	0.17	0.122	2.218	2.212	0.006	8.446	9.199	0.088
189	2.893	0.447	0.525	0.717	0.295	3.889	3.712	0.021	17.424	17.64	0.403
240	1.599	0.383	0.443	0.279	0.098	2.256	2.099	0.004	7.931	9.281	0.075
243	3.479	0.736	0.759	0.319	0.124	4.456	4.23	0.158	19.333	18.174	0.761
244	1.858	0.107	0.474	0.452	0.159	2.416	2.404	0.022	13.455	13.492	0.113
245	1.642	0.548	0.78	0.153	0.257	2.249	2.679	0.005	12.037	12.202	0.062
246	3.476	0.663	0.592	0.261	0.271	4.297	4.32	0.026	18.827	18.931	0.327
249	2.611	0.341	0.413	0.488	0.141	3.433	3.158	0.005	10.915	11.799	0.073
285	3.659	0.468	0.445	0.431	0.123	4.488	4.184	0.033	11.119	12.495	0.163
288	3.98	0.65	0.692	0.344	0.249	4.975	4.863	0.117	20.025	19.31	0.544
289	2.383	0.144	0.454	0.471	0.153	2.975	2.888	0.006	13.709	13.62	0.067
290	1.947	0.537	0.801	0.144	0.276	2.576	3.012	0.006	11.577	11.782	0.066
291	4.27	0.47	0.57	0.434	0.136	5.092	4.976	0.004	13.445	14.516	0.062
294	4.003	0.721	0.606	0.228	0.275	4.953	4.744	0.143	20.149	19.641	0.565
330	2.913	0.381	0.502	0.336	0.117	3.63	3.498	0.03	11.088	12.36	0.134
333	3.385	0.748	0.836	0.268	0.225	4.292	4.446	0.031	17.581	17.777	0.31
334	1.73	0.166	0.58	0.336	0.139	2.232	2.442	0.002	11.212	11.56	0.011
335	1.462	0.675	0.986	0.135	0.234	2.257	2.682	0.005	10.133	10.332	0.046
336	3.195	0.351	0.426	0.364	0.168	3.866	3.753	0.011	9.886	10.668	0.029
339	3.473	0.82	0.895	0.305	0.275	4.554	4.581	0.105	18.124	18.421	0.135
359	3.172	0.42	0.383	0.625	0.516	4.083	4.071	0.008	7.45	6.466	0.082

^a Seismic excitation cases described in Table 5.1

Table 5.4 Stresses (ksi) in Members due to Seismic Excitation Case L2T1V3^a, Dead Load and Temperature

Member No.	Stresses due to L2T1V3 Earthquake								Maximum Stresses from (DL ± EQ ± Temperature)		
	Axial Stress	Bending Stress in 1-2 plane		Bending Stress in 1-3 plane		Combined Stress		Shear stress	Combined Stress at Node I	Combined Stress at Node J	Shear stress
		Node I	Node J	Node I	Node J	Node I	Node J				
1	1.9	0.687	0.494	1.467	1.117	4.054	3.316	0.043	4.054	3.316	0.043
10	1.605	0.647	0.879	0.772	1.427	2.719	3.912	0.042	2.719	3.912	0.042
11	2.327	0.815	0.559	1.652	0.972	4.566	3.859	0.048	4.566	3.859	0.048
34	3.862	0.598	1.167	0.745	1.407	5.205	6.434	0.018	5.205	6.434	0.018
35	3.707	1.035	0.844	1.506	0.926	6.075	5.161	0.015	6.075	5.161	0.015
51	4.171	0.644	1.322	0.557	1.379	5.34	6.755	0.017	5.34	6.755	0.017
52	4.189	1.333	0.955	1.649	0.843	6.665	5.93	0.019	6.665	5.93	0.019
68	3.67	0.859	0.92	0.572	1.259	4.661	5.85	0.043	4.661	5.85	0.043
69	1.972	1.011	0.671	1.177	0.697	4.097	3.34	0.046	4.097	3.34	0.046
78	2.397	0.487	0.648	1.106	1.431	3.776	4.443	0.023	3.776	4.443	0.023
89	1.911	0.842	0.96	0.215	0.328	2.729	3.199	0.014	2.729	3.199	0.014
90	1.778	0.822	0.71	0.227	0.195	2.744	2.611	0.015	2.744	2.611	0.015
113	2.032	1.047	1.096	0.259	0.339	3.187	3.455	0.044	3.187	3.455	0.044
114	2.07	0.837	0.73	0.443	0.198	3.35	2.954	0.062	3.35	2.954	0.062
130	2.173	0.804	0.871	0.165	0.443	3.113	3.487	0.012	3.113	3.487	0.012
131	2.659	0.727	0.578	0.553	0.186	3.86	3.367	0.013	3.86	3.367	0.013
147	1.817	1.148	1.115	0.15	0.304	2.844	3.236	0.013	2.844	3.236	0.013
148	1.965	1.29	1.156	0.305	0.196	3.297	3.317	0.048	3.297	3.317	0.048
161	2.321	0.311	0.278	1.255	1.012	3.856	3.588	0.11	3.856	3.588	0.11
182	2.857	0.707	0.753	0.287	0.274	3.79	3.883	0.158	3.79	3.883	0.158
184	2.68	0.343	0.357	0.808	0.284	3.796	3.271	0.041	3.796	3.271	0.041
185	1.548	0.166	0.446	0.728	0.252	2.442	2.119	0.021	2.442	2.119	0.021
186	1.329	0.527	0.782	0.271	0.368	2.128	2.388	0.005	2.128	2.388	0.005
187	2.298	0.321	0.338	0.328	0.222	2.947	2.858	0.01	2.947	2.858	0.01
189	2.854	0.477	0.544	0.986	0.438	4.279	3.782	0.044	4.279	3.782	0.044
240	3.296	0.527	0.386	0.442	0.111	4.089	3.778	0.01	4.089	3.778	0.01
243	4.083	0.803	0.805	0.763	0.227	5.458	5.108	0.188	5.458	5.108	0.188
244	2.061	0.133	0.395	0.881	0.266	2.837	2.721	0.024	2.837	2.721	0.024
245	1.69	0.458	0.671	0.252	0.565	2.4	2.893	0.008	2.4	2.893	0.008
246	3.984	0.677	0.567	0.608	0.79	5.138	5.108	0.045	5.138	5.108	0.045
249	3.058	0.366	0.533	0.945	0.29	4.369	3.863	0.012	4.369	3.863	0.012
285	2.867	0.697	0.425	1.047	0.29	4.422	3.581	0.036	4.422	3.581	0.036
288	6.099	0.573	0.615	0.653	0.51	7.312	7.217	0.109	7.312	7.217	0.109
289	2.937	0.134	0.397	0.857	0.271	3.72	3.515	0.008	3.72	3.515	0.008
290	2.146	0.469	0.688	0.264	0.626	2.795	3.46	0.007	2.795	3.46	0.007
291	3.543	0.578	0.645	0.812	0.301	4.546	4.44	0.007	4.546	4.44	0.007
294	6.061	0.6	0.504	0.471	0.547	7.116	7.069	0.173	7.116	7.069	0.173
330	2.597	0.473	0.686	0.651	0.244	3.697	3.27	0.042	3.697	3.27	0.042
333	4.214	0.914	1.029	0.397	0.311	5.228	5.553	0.072	5.228	5.553	0.072
334	1.917	0.119	0.748	0.642	0.244	2.657	2.909	0.002	2.657	2.909	0.002
335	1.552	0.885	1.301	0.239	0.408	2.489	3.261	0.008	2.489	3.261	0.008
336	3.247	0.378	0.438	0.723	0.323	4.348	4.007	0.018	4.348	4.007	0.018
339	4.213	1.049	1.11	0.387	0.494	5.301	5.768	0.115	5.301	5.768	0.115
359	3.203	0.513	0.423	1.237	1.048	4.919	4.674	0.008	4.919	4.674	0.008

^a Seismic excitation cases described in Table 5.1

Table 5.5 Stresses (ksi) in Members due to Seismic Excitation Case: LL11^a

Member No.	Axial Stress	Bending Stress in 1-2 plane		Bending Stress in 1-3 plane		Combined Stress		Shear stress
		Node I	Node J	Node I	Node J	Node I	Node J	
1	1.655	0.658	0.431	0.129	0.072	2.441	2.074	0.014
10	1.136	0.606	0.775	0.07	0.185	1.656	2.059	0.015
11	1.684	0.784	0.582	0.161	0.071	2.557	2.244	0.016
34	1.498	0.483	0.822	0.068	0.146	2.043	2.466	0.005
35	1.285	0.931	0.664	0.13	0.055	2.326	1.953	0.004
51	2.012	0.581	0.976	0.049	0.132	2.637	3.12	0.006
52	1.283	1.161	0.764	0.163	0.065	2.406	2.1	0.006
68	1.561	0.699	0.793	0.058	0.168	2.123	2.522	0.014
69	1.205	0.944	0.579	0.208	0.082	2.31	1.866	0.017
78	1.837	0.4	0.422	0.043	0.063	2.276	2.272	0.011
89	1.45	0.786	0.889	0.032	0.034	2.268	2.144	0.006
90	1.406	0.676	0.614	0.049	0.065	2.131	2.085	0.007
113	2.153	0.969	0.946	0.043	0.031	3.057	3.129	0.022
114	2.119	0.748	0.739	0.05	0.084	2.851	2.942	0.03
130	2.177	0.837	0.86	0.052	0.025	3.049	3.062	0.005
131	2.65	0.86	0.708	0.037	0.079	3.543	3.292	0.007
147	1.65	0.974	0.995	0.056	0.033	2.676	2.529	0.007
148	1.697	0.983	0.883	0.028	0.042	2.708	2.459	0.024
161	2.286	0.355	0.267	0.129	0.073	2.715	2.61	0.054
182	2.869	0.671	0.736	0.204	0.122	3.615	3.717	0.045
184	2.5	0.307	0.374	0.163	0.047	2.922	2.826	0.034
185	1.188	0.157	0.383	0.197	0.043	1.531	1.615	0.016
186	1.057	0.453	0.678	0.051	0.033	1.556	1.73	0.003
187	1.553	0.346	0.354	0.136	0.069	2.035	1.974	0.005
189	2.861	0.462	0.529	0.46	0.261	3.739	3.606	0.019
240	1.376	0.348	0.416	0.195	0.069	1.906	1.831	0.004
243	3.152	0.751	0.769	0.136	0.051	4.038	3.919	0.156
244	1.932	0.108	0.432	0.261	0.049	2.239	2.365	0.019
245	1.725	0.503	0.726	0.047	0.019	2.217	2.468	0.004
246	3.172	0.673	0.627	0.046	0.136	3.892	3.885	0.025
249	2.514	0.355	0.441	0.165	0.048	3.034	2.997	0.004
285	3.146	0.486	0.465	0.206	0.046	3.697	3.603	0.032
288	4.194	0.638	0.679	0.21	0.09	4.937	4.941	0.104
289	2.281	0.131	0.428	0.273	0.051	2.657	2.705	0.006
290	1.901	0.508	0.765	0.055	0.016	2.404	2.682	0.006
291	3.886	0.459	0.559	0.189	0.049	4.432	4.481	0.002
294	4.253	0.682	0.564	0.087	0.2	5.006	4.904	0.143
330	2.706	0.373	0.521	0.138	0.037	3.192	3.191	0.031
333	3.255	0.761	0.851	0.21	0.105	4.048	4.201	0.017
334	1.603	0.151	0.579	0.226	0.041	1.902	2.167	0.002
335	1.319	0.673	0.988	0.042	0.011	2.03	2.247	0.004
336	2.705	0.348	0.414	0.184	0.06	3.209	3.147	0.01
339	3.348	0.761	0.83	0.153	0.075	4.263	4.226	0.095
359	3.136	0.38	0.37	0.096	0.034	3.586	3.54	0.007

^a Seismic excitation cases described in Table 5.1

Table 5.6 Stresses (ksi) in Members due to Seismic Excitation Case: LL22^a

Member No.	Axial Stress	Bending Stress in 1-2 plane		Bending Stress in 1-3 plane		Combined Stress		Shear stress
		Node I	Node J	Node I	Node J	Node I	Node J	
1	1.312	0.463	0.407	0.087	0.053	1.794	1.766	0.011
10	1.229	0.58	0.831	0.064	0.144	1.729	2.204	0.015
11	1.108	0.796	0.555	0.175	0.087	2.036	1.718	0.016
34	1.325	0.5	0.904	0.06	0.142	1.85	2.37	0.005
35	0.987	0.914	0.662	0.105	0.043	1.938	1.692	0.004
51	1.689	0.582	1.046	0.042	0.096	2.305	2.585	0.005
52	1.212	1.099	0.764	0.106	0.051	2.394	1.949	0.005
68	1.284	0.714	0.861	0.048	0.129	2.041	2.155	0.015
69	1.023	0.87	0.593	0.134	0.058	2.003	1.64	0.016
78	1.558	0.407	0.451	0.042	0.057	1.986	1.914	0.011
89	1.269	0.822	0.922	0.032	0.034	2.124	2.203	0.006
90	1.251	0.659	0.591	0.046	0.062	1.956	1.884	0.008
113	2.076	0.92	0.897	0.04	0.025	3.018	2.997	0.021
114	2.05	0.777	0.719	0.047	0.08	2.774	2.85	0.029
130	2.168	0.784	0.819	0.056	0.027	3.009	2.981	0.006
131	2.638	0.886	0.723	0.035	0.076	3.558	3.239	0.007
147	1.429	0.982	0.983	0.057	0.034	2.459	2.353	0.008
148	1.425	1.059	0.958	0.025	0.041	2.506	2.312	0.023
161	2.08	0.311	0.252	0.121	0.075	2.455	2.372	0.051
182	2.882	0.613	0.631	0.206	0.122	3.667	3.621	0.047
184	2.299	0.31	0.343	0.161	0.047	2.749	2.623	0.036
185	1.177	0.125	0.382	0.199	0.043	1.501	1.56	0.016
186	1.066	0.449	0.669	0.05	0.033	1.512	1.766	0.002
187	1.64	0.34	0.338	0.116	0.074	2.091	2.051	0.005
189	2.833	0.431	0.481	0.469	0.265	3.733	3.523	0.019
240	1.275	0.381	0.416	0.193	0.076	1.822	1.706	0.003
243	3.2	0.679	0.69	0.136	0.049	3.961	3.937	0.148
244	1.86	0.065	0.388	0.252	0.051	2.145	2.283	0.019
245	1.658	0.451	0.65	0.048	0.019	2.138	2.325	0.004
246	3.129	0.596	0.537	0.048	0.14	3.768	3.803	0.025
249	2.452	0.329	0.436	0.156	0.041	2.924	2.929	0.004
285	2.971	0.529	0.442	0.217	0.052	3.564	3.387	0.03
288	4.203	0.571	0.617	0.21	0.085	4.984	4.82	0.106
289	2.261	0.112	0.379	0.276	0.053	2.611	2.679	0.005
290	1.889	0.449	0.67	0.057	0.017	2.385	2.57	0.005
291	3.886	0.413	0.556	0.176	0.049	4.451	4.479	0.002
294	4.193	0.713	0.594	0.089	0.195	4.973	4.89	0.143
330	2.643	0.413	0.529	0.166	0.037	3.168	3.107	0.033
333	3.255	0.78	0.878	0.21	0.102	4.06	4.229	0.014
334	1.545	0.123	0.59	0.226	0.041	1.829	2.099	0.002
335	1.269	0.696	1.04	0.043	0.011	2.002	2.208	0.004
336	2.814	0.315	0.429	0.174	0.064	3.27	3.247	0.01
339	3.272	0.824	0.876	0.151	0.074	4.15	4.221	0.094
359	3.163	0.448	0.38	0.085	0.03	3.578	3.571	0.007

^a Seismic excitation cases described in Table 5.1

Table 5.7 Stresses (ksi) in Members due to Seismic Excitation Case: TT11^a

Member No.	Axial Stress	Bending Stress in 1-2 plane		Bending Stress in 1-3 plane		Combined Stress		Shear stress
		Node I	Node J	Node I	Node J	Node I	Node J	
1	1.826	0.52	0.494	1.42	1.103	3.767	3.328	0.041
10	1.454	0.649	0.878	0.754	1.369	2.559	3.7	0.041
11	2.465	0.893	0.547	1.633	0.972	4.992	3.642	0.048
34	3.681	0.609	1.128	0.726	1.463	5.016	6.273	0.018
35	4.101	1.089	0.844	1.499	0.926	6.47	5.555	0.015
51	4.781	0.622	1.284	0.547	1.338	5.907	6.913	0.017
52	3.908	1.371	0.948	1.64	0.841	6.473	5.638	0.019
68	3.488	0.855	0.872	0.583	1.298	4.486	5.658	0.042
69	1.942	1.002	0.684	1.227	0.714	4.062	3.34	0.046
78	2.116	0.484	0.576	1.111	1.453	3.681	4.077	0.022
89	1.826	0.844	0.996	0.211	0.329	2.636	3.151	0.013
90	1.702	0.839	0.748	0.228	0.196	2.685	2.571	0.015
113	2.038	1.023	1.078	0.254	0.342	3.183	3.439	0.044
114	2.077	0.848	0.721	0.445	0.2	3.37	2.951	0.062
130	2.2	0.888	0.942	0.165	0.443	3.084	3.585	0.012
131	2.704	0.732	0.554	0.553	0.186	3.963	3.422	0.013
147	1.821	1.148	1.131	0.149	0.302	2.878	3.254	0.013
148	1.981	1.278	1.141	0.308	0.197	3.325	3.318	0.049
161	2.364	0.324	0.285	1.237	1.006	3.925	3.561	0.112
182	2.798	0.684	0.721	0.29	0.275	3.771	3.787	0.157
184	2.741	0.291	0.368	0.782	0.277	3.766	3.349	0.041
185	1.48	0.084	0.431	0.724	0.253	2.288	2.096	0.021
186	1.265	0.508	0.751	0.273	0.366	2.046	2.305	0.006
187	2.321	0.294	0.351	0.35	0.222	2.965	2.893	0.011
189	2.848	0.527	0.548	0.977	0.436	4.325	3.756	0.046
240	3.371	0.502	0.392	0.46	0.112	4.138	3.866	0.009
243	4.087	0.759	0.753	0.758	0.226	5.44	5.059	0.184
244	2.142	0.092	0.416	0.874	0.264	2.914	2.791	0.024
245	1.693	0.475	0.664	0.25	0.565	2.389	2.922	0.008
246	4.043	0.654	0.585	0.61	0.789	5.175	5.16	0.044
249	3.117	0.394	0.533	0.917	0.295	4.349	3.945	0.012
285	2.903	0.671	0.454	1.045	0.294	4.387	3.645	0.039
288	6.119	0.652	0.69	0.655	0.51	7.315	7.318	0.109
289	2.972	0.099	0.44	0.857	0.271	3.725	3.553	0.008
290	2.175	0.521	0.774	0.264	0.624	2.826	3.573	0.007
291	3.591	0.61	0.643	0.79	0.297	4.662	4.49	0.008
294	6.124	0.673	0.567	0.471	0.55	7.142	7.195	0.174
330	2.8	0.446	0.691	0.68	0.25	3.854	3.468	0.042
333	4.211	0.916	1.031	0.405	0.311	5.289	5.552	0.072
334	1.946	0.083	0.75	0.644	0.244	2.653	2.94	0.002
335	1.56	0.887	1.3	0.239	0.408	2.495	3.268	0.008
336	3.347	0.411	0.447	0.704	0.32	4.462	4.114	0.018
339	4.269	1.037	1.098	0.388	0.496	5.427	5.81	0.111
359	3.276	0.492	0.429	1.245	1.051	4.967	4.756	0.008

^a Seismic excitation cases described in Table 5.1

Table 5.8 Stresses (ksi) in Members due to Seismic Excitation Case: TT22^a

Member No.	Axial Stress	Bending Stress in 1-2 plane		Bending Stress in 1-3 plane		Combined Stress		Shear stress
		Node I	Node J	Node I	Node J	Node I	Node J	
1	1.228	0.378	0.422	0.72	0.575	2.327	2.176	0.023
10	1.11	0.575	0.735	0.415	0.638	2.016	2.415	0.022
11	1.696	0.765	0.554	0.802	0.458	3.188	2.451	0.026
34	2.221	0.48	0.885	0.276	0.473	2.913	3.517	0.008
35	1.566	0.927	0.612	0.56	0.369	2.914	2.531	0.006
51	1.903	0.552	1.013	0.347	0.67	2.783	3.495	0.008
52	1.685	1.192	0.767	0.87	0.48	3.747	2.83	0.008
68	1.664	0.681	0.82	0.365	0.73	2.629	3.034	0.02
69	1.398	0.91	0.617	0.618	0.447	2.683	2.429	0.023
78	1.79	0.434	0.325	0.482	0.588	2.674	2.678	0.013
89	1.138	0.772	0.88	0.098	0.174	2.007	2.136	0.008
90	1.206	0.676	0.63	0.126	0.093	2.008	1.891	0.009
113	1.875	0.92	0.853	0.085	0.176	2.854	2.9	0.028
114	1.892	0.915	0.808	0.196	0.117	2.82	2.815	0.041
130	2.222	0.853	0.879	0.088	0.173	3.082	3.273	0.009
131	2.771	0.928	0.744	0.233	0.131	3.932	3.438	0.01
147	1.533	0.958	0.989	0.121	0.149	2.589	2.619	0.009
148	1.551	1.005	0.916	0.158	0.107	2.691	2.44	0.03
161	2.303	0.293	0.253	0.485	0.412	3.02	2.919	0.074
182	3.055	0.564	0.613	0.261	0.187	3.881	3.835	0.077
184	2.613	0.302	0.349	0.34	0.144	3.255	3.045	0.035
185	1.093	0.071	0.382	0.268	0.115	1.433	1.58	0.017
186	0.961	0.446	0.659	0.127	0.205	1.515	1.825	0.003
187	1.838	0.311	0.348	0.155	0.122	2.235	2.286	0.006
189	2.947	0.443	0.489	0.72	0.304	3.943	3.733	0.022
240	1.535	0.378	0.416	0.265	0.093	2.151	2.022	0.004
243	3.434	0.623	0.65	0.306	0.124	4.294	4.206	0.148
244	1.769	0.061	0.403	0.437	0.156	2.267	2.326	0.022
245	1.587	0.47	0.69	0.151	0.257	2.208	2.502	0.005
246	3.429	0.671	0.602	0.263	0.271	4.231	4.302	0.028
249	2.635	0.335	0.41	0.437	0.139	3.404	3.17	0.005
285	3.526	0.486	0.431	0.427	0.121	4.351	4.042	0.033
288	3.93	0.615	0.648	0.339	0.25	4.858	4.828	0.116
289	2.389	0.088	0.427	0.462	0.153	2.94	2.892	0.006
290	1.975	0.509	0.762	0.143	0.276	2.541	3	0.005
291	4.254	0.459	0.562	0.427	0.128	5.063	4.944	0.004
294	4.007	0.717	0.602	0.232	0.274	4.955	4.83	0.143
330	3.053	0.394	0.518	0.34	0.117	3.787	3.618	0.032
333	3.383	0.769	0.866	0.268	0.224	4.307	4.472	0.031
334	1.664	0.09	0.59	0.334	0.139	2.088	2.355	0.002
335	1.401	0.698	1.034	0.135	0.234	2.183	2.669	0.005
336	3.404	0.339	0.447	0.333	0.158	4.03	3.96	0.011
339	3.452	0.855	0.935	0.298	0.27	4.561	4.566	0.095
359	3.271	0.432	0.398	0.615	0.508	4.177	4.177	0.007

^a Seismic excitation cases described in Table 5.1

Table 5.9 Stresses (ksi) Due to a Temperature of 90° F

Member No.	Axial Stress	Bending Stress in 1-2 plane		Bending Stress in 1-3 plane		Combined Stress		Shear stress
		Node I	Node J	Node I	Node J	Node I	Node J	
1	9.242	-2.177	-0.203	0.094	-0.08	11.325	9.525	0.034
10	1.557	-0.199	0.888	-0.008	0.013	1.764	2.458	0.013
11	6.18	-0.612	-0.222	0.066	-0.048	6.726	6.45	0.005
34	6.401	-0.392	0.29	-0.06	0.088	6.853	6.778	0.013
35	6.764	0.021	-0.291	0.06	-0.044	6.845	7.099	0.011
51	7.064	-0.296	-0.064	-0.065	0.09	7.425	7.09	0.013
52	5.131	0.255	-0.171	0.049	-0.037	5.436	5.339	0.012
68	5.794	-0.13	-0.57	-0.052	0.074	5.976	6.291	0.009
69	0.498	0.738	-0.087	0.006	-0.004	1.242	0.589	0.004
78	6.287	-0.161	-1.6	-0.055	0.062	6.504	7.825	0.042
89	2.754	0.696	-0.897	0.001	0.002	3.452	3.649	0.019
90	2.761	-0.625	0.252	-0.003	0.044	3.388	3.057	0.019
113	2.454	0.354	-0.675	0.034	0.007	2.843	3.122	0.005
114	2.44	-0.734	0.382	0.009	0.013	3.164	2.835	0.007
130	3.375	0.497	-0.933	0.017	0.016	3.888	4.291	0.017
131	4.123	-1.231	0.793	0.025	0.005	5.329	4.921	0.021
147	3.097	0.34	-0.742	0.014	0.017	3.451	3.822	0.017
148	3.12	-1.034	0.809	0.019	-0.003	4.134	3.927	0.008
161	1.739	-0.961	-0.208	0.002	-0.005	2.698	1.953	0.029
182	2.203	0.61	-0.56	0.008	0.016	2.821	2.747	0.094
184	0.575	-0.58	0.098	0	0.003	1.155	0.676	0.033
185	-2.434	-0.548	-0.019	-0.047	0.022	-1.839	-2.431	0.011
186	-2.188	-0.046	0.181	0.041	0	-2.184	-2.007	0.015
187	1.638	-0.328	-0.005	0.051	-0.085	1.915	1.728	0.02
189	2.162	-0.171	0.095	-0.505	0.342	2.837	2.599	0.092
240	1.694	-0.245	0.143	0.019	-0.008	1.921	1.829	0.02
243	2.914	0.397	-0.344	-0.046	0.077	3.265	3.181	0.084
244	-2.265	-0.055	0.032	-0.033	0.031	-2.176	-2.202	0.014
245	-1.966	0.037	-0.037	0.04	-0.018	-1.889	-1.911	0.02
246	2.88	-0.388	0.423	0.082	-0.054	3.186	3.25	0.113
249	2.437	0.113	-0.081	0.024	-0.009	2.575	2.528	0.027
285	2.582	-0.072	0.119	0.02	-0.002	2.634	2.699	0.027
288	3.138	0.45	-0.387	-0.061	0.1	3.527	3.424	0.133
289	-3.374	0.143	0.044	-0.046	0.042	-3.277	-3.289	0.016
290	-3.012	0.06	-0.09	0.056	-0.026	-2.896	-2.896	0.018
291	2.488	0.281	-0.027	0.021	-0.004	2.79	2.519	0.019
294	3.133	-0.618	0.691	0.11	-0.081	3.641	3.743	0.079
330	2.402	0.295	-0.005	0.02	-0.003	2.717	2.41	0.031
333	1.957	0.248	-0.183	-0.052	0.075	2.154	2.065	0.02
334	-2.61	0.452	0.057	-0.037	0.034	-2.195	-2.52	0.001
335	-2.396	0.082	-0.199	0.043	-0.021	-2.271	-2.177	0.004
336	0.566	0.522	-0.028	0	0.009	1.089	0.585	0.011
339	1.976	-0.645	0.582	-0.056	0.081	2.676	2.639	0.019
359	1.804	0.652	0.192	0.004	-0.006	2.46	1.991	0.004

Table 5.10 Self-Weight Induced Stresses (ksi)

Member No.	Axial Stress	Bending Stress in 1-2 plane		Bending Stress in 1-3 plane		Combined Stress		Shear stress
		Node I	Node J	Node I	Node J	Node I	Node J	
1	1.032	1.128	5.299	-0.002	-0.001	2.158	6.33	0.591
10	-4.803	2.017	5.407	0.033	-0.049	-2.752	0.555	0.26
11	-4.944	6.353	2.301	-0.028	0.031	1.38	-2.613	0.288
34	-5.586	2.381	6.28	0.056	-0.078	-3.149	0.616	0.228
35	-4.898	6.349	2.576	-0.043	0.032	1.407	-2.291	0.204
51	-3.843	2.423	6.001	0.036	-0.05	-1.384	2.108	0.242
52	-3.283	6.073	2.259	-0.032	0.023	2.758	-1.001	0.223
68	-3.352	2.284	5.894	0.032	-0.044	-1.036	2.497	0.293
69	-3.262	5.752	1.791	-0.035	0.025	2.455	-1.445	0.269
78	1.458	5.439	1.296	-0.012	0.014	6.885	2.768	0.568
89	8.894	1.496	-0.117	-0.036	0.133	10.354	8.941	0.281
90	8.88	-0.132	1.664	0.156	-0.063	8.904	10.45	0.28
113	9.508	1.884	-0.42	-0.079	0.103	11.313	9.856	0.367
114	9.47	-0.004	1.496	0.097	-0.027	9.563	10.908	0.379
130	6.681	1.349	0.291	-0.003	0.062	8.027	7.065	0.292
131	8.194	0.779	0.94	0.086	-0.028	9.059	9.075	0.353
147	6.909	1.015	0.703	-0.017	0.066	7.907	7.709	0.312
148	6.991	0.588	1.004	0.07	-0.016	7.648	7.947	0.405
161	-1.132	-1.695	1.986	-0.018	0.054	0.582	1.051	0.775
182	9.877	1.333	1.074	0.099	-0.018	11.308	10.964	2.228
184	-6.367	-1.529	-0.355	-0.053	0.086	-4.785	-6.003	0.116
185	-8.351	0.205	-0.061	-0.077	0.188	-8.224	-8.098	0.076
186	-7.274	-0.054	-0.003	0.066	-0.083	-7.262	-7.063	0.038
187	-6.058	1.998	0.33	-0.253	0.376	-4.313	-5.259	0.062
189	9.923	-1.451	-0.956	0.676	-0.418	10.698	11.329	0.29
240	-5.784	-1.927	-0.464	-0.103	0.128	-3.754	-5.353	0.051
243	9.967	1.692	0.72	-0.047	0.045	11.612	10.763	0.519
244	-9.12	-0.077	-0.101	-0.18	0.209	-8.863	-8.886	0.077
245	-7.931	-0.119	0.239	0.087	-0.045	-7.899	-7.612	0.037
246	9.986	1.306	1.337	0.052	0.07	11.344	11.361	0.188
249	-6.665	1.844	0.369	-0.086	0.088	-4.907	-6.113	0.041
285	-6.04	-1.97	-0.406	-0.072	0.072	-3.997	-5.612	0.103
288	9.936	1.479	1.067	0.108	-0.011	11.523	11.023	0.294
289	-7.607	-0.016	-0.198	-0.133	0.159	-7.457	-7.443	0.045
290	-6.303	-0.233	0.298	0.036	0.005	-6.105	-5.874	0.042
291	-7.427	1.953	0.23	-0.089	0.082	-5.563	-7.021	0.039
294	10.025	1.58	1.026	-0.05	0.134	11.555	11.154	0.343
330	-6.773	-1.951	-0.299	-0.08	0.073	-4.741	-6.452	0.073
333	9.859	1.135	1.426	0.141	-0.051	11.135	11.266	0.259
334	-6.896	0.012	0.026	-0.122	0.147	-6.785	-6.598	0.008
335	-5.675	0.039	-0.081	0.031	0.005	-5.605	-5.473	0.037
336	-6.723	1.874	0.22	-0.082	0.078	-4.931	-6.33	0.007
339	9.901	-1.125	-1.224	0.132	-0.044	10.894	11.201	0.011
359	-2.658	1.784	-2.174	-0.033	0.061	-0.907	-0.404	0.07

Table 5.11 Stress Requirement Based on AASHTO Equations for L1T2V3 Earthquake

Member No.	Axial Stress (ksi) f_a	Bending Stress (ksi)		Euler Buckling Stress (ksi) , AASHTO Eq. (10-44)		Stress Requirement ≤ 1.0	
		f_{bx}	f_{by}	F_{ex}	F_{ey}	AASHTO Eq. (10-42)	AASHTO Eq. (10-43)
1	12.119	8.209	0.838	250.006	167.155	0.225	0.588
10	7.714	7.067	0.849	180.716	222.549	0.195	0.434
11	13.846	7.722	0.759	196.517	219.192	0.215	0.620
34	14.296	7.556	0.619	196.517	219.192	0.208	0.624
35	13.112	7.574	0.662	164.288	201.138	0.211	0.593
51	13.537	7.274	0.817	181.250	191.654	0.206	0.601
52	9.966	7.536	0.975	166.761	191.775	0.214	0.513
68	11.370	7.262	0.858	178.108	195.570	0.205	0.541
69	5.131	7.421	0.727	180.469	222.244	0.198	0.369
78	10.133	7.485	0.681	249.663	166.926	0.201	0.508
89	12.922	3.393	0.305	142.932	204.460	0.096	0.462
90	12.875	2.965	0.331	142.757	204.210	0.085	0.449
113	13.908	3.552	0.311	142.757	204.210	0.101	0.494
114	13.864	3.127	0.302	130.536	186.728	0.090	0.480
130	12.235	3.162	0.255	130.536	186.728	0.089	0.435
131	15.035	3.108	0.344	136.599	173.659	0.091	0.514
147	11.649	2.740	0.236	132.892	181.388	0.077	0.406
148	11.874	2.977	0.246	145.335	198.372	0.083	0.419
161	5.276	3.280	0.562	52.299	48.266	0.101	0.253
182	14.993	2.735	0.373	46.507	165.285	0.105	0.503
184	9.714	2.480	0.499	87.077	83.518	0.079	0.353
185	11.882	1.175	0.503	164.441	89.209	0.044	0.377
186	10.442	0.959	0.329	164.441	89.209	0.033	0.326
187	9.455	2.707	0.631	83.339	87.868	0.089	0.355
189	14.978	2.147	1.898	46.450	165.082	0.124	0.528
240	9.077	2.615	0.426	83.339	87.868	0.081	0.337
243	16.360	2.848	0.443	46.450	165.083	0.115	0.546
244	13.243	0.630	0.694	168.519	87.830	0.035	0.405
245	11.539	1.056	0.384	168.519	87.830	0.037	0.361
246	16.342	2.423	0.423	42.473	150.951	0.104	0.533
249	11.713	2.370	0.600	80.515	82.505	0.082	0.408
285	12.281	2.557	0.523	81.805	81.046	0.086	0.427
288	17.054	2.621	0.552	42.473	150.951	0.118	0.562
289	13.364	0.795	0.676	168.274	87.077	0.039	0.412
290	11.262	1.189	0.368	168.274	87.077	0.040	0.356
291	14.185	2.804	0.544	79.514	83.835	0.096	0.487
294	17.161	2.992	0.519	42.473	150.951	0.132	0.574
330	12.088	2.748	0.436	79.514	83.835	0.089	0.424
333	15.201	2.510	0.484	42.473	150.951	0.105	0.505
334	11.236	1.058	0.520	171.466	86.479	0.041	0.356
335	9.533	1.266	0.308	171.466	86.479	0.040	0.309
336	10.484	2.822	0.455	87.022	83.466	0.088	0.382
339	15.350	2.764	0.518	46.450	165.084	0.111	0.518
359	7.634	3.246	0.692	52.279	48.248	0.109	0.321

Table 5.12 Stress Requirement Based on AASHTO Equations for L2T1V3

Member No.	Axial Stress (ksi) f_a	Bending Stress (ksi)		Euler Buckling Stress (ksi), AASHTO Eq. (10-44)		Stress Requirement ≤ 1.0	
		f_{bx}	f_{by}	F_{ex}	F_{ey}	AASHTO Eq. (10-42)	AASHTO Eq. (10-43)
1	12.174	8.163	1.563	250.006	167.155	0.242	0.608
10	7.965	7.174	1.489	180.716	222.549	0.214	0.462
11	13.451	7.780	1.749	196.517	219.192	0.241	0.638
34	15.849	7.839	1.573	196.517	219.192	0.241	0.702
35	15.369	7.675	1.609	164.288	201.138	0.241	0.685
51	15.078	7.619	1.519	181.250	191.654	0.235	0.673
52	12.603	7.661	1.730	166.761	191.775	0.239	0.611
68	12.816	7.384	1.377	178.108	195.570	0.223	0.599
69	5.732	7.501	1.218	180.469	222.244	0.212	0.401
78	10.142	7.687	1.507	249.663	166.926	0.227	0.537
89	13.559	3.353	0.463	142.932	204.460	0.099	0.483
90	13.419	3.111	0.427	142.757	204.210	0.092	0.471
113	13.994	3.655	0.476	142.757	204.210	0.108	0.503
114	13.980	3.067	0.553	130.536	186.728	0.095	0.489
130	12.229	3.153	0.522	130.536	186.728	0.095	0.442
131	14.976	2.898	0.664	136.599	173.659	0.094	0.515
147	11.823	2.905	0.387	132.892	181.388	0.085	0.420
148	12.076	3.328	0.394	145.335	198.372	0.096	0.439
161	5.192	3.258	1.314	52.299	48.266	0.120	0.271
182	14.937	2.696	0.402	46.507	165.285	0.104	0.501
184	9.622	2.466	0.897	87.077	83.518	0.089	0.361
185	12.333	1.199	0.963	164.441	89.209	0.057	0.403
186	10.791	1.017	0.492	164.441	89.209	0.039	0.342
187	9.994	2.664	0.789	83.339	87.868	0.092	0.374
189	14.939	2.166	2.167	46.450	165.082	0.132	0.535
240	10.774	2.699	0.589	83.339	87.868	0.089	0.391
243	16.964	2.894	0.887	46.450	165.083	0.131	0.576
244	13.446	0.551	1.123	168.519	87.830	0.045	0.420
245	11.587	0.947	0.692	168.519	87.830	0.043	0.367
246	16.850	2.437	0.942	42.473	150.951	0.120	0.562
249	12.160	2.490	1.057	80.515	82.505	0.099	0.436
285	11.489	2.786	1.139	81.805	81.046	0.108	0.428
288	19.173	2.544	0.861	42.473	150.951	0.133	0.627
289	13.918	0.738	1.062	168.274	87.077	0.049	0.437
290	11.461	1.076	0.718	168.274	87.077	0.047	0.368
291	13.458	2.879	0.922	79.514	83.835	0.108	0.479
294	19.219	2.871	0.791	42.473	150.951	0.145	0.636
330	11.772	2.932	0.751	79.514	83.835	0.102	0.429
333	16.030	2.703	0.613	42.473	150.951	0.119	0.537
334	11.423	1.226	0.826	171.466	86.479	0.053	0.374
335	9.623	1.581	0.482	171.466	86.479	0.052	0.325
336	10.536	2.834	0.814	87.022	83.466	0.098	0.394
339	16.090	2.979	0.707	46.450	165.084	0.126	0.549
359	7.665	3.339	1.304	52.279	48.248	0.129	0.342

Table 5.13 Displacements (in) due to Seismic Excitation of the 50-year Earthquake

Joint No.	L1T2V3 ^a			L2TIV3 ^a			LL1I ^a			LL2 ^a			TT1I ^a			TT2 ^a		
	Ux	Uy	Uz	Ux	Uy	Uz	Ux	Uy	Uz	Ux	Uy	Uz	Ux	Uy	Uz	Ux	Uy	Uz
1	0.789	0.001	0.011	0.502	0.002	0.012	0.777	0	0.01	0.476	0	0.01	0.2	0.002	0.012	0.175	0.001	0.012
6	0.743	0.664	0.81	0.506	1.458	0.903	0.742	0.02	0.798	0.486	0.021	0.861	0.08	1.46	0.818	0.08	0.666	0.795
7	0.747	0.608	0.709	0.545	1.372	0.795	0.732	0.02	0.702	0.489	0.02	0.76	0.084	1.374	0.72	0.086	0.61	0.693
8	0.754	0.497	0.594	0.569	1.156	0.645	0.735	0.013	0.572	0.489	0.013	0.609	0.109	1.158	0.583	0.091	0.499	0.586
11	0.76	0.023	0.027	0.598	0.043	0.039	0.74	0.003	0.023	0.484	0.003	0.023	0.155	0.043	0.039	0.097	0.023	0.027
15	0.851	0.97	0.867	0.706	2.562	0.909	0.844	0.037	0.862	0.534	0.037	0.903	0.219	2.562	0.853	0.139	0.969	0.852
17	0.904	1.199	1.072	0.708	2.91	1.125	0.875	0.027	1.06	0.541	0.028	1.113	0.202	2.91	1.053	0.152	1.197	1.054
22	0.996	1.58	1.244	0.649	4.168	1.545	1.009	0.016	1.187	0.581	0.018	1.391	0.227	4.167	1.508	0.115	1.577	1.312
23	0.989	1.523	1.217	0.665	3.982	1.579	1.015	0.017	1.203	0.583	0.018	1.432	0.222	3.981	1.535	0.112	1.522	1.346
24	0.997	1.403	1.194	0.672	3.498	1.565	1.011	0.026	1.232	0.598	0.028	1.429	0.208	3.496	1.516	0.102	1.402	1.342
29	1.158	1.209	0.95	0.626	3.549	0.961	1.101	0.035	0.98	0.656	0.035	0.986	0.295	3.549	1.007	0.202	1.211	0.991
31	1.055	1.094	0.777	0.745	3.333	0.751	1.012	0.044	0.8	0.683	0.044	0.785	0.331	3.333	0.788	0.216	1.096	0.768
35	0.92	0.025	0.042	0.802	0.065	0.068	0.911	0.003	0.034	0.656	0.003	0.033	0.293	0.065	0.069	0.122	0.025	0.04
44	1.057	1.61	1.774	0.633	5.001	1.851	1.057	0.012	1.729	0.653	0.013	1.81	0.161	5.002	1.923	0.137	1.61	1.927
45	1.104	1.486	1.446	0.699	4.456	1.546	1.083	0.013	1.411	0.659	0.013	1.506	0.257	4.456	1.625	0.172	1.486	1.622
46	1.123	1.311	1.154	0.753	3.717	1.221	1.085	0.009	1.139	0.645	0.01	1.166	0.318	3.719	1.307	0.182	1.311	1.289
52	0.974	0.032	0.049	0.588	0.058	0.054	0.959	0.002	0.042	0.595	0.002	0.041	0.17	0.058	0.055	0.145	0.032	0.049
60	0.931	1.799	1.39	0.678	3.781	1.38	0.933	0.007	1.335	0.63	0.009	1.278	0.164	3.781	1.502	0.128	1.8	1.446
61	0.924	1.697	1.263	0.665	4.006	1.205	0.926	0.008	1.227	0.64	0.01	1.282	0.11	4.006	1.305	0.11	1.698	1.298
62	0.912	1.75	1.214	0.655	4.097	1.075	0.917	0.004	1.192	0.649	0.005	1.255	0.128	4.097	1.107	0.12	1.75	1.281
69	0.836	0.022	0.032	0.55	0.038	0.045	0.82	0.001	0.034	0.568	0.001	0.034	0.288	0.038	0.046	0.189	0.022	0.032
73	0.874	0.616	1.054	0.535	1.715	1.042	0.865	0.006	1.026	0.565	0.006	1.038	0.203	1.715	1.081	0.208	0.617	1.104
74	0.86	0.652	1.191	0.548	1.842	1.197	0.857	0.008	1.166	0.554	0.009	1.187	0.179	1.842	1.238	0.192	0.653	1.251
75	0.844	0.632	1.117	0.559	1.782	1.132	0.848	0.007	1.095	0.547	0.008	1.121	0.184	1.782	1.167	0.173	0.631	1.177
79	0.715	0.004	0.016	0.553	0.01	0.015	0.741	0	0.016	0.481	0	0.016	0.146	0.01	0.015	0.166	0.004	0.016
118	0.887	1.022	1.035	0.725	2.335	1.092	0.889	0.08	1.03	0.601	0.082	1.083	0.198	2.332	1.02	0.127	1.021	1.017
120	0.883	1.215	1.182	0.726	3.146	1.247	0.916	0.066	1.173	0.623	0.071	1.234	0.188	3.15	1.162	0.119	1.214	1.161
130	0.919	1.322	1.012	0.662	3.299	1.001	0.941	0.111	1.028	0.607	0.114	1.043	0.251	3.304	1.041	0.144	1.324	1.032
132	1.1	1.208	0.935	0.671	3.524	0.938	1.088	0.037	0.963	0.608	0.04	0.959	0.272	3.527	0.982	0.19	1.208	0.965
813	0.77	0.001	0.001	0.472	0.002	0.001	0.768	0	0.001	0.47	0	0.001	0.15	0.002	0.001	0.145	0.001	0.001
814	0.718	0.023	0.004	0.47	0.042	0.004	0.718	0.003	0.004	0.472	0.003	0.004	0.089	0.042	0.004	0.087	0.023	0.004
815	0.896	0.025	0.006	0.649	0.064	0.005	0.894	0.003	0.006	0.646	0.003	0.006	0.115	0.064	0.005	0.107	0.025	0.005
816	0.942	0.032	0.007	0.578	0.058	0.007	0.942	0.001	0.007	0.583	0.001	0.007	0.134	0.058	0.007	0.13	0.032	0.007
817	0.8	0.022	0.005	0.555	0.038	0.005	0.799	0.001	0.005	0.554	0.001	0.005	0.179	0.038	0.005	0.179	0.022	0.005
818	0.733	0.004	0.002	0.482	0.01	0.002	0.734	0	0.002	0.477	0	0.002	0.141	0.01	0.002	0.153	0.004	0.002

^a Seismic excitation cases are described in Table 5.1

Ux = Longitudinal displacement; Uy = Transverse displacement; Uz = Vertical displacement

Table 5.14 Displacements (in) due to Self-weight and Temperature

Joint Number	Thermal Displacement			Self-weight Displacement		
	U _x	U _y	U _z	U _x	U _y	U _z
1	4.021	0.097	0.000	0.188	0.000	-0.001
6	3.287	0.110	0.156	0.179	-0.007	0.128
7	3.080	0.108	0.216	0.142	-0.007	0.304
8	2.853	0.106	0.177	0.072	-0.008	0.379
11	2.162	0.096	-0.003	-0.142	0.000	-0.025
15	1.611	0.096	0.053	-0.492	0.031	-3.601
17	1.557	0.096	-0.100	-0.489	0.042	-4.825
22	1.152	0.112	-0.212	0.025	0.022	-8.859
23	1.031	0.115	-0.077	0.157	0.017	-8.905
24	0.911	0.117	-0.042	0.288	0.014	-8.755
29	0.525	0.161	0.970	0.761	-0.007	-4.335
31	1.274	0.159	0.893	0.705	-0.013	-3.156
35	0.742	0.097	-0.001	0.311	0.000	-0.029
44	-0.242	0.109	-0.368	0.035	0.005	-1.491
45	-0.270	0.110	-0.192	0.079	0.004	-1.296
46	-0.303	0.110	-0.206	0.094	0.002	-1.092
52	-0.905	0.097	-0.002	-0.190	0.000	-0.024
60	-2.230	0.108	0.209	-0.188	0.006	-4.548
61	-2.348	0.108	-0.063	-0.095	0.007	-4.593
62	-2.467	0.110	-0.157	-0.002	0.006	-4.284
69	-2.664	0.097	-0.003	0.014	0.000	-0.022
73	-3.651	0.098	0.444	-0.173	-0.002	-0.369
74	-3.883	0.098	0.409	-0.180	0.000	-0.564
75	-4.115	0.100	0.326	-0.186	0.001	-0.626
79	-4.817	0.097	0.000	-0.090	0.000	-0.002
118	1.684	0.141	-0.521	0.796	0.033	-4.613
120	1.604	0.118	-0.705	0.785	0.036	-5.845
130	0.149	0.129	0.174	-0.568	-0.011	-5.398
132	1.571	0.118	0.546	-0.486	-0.005	-4.114
813	4.017	0.000	0.001	0.184	0.000	-0.001
814	2.161	0.000	-0.001	-0.144	0.000	-0.022
815	0.742	0.000	0.000	0.312	0.000	-0.027
816	-0.904	0.000	0.000	-0.192	0.000	-0.022
817	-2.661	0.000	-0.001	0.015	0.000	-0.019
818	-4.815	0.000	0.001	-0.086	0.000	-0.002

U_x = Longitudinal displacement; U_y = Transverse displacement; U_z=Vertical displacement

Table 5.15 Maximum and Minimum Base Shears from Modal Time-History
for the 50-Year Earthquake

Seismic Excitation Cases	Longitudinal direction			Transverse direction			Vertical direction			
	Maximum (Kip)	Time (sec)	Minimum m (Kip)	Time (sec)	Maximum (Kip)	Minimum (Kip)	Time (sec)	Maximum (Kip)	Minimum m (Kip)	Time (sec)
LL11	2174	2.99	-1975	4.7	36.58	-32.54	3.41	2087	-2567	3.025
LL22	1413	3.81	-1413	4.16	42.03	-36.33	3.41	2001	-2598	3.025
TT11	224.2	3.875	-173.4	4.13	896.2	-1221	2.535	2064	-2630	3.025
TT22	225.4	3.875	-177.1	4.14	454.2	-469.9	3.42	2070	-2639	3.025
L1T2V3	2174	2.99	-1974	4.7	453	-467.7	3.42	2080	-2570	3.025
L2T1V3	1412	3.81	-1410	4.16	896.1	-1220	2.535	1988	-2591	3.025

Table 5.16 Bearing Force Capacity/Demand Ratios of the Main bridge without site soil coefficients for the 50-Year Earthquake

Pier	Anchor Bolt Capacity (kip), V_c	Seismic Force (kip)			Seismic Demand, $V_B=1.25 \times H_R$	Force C/D ratio $r_{bf}=V_c/V_b$
		Longitudinal H_L	Transverse H_T	Resultant H_R		
A	857.88	249.76	780.25	819.25	1024.06	0.8377
B	857.88	559.4	86.23	566.01	707.51	1.2125
C	857.88	364.3	62.42	369.61	462.01	1.8568
D	857.88	389.9	64.887	395.26	494.08	1.7363
E	857.88	528.66	76.48	534.16	667.70	1.2848
F	857.88	149.9	162.89	221.37	276.71	3.1003

Table 5.17 Bearing Displacement Capacity/Demand Ratio for the 50-Year Earthquake

Seismic Excitation Cases	Seismic Displacement (in) $\Delta_{eq}(d)$		Displacement Capacity (in) $\Delta_s(c)$		Thermal Displacement (in) $\Delta_t(d)$		Capacity/Demand Ratio $r_{bd} = (\Delta_s(c) - \Delta_t(d)) / \Delta_{eq}(d)$	
	Pier A	Pier F	Pier A	Pier F	Pier A	Pier F	Pier A	Pier F
L1T2V3	0.77	0.73	28.56	30	4.017	4.815	31.87	34.50
L2T1V3	0.145	0.153	28.56	30	4.017	4.815	169.26	164.61
LL11	0.15	0.14	28.56	30	4.017	4.815	163.62	179.89
LL22	0.47	0.47	28.56	30	4.017	4.815	52.22	53.59
TT11	0.47	0.48	28.56	30	4.017	4.815	52.22	52.47
TT22	0.77	0.73	28.56	30	4.017	4.815	31.87	34.50

Table 6.1 Dimensions and Stiffnesses of the Approach Span Piers

Pier	Pier Dimensions (in)					Pier Area (in ²)		M.I. for Longitudinal Bending (in ⁴)		Pier Stiffness (K _l) for Longitudinal bending, (kip/ft) = 3EI/L ³	Pier Stiffness (K _p) with pile effect (kip/ft)
	A	B	C	D	D	Pier Area (in ²)		M.I. for Longitudinal Bending (in ⁴)			
						Bottom	Top	Top	Bottom		
K1	208	376	616.5625	111.375	31460.53	10747.4	1829863	3598903	1511.299	540.603	
K2	172	348	483	100.25	27442.07	10747.4	1829863	3598903	3143.694	892.113	
K3	172	348	457.4375	98.125	26696.61	10747.4	1829863	3598903	3700.721	992.063	
K4	172	348	432	96	25958.25	10747.4	1829863	3598903	4393.700	1106.913	
K5	172	348	406.3125	93.875	25226.97	10747.4	1829863	3598903	5280.817	1241.610	
K6	172	328	380.75	91.75	24502.8	10747.4	1829863	3598903	6417.441	1398.251	
K7	172	328	355.1875	89.625	23785.71	14527.44	3598903	12584024	23564.840	4717.035	
K8	172	328	329.625	87.5	23075.72	14527.44	3598903	11690450	27855.390	5070.379	
K9	172	328	412.0625	94.375	25398.4	14527.44	3598903	14747522	17109.710	4087.946	
K10	136	304	471.375	71.4375	17938.46	8037.878	781203.7	6281544	4400.019	1217.485	
K11	136	304	458.75	70.6875	17708.49	8037.878	781203.7	6082136	4638.609	1247.284	
K12	136	304	463.9375	71	17804.2	8037.878	781203.7	6164692	4538.688	1235.047	
K13	136	304	446.75	69.9375	17479.4	8037.878	781203.7	5887067	4879.778	1275.347	
K14	136	304	443.5625	69.75	17422.27	8037.878	781203.7	5838972	4949.776	1283.635	
K15	136	304	421.125	68.3125	16986.08	8037.878	781203.7	5479062	5469.407	1339.325	
K16	136	304	405.25	67.3125	16684.56	8037.878	781203.7	5237765	5901.108	1383.282	
K17	136	304	378.5	65.625	16179.31	8037.878	781203.7	4847088	6772.664	1465.217	
K18	136	304	398.75	66.9375	16571.9	8037.878	781203.7	5149170	6103.240	1404.171	
K19	136	304	323.875	62.25	15182.22	8037.878	781203.7	4125883	9424.797	1676.562	
K20	136	292	260.8125	58.25	14023.66	8037.878	781203.7	3369698	15266.440	2008.386	
I 1	172	328	219.75	78.3125	20087.68	14527.44	3598903	8320548	73290.910	7408.001	
I 2	136	304	350.875	63.9375	15678.53	8037.878	781203.7	4476651	7942.036	1565.696	
I 3	136	304	399	66.9375	16571.9	8037.878	781203.7	5149170	6091.775	1402.554	
I 4	136	304	299.75	60.75	14744.82	8037.878	781203.7	3830142	11171.990	1791.353	
I 5	136	304	274.3125	59.125	14274.95	8037.878	781203.7	3526325	13616.700	1927.870	

Table 6.2 Weight of the Superstructure of the Illinois Approach Spans (Girder Spans)
 Note: The dimensions are in kip and ft units

Span	Deck			Beams		Girders		Knee Bracing		Lateral Bracing		Bracing Total Weight		Handrails		Span Total Weight	Span Total Mass			
	Length	Area of Cross section.	Weight/ft	Total weight	Total length	Weight/ft	Total length	Total weight	Total length	Weight/ft	Total length	Weight/ft	Total Weight	Length	Weight/ft			Total Weight		
Abut-15	59.5	14.788	2.218	131.985	244	0.045	10.98	119	0.237	28.203	61.81	0.0079	80.442	0.01	1.293	119	0.0167	1.987	174.448	5.420
15-14	90	14.788	2.218	199.641	352	0.045	15.84	180	0.258	46.35	85.534	0.0079	118	0.01	1.886	180	0.0167	3.006	266.692	8.286
14-13	80	14.788	2.218	177.458	332	0.045	14.94	160	0.237	37.872	74.17	0.0079	116.33	0.01	1.749	160	0.0167	2.672	234.692	7.292
13-12	80	14.788	2.218	177.458	332	0.045	14.94	160	0.237	37.872	74.17	0.0079	116.33	0.01	1.749	160	0.0167	2.672	234.692	7.292
12-11	80	14.788	2.218	177.458	332	0.045	14.94	160	0.237	37.872	74.17	0.0079	116.33	0.01	1.749	160	0.0167	2.672	234.692	7.292

Table 6.3 Weight of the Superstructure of the Illinois Approach Spans (Deck-truss Span)
 Note: The dimensions are in kip and ft units

Span	Deck			Beams		Truss			Lower beams		Lower lateral		Upper lateral		Hand rails		Span Total Weight	Span Total Mass			
	Length	Area/ft	Weight/ft	Total Weight	Total length	Weight/ft	Total length	Total Weight	Total length	Weight/ft	Total length	Weight/ft	Total length	Weight/ft	Total length	Weight/ft					
11-Main	181.021	14.7882	2.218	401.5458	684	0.045	30.78	20	4.993	99.86	120	0.027	217.54	0.025	2.35	10.9414	362.1875	0.0167	6.0485	552.019	17.151

Table 6.4 Weight of the Superstructure of the Kentucky Approach Spans (From Pier F to Pier K9)

Note: The dimensions are in kip and ft units

Span	Deck				Beams			Truss			Lower beams		lower lateral Bracing		Upper lateral Bracing		Handrails	
	Length	Cross Section Area	Weight/ft	Total Weight	Total length	Weight/ft	Total Weight	# Panel	Weight/ Panel	Total Weight	Total length	Weight/ft	Total length	Weight/ft	Total Weight	Total Weight	Length	Weight/ft
Main-K1	182.5	14.788	2.218	404.827	684	0.045	30.78	20	4.993	99.86	120	0.027	217.54	0.025	2.35	10.941	362.188	0.0167
K1-K2	182	14.788	2.218	403.718	684	0.045	30.78	20	4.993	99.86	120	0.027	217.54	0.025	2.35	10.941	362.188	0.0167
K2-K3	182	14.788	2.218	403.718	684	0.045	30.78	20	4.993	99.86	120	0.027	217.54	0.025	2.35	10.941	362.188	0.0167
K3-K4	182	14.788	2.218	403.718	684	0.045	30.78	20	4.993	99.86	120	0.027	217.54	0.025	2.35	10.941	362.188	0.0167
K4-K5	182	14.788	2.218	403.718	684	0.045	30.78	20	4.993	99.86	120	0.027	217.54	0.025	2.35	10.941	362.188	0.0167
K5-K6	182	14.788	2.218	403.718	684	0.045	30.78	20	4.993	99.86	120	0.027	217.54	0.025	2.35	10.941	362.188	0.0167
K6-K7	182	14.788	2.218	403.718	684	0.045	30.78	20	4.993	99.86	120	0.027	217.54	0.025	2.35	10.941	362.188	0.0167
K7-K8	182	14.788	2.218	403.718	684	0.045	30.78	20	4.993	99.86	120	0.027	217.54	0.025	2.35	10.941	362.188	0.0167
K8-K9	181	14.788	2.218	401.500	684	0.045	30.78	20	4.993	99.86	120	0.027	217.54	0.025	2.35	10.941	362.188	0.0167

Table 6.5 Weight of the Superstructure of the Kentucky Approach Spans (From Pier K9 to K20)

Note: The dimensions are in kip and ft units

Span	Deck				Beams			Girders	Knee Bracing		Lateral Bracing		Handrails			Span Total Weight	Span Total Mass
	Length	Area/ft	Weight/ft	Total weight	Total length	Weight/ft	Total Weight	Total Weight	Total length	Weight/ft	Total length	Weight/ft	Length	Weight/ft	Total Weight		
K9-K10	89.71	14.788	2.218	198.997	376	0.045	16.92	48.42	74.17	0.0079	126.2	0.0098	538	0.0167	8.985	275.150	8.5490
K10-K	25	14.788	2.218	55.456	84	0.045	3.78	13.37	12.36	0.0079	38.66	0.0098	150	0.0167	2.505	75.600	2.3489
K-K	40	14.788	2.218	88.729	$2 \times 20 \times 0.074 + 6 \times 6.8125 \times 0.0318 + 40 \times 5 \times 0.080 = 20.25$								240	0.0167	4.0	113.000	3.5110
K-K11	25	14.788	2.218	55.456	84	0.045	3.78	13.37	12.36	0.0079	38.66	0.0098	150	0.0167	2.505	75.600	2.3489
K11-K12	48	14.788	2.218	106.475	176	0.045	7.92	27.22	12.36	0.0079	76.52	0.0098	288	0.0167	2.8096	147.500	4.5829
K12-K	25	14.788	2.218	55.456	84	0.045	3.78	13.37	12.36	0.0079	38.66	0.0098	150	0.0167	2.505	75.600	2.3489
K-K	40	14.788	2.218	88.729	$2 \times 20 \times 0.074 + 6 \times 6.8125 \times 0.0318 + 40 \times 5 \times 0.080 = 20.25$								240	0.0167	4.0	113.000	3.5110
K-K13	25	14.788	2.218	55.456	84	0.045	3.78	13.37	12.36	0.0079	38.66	0.0098	150	0.0167	2.505	75.600	2.3489
K13-K14	89.677	14.788	2.218	198.924	376	0.045	16.92	48.42	74.28	0.0079	126.2	0.0098	538	0.0167	8.985	275.000	8.5444
K14-K15	60	14.788	2.218	133.094	244	0.045	10.98	22.52	371.4	0.0079	126.2	0.0098	360	0.0167	6.012	175.500	5.4529
K15-K16	60	14.788	2.218	133.094	244	0.045	10.98	22.52	371.4	0.0079	126.2	0.0098	360	0.0167	6.012	175.500	5.4529
K16-K17	60	14.788	2.218	133.094	244	0.045	10.98	22.52	371.4	0.0079	126.2	0.0098	360	0.0167	6.012	175.500	5.4529
K17-K18	60	14.788	2.218	133.094	244	0.045	10.98	22.52	371.4	0.0079	126.2	0.0098	360	0.0167	6.012	175.500	5.4529
K18-K19	60	14.788	2.218	133.094	244	0.045	10.98	22.52	371.4	0.0079	126.2	0.0098	360	0.0167	6.012	175.500	5.4529
K19-K20	60	14.788	2.218	133.094	244	0.045	10.98	22.52	371.4	0.0079	126.2	0.0098	360	0.0167	6.012	175.500	5.4529
K20-Abut.	59.5	14.788	2.218	131.985	244	0.045	10.98	22.33	371.4	0.0079	126.2	0.0098	357	0.0167	5.962	174.000	5.4062

Table 6.6 Natural Frequencies of the Approach Spans - Flexible System

Model Designation ^a	Longitudinal Bending Stiffness K/ft	Mass (k-sec ² /ft)	Frequency (Hz)	Period (sec)	Minimum Force Demand ^b (Kip)
Ka	540.603	24.2	0.7522	1.3294	155.78
Kb	892.113	22.66	0.9986	1.0014	145.86
Kc	992.063	22.27	1.0623	0.9414	143.35
Kd	1106.913	21.97	1.1297	0.8852	141.42
Ke	1241.610	21.68	1.2044	0.8303	139.55
Kf	1398.251	21.38	1.2871	0.7769	137.62
Kg	23564.840	23.2	5.0723	0.1971	149.34
Kh	27855.390	22.65	5.5814	0.1792	145.80
Ki	17109.710	24.4	4.2145	0.2373	157.06
Kj	1217.485	16.4	1.3713	0.7292	105.57
Kk	2482.000	23.54	1.6342	0.6119	151.53
Kl	1275.347	19.51	1.2868	0.7771	125.59
Km	1339.325	15.64	1.4728	0.6790	100.67
Kn	1465.217	15.02	1.5719	0.6362	96.68
Ko	1676.562	14.266	1.7254	0.5796	91.83
Kp	1950.000	8.46	2.4163	0.4139	54.46
Ia	73290.910	8.78	14.5411	0.0688	56.52
Ib	1791.353	18.58	1.5627	0.6399	119.60
Ic	1565.696	18.27	1.4733	0.6787	117.60
Id	1791.353	20.49	1.4881	0.6720	131.89

^a Shown in Figures 6.8 and 6.9

^b As per Section A.2 in "Seismic Retrofitting Manual for Highway Bridges (1995)".

Table 6.7 Natural Frequencies of the Approach Spans - Stiff System

Model Designation ^a	Longitudinal Bending Stiffness (k/ft)	Mass (k-sec ² /ft)	Frequency (Hz)	Period (sec)	Minimum Force Demand ^b (Kip)
Ka	1512.500	24.2	1.2582	0.7948	155.78
Kb	3146.000	22.66	1.8753	0.5333	145.86
Kc	3703.250	22.27	2.0524	0.4872	143.35
Kd	4397.000	21.97	2.2516	0.4441	141.42
Ke	5284.750	21.68	2.4849	0.4024	139.55
Kf	6422.250	21.38	2.7584	0.3625	137.62
Kg	24155.750	23.2	5.1355	0.1947	149.34
Kh	28400.000	22.65	5.6357	0.1774	145.80
Ki	17327.000	24.4	4.2412	0.2358	157.06
Kj	4399.250	16.4	2.6067	0.3836	105.57
Kk	9172.500	23.54	3.1417	0.3183	151.53
Kl	4886.250	19.51	2.5187	0.3970	125.59
Km	5471.250	15.64	2.9768	0.3359	100.67
Kn	6787.000	15.02	3.3832	0.2956	96.68
Ko	9399.000	14.266	4.0852	0.2448	91.83
Kp	174000.000	8.46	22.8407	0.0438	54.46
Ia	174000.000	8.78	22.4206	0.0446	56.52
Ib	11152.750	18.58	3.8993	0.2565	119.60
Ic	7955.750	18.27	3.3212	0.3011	117.60
Id	73186.250	20.49	9.5118	0.1051	131.89

^a Shown in Figures 6.8 and 6.9

^b As per Section A.2 in "Seismic Retrofitting Manual for Highway Bridges (1995)".

Table 6.8 Seismic Response using Response Spectrum Method - Flexible System

Model Designation ^a	Longitudinal Displacement, D _L =PSA. M/K (in)	Longitudinal Displacement, D _L =1.2. PSA. S/g W/K (in)	Based on C _s ≤ 2A; D _L =2A M/K (in)	Horizontal Seismic Force H _L = PSA.M (kip)	Horizontal Seismic Force H _L =1.2. PSA. S/g. W (kip)	H _L =2A.M.K Based on C _s ≤ 2A (kip)
Ka	4.17	10.01	10.37	188.00	451.20	451.20
Kb	3.02	7.24	5.89	224.00	537.60	437.59
Kc	2.73	6.55	5.20	226.00	542.40	430.06
Kd	2.48	5.95	4.60	229.00	549.60	424.26
Ke	2.27	5.45	4.05	235.00	564.00	418.66
Kf	2.09	5.01	3.54	243.00	583.20	412.87
Kg	0.31	0.74	0.23	607.60	1458.24	448.02
Kh	0.28	0.68	0.19	656.24	1574.98	437.39
Ki	0.41	0.98	0.33	581.41	1395.38	471.19
Kj	1.94	4.65	3.12	197.00	472.80	316.70
Kk	1.48	3.54	2.20	305.00	732.00	454.58
Kl	2.09	5.01	3.55	222.00	532.80	376.76
Km	1.75	4.21	2.71	252.00	604.80	302.02
Kn	1.58	3.78	2.38	425.00	1020.00	290.05
Ko	1.36	3.27	1.97	523.00	1255.20	275.49
Kp	0.87	2.08	0.01	191.00	458.40	163.37
Ia	0.07	0.17	0.01	444.77	1067.45	169.55
Ib	1.59	3.82	2.40	237.00	568.80	358.80
Ic	1.75	4.20	2.70	229.00	549.60	352.81
Id	1.72	4.14	2.65	257.00	616.80	395.68

Note: M and K are the Mass and Stiffness of the System; A = Acceleration Coefficient=0.3;
PSA = Psuedo-spectral acceleration from the response spectra; S = Soil Site Coefficient=2, and
g = Acceleration due to gravity
^aShown in Figures 6.8 and 6.9

Table 6.9 Seismic Response using Response Spectrum Method - Stiff System

Model Designation ^a	Longitudinal Displacement, $D_L=PSA \cdot M/K$ (in)	Longitudinal Displacement, $D_L=1.2 \cdot PSA \cdot S/g \cdot W/K$ (in)	Based on $C_s \leq 2A$; $D_L=2A \cdot M/K$ (in)	Horizontal Seismic Force $H_L=PSA \cdot M$ (kip)	Horizontal Seismic Force $H_L=1.2 \cdot PSA \cdot S/g \cdot W$ (kip)	$H_L=2A \cdot M \cdot K$ Based on $C_s \leq 2A$ (kip)
Ka	2.14	5.14	3.71	269.80	647.52	467.33
Kb	1.21	2.90	1.67	316.60	759.84	437.59
Kc	1.07	2.56	1.39	328.50	788.40	430.06
Kd	0.95	2.28	1.16	348.40	836.16	424.26
Ke	0.83	2.00	0.95	366.90	880.56	418.66
Kf	0.73	1.76	0.77	392.00	940.80	412.87
Kg	0.31	0.74	0.22	607.60	1458.24	448.02
Kh	0.28	0.68	0.18	656.24	1574.98	437.39
Ki	0.41	0.98	0.33	581.40	1395.36	471.19
Kj	0.79	1.89	0.86	288.40	692.16	316.70
Kk	0.61	1.47	0.59	469.41	1126.58	454.58
Kl	0.82	1.97	0.93	333.40	800.16	376.76
Km	0.66	1.59	0.66	482.90	1158.96	302.02
Kn	0.55	1.33	0.51	479.50	1150.80	290.05
Ko	0.43	1.02	0.35	480.70	1153.68	275.49
Kp	0.03	0.07	0.01	305.30	732.72	163.37
Ia	0.03	0.08	0.01	469.63	1127.11	169.55
Ib	0.46	1.09	0.39	424.60	1019.04	358.80
Ic	0.57	1.36	0.53	375.44	901.06	352.81
Id	0.14	0.33	0.06	828.75	1989.00	395.68

Note: M and K are the Mass and Stiffness of the System; A =

Acceleration Coefficient=0.3;

PSA = Psuedo-spectral acceleration from the response spectra; S = Soil Site Coefficient=2, and

g = Acceleration due to gravity

^aShown in Figures 6.8 and 6.9

Table 6.10 Bearing Force Capacity/Demand Ratios and Retrofitting Recommendations - Flexible System
 (Note: The additional bolts are to be provided at the fixed bearing locations only)

Span	Location	Seismic Force (Kip)	Seismic Demand, $V_b=1.25 \times SF$	Available Number of Bolts	Available Bolt Capacity ^a , V_c (Kip)	C/D ratio $r_{br}=V_c/V_b$	Required Additional Bolt Capacity (kip)	Required Additional Bolt Area (in ²)	Required Number of Additional Bolts	Provided Additional Anchor Bolt Area (in ²)	Pier and Number of Bolts at Each Pier
Pier F-K1	K1	451.20	564.00	8, 1.5"	381.28	0.676	182.72	6.775	4#, 2"	12.570	4 @ K1
K1-K2	K2	437.59	546.98	8, 1.5"	381.28	0.697	165.71	6.144	4#, 1.5"	7.068	4 @ K2
K2-K3	K3	430.06	537.57	8, 1.5"	381.28	0.709	156.29	5.795	4#, 1.5"	7.068	4 @ K3
K3-K4	K4	424.26	530.33	8, 1.5"	381.28	0.719	149.05	5.526	4#, 1.5"	7.068	4 @ K4
K4-K5	K5	418.66	523.33	8, 1.5"	381.28	0.729	142.05	5.267	4#, 1.5"	7.068	4 @ K5
K5-K6	K6	412.87	516.09	8, 1.5"	381.28	0.739	134.81	4.998	4#, 1.5"	7.068	4 @ K6
K6-K7	K7	448.02	560.02	8, 1.5"	381.28	0.681	178.74	6.627	4#, 1.5"	7.068	4 @ K7
K7-K8	K8	437.39	546.74	8, 1.5"	381.28	0.697	165.46	6.135	4#, 1.5"	7.068	4 @ K8
K8-K9	K9	471.19	588.99	4, 1.5"	190.64	0.324	398.35	14.770	8#, 1.5"	14.136	8 @ K9
K9-K10K	K10	316.70	395.88	4, 1.25"	132.39	0.334	263.49	9.770	4#, 2"	12.570	4 @ K10
KK11-K12K	K11-K12	454.58	568.23	8, 1.25"	264.78	0.466	303.45	11.251	8#, 1.5"	14.136	4@K11, 4@K12
KK13-K14	K13	376.76	470.95	4, 1.25"	132.39	0.281	338.56	12.553	8#, 1.5"	14.136	8@K13
K14K15K16	K15	302.02	377.53	8, 1.25"	264.78	0.701	112.75	4.181	8#, 1.5"	14.136	8@K15
K16K17K18	K17	290.05	362.56	8, 1.25"	264.78	0.730	97.79	3.626	8#, 1.5"	14.136	8@K17
K18K19K20	K19	275.49	344.36	8, 1.25"	264.78	0.769	79.59	2.951	8#, 1.5"	14.136	8@K19
K20-Abut.	Abutment	163.37	204.21	4, 1.25"	132.39	0.648	71.83	2.663	4#, 1.5"	7.068	4@KY-Abutment
Abut.-I5	Abutment	169.55	211.94	4, 1.25"	132.39	0.625	79.55	2.950	4#, 1.5"	7.068	4@IL-Abutment
I5I4I3	I4	358.80	448.50	8, 1.25"	264.78	0.590	183.72	6.812	8#, 1.5"	14.136	8@I4
I3I2I1	I2	352.81	441.02	8, 1.25"	264.78	0.600	176.24	6.535	8#, 1.5"	14.136	8@I2
I1-Pier A	I1	395.68	494.60	4, 1.5"	190.64	0.385	303.96	11.270	8#, 1.5"	14.136	8@I1

^aBolt Shear Strength is assumed as 26.97 ksi (186 MPa)

Table 6.11 Bearing Force Capacity/Demand Ratios and Retrofitting Recommendations - Stiff System
 (Note: The additional bolts are to be provided at the fixed bearing locations only)

Span	Fixed Bearing Location	Seismic Force (Kip)	Seismic Demand, $V_b = 1.25 \times SF$	Available Number of anchor Bolts	Available Bolt Capacity ^a , V_c (Kip)	C/D ratio $r_u = V_c/V_d$	Required Additional Bolt Capacity (kip)	Required Additional Anchor Bolt Area (in ²)	Required Additional Number of Bolts	Provided Additional Anchor Bolt Area (in ²)	Pier and Number of Bolts at Each Pier ^b
Pier F-K1	K1	467.33	584.16	8, 1.5"	381.28	0.653	202.88	7.522	4#, 2"	12.570	4 @ K1
K1-K2	K2	437.59	546.98	8, 1.5"	381.28	0.697	165.71	6.144	4#, 1.5"	7.068	4 @ K2
K2-K3	K3	430.06	537.57	8, 1.5"	381.28	0.709	156.29	5.795	4#, 1.5"	7.068	4 @ K3
K3-K4	K4	424.26	530.33	8, 1.5"	381.28	0.719	149.05	5.526	4#, 1.5"	7.068	4 @ K4
K4-K5	K5	418.66	523.33	8, 1.5"	381.28	0.729	142.05	5.267	4#, 1.5"	7.068	4 @ K5
K5-K6	K6	412.87	516.09	8, 1.5"	381.28	0.739	134.81	4.998	4#, 1.5"	7.068	4 @ K6
K6-K7	K7	448.02	560.02	8, 1.5"	381.28	0.681	178.74	6.627	4#, 1.5"	7.068	4 @ K7
K7-K8	K8	437.39	546.74	8, 1.5"	381.28	0.697	165.46	6.135	4#, 1.5"	7.068	4 @ K8
K8-K9	K9	471.19	588.99	4, 1.5"	190.64	0.324	398.35	14.770	8#, 1.5"	14.136	8 @ K9
K9-K10K	K10	316.70	395.88	4, 1.25"	132.39	0.334	263.49	9.770	4#, 2"	12.570	4 @ K10
KK11-K12K	K11-K12	454.58	568.23	8, 1.25"	264.78	0.466	303.45	11.251	8#, 1.5"	14.136	4@K11, 4@K12
KK13-K14	K13	376.76	470.95	4, 1.25"	132.39	0.281	338.56	12.553	8#, 1.5"	14.136	8@K13
K14K15K16	K15	302.02	377.53	8, 1.25"	264.78	0.701	112.75	4.181	8#, 1.5"	14.136	8@K15
K16K17K18	K17	290.05	362.56	8, 1.25"	264.78	0.730	97.79	3.626	8#, 1.5"	14.136	8@K17
K18K19K20	K19	275.49	344.36	8, 1.25"	264.78	0.769	79.59	2.951	8#, 1.5"	14.136	8@K19
K20-Abut.	Abutment	163.37	204.21	4, 1.25"	132.39	0.648	71.83	2.663	4#, 1.5"	7.068	4@KY-Abutment
Abut.-I5	Abutment	169.55	211.94	4, 1.25"	132.39	0.625	79.55	2.950	4#, 1.5"	7.068	4@IL-Abutment
I5I4I3	I4	358.80	448.50	8, 1.25"	264.78	0.590	183.72	6.812	8#, 1.5"	14.136	8@I4
I3I2I1	I2	352.81	441.02	8, 1.25"	264.78	0.600	176.24	6.535	8#, 1.5"	14.136	8@I2
I1-Pier A	I1	395.68	494.60	4, 1.5"	190.64	0.385	303.96	11.270	8#, 1.5"	14.136	8@I1

^a Bolt Shear Strength is assumed as 26.97 ksi (186 MPa)

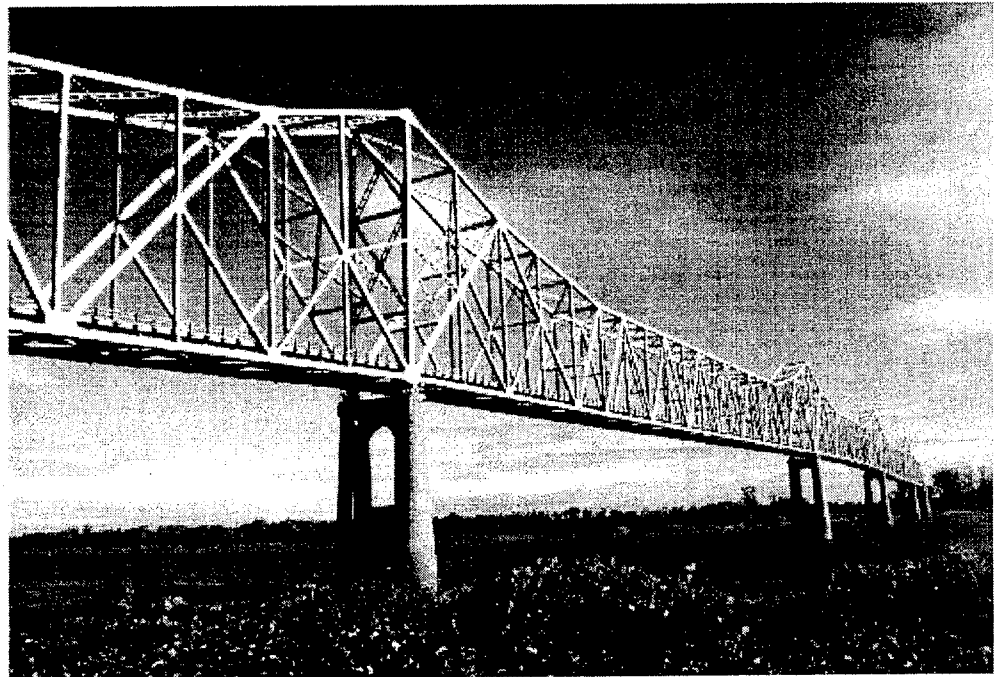
^b Arrangement of additional anchor bolts is shown in Figures 6.10 to 6.30

Table 6.12 Bearing Displacement Capacity/Demand Ratio for the Flexible System

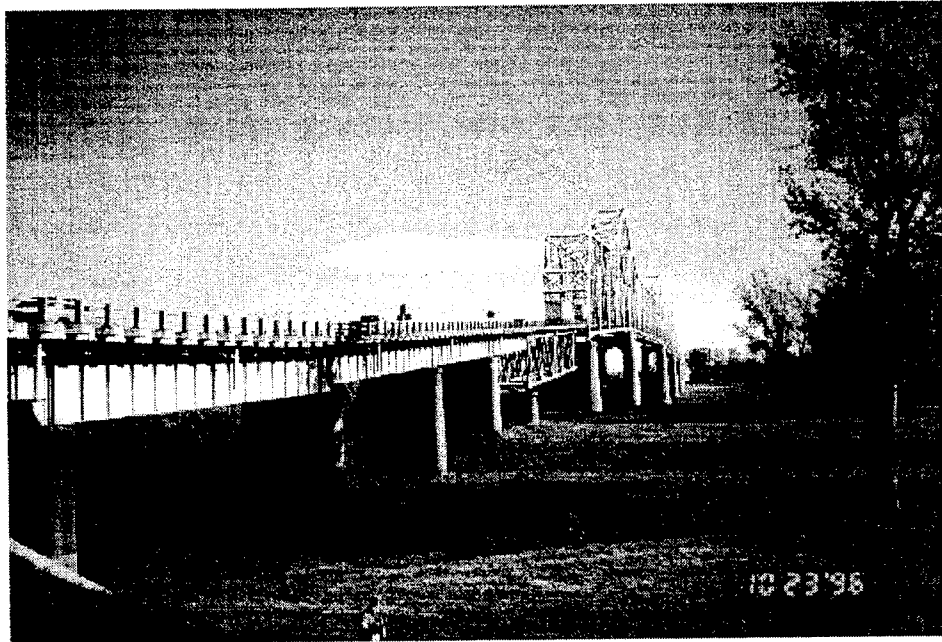
Span	Location	Span Length (ft)	Thermal displacement $\Delta_1(d)$ (ft)	Available Seat Width (ft), $\Delta_3(c)$	Seismic Displacement, $\Delta_{eq}(d)$		C/D ratio $r_{int} = (\Delta_3(c) - \Delta_1(d)) / \Delta_{eq}(d)$
					(ft)	(in)	
Abutment-I5	I5	59.5	0.0348	0.75	0.20	2.4117	3.56
I5-I4	I5	90	0.0527	0.75	0.20	2.4117	3.47
I4-I3	I3	80	0.0468	0.75	0.43	5.1040	1.65
I3-I2	I3	80	0.0468	0.75	0.43	5.1040	1.65
I2-I1	I1	80	0.0468	1.5	0.45	5.3550	3.26
I1-PIER A	PIER A	180	0.1053	2.75	0.44	5.3020	5.99
PIER F-K1	PIER F	180	0.1053	2.5	1.67	20.0200	1.44
K1-K2	K1	180	0.1053	1.5	1.33	15.8960	1.05
K2-K3	K2	180	0.1053	1.5	0.92	11.0880	1.51
K3-K4	K3	180	0.1053	1.5	0.82	9.8010	1.71
K4-K5	K4	180	0.1053	1.5	0.72	8.6450	1.94
K5-K6	K5	180	0.1053	1.5	0.63	7.5890	2.21
K6-K7	K6	180	0.1053	1.5	0.31	3.7710	4.44
K7-K8	K7	180	0.1053	1.5	0.03	0.4160	40.23
K8-K9	K8	180	0.1053	1.5	0.04	0.5185	32.28
K9-K10	K9	89.677	0.0525	1.5	0.29	3.4505	5.03
K9-K10K	K	25	0.0146	0.75	0.44	5.3180	1.66
K12K	K	25	0.0146	0.75	0.48	5.7430	1.54
KK13	K	65	0.0380	0.75	0.20	3.5640	2.40
K13-K14	K14	154.7	0.0905	0.75	0.52	6.2510	1.27
K14-K15	K14	60	0.0351	0.75	0.52	6.2510	1.37
K15-K16	K16	60	0.0351	0.75	0.42	5.0810	1.69
K16-K17	K16	60	0.0351	0.75	0.42	5.0810	1.69
K17-K18	K18	60	0.0351	0.75	0.36	4.3470	1.97
K18-K19	K18	60	0.0351	0.75	0.36	4.3470	1.97
K19-K20	K20	60	0.0351	0.75	0.17	1.9830	4.33
K20-A	K20	59.5	0.0348	0.75	0.17	1.9830	4.33



2.1a View showing Illinois approach and US51 main bridge



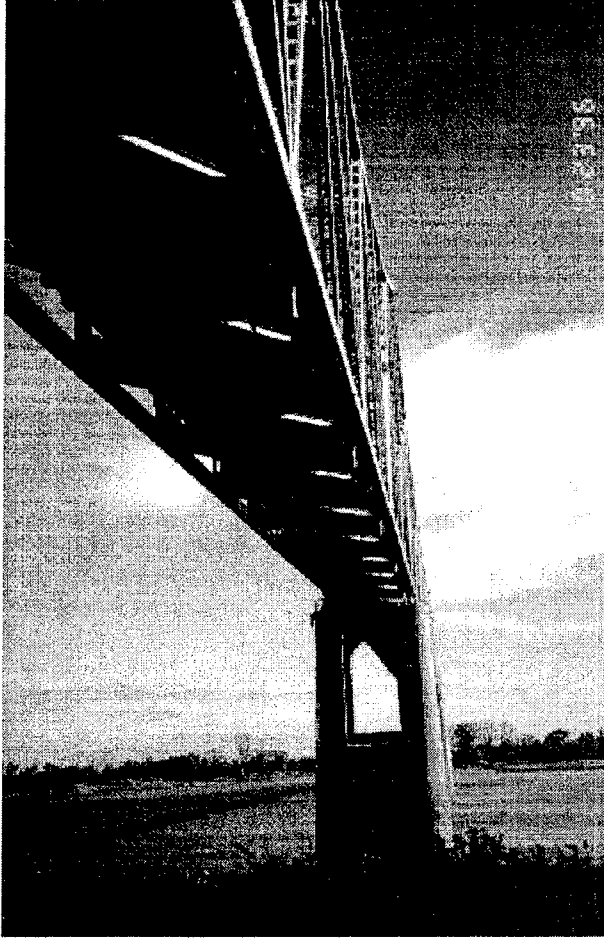
2.1b US51 main bridge across the Ohio river



2.1c Illinois approach and end view of the main bridge



2.1d End portal of the main bridge



2.1e Bottom view of the main bridge

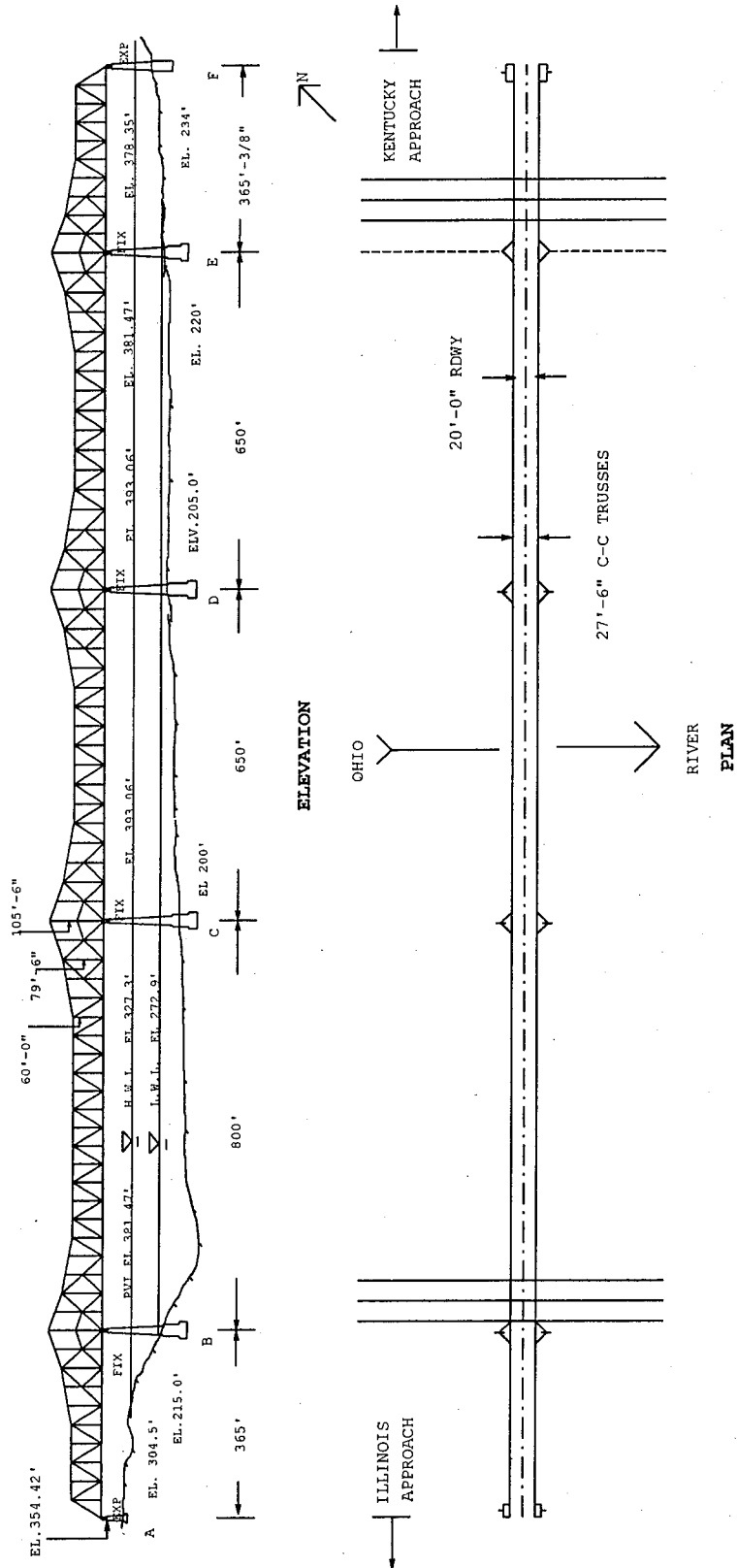


Figure 2.2 Plan and Elevation Views of the US51 Bridge over the Ohio River

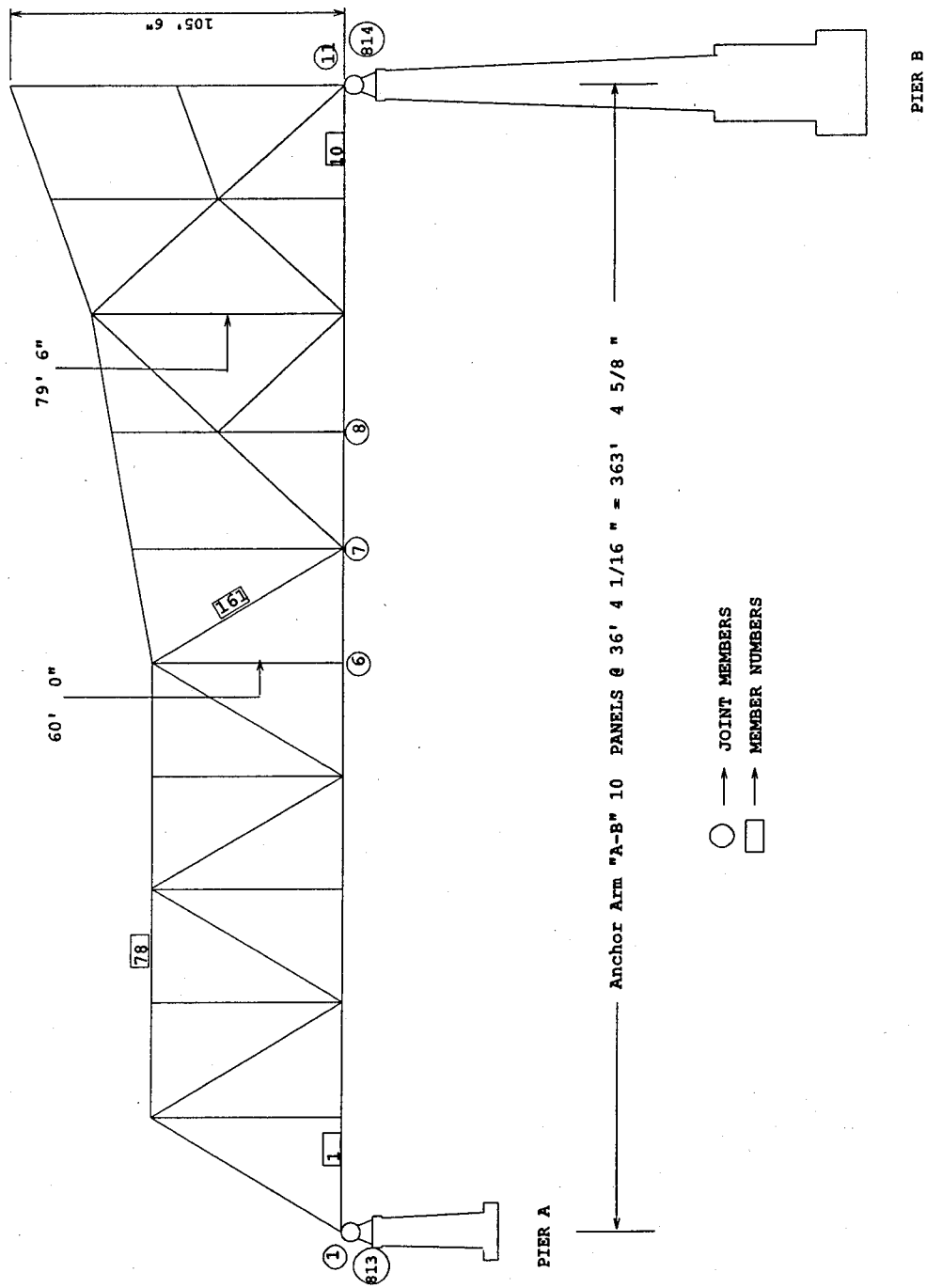


Figure 2.3 Elevation View of the First Span A-B

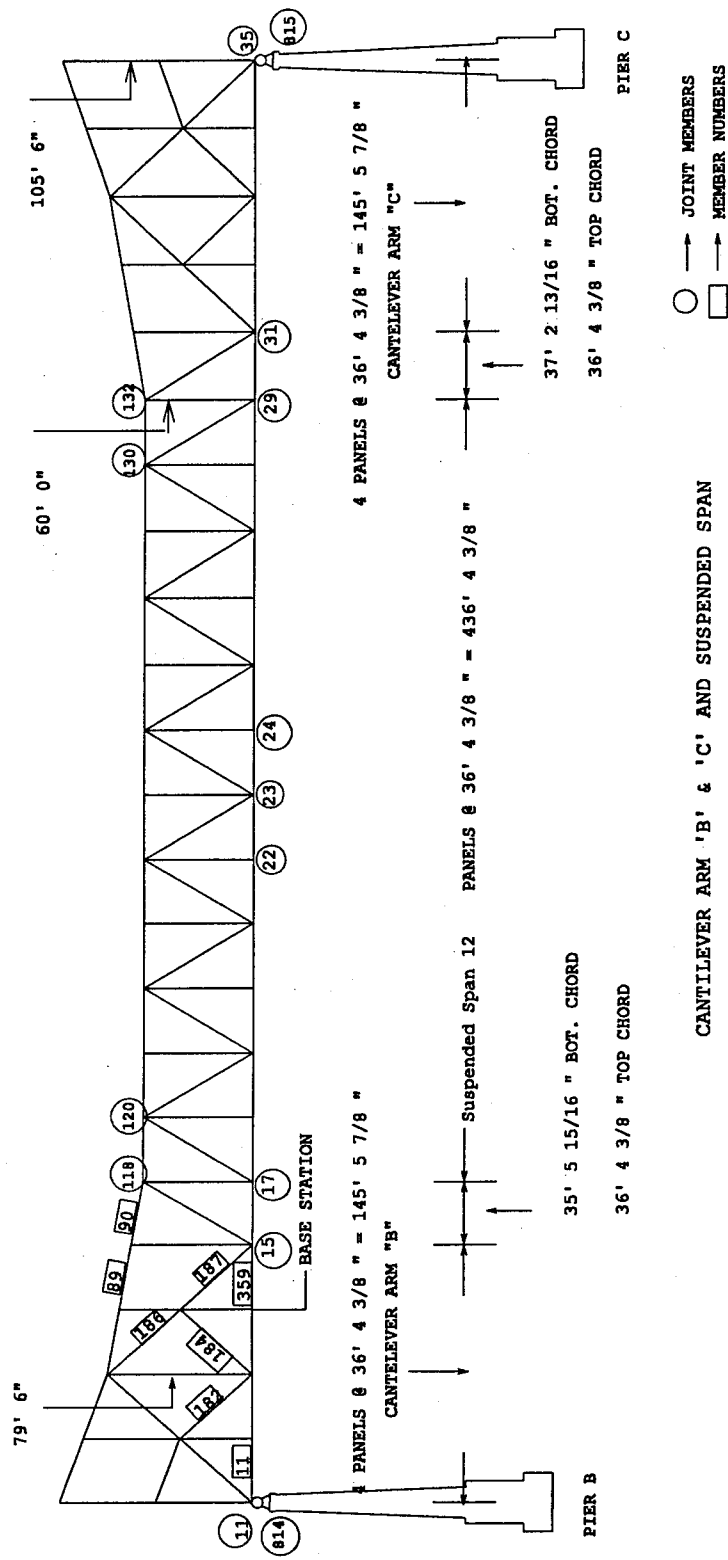


Figure 2.4 Elevation View of the Second Span B-C

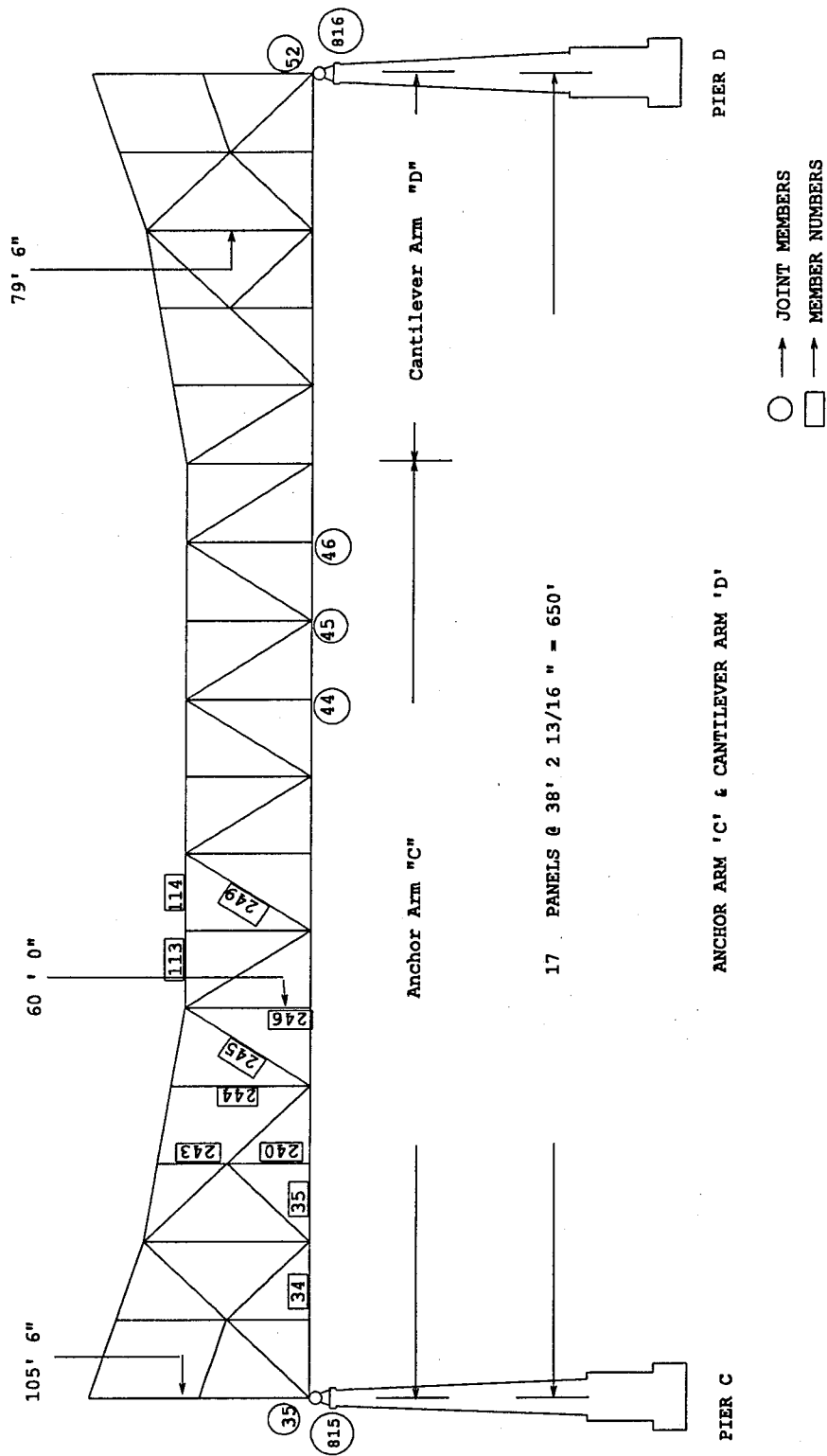


Figure 2.5 Elevation View of the Third Span C-D

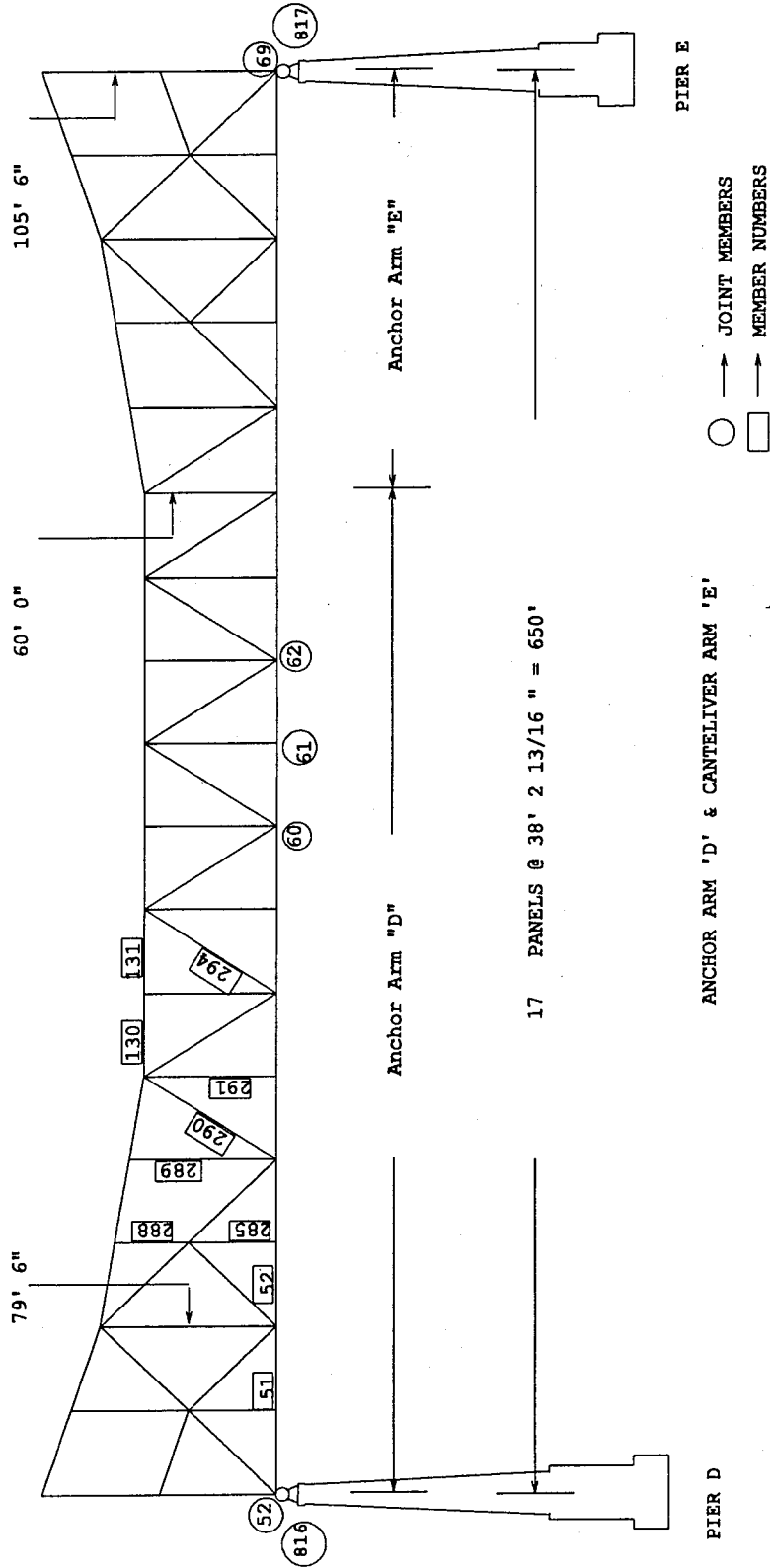


Figure 2.6 Elevation View of the Fourth Span D-E

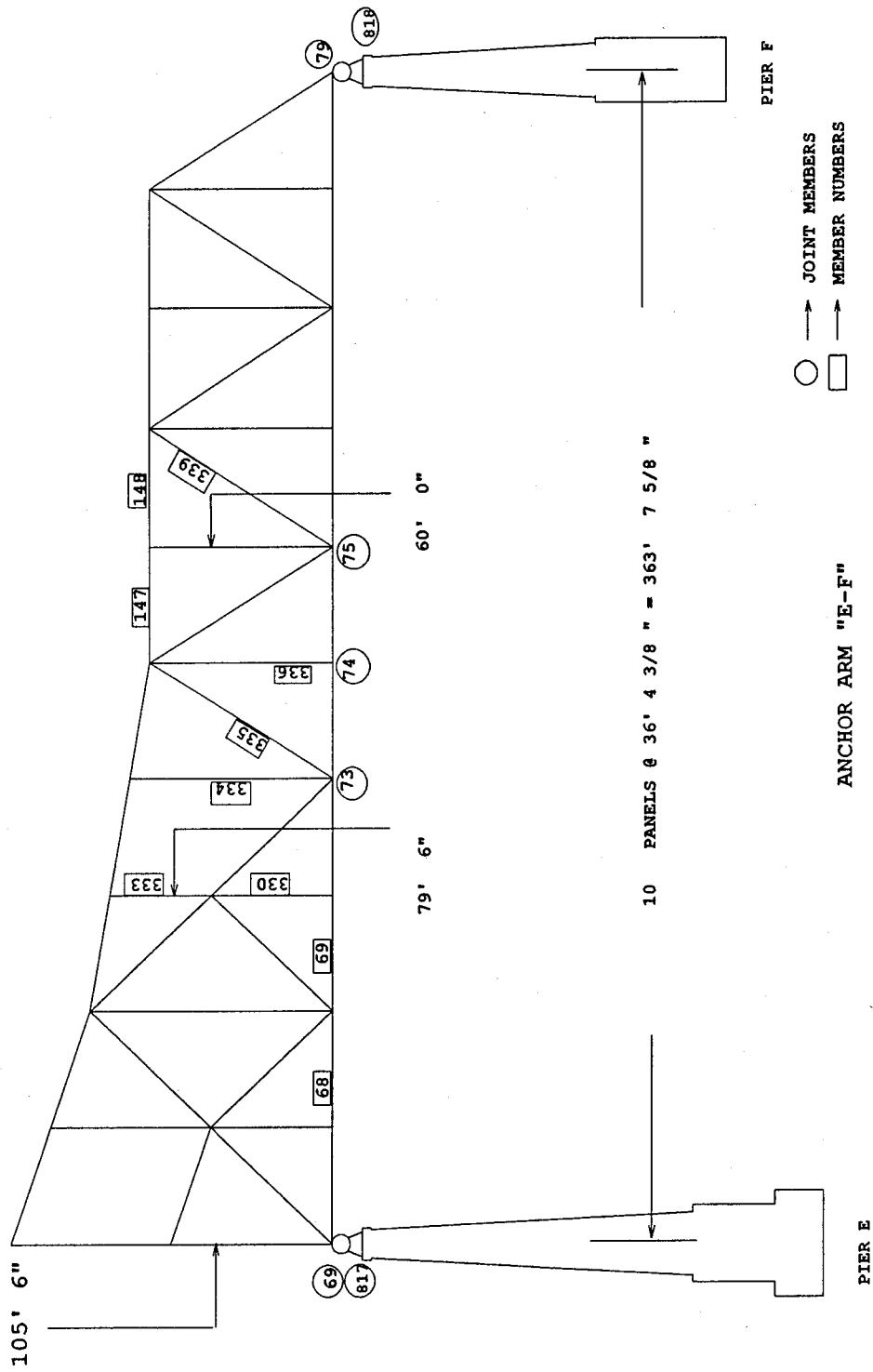


Figure 2.7 Elevation View of the Fifth Span E-F

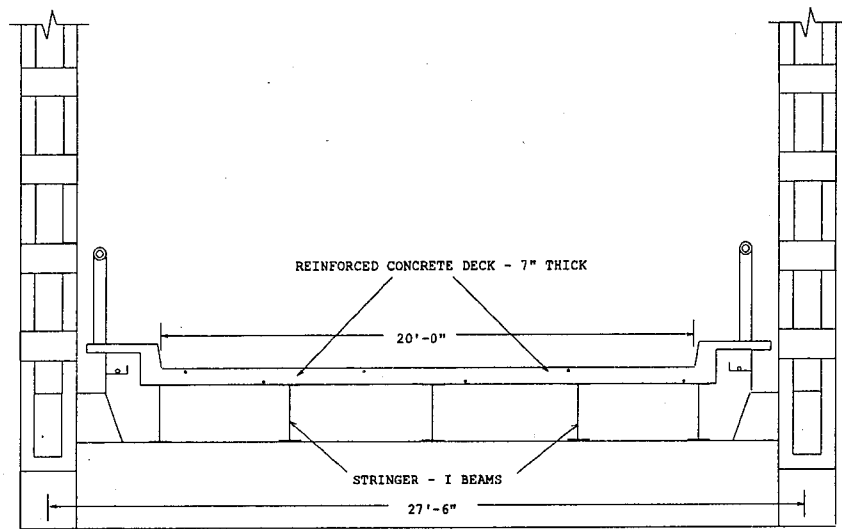


Figure 2.8 Transverse Cross Section of the US51 Main Bridge

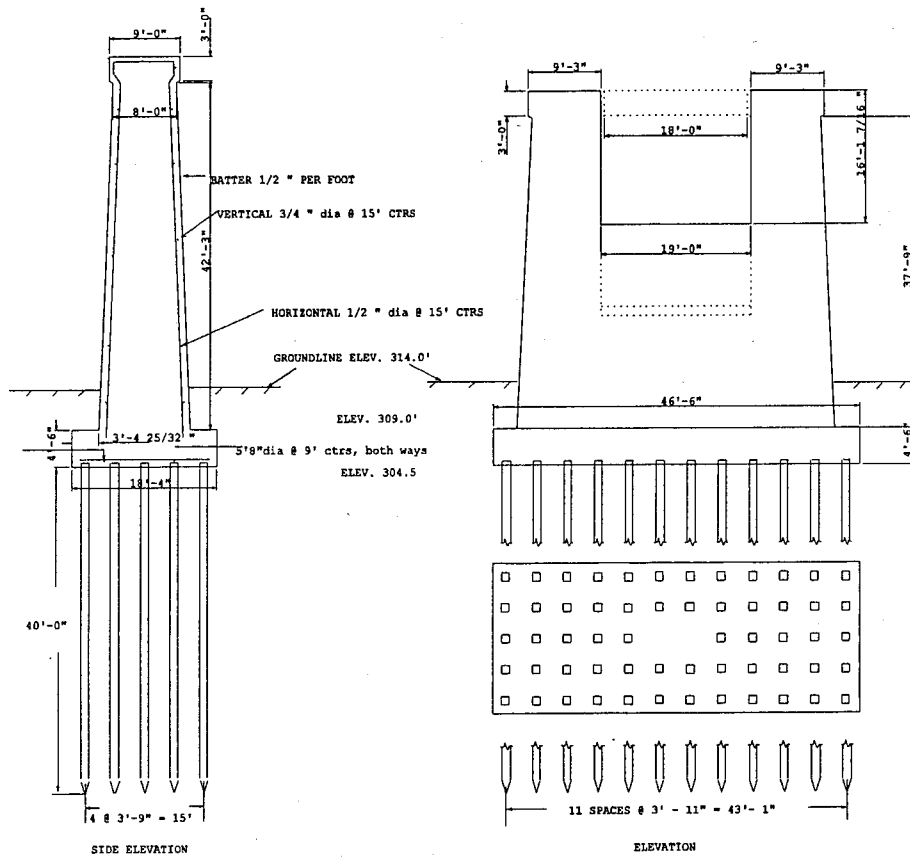


Figure 2.9 Elevation and Sectional Views of Pier A

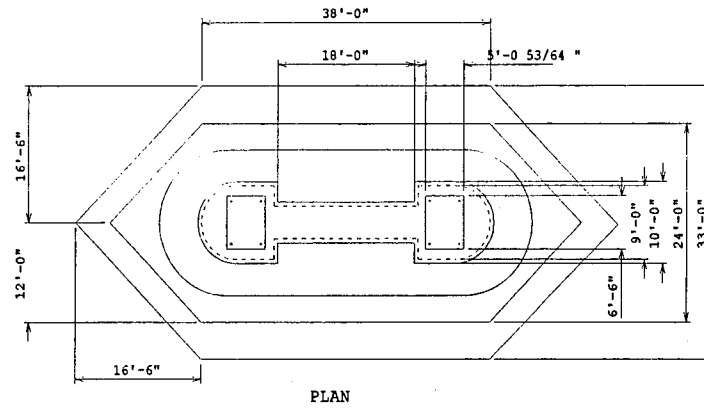


Figure 2.10a Plan View of Pier B, C, D and E

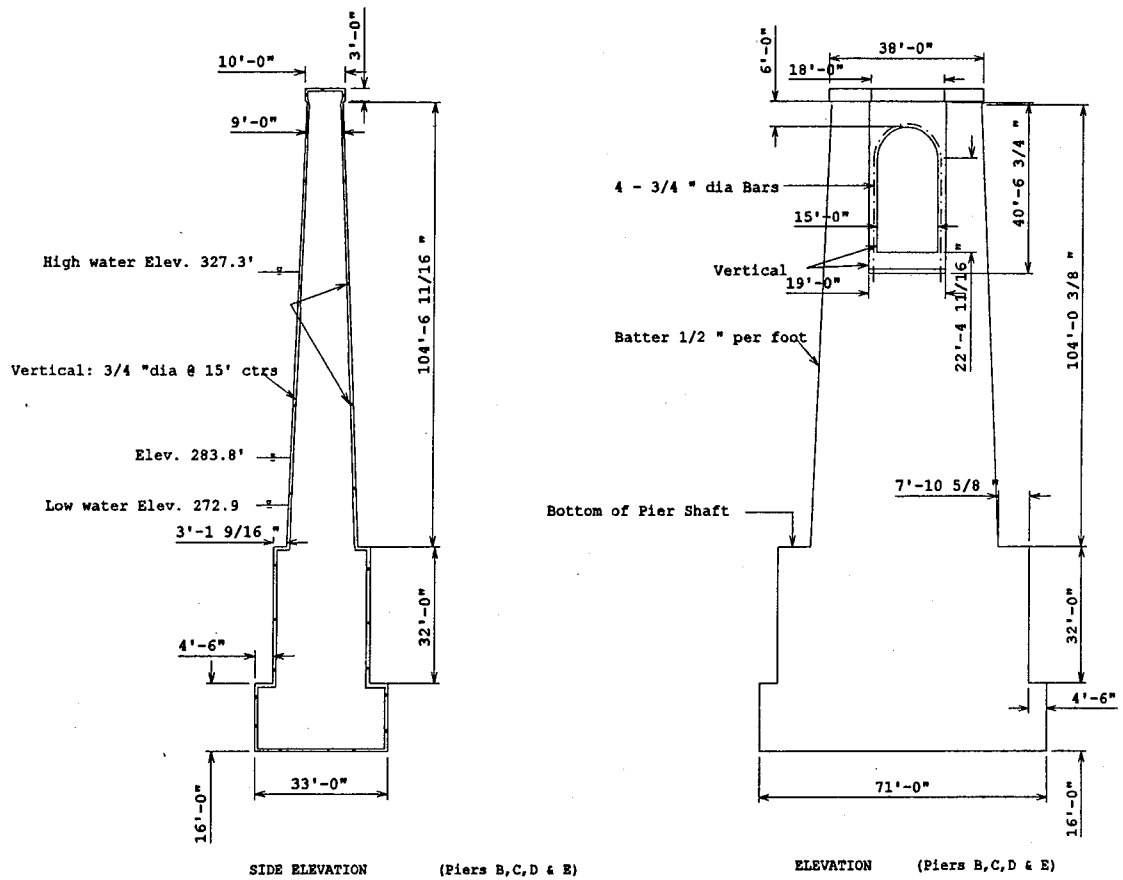


Figure 2.10b Elevation and Sectional Views of Pier B, C, D and E

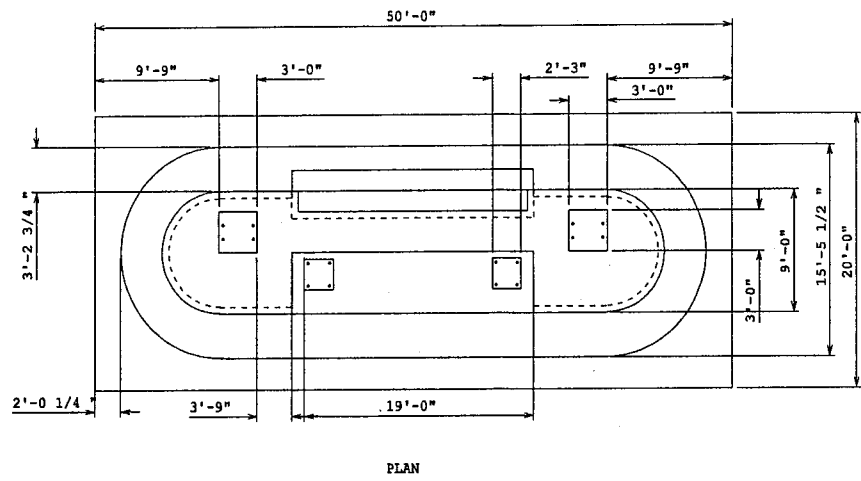


Figure 2.11a Plan View of Pier F

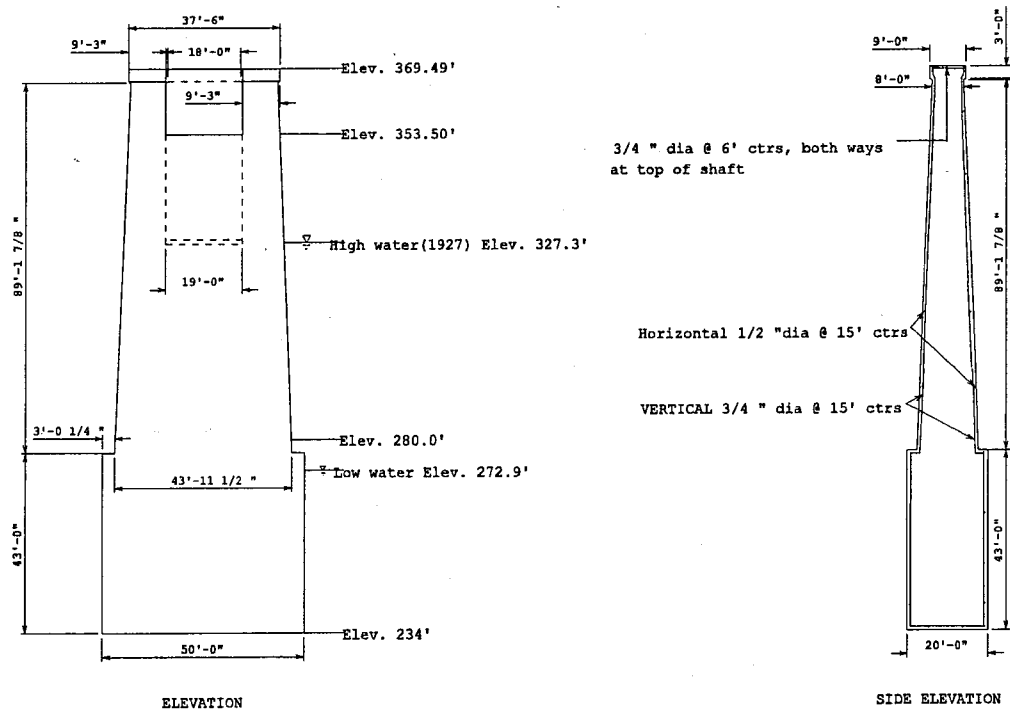


Figure 2.11b Elevation and sectional views of Pier F

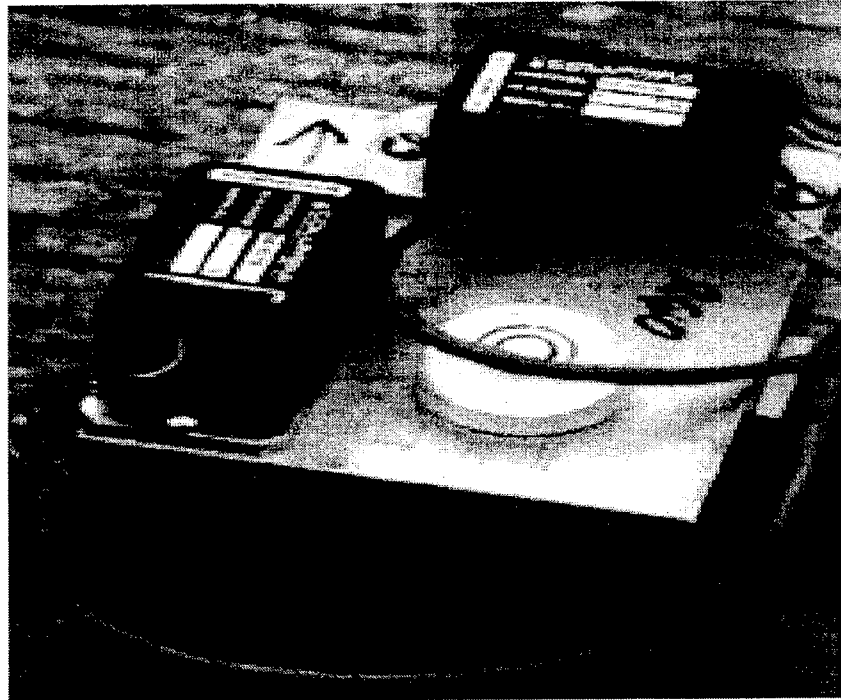


Figure 3.1a Triaxial Accelerometer Block

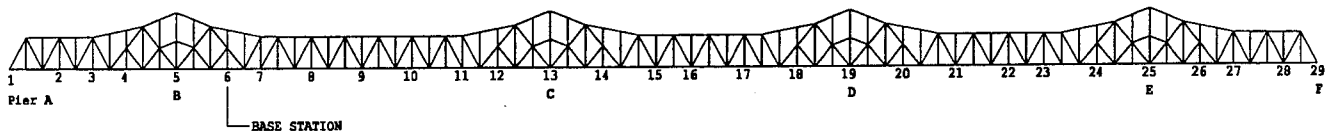


Figure 3.1b Accelerometer Locations (Moving and Base Stations) on One Side of the Bridge

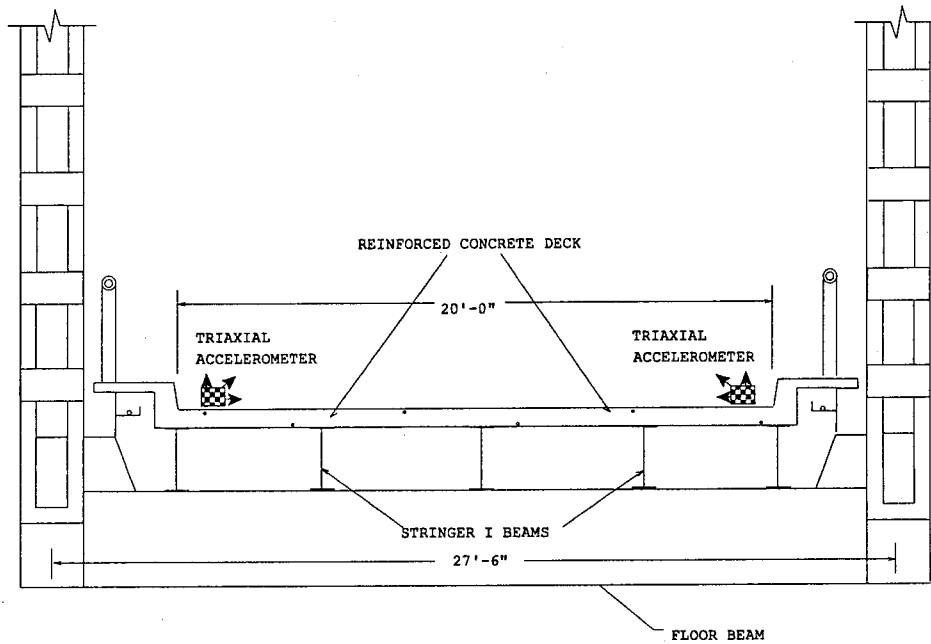


Figure 3.1c Accelerometer Placement on the Deck

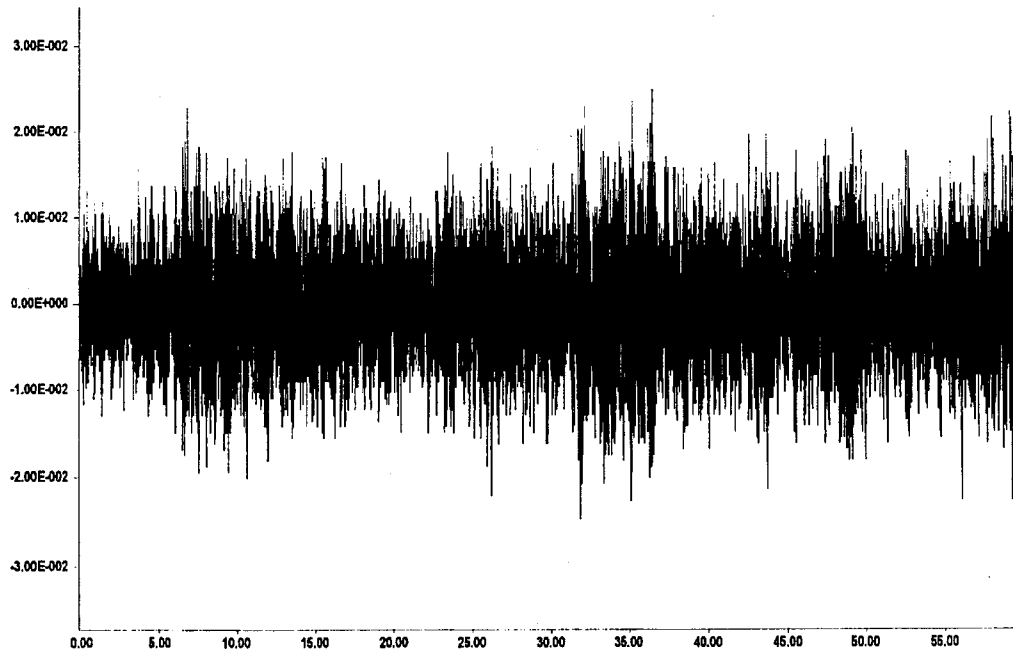


Figure 3.2a Transverse acceleration-time history obtained from field testing at moving station 6

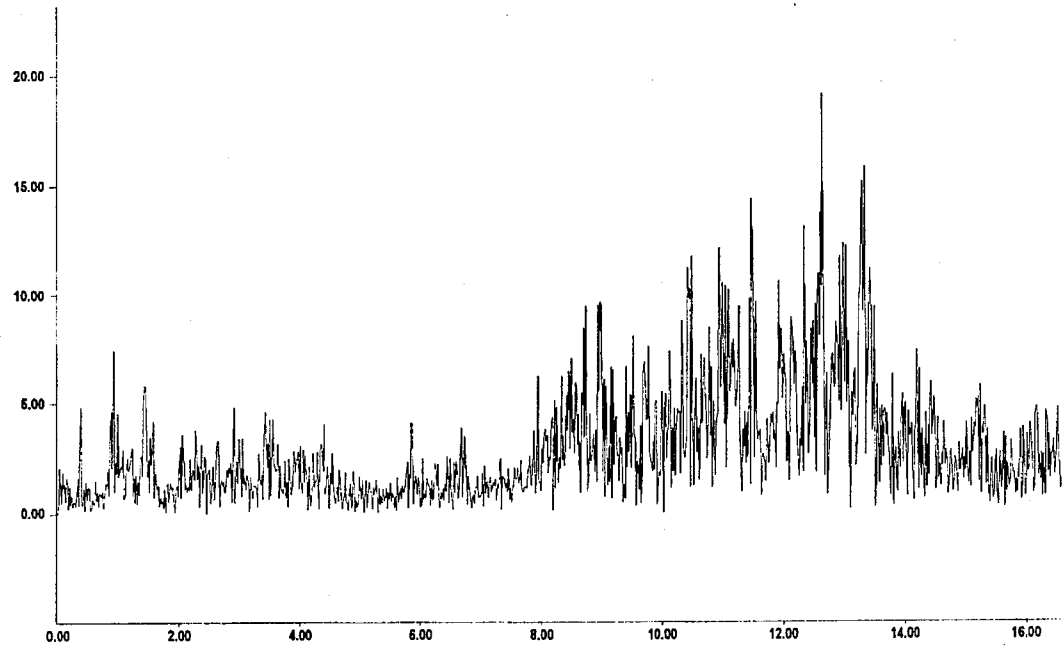


Figure 3.2b FFT of transverse acceleration-time history at moving station 6

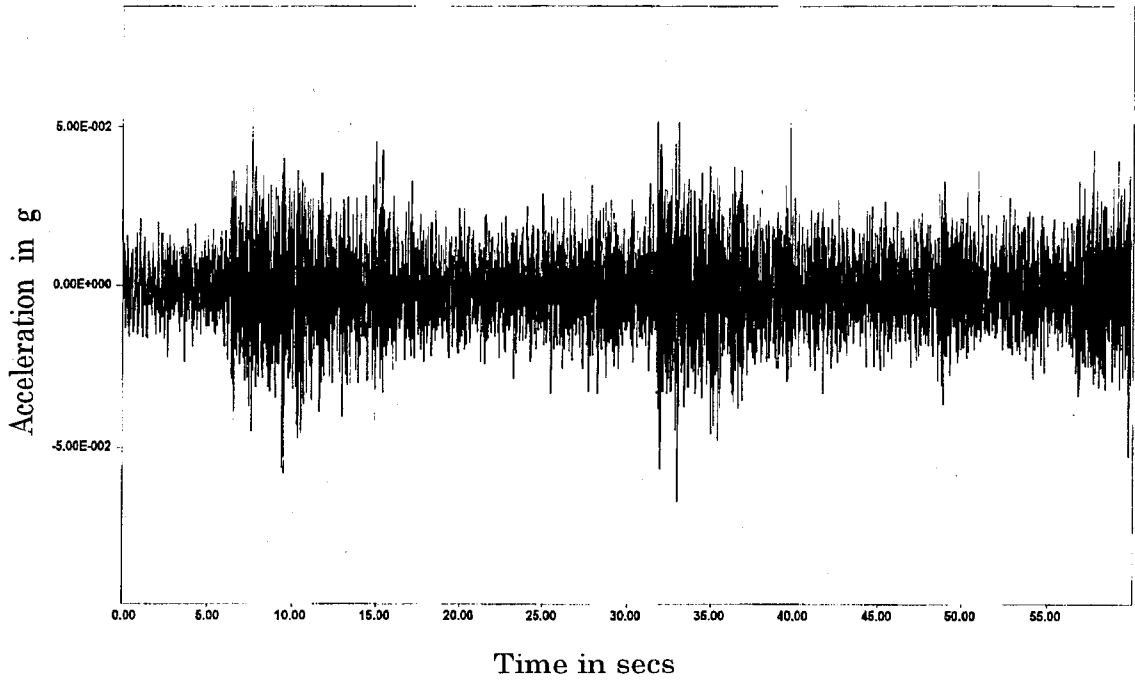


Figure 3.2c Vertical acceleration time-history obtained from field testing at moving station 6

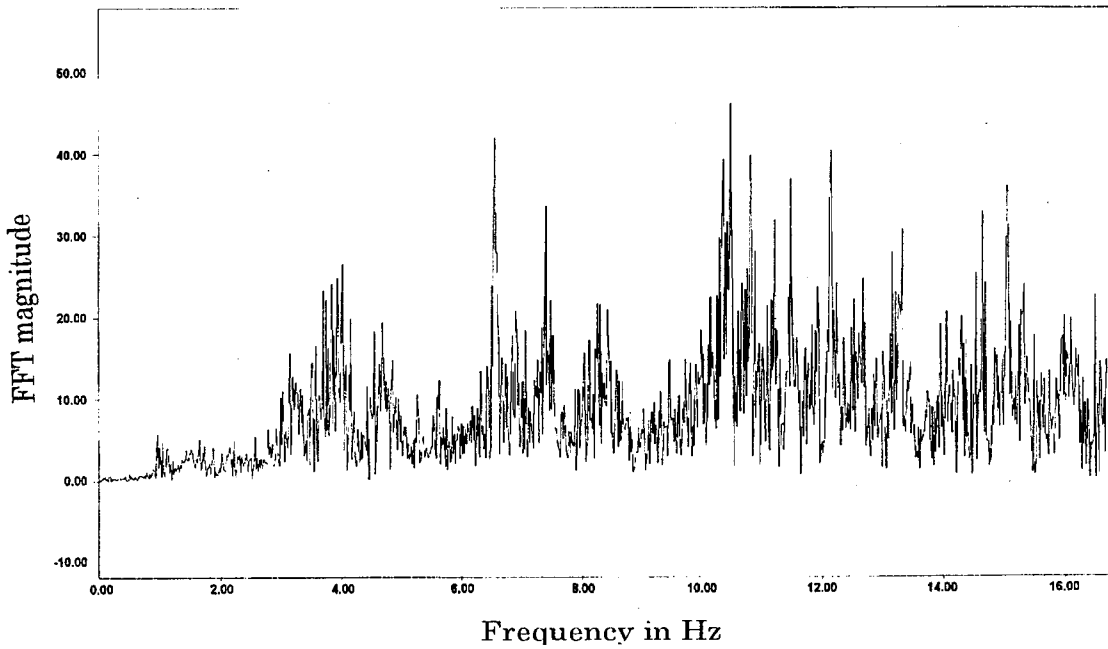


Figure 3.2d FFT of vertical acceleration time-history at moving station 6

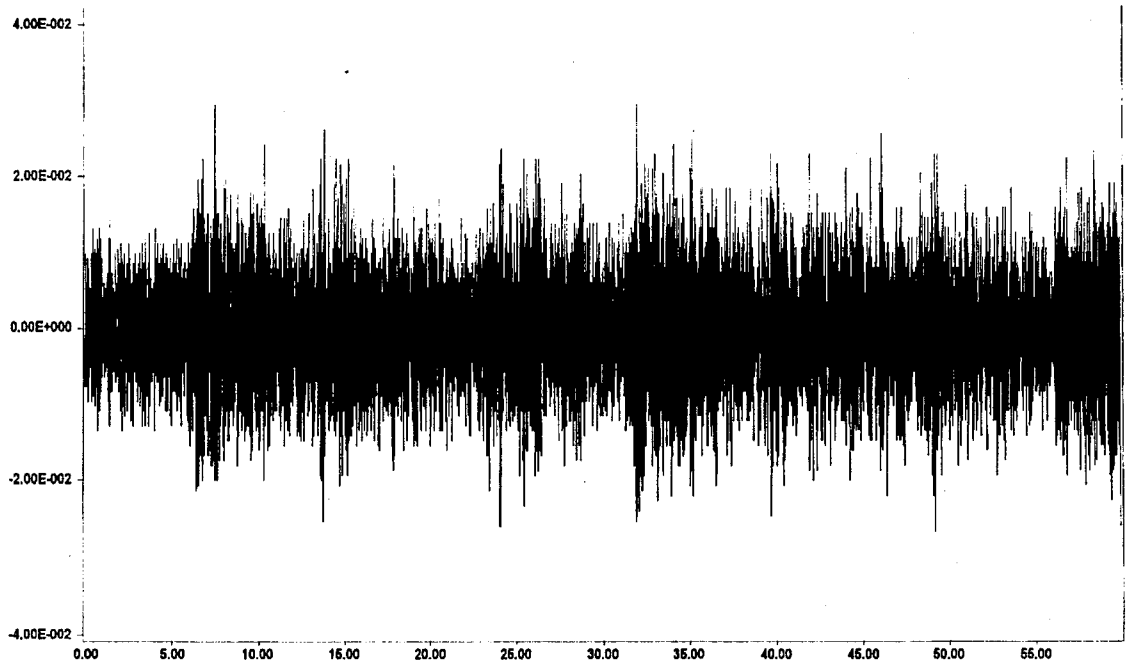


Figure 3.2e Longitudinal acceleration-time history obtained from field testing at moving station 6

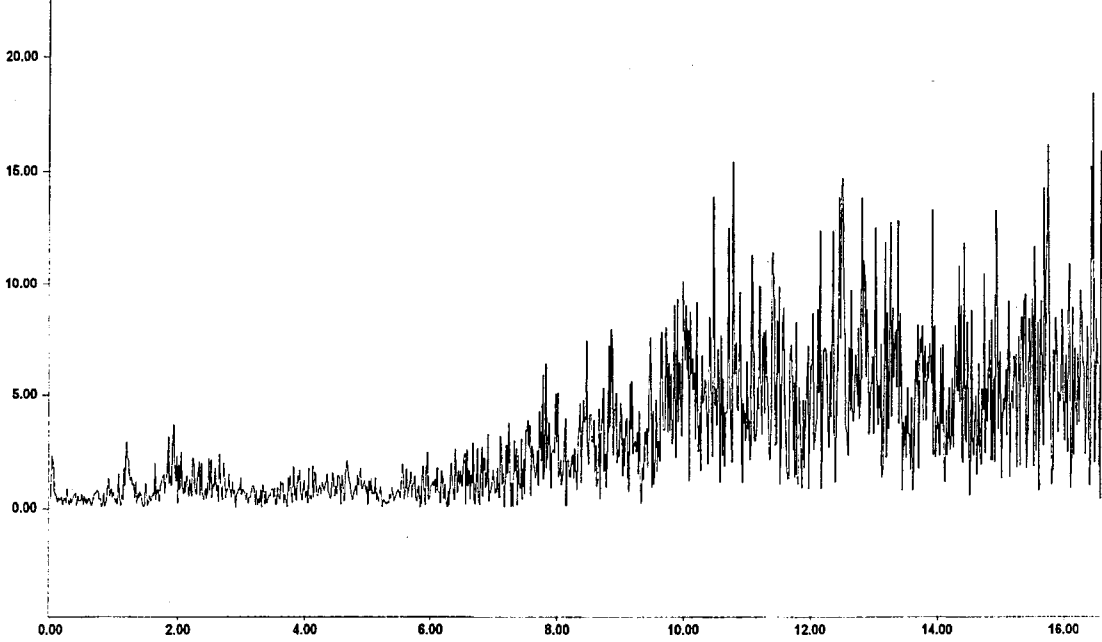


Figure 3.2f FFT of longitudinal acceleration-time history at moving station 6

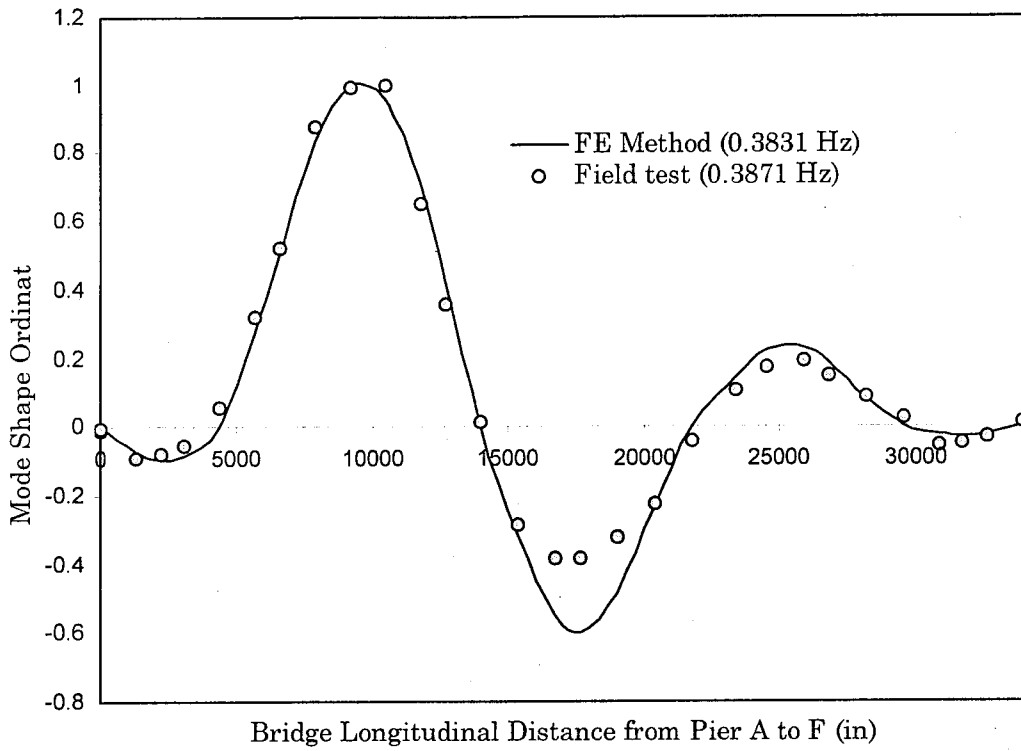


Figure 3.3a First Transverse Mode

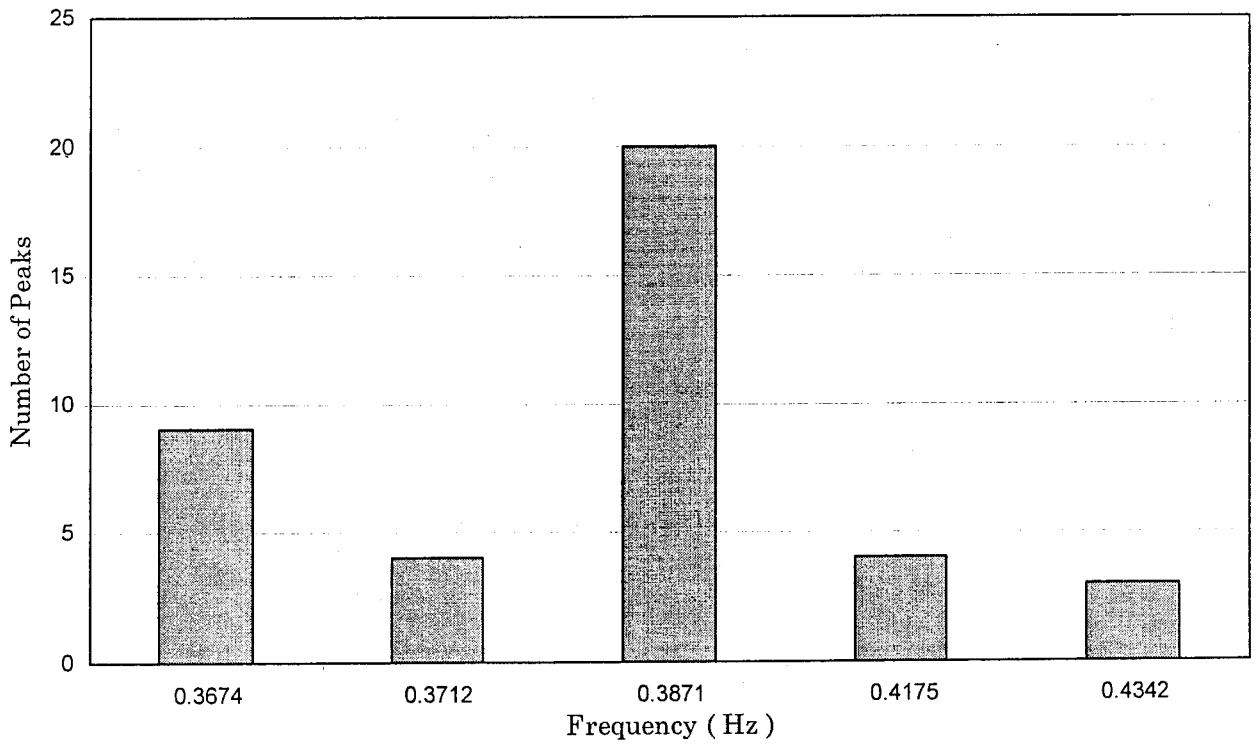


Figure 3.3b Peak Comparison for the First Transverse Mode

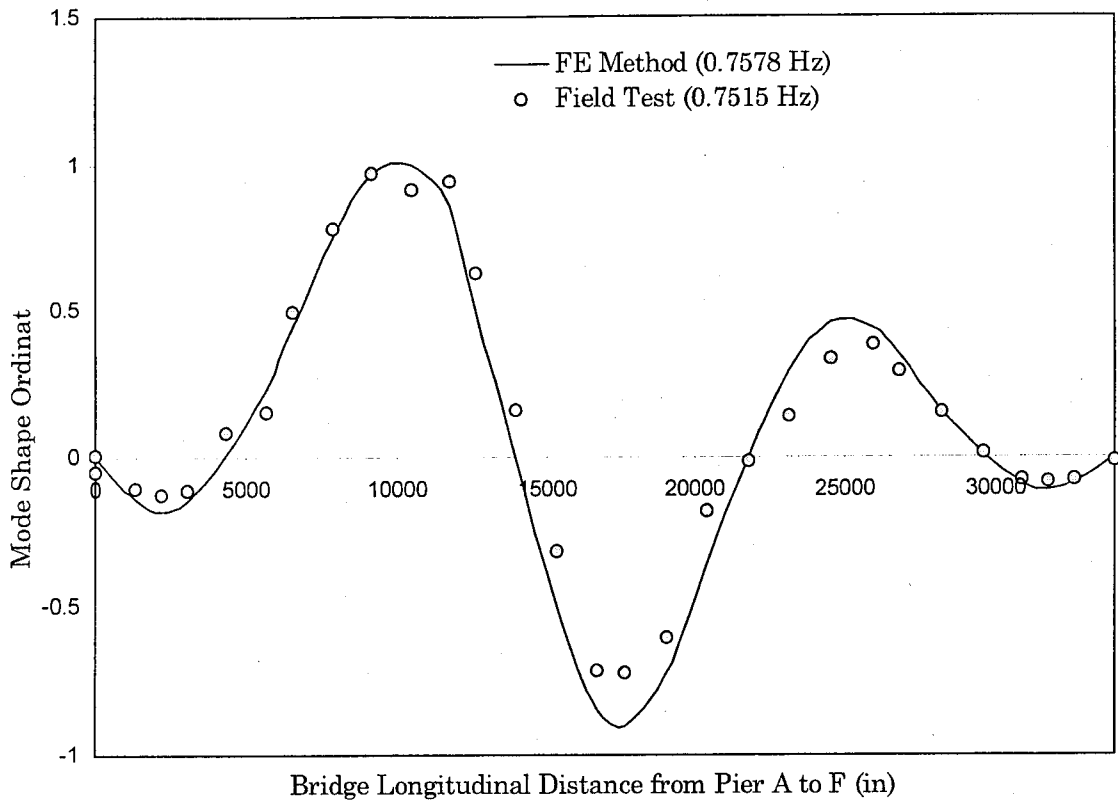


Figure 3.4a First Vertical Mode

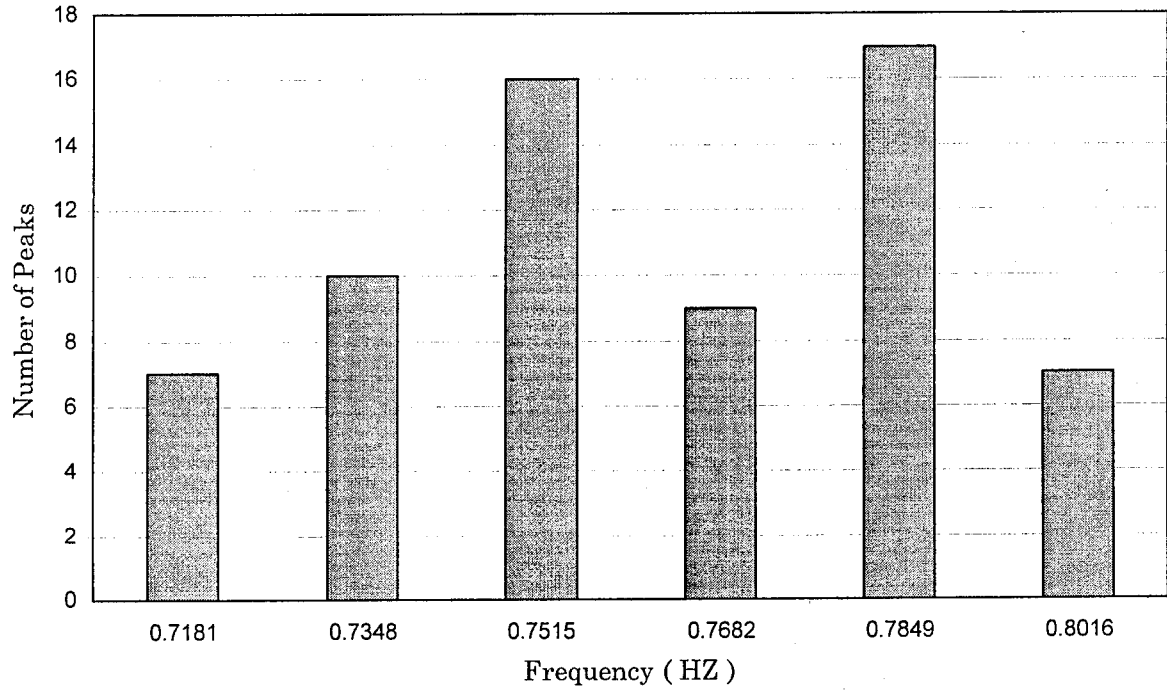
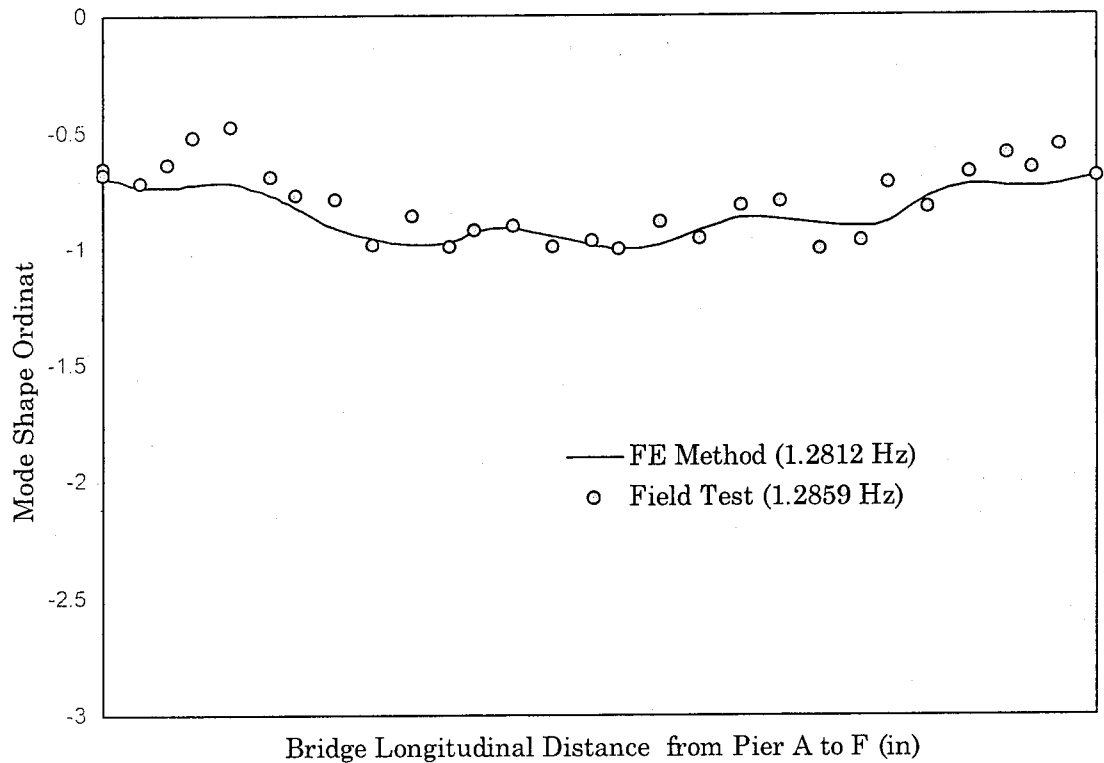


Figure 3.4b Peak Comparison for the First Vertical Mode



Bridge Longitudinal Distance from Pier A to F (in)

Figure 3.5a First Longitudinal Mode

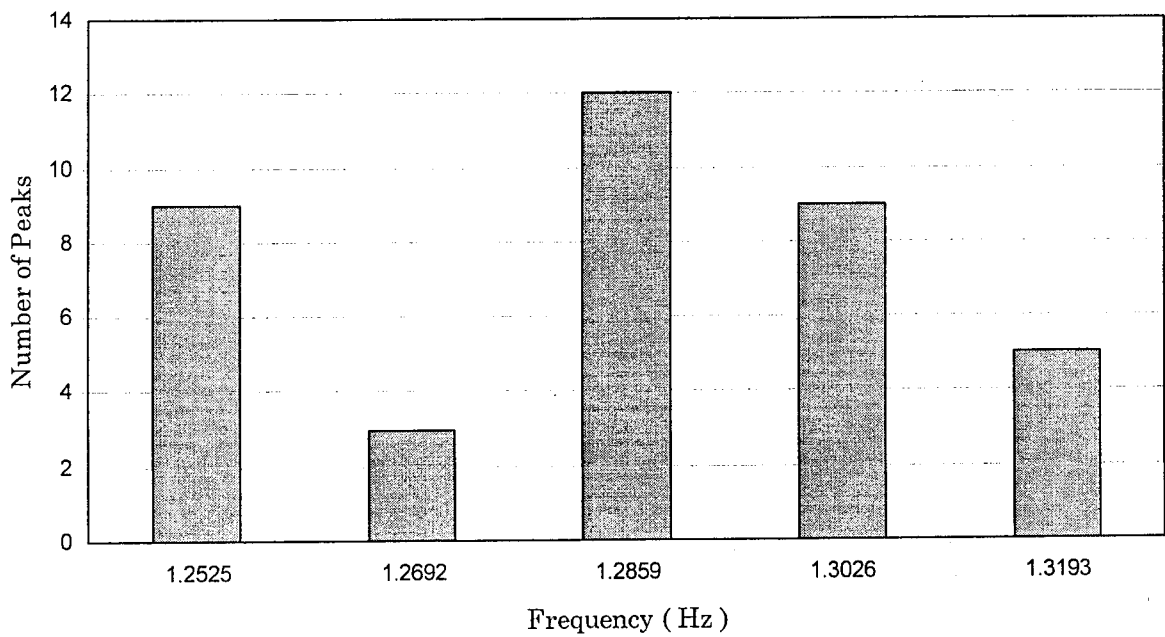


Figure 3.5b Peak Number Comparison for the First Longitudinal Mode

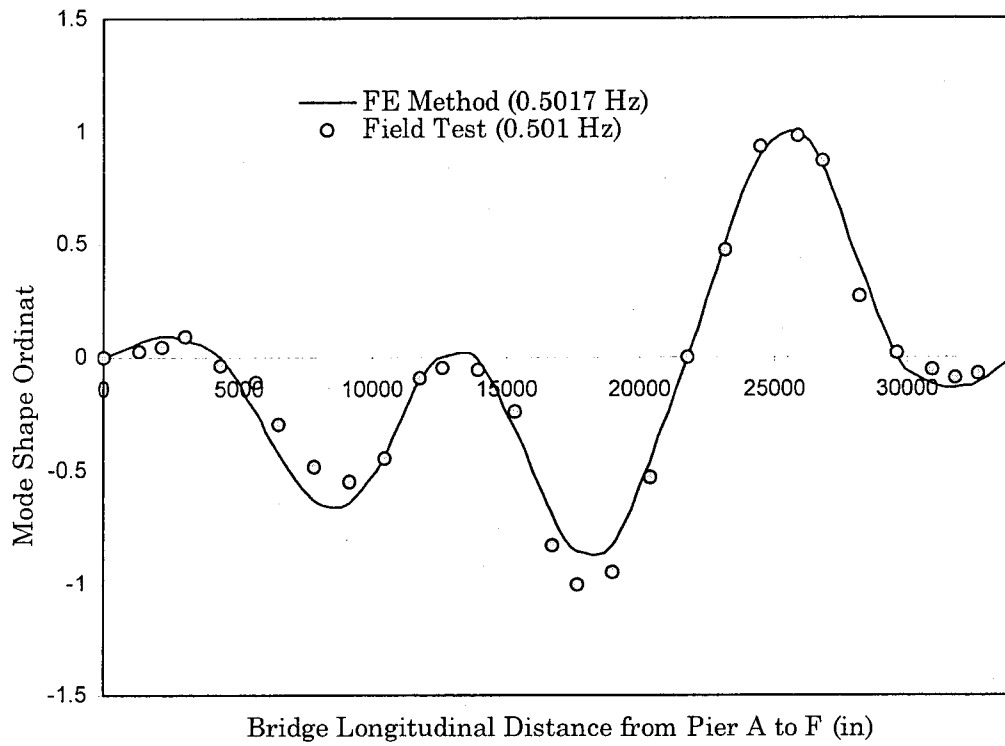


Figure 3.6a Second Transverse Mode

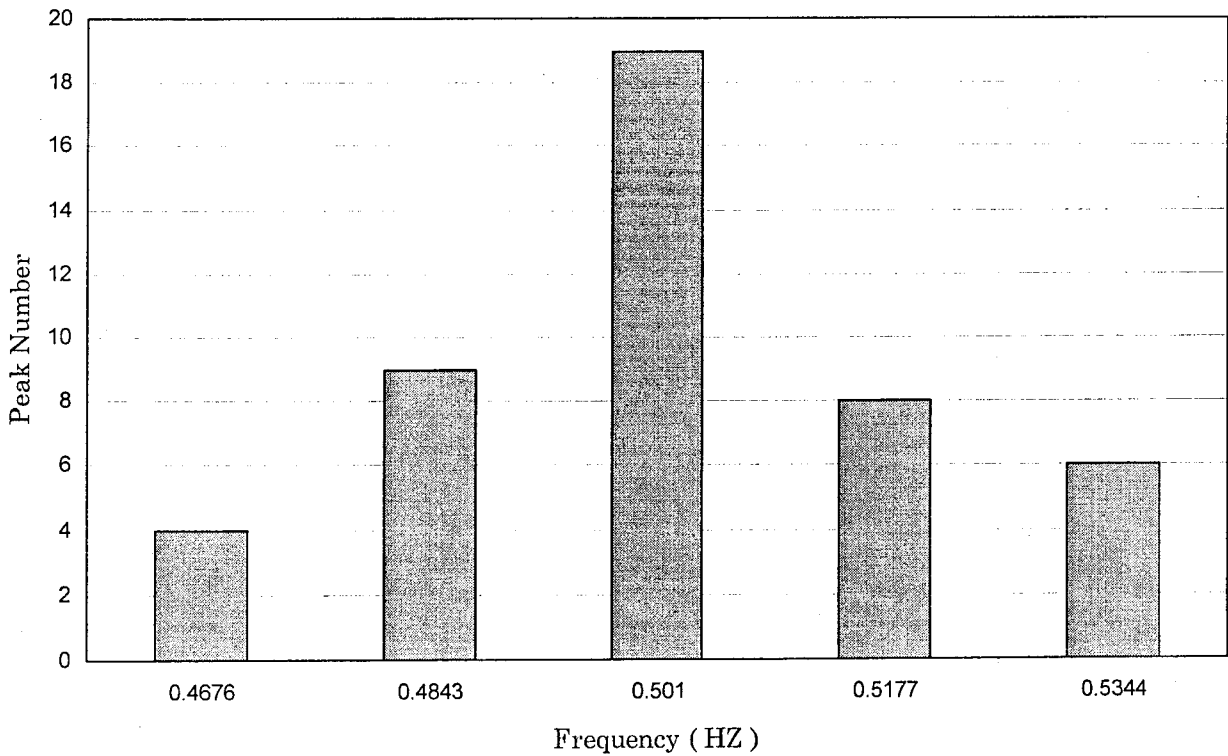


Figure 3.6b Peak Comparison for the Second Transverse Mode

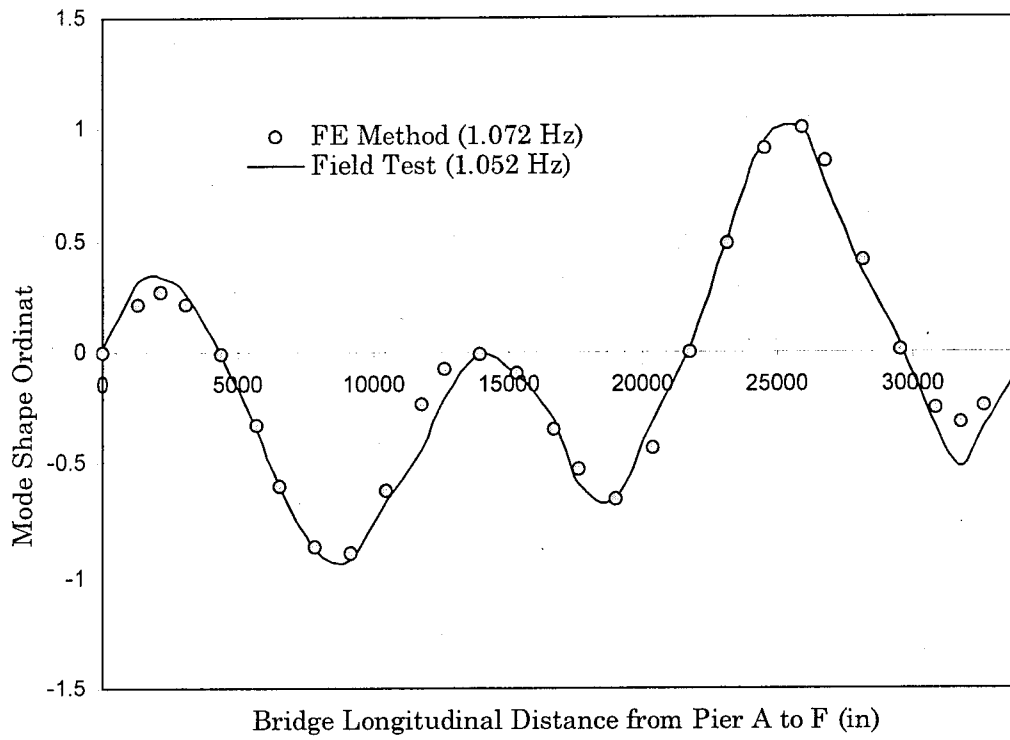


Figure 3.7a Second Vertical Mode

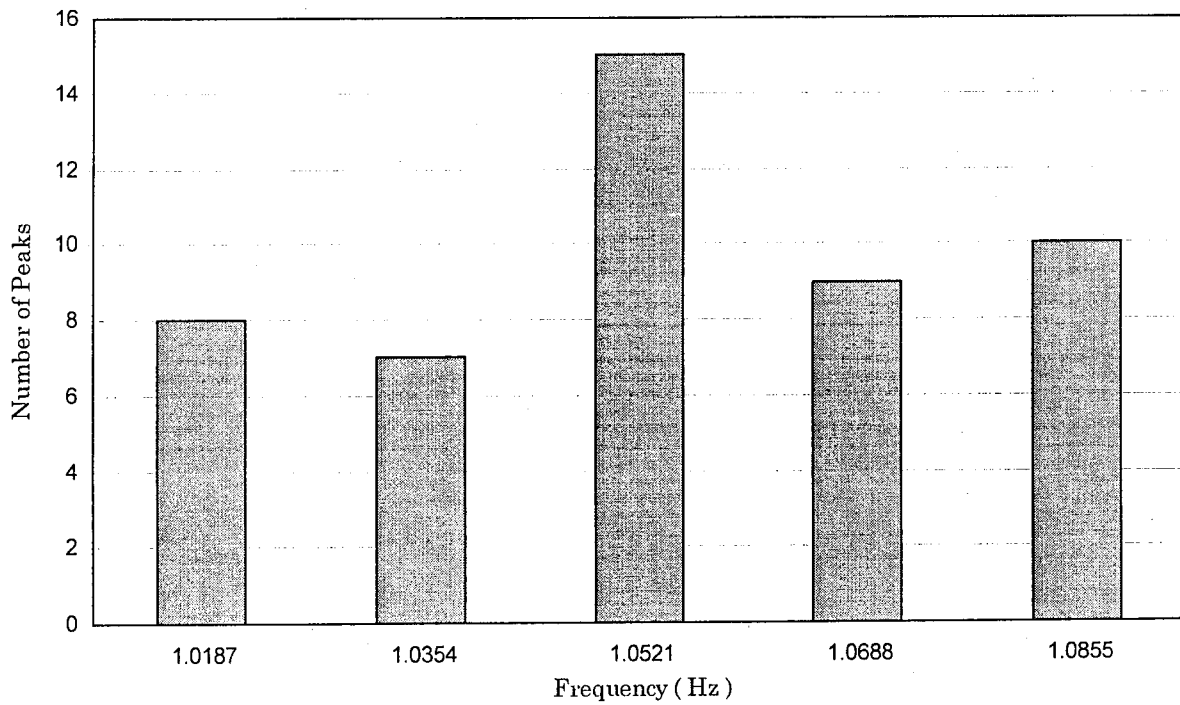


Figure 3.7b Peak Comparison for the Second Vertical Mode

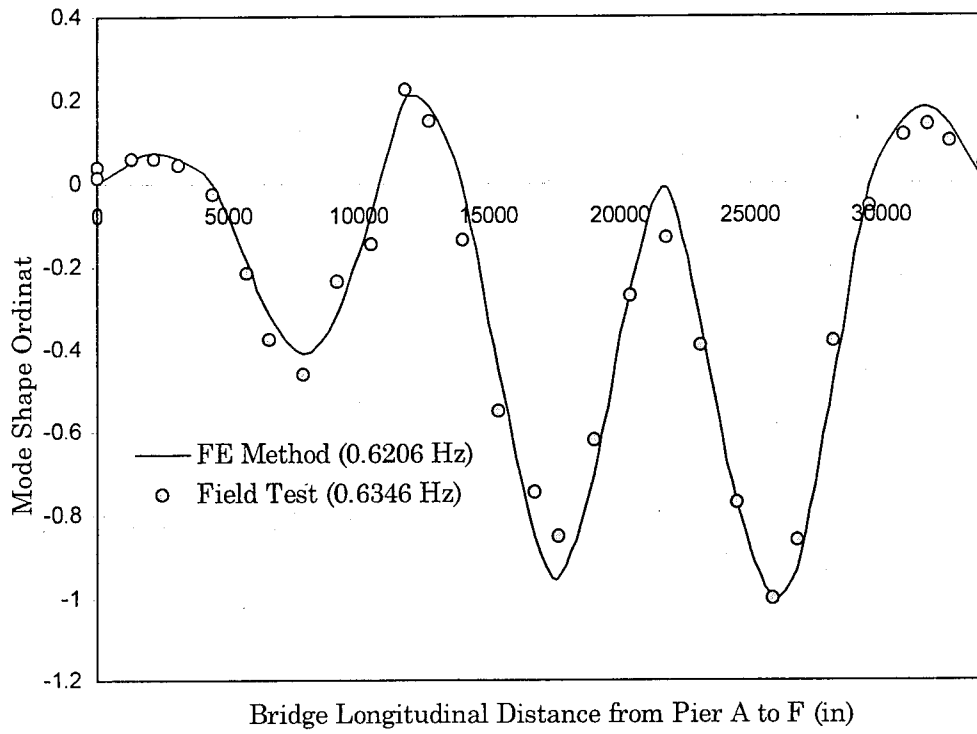


Figure 3.8a Third Transverse Mode

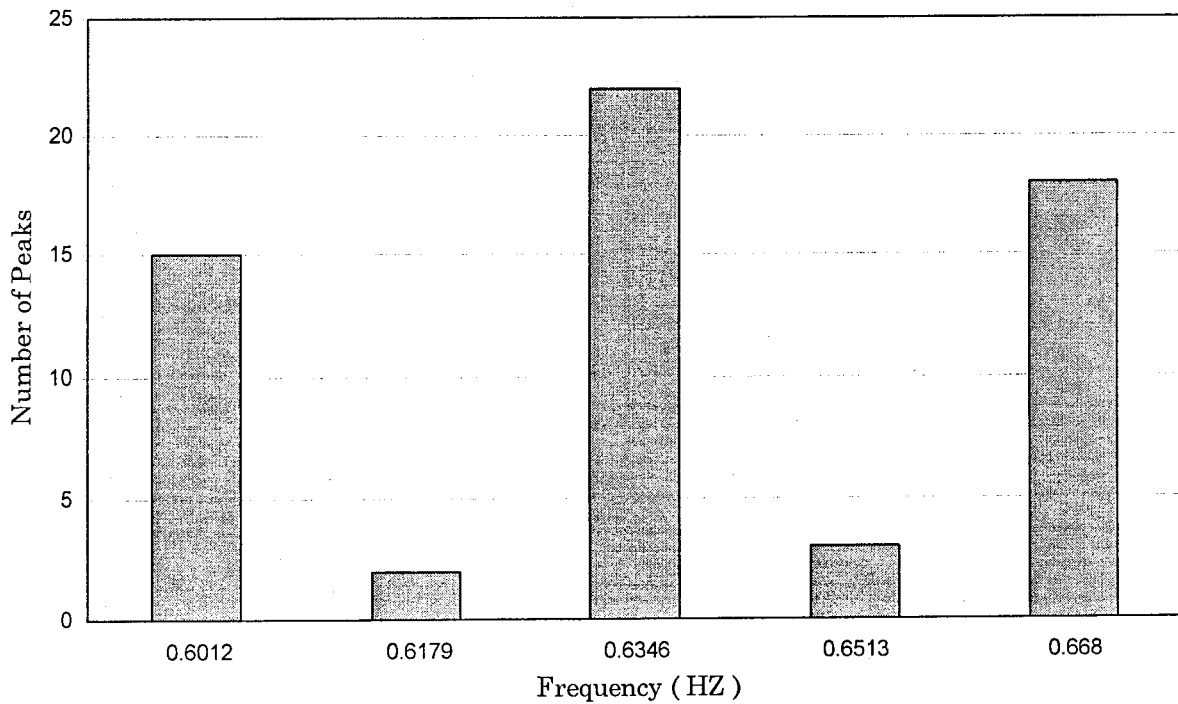


Figure 3.8b Peak Comparison for the Third Transverse Mode

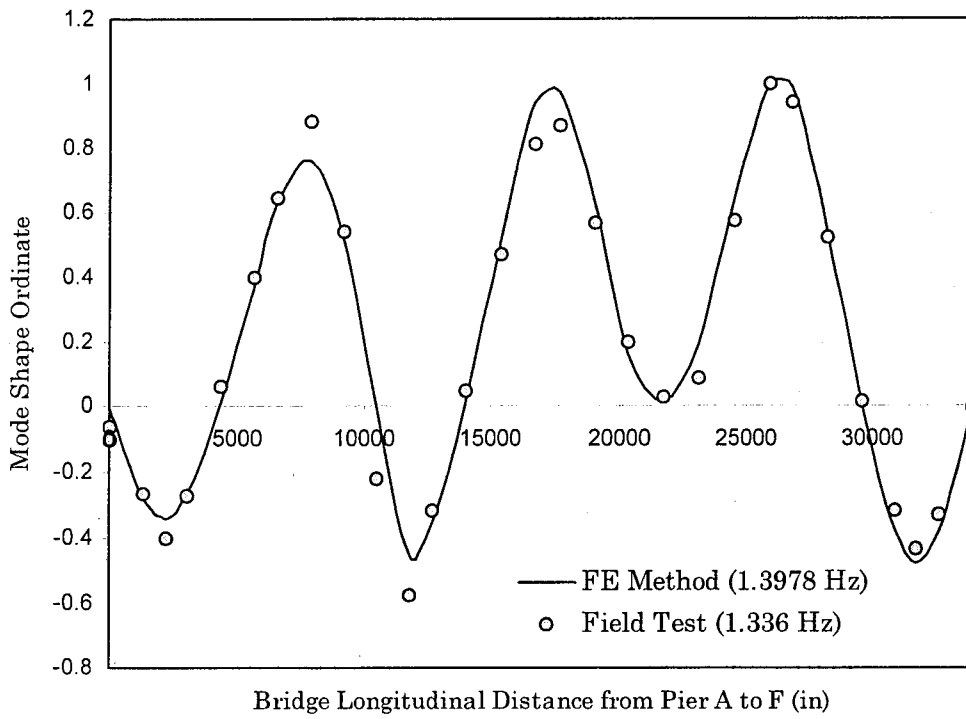


Figure 3.9a Third Vertical Mode

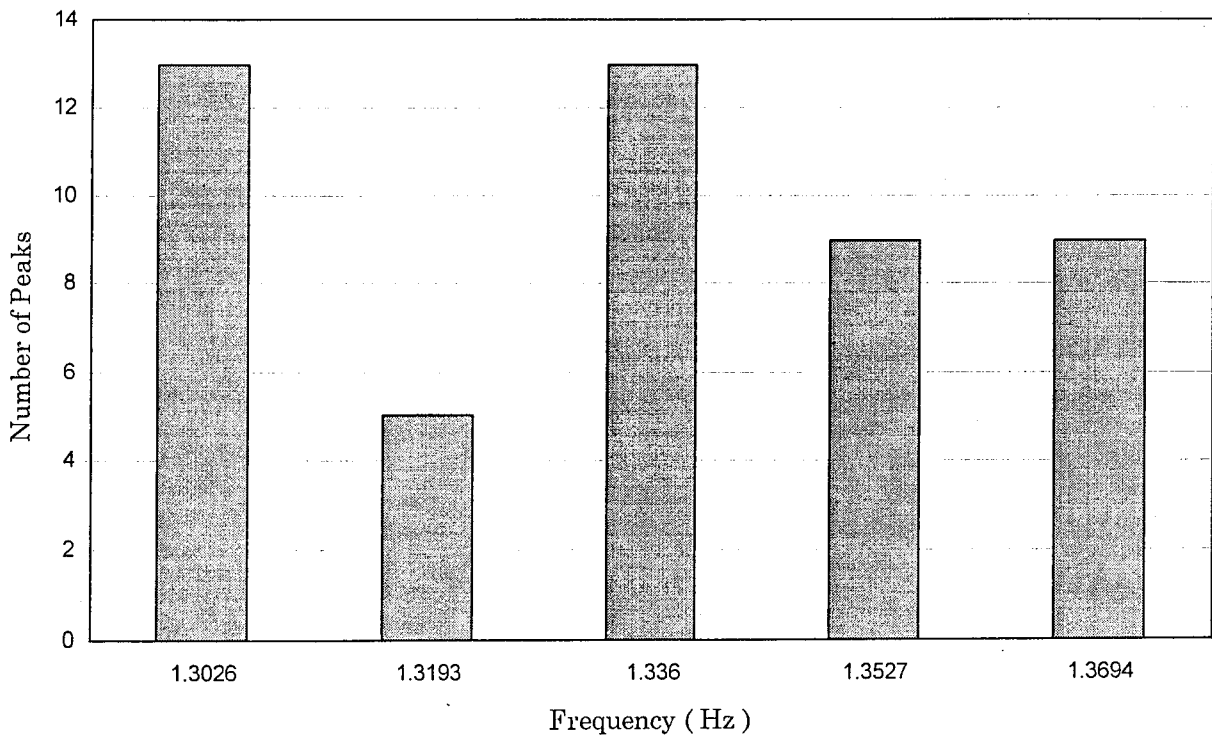


Figure 3.9b Peak Comparison for the Third Vertical Mode

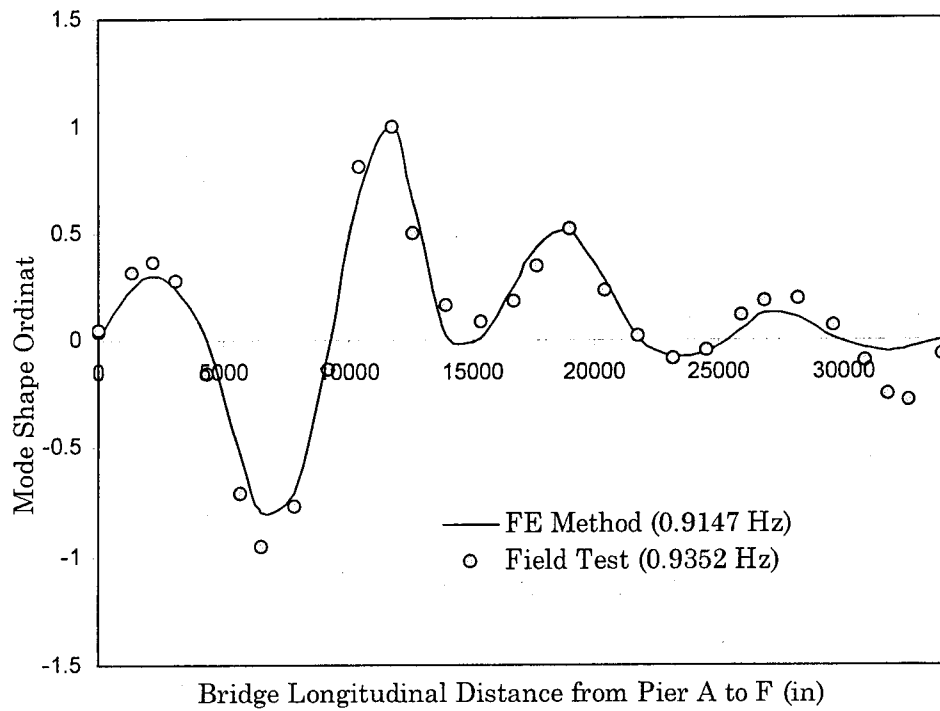


Figure 3.10a Fourth Transverse Mode

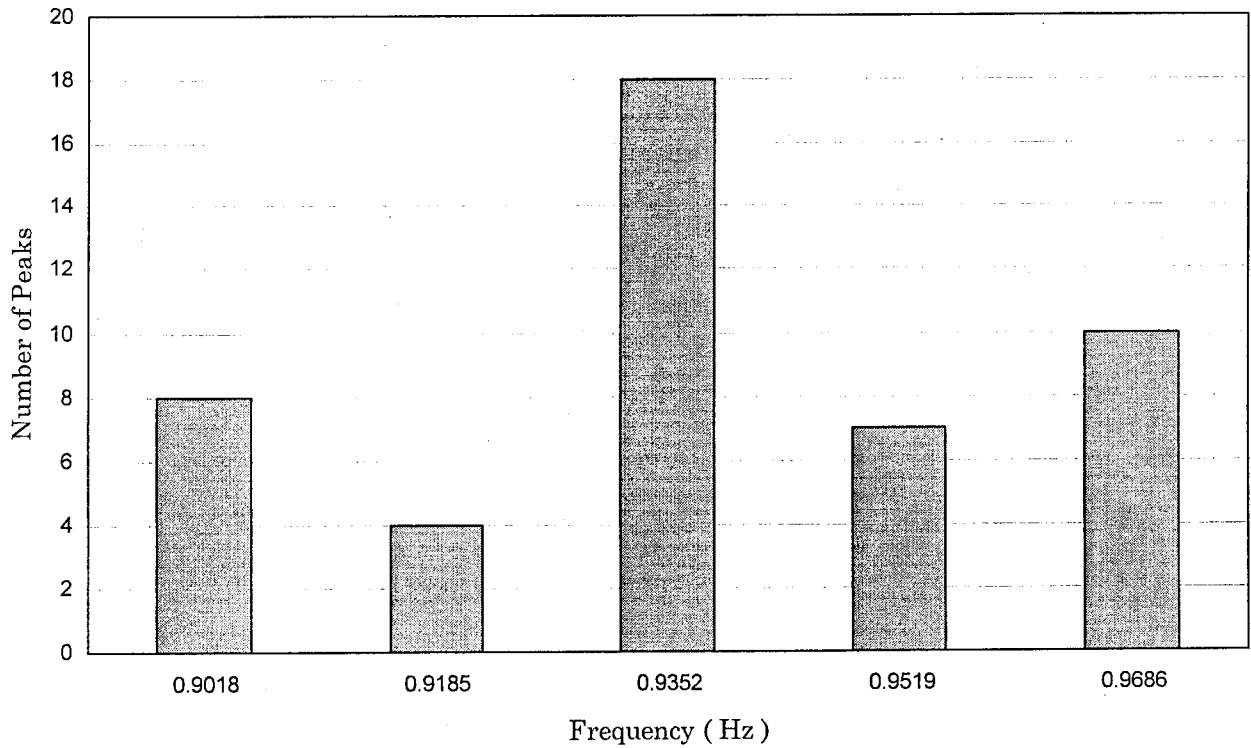


Figure 3.10b Peak Comparison for the Fourth Transverse Mode

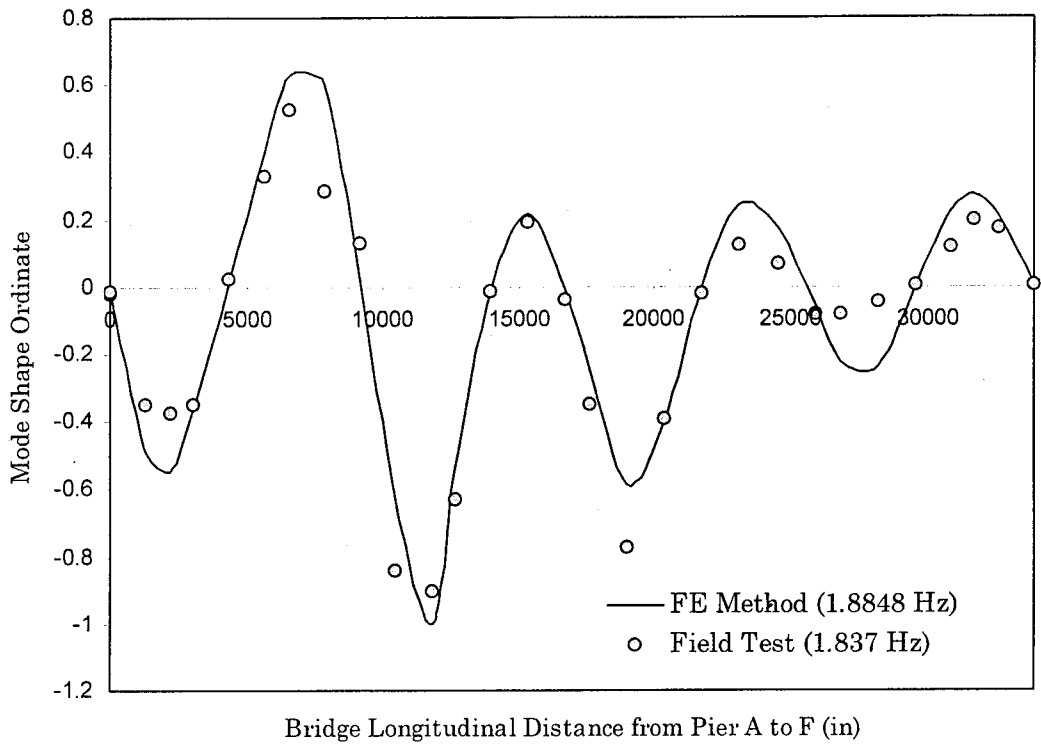


Figure 3.11a Fourth Vertical Mode

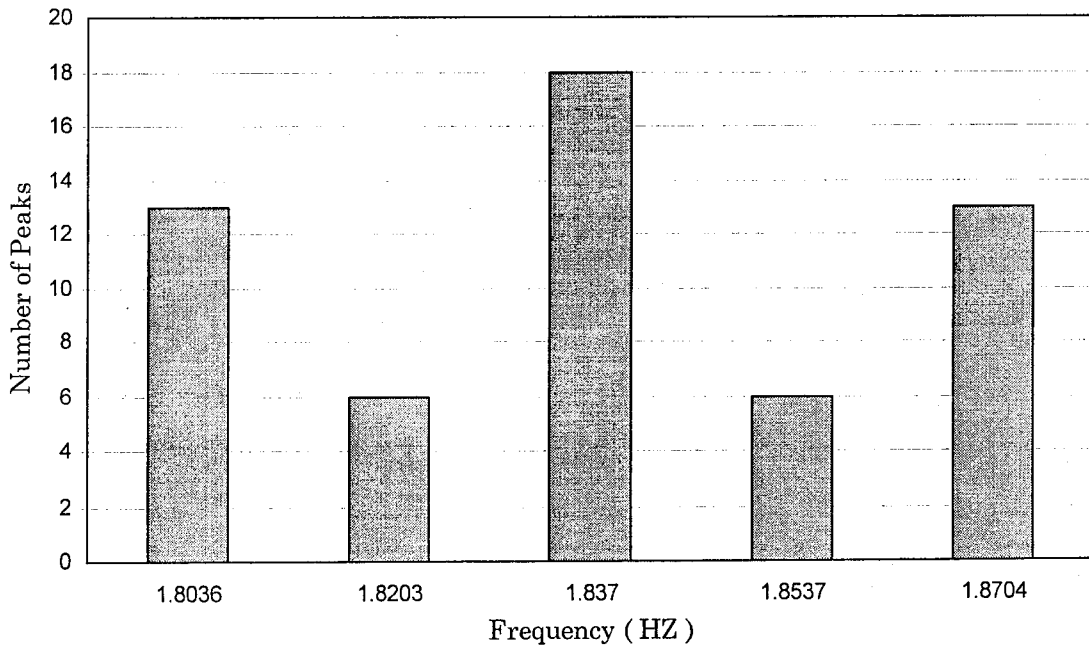


Figure 3.11b Peak Comparison for the Fourth Vertical Mode

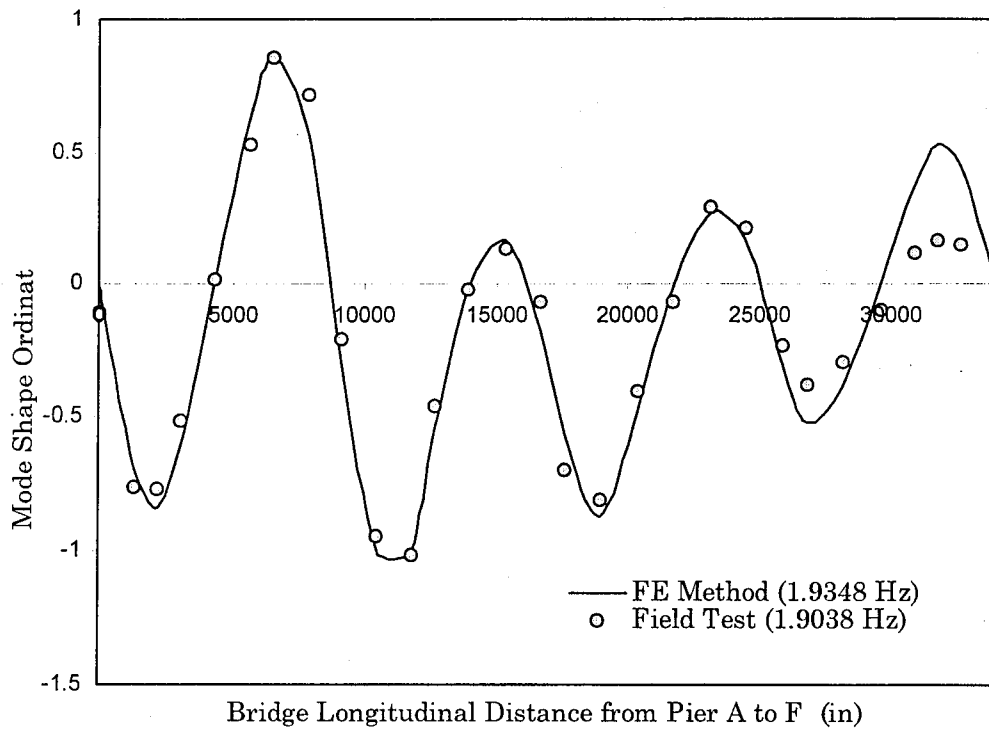


Figure 3.12a Fifth Vertical Mode

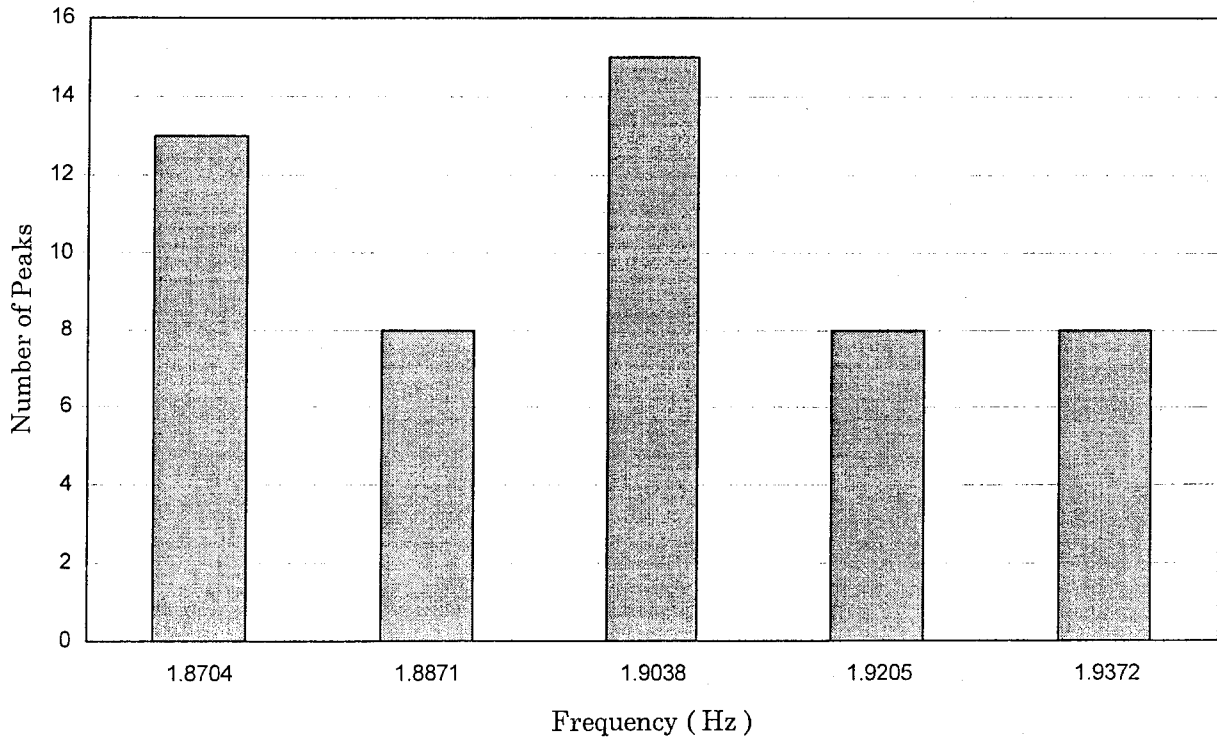


Figure 3.12b Peak Comparison for the Fifth Vertical Mode

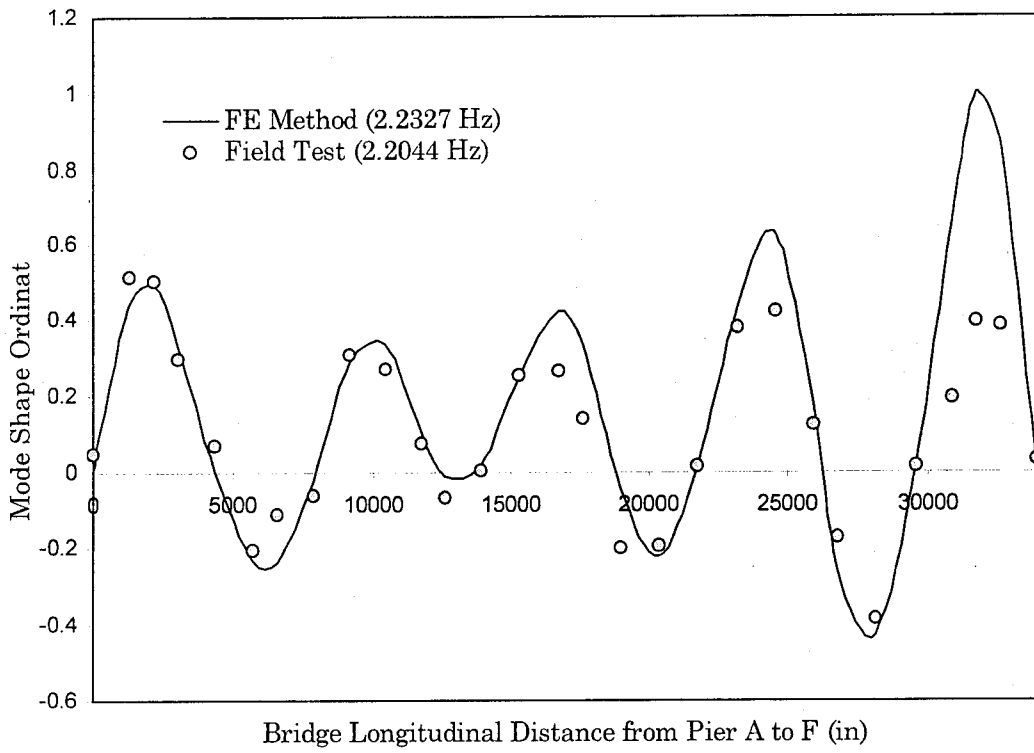


Figure 3.13a Sixth Vertical Mode

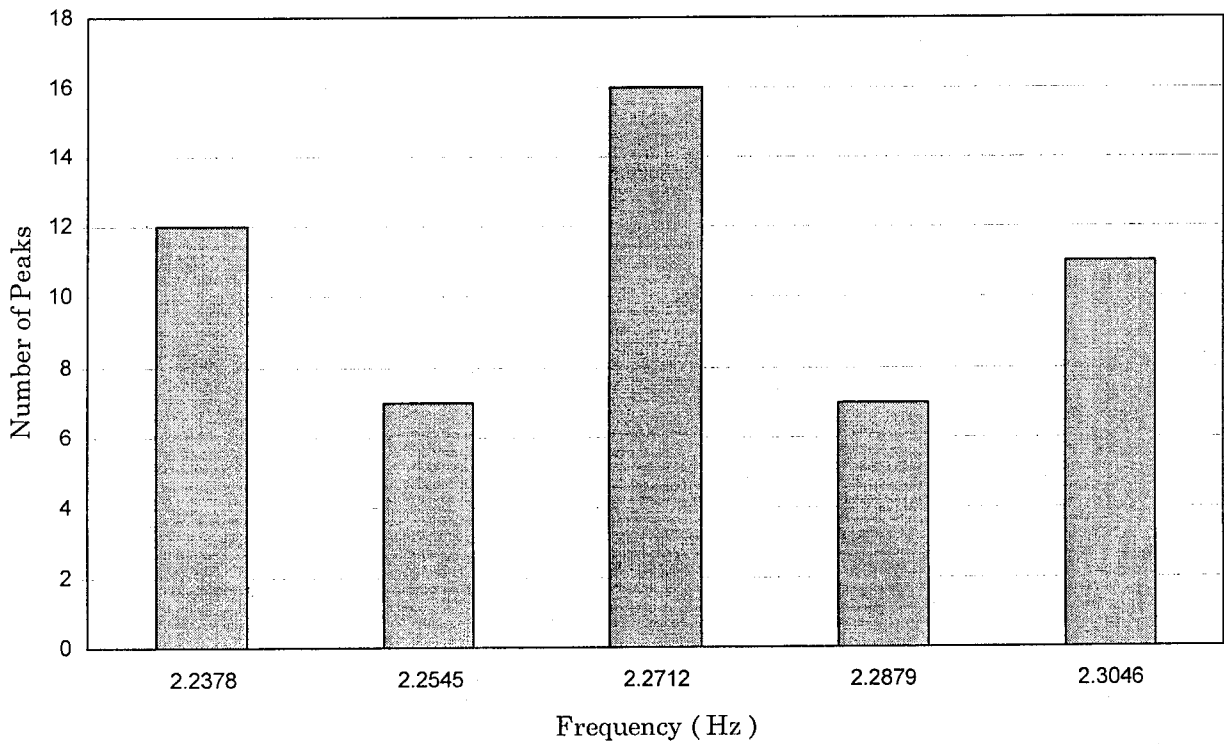


Figure 3.13b Peak Comparison for the Sixth Vertical Mode

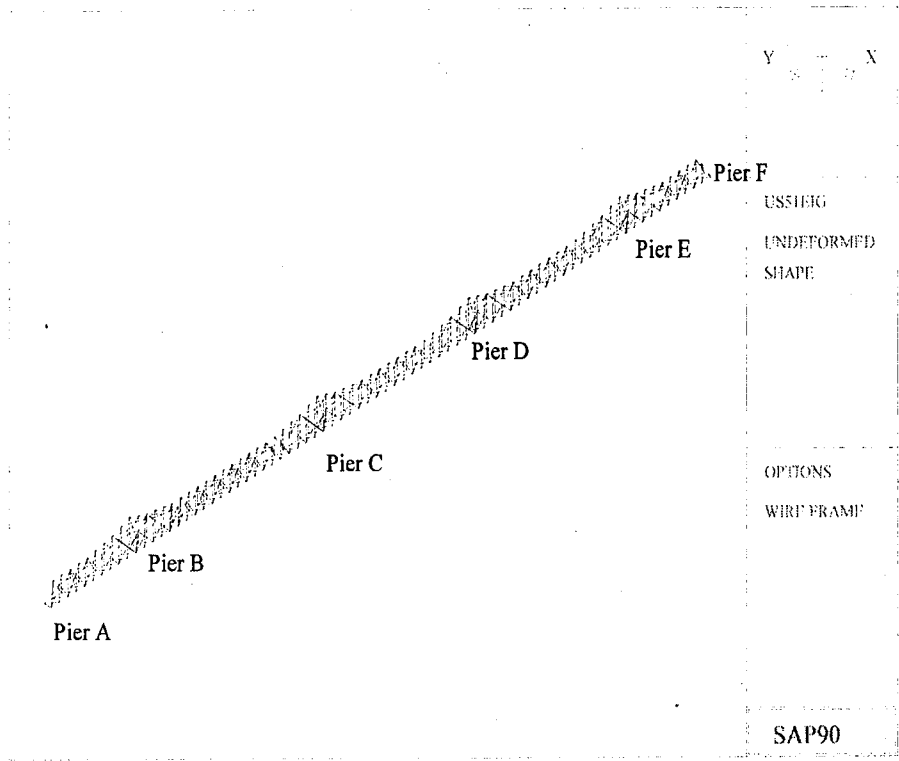
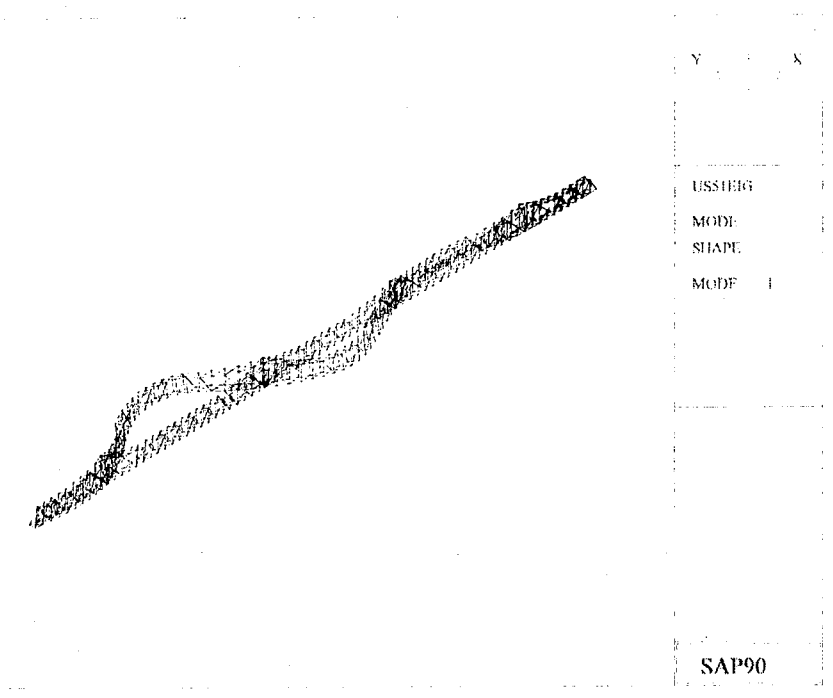
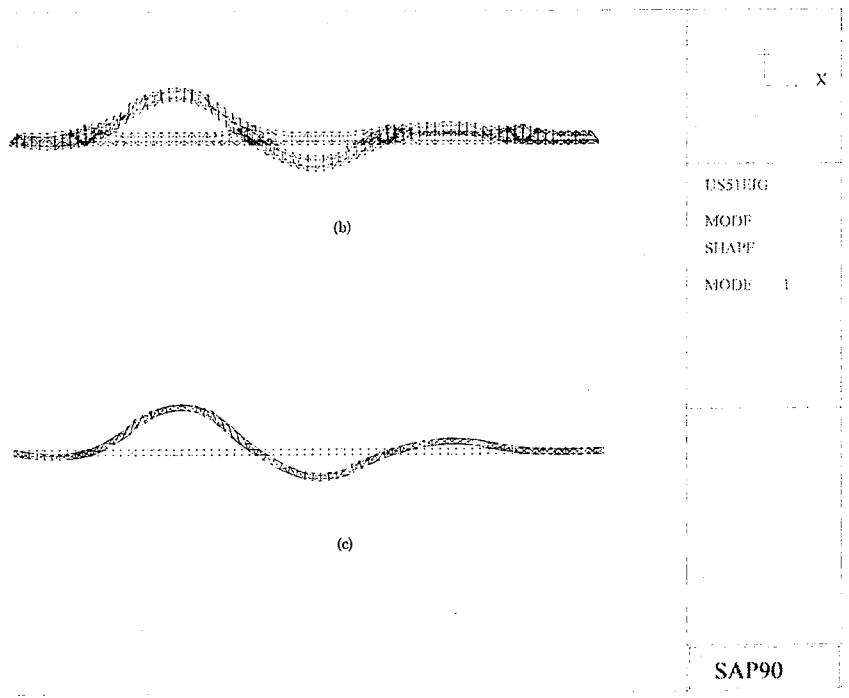


Figure 4.1 3D Finite Element Model of the Ohio River Bridge on US51



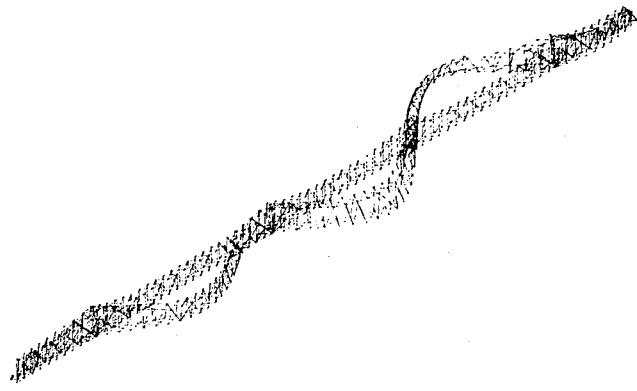
(a)



(b)

(c)

Figure 4.2 Mode Shape of the First Natural Frequency (0.3831 Hz)
 (a) Isometric View (b) Elevation View (c) Plan View



(a)



(b)



(c)

Y X

USS11IG
 MODE
 SHAPE
 MODE 2

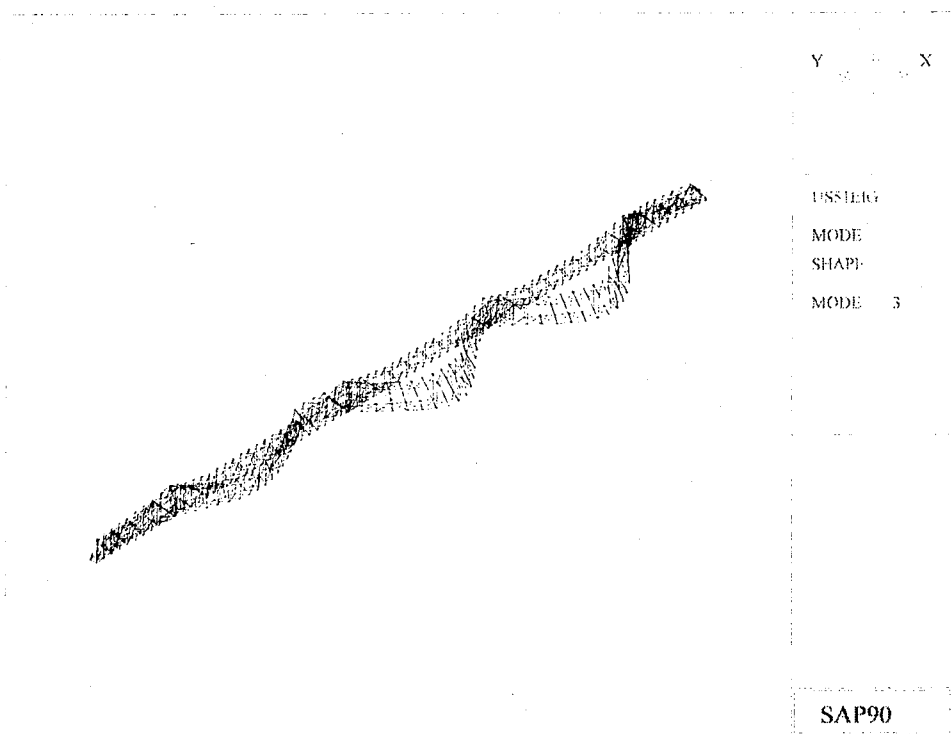
SAP90

Y X

USS11IG
 MODE
 SHAPE
 MODE 2

SAP90

Figure 4.3 Mode Shape of the Second Natural Frequency (0.5017 Hz)
 (a) Isometric View, (b) Elevation View and (c) Plan View



(a)



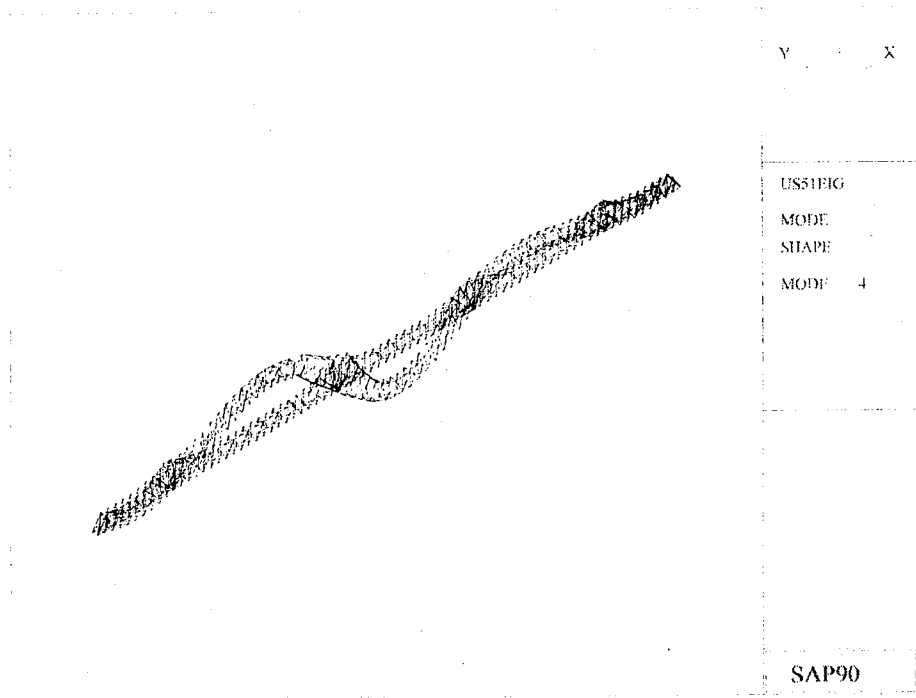
(b)



(c)

SAP90

Figure 4.4 Mode Shape of the Third Natural Frequency (0.6206 Hz)
 (a) Isometric View, (b) Elevation View, and (c) Plan View



(a)

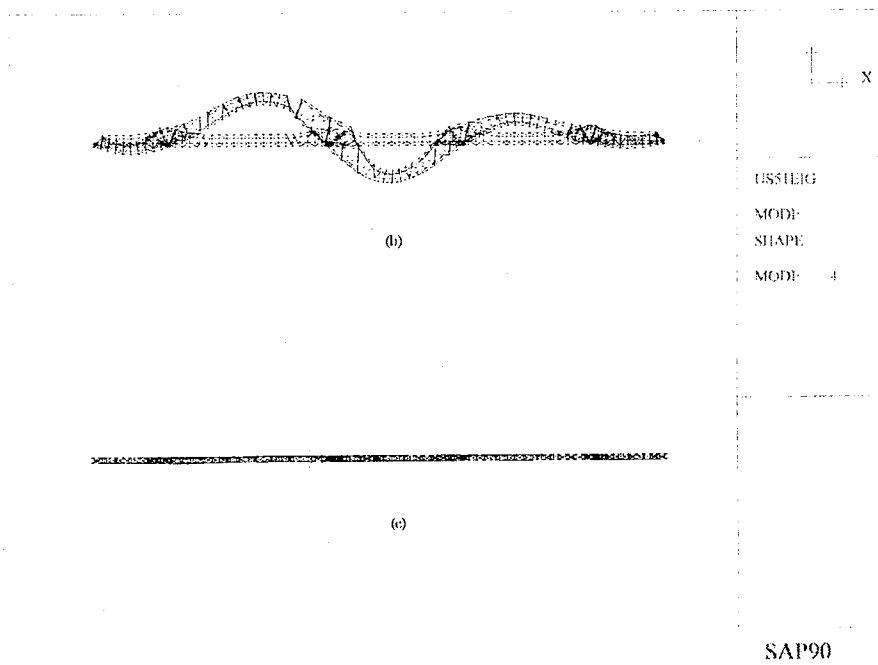


Figure 4.5 Mode Shape of the Fourth Natural Frequency (0.7578 Hz)
 (a) Isometric View, (b) Elevation View, and (c) Plan View

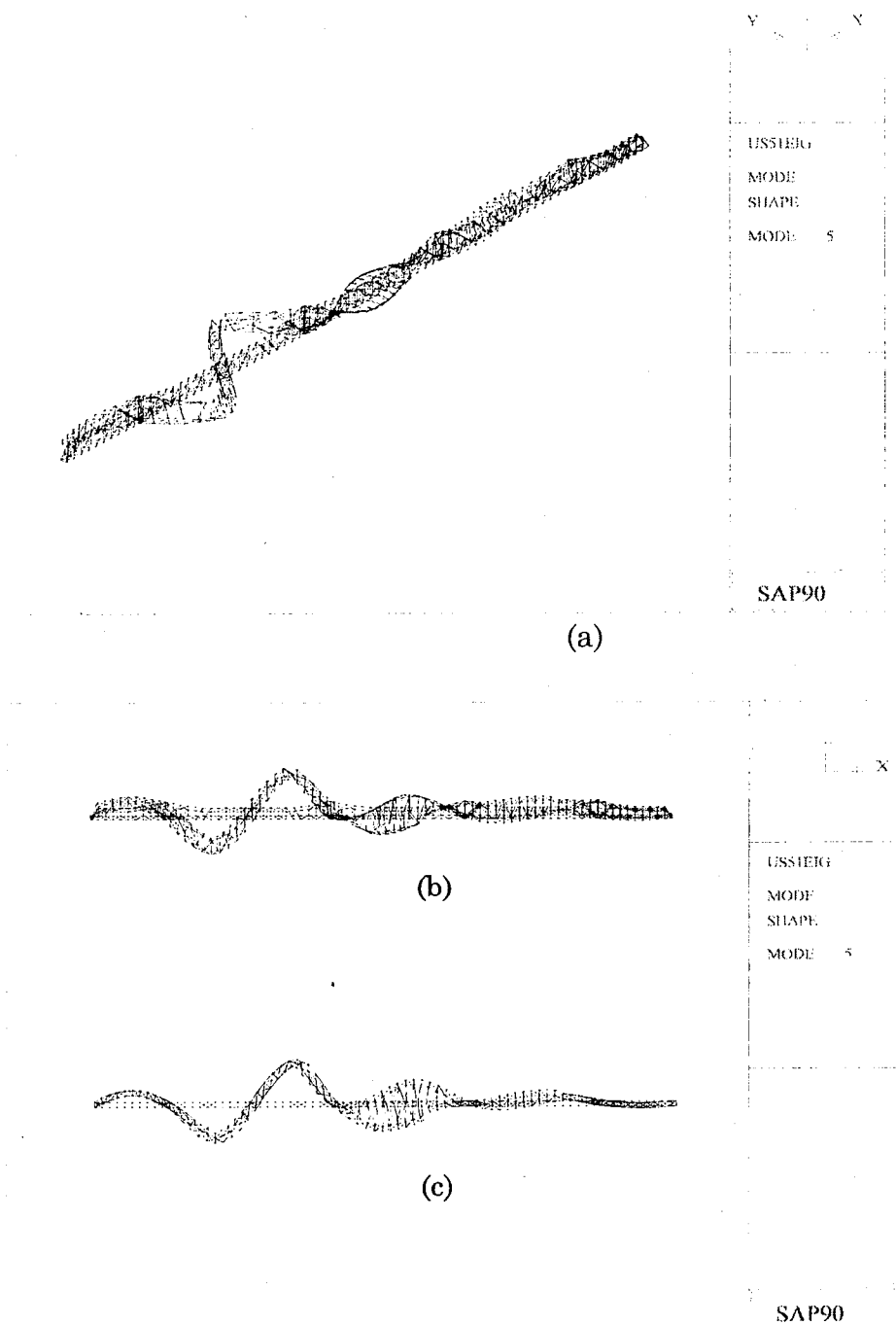
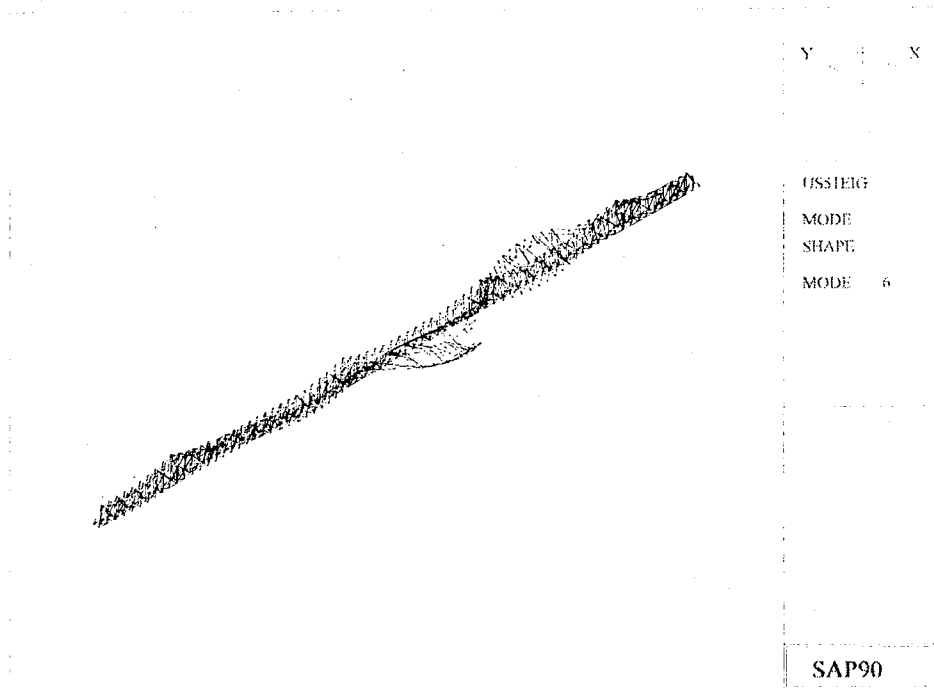
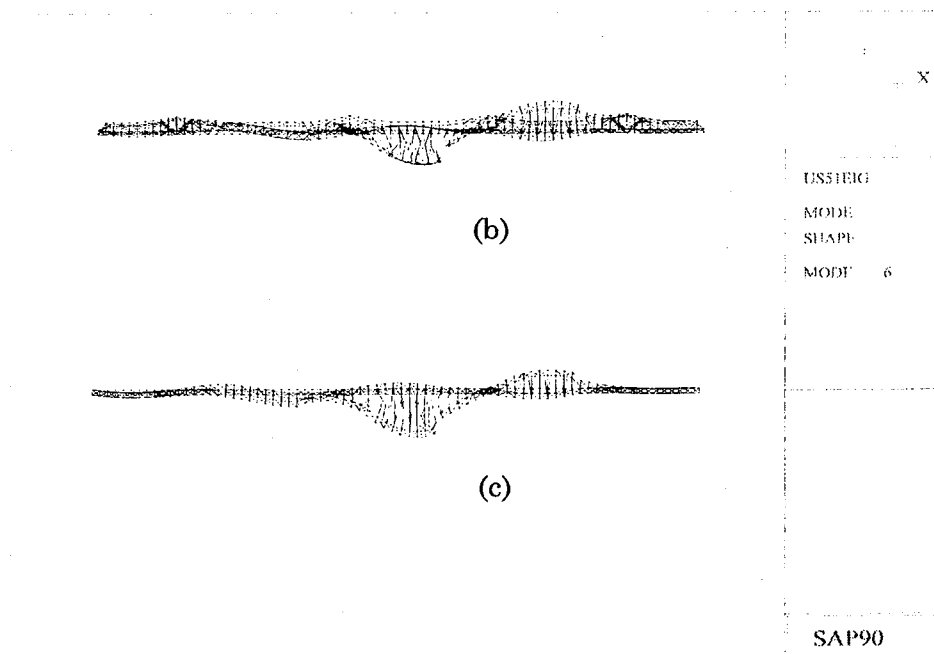


Figure 4.6 Mode Shape of the Fifth Natural Frequency (0.9147 Hz)
 (a) Isometric View, (b) Elevation View, and (c) Plan View



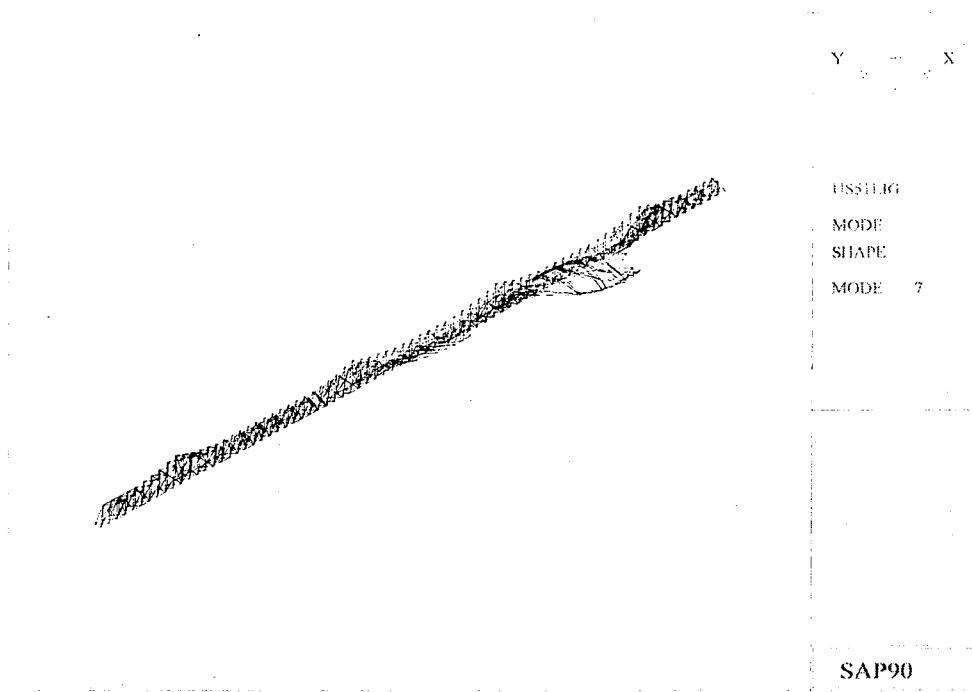
(a)



(b)

(c)

Figure 4.7 Mode Shape of the Sixth Natural Frequency (0.9725 Hz)
(a) Isometric View, (b) Elevation View, and (c) Plan View



(a)

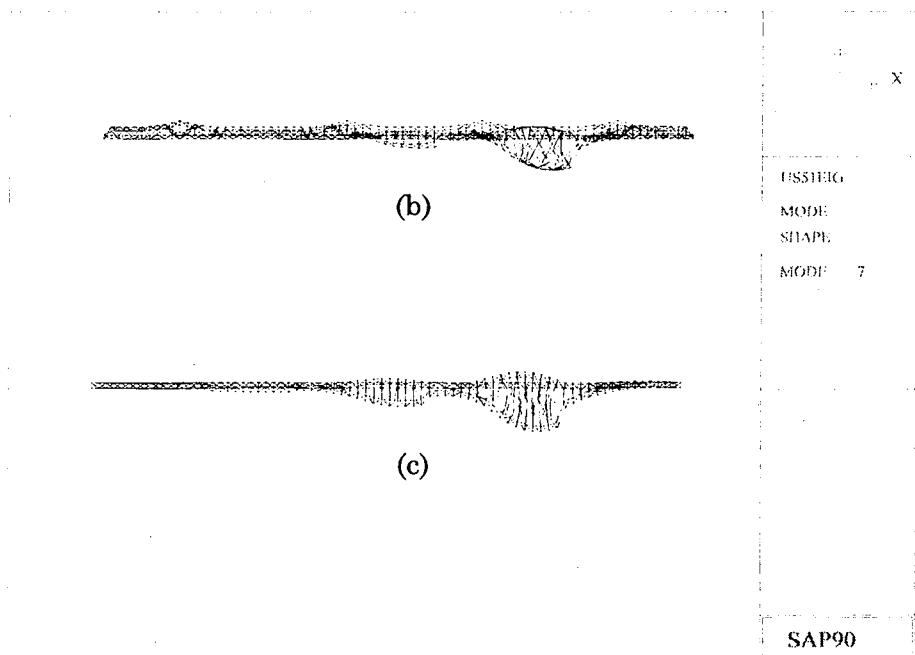
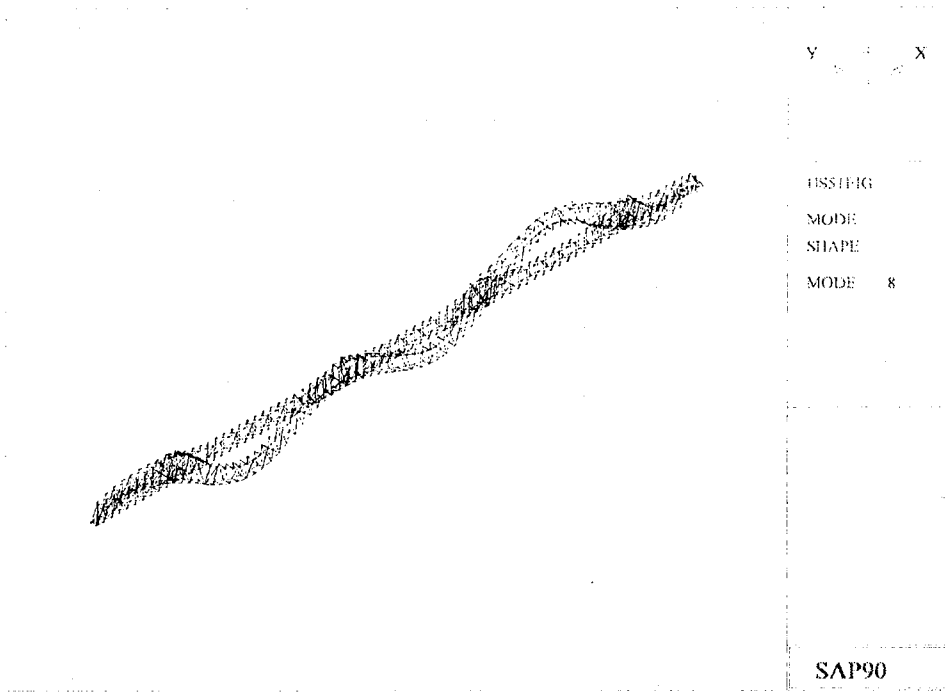
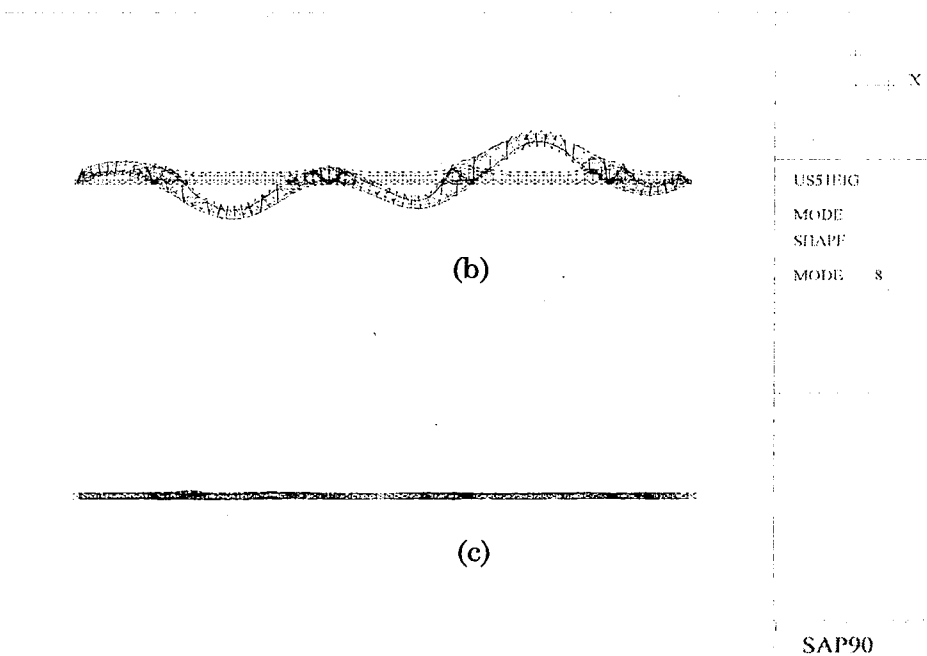


Figure 4.8 Mode Shape of the Seventh Natural Frequency (0.993 Hz)
 (a) Isometric View, (b) Elevation View, and (c) Plan View



(a)



(b)

(c)

Figure 4.9 Mode Shape of the Eighth Natural Frequency (1.072 Hz)
 (a) Isometric View, (b) Elevation View, and (c) Plan View

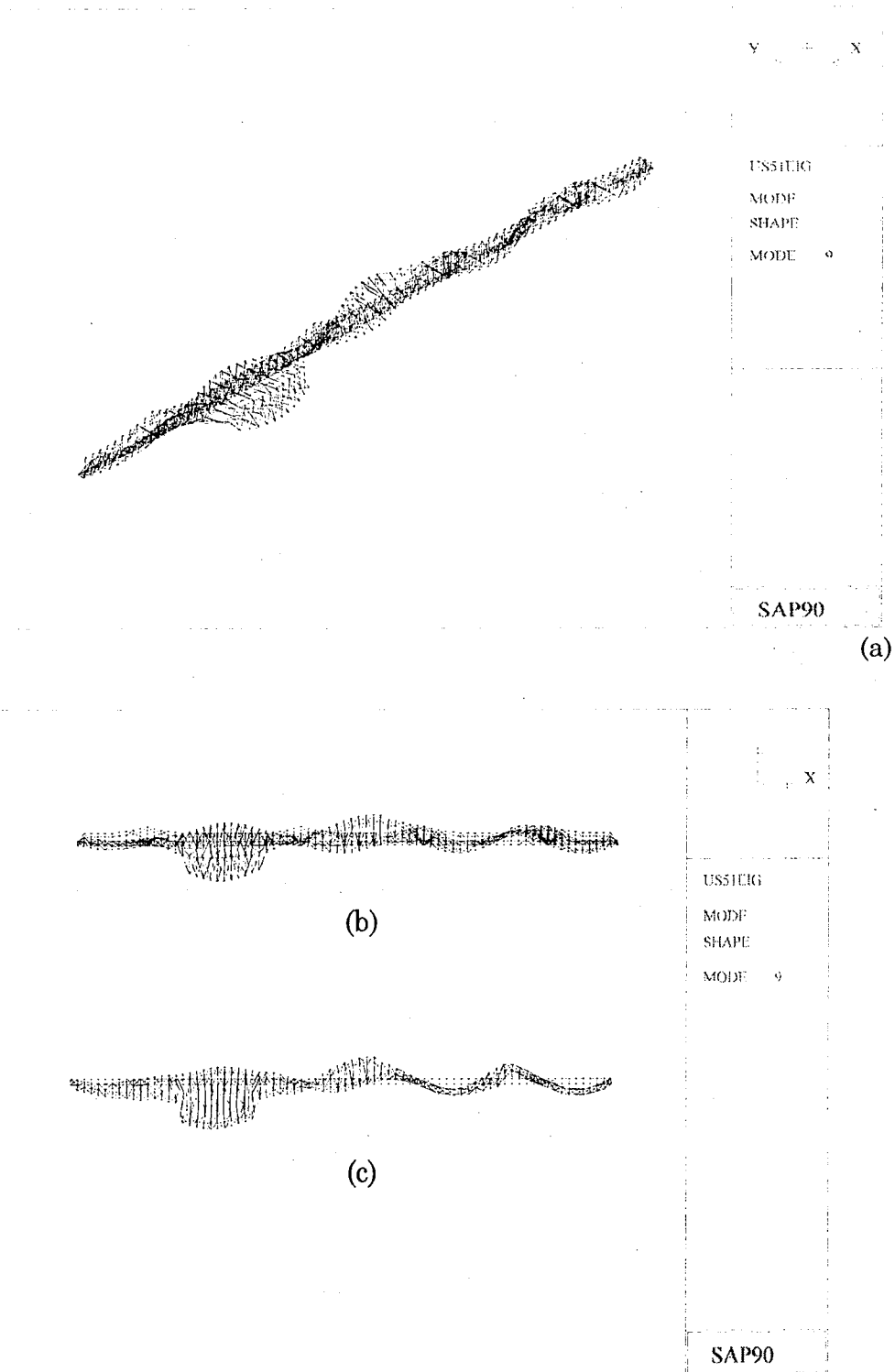


Figure 4.10 Mode Shape of the Ninth Natural Frequency (1.1318 Hz)
 (a) Isometric View, (b) Elevation View, and (c) Plan View

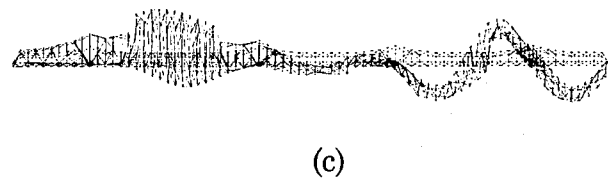
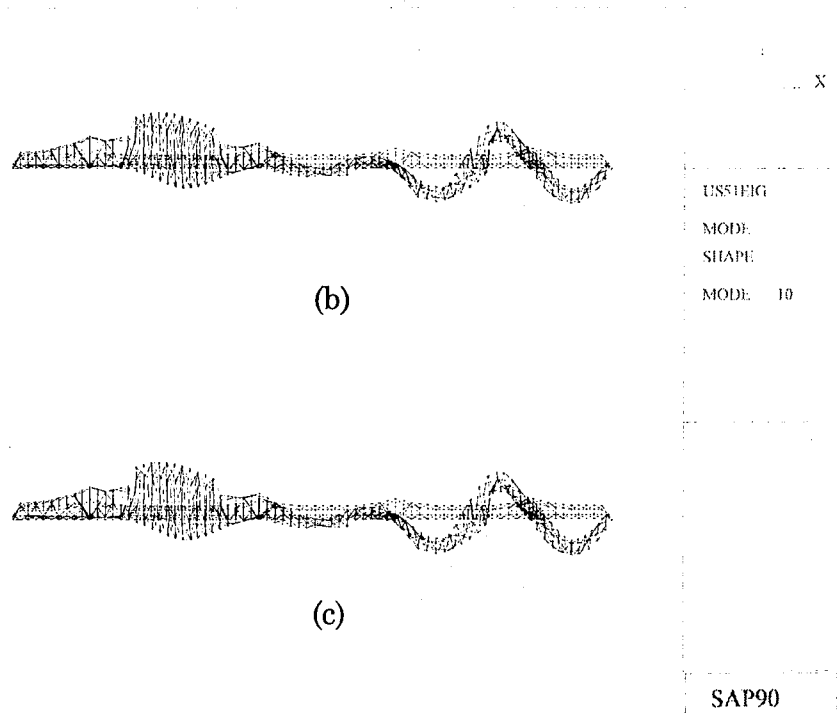
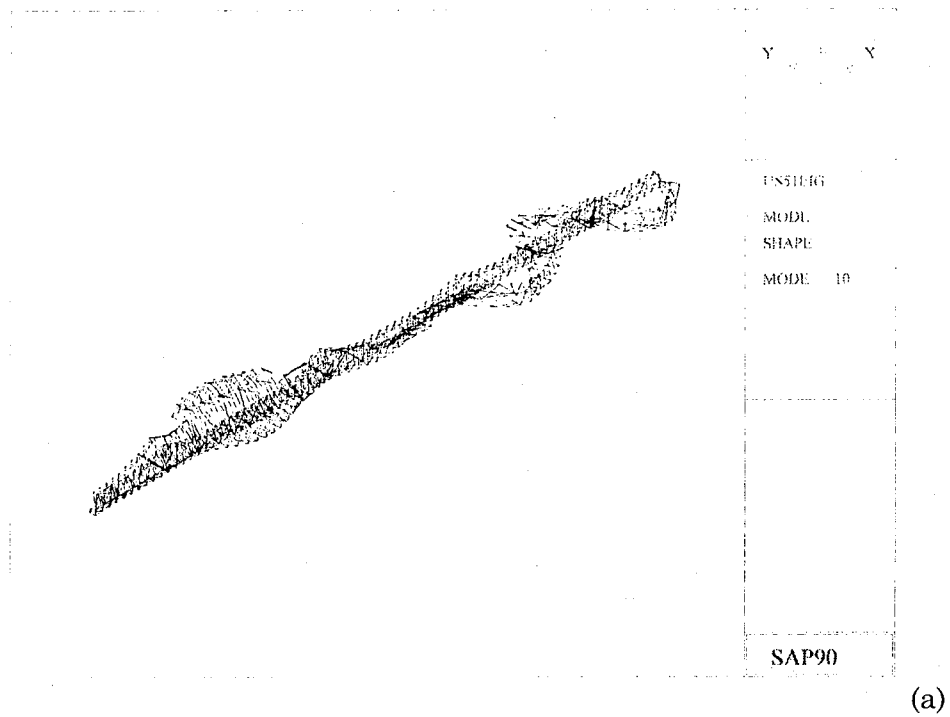


Figure 4.11 Mode Shape of the Tenth Natural Frequency (1.1435 Hz)
 (a) Isometric View, (b) Elevation View, and (c) Plan View

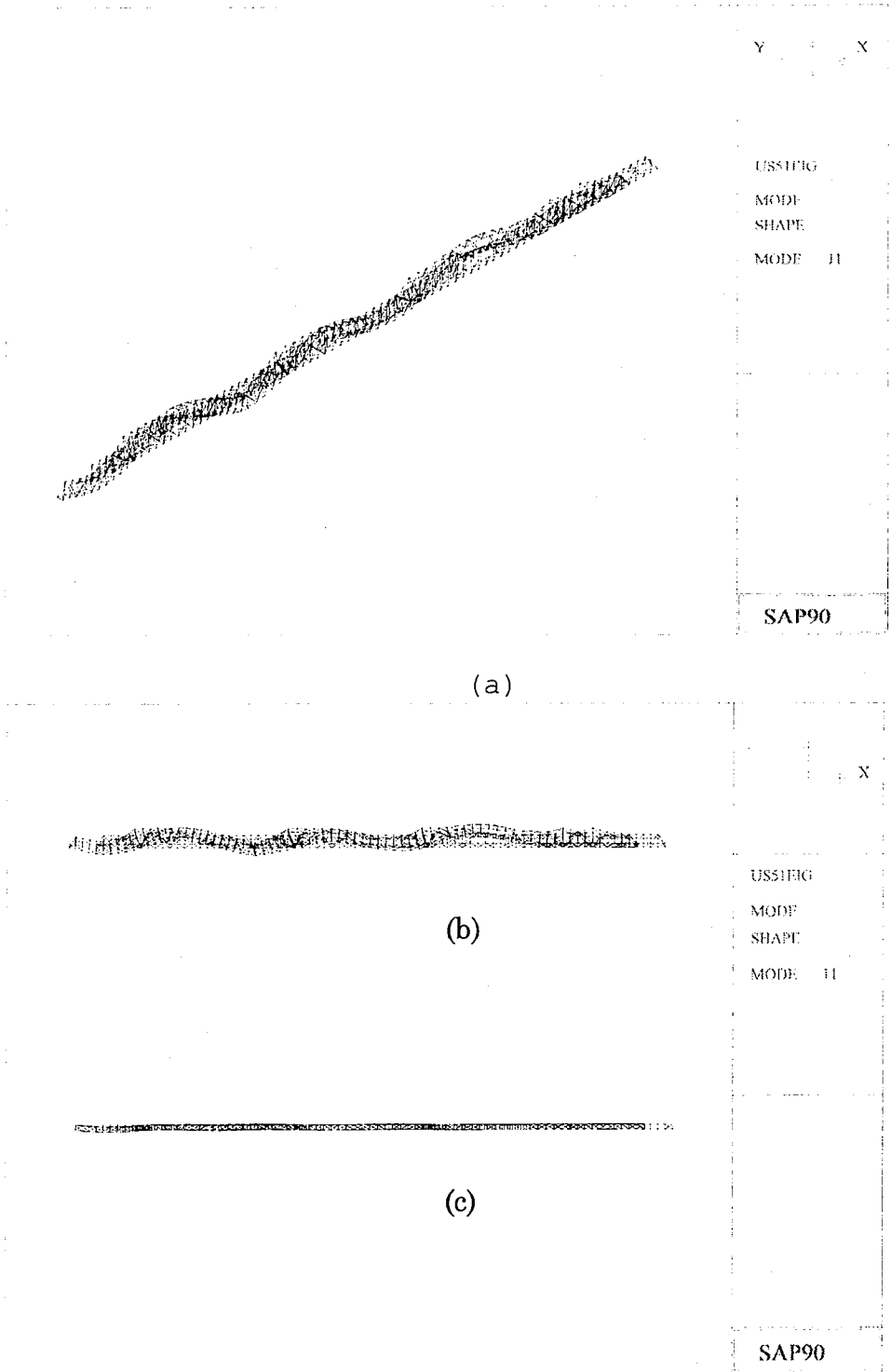


Figure 4.12 Mode Shape of the Eleventh Natural Frequency (1.2812 Hz)
 (a) Isometric View, (b) Elevation View, and (c) Plan View

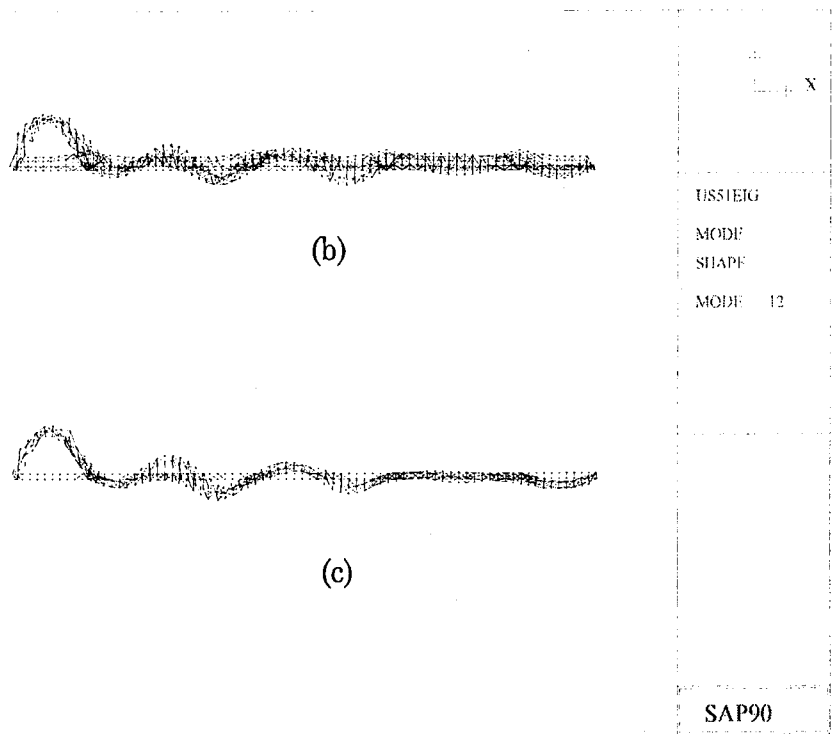
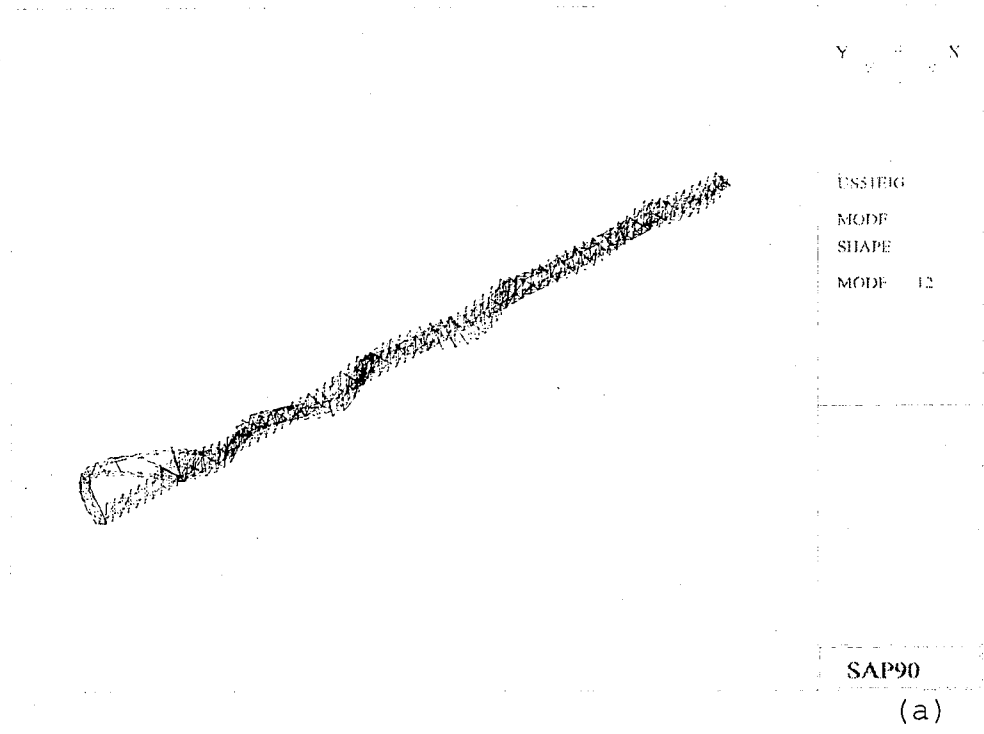
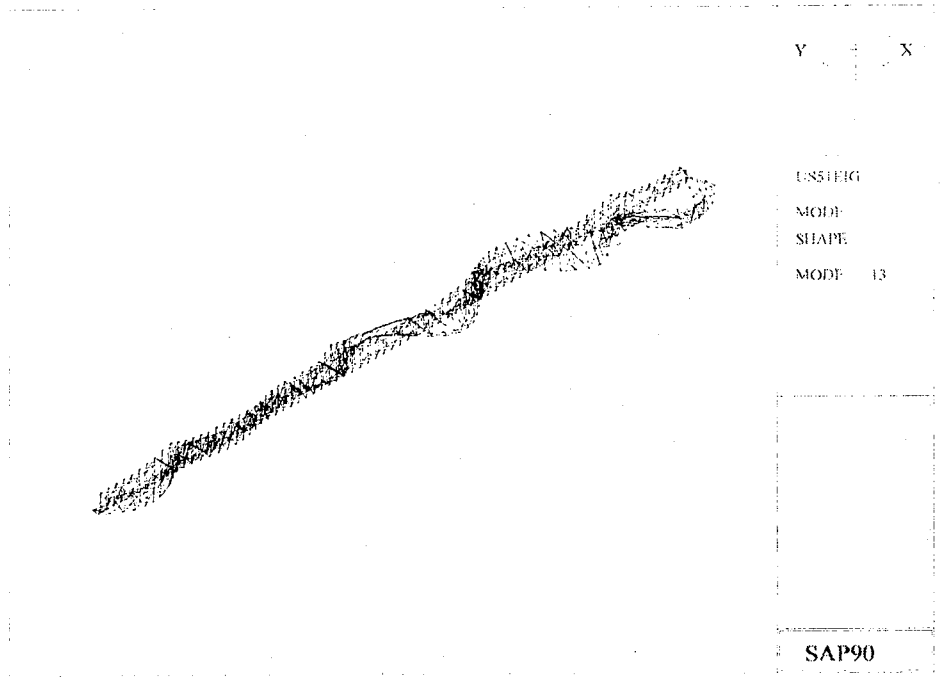
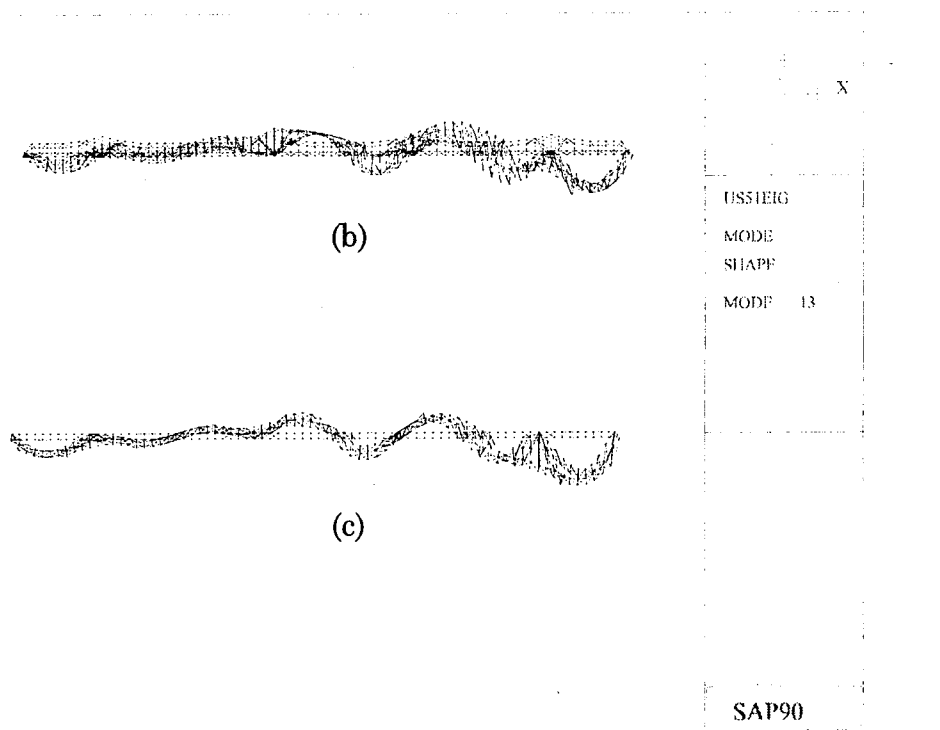


Figure 4.13 Mode Shape of the Twelveth Natural Frequency (1.2866 Hz)
 (a) Isometric View, (b) Elevation View, and (c) Plan View



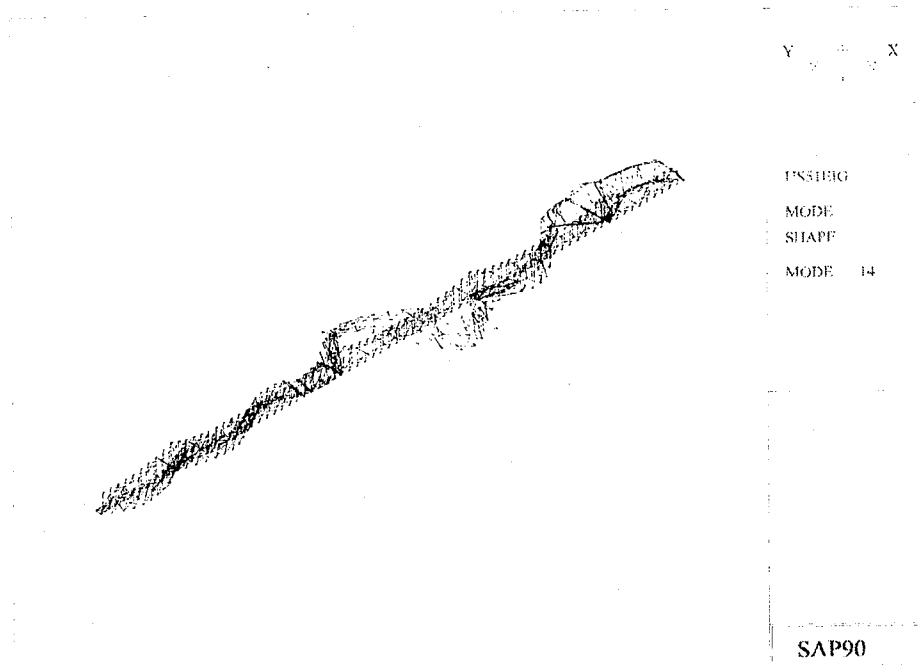
(a)



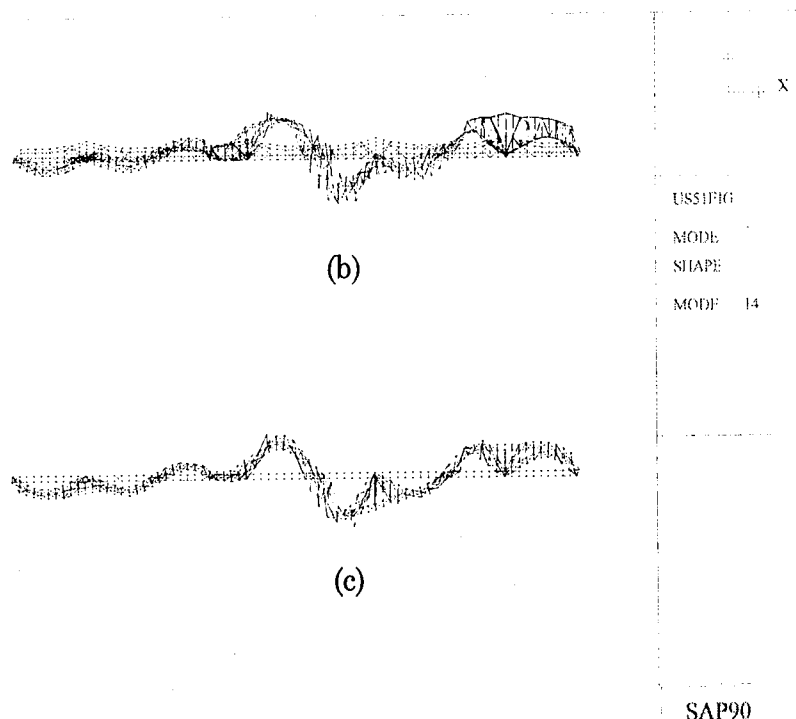
(b)

(c)

Figure 4.14 Mode Shape of the Thirteenth Natural Frequency (1.3279 Hz)
 (a) Isometric View, (b) Elevation View, and (c) Plan View



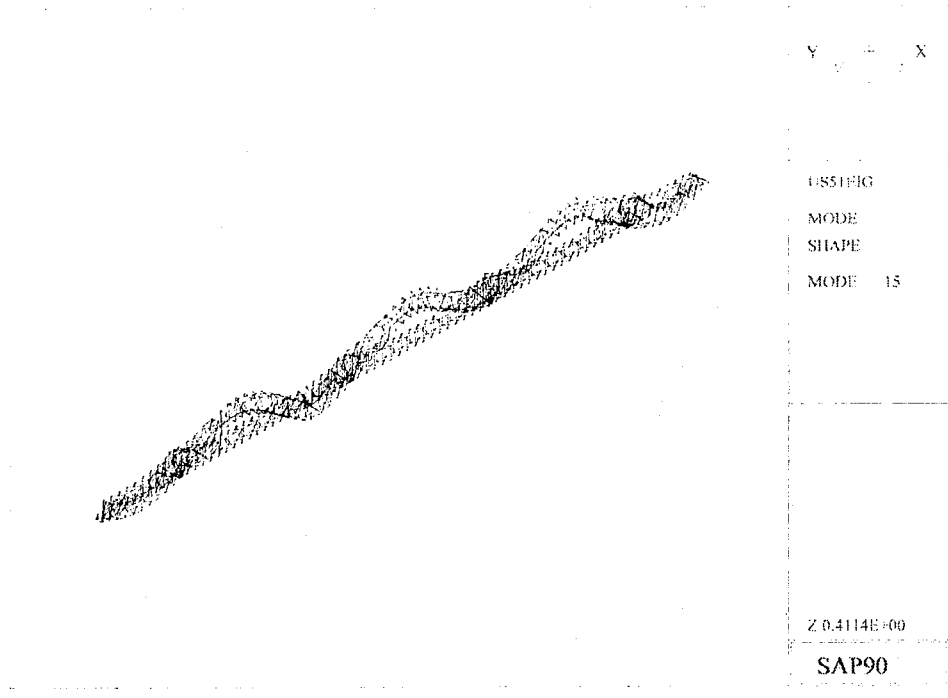
(a)



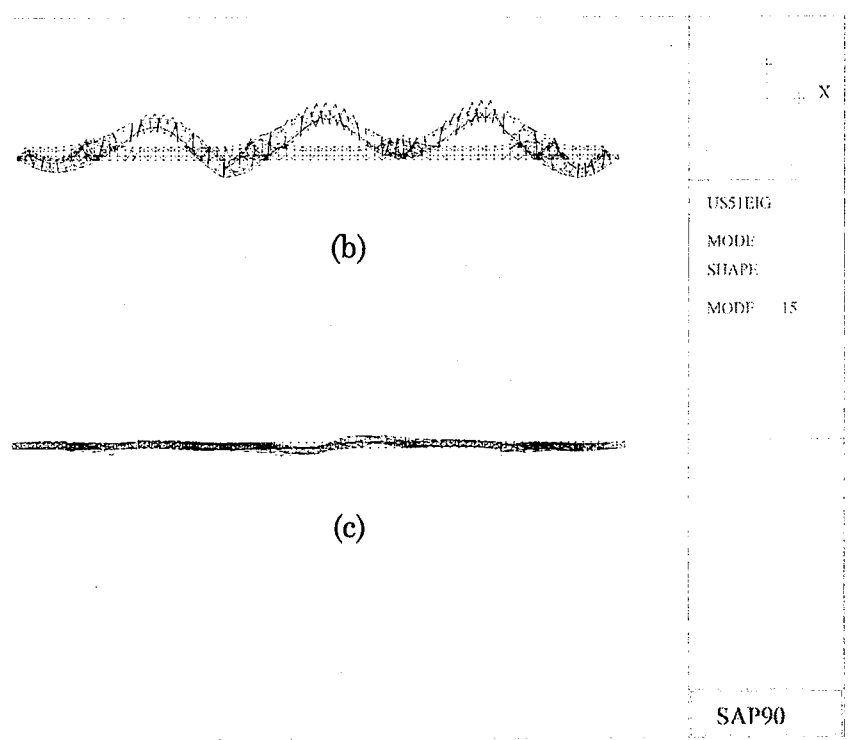
(b)

(c)

Figure 4.15 Mode Shape of the Fourteenth Natural Frequency (1.3849 Hz)
 (a) Isometric View, (b) Elevation View, and (c) Plan View



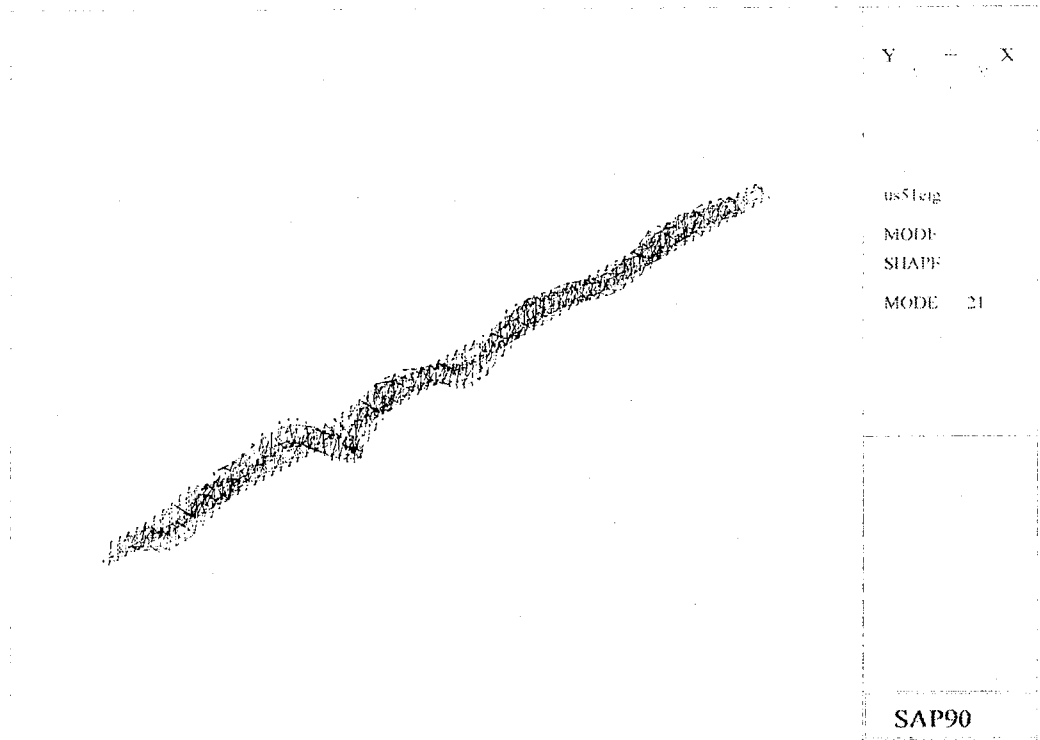
(a)



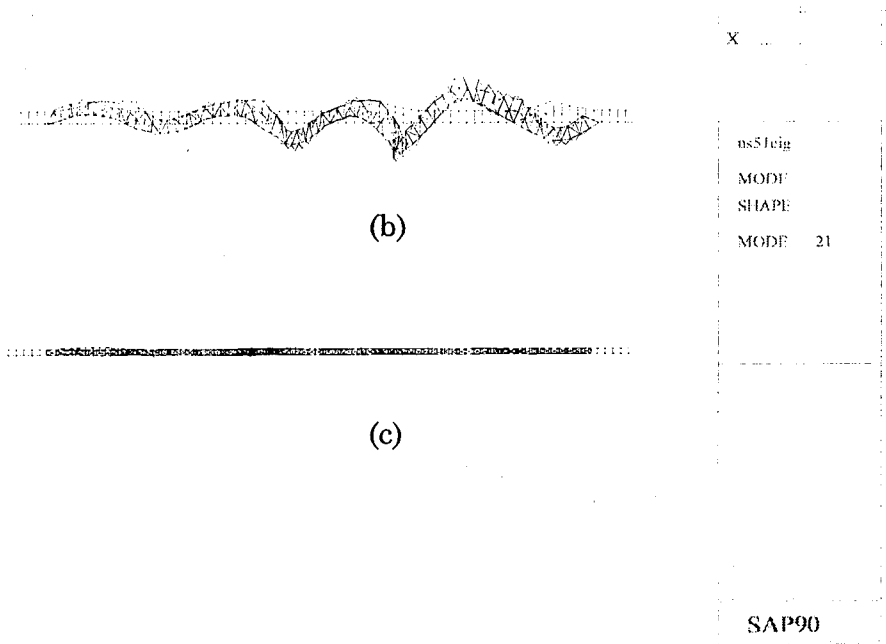
(b)

(c)

Figure 4.16 Mode Shape of the Fifteenth Natural Frequency (1.3978 Hz)
 (a) Isometric View, (b) Elevation View, and (c) Plan View



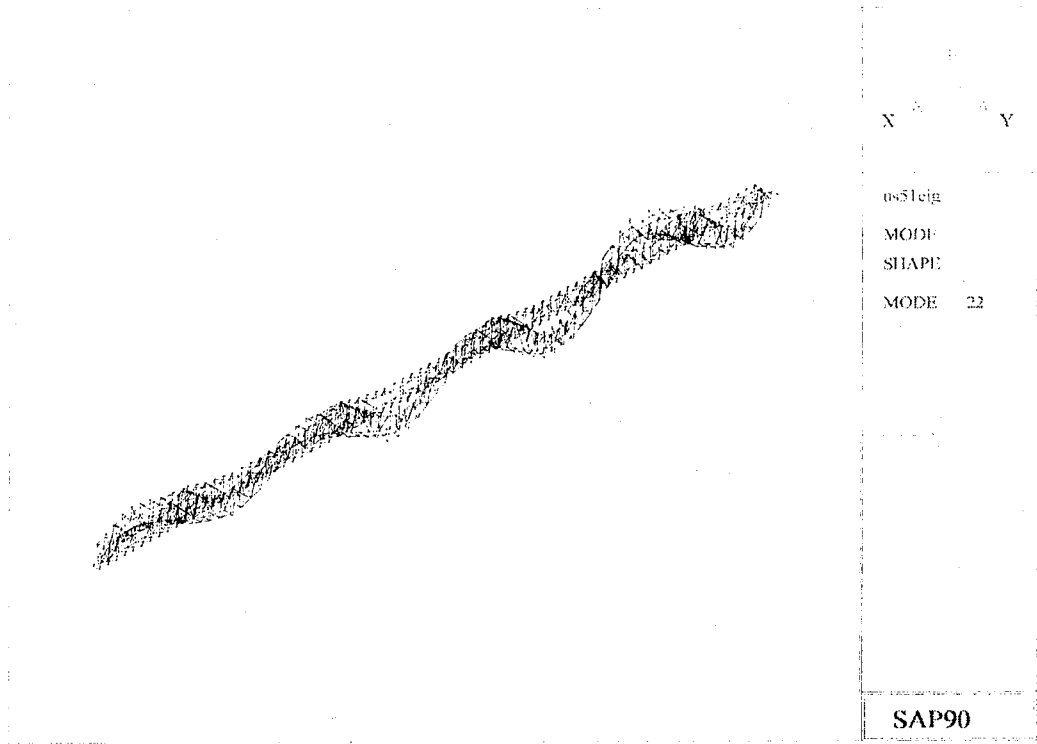
(a)



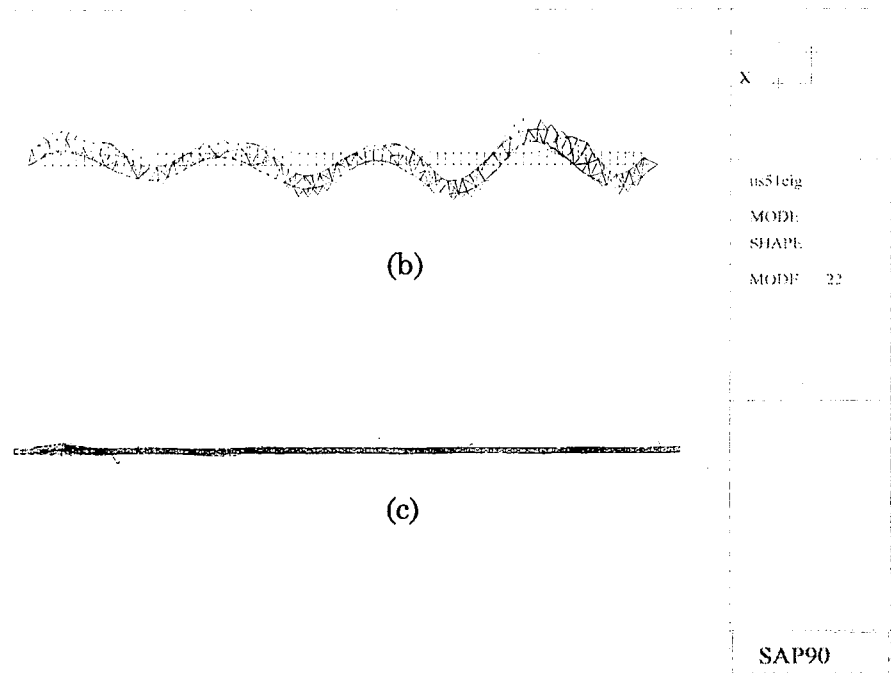
(b)

(c)

Figure 4.17 Mode Shape of the 21st Natural Frequency (1.8848 Hz)
 (a) Isometric View, (b) Elevation View, and (c) Plan View



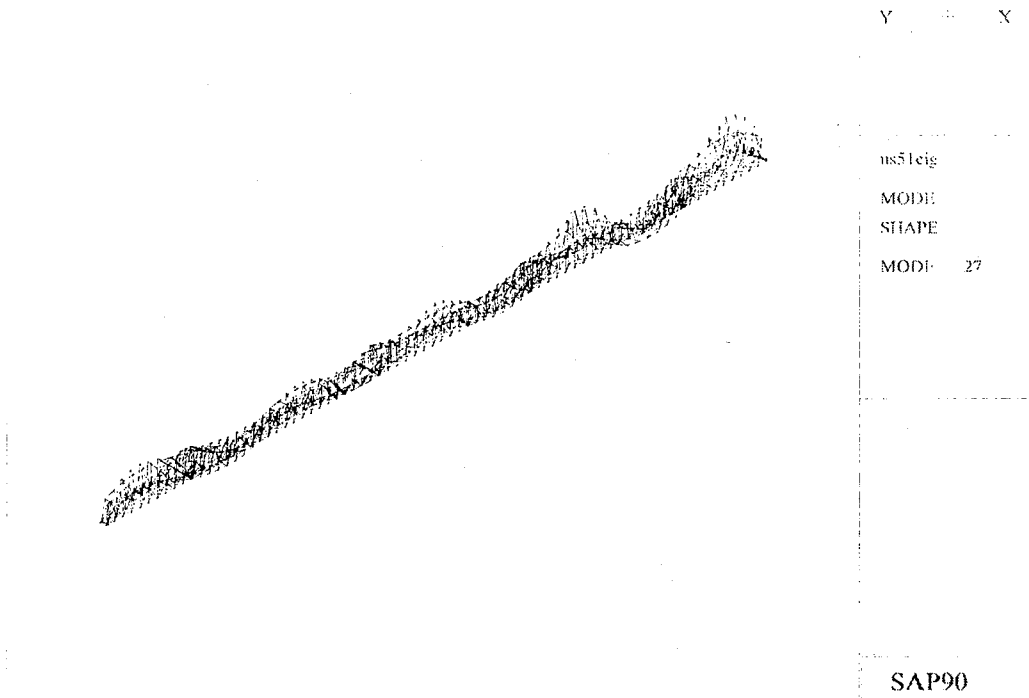
(a)



(b)

(c)

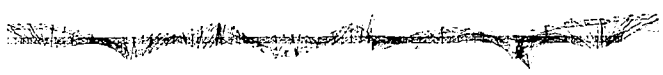
Figure 4.18 Mode Shape of the 22nd Natural Frequency (1.9348 Hz)
 (a) Isometric View, (b) Elevation View, and (c) Plan View



(a)



(b)



(c)

ms51eig
MODE
SHAPE
MODE 27

SAP90

Figure 4.19 Mode Shape of the 27th Natural Frequency (2.2327 Hz)
 (a) Isometric View, (b) Elevation View, and (c) Plan View

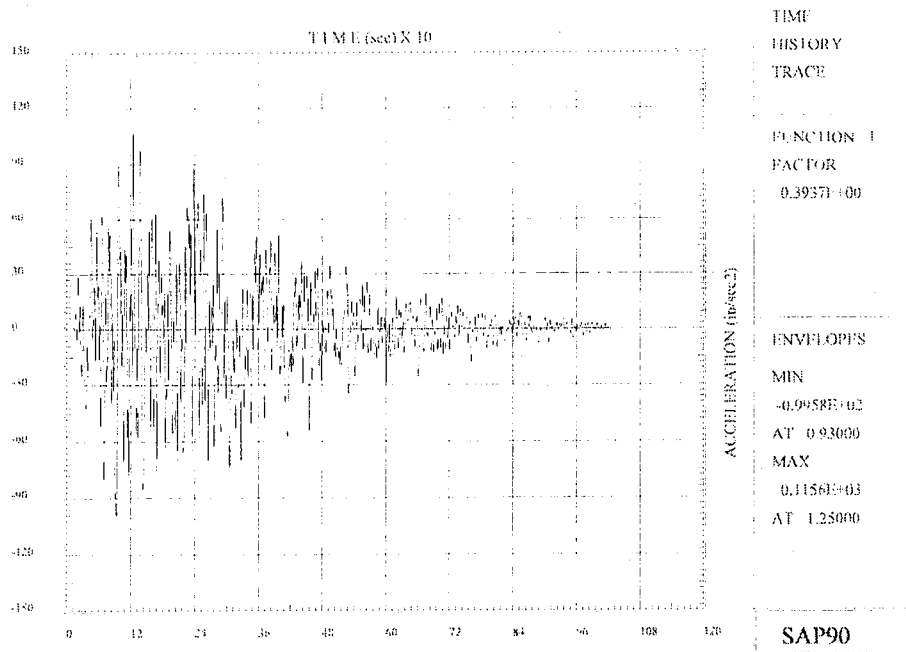


Figure 5.2 Acceleration-Time History in the Horizontal Direction (Direction 1) for the 50-year Earthquake

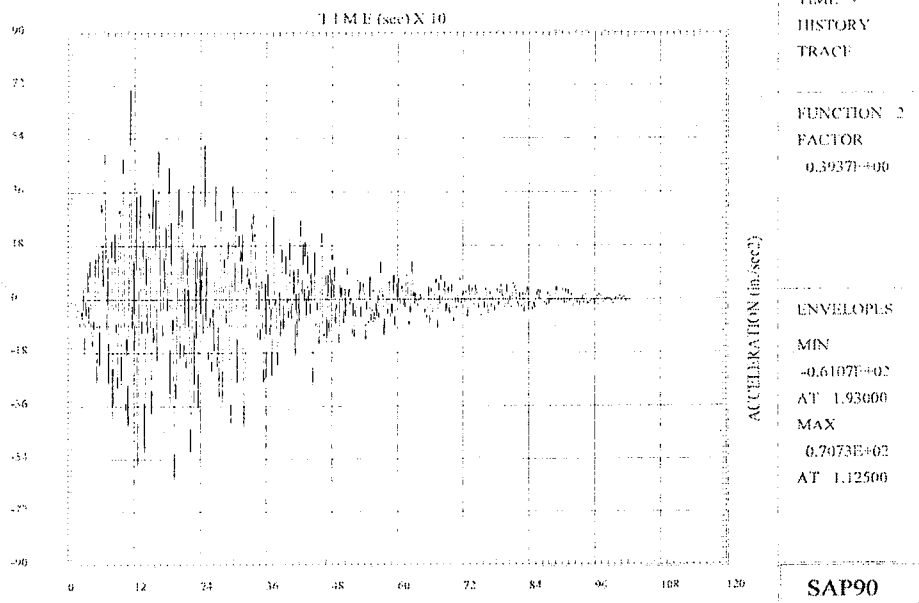


Figure 5.3 Acceleration-Time History in the Transverse Direction (Direction 2) for the 50-Year Earthquake

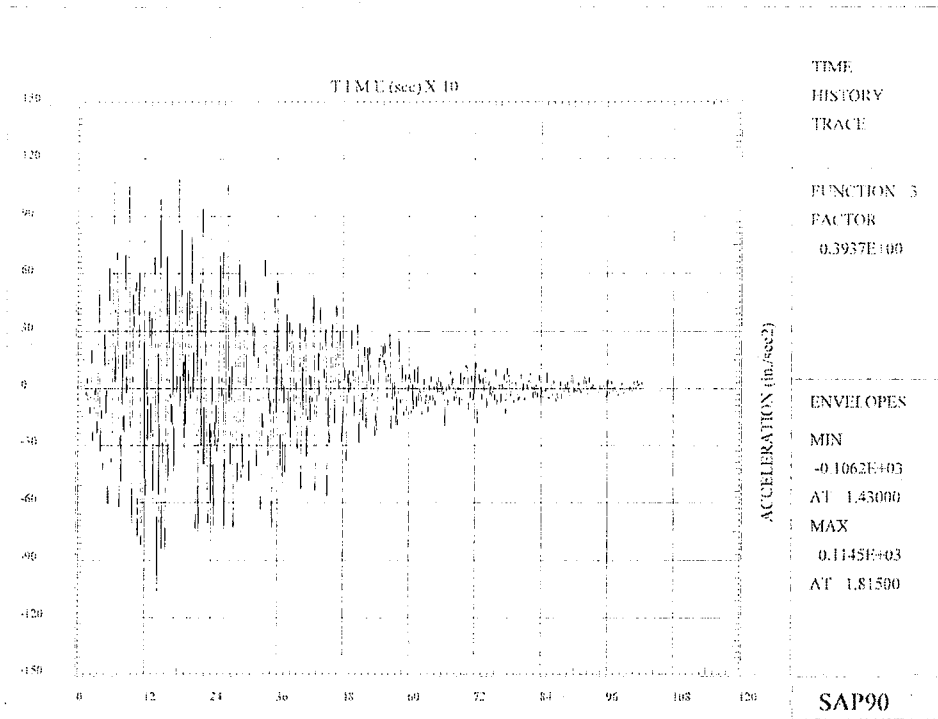


Figure 5.4 Acceleration-Time History in the Vertical Direction (Direction 3) for the 50-Year Earthquake

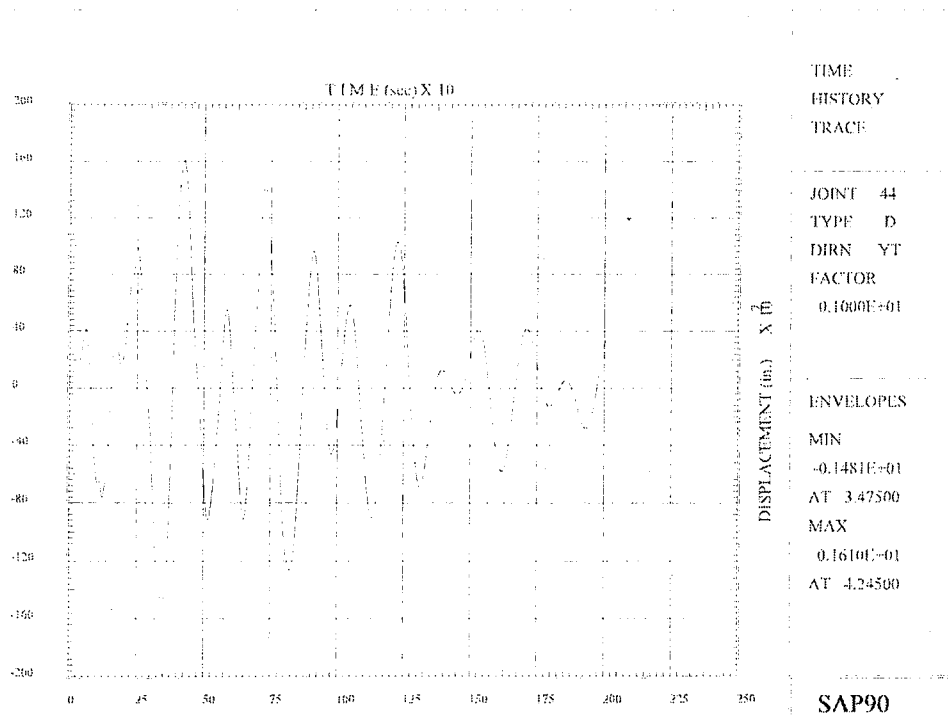


Figure 5.5 Displacement-Time History in the Transverse Direction at Node 44 for L1T2V3 Excitation Case

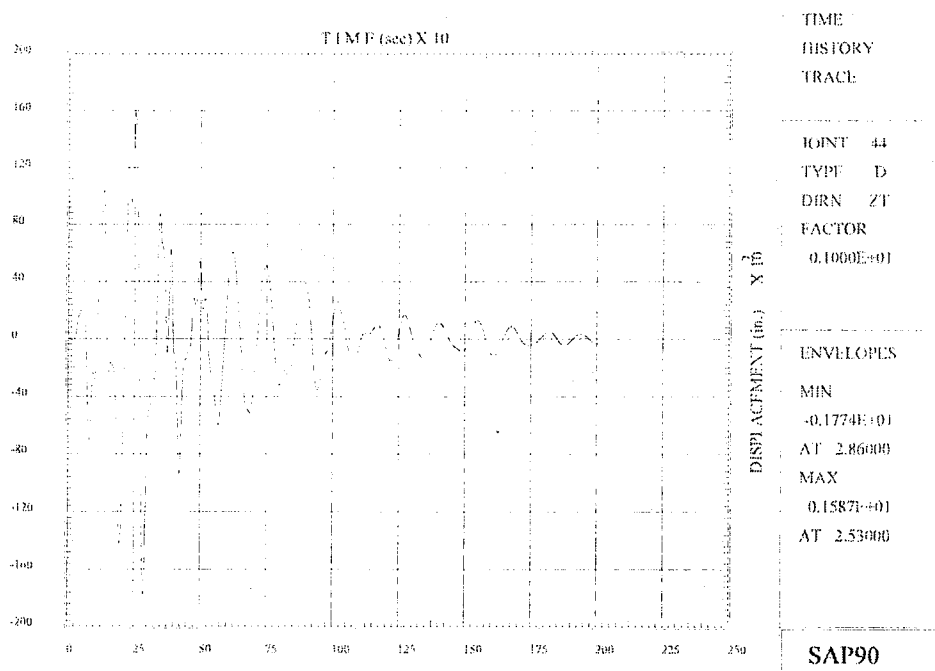


Figure 5.6 Displacement-Time History in the Vertical Direction at Node 44 for L1T2V3 Excitation Case

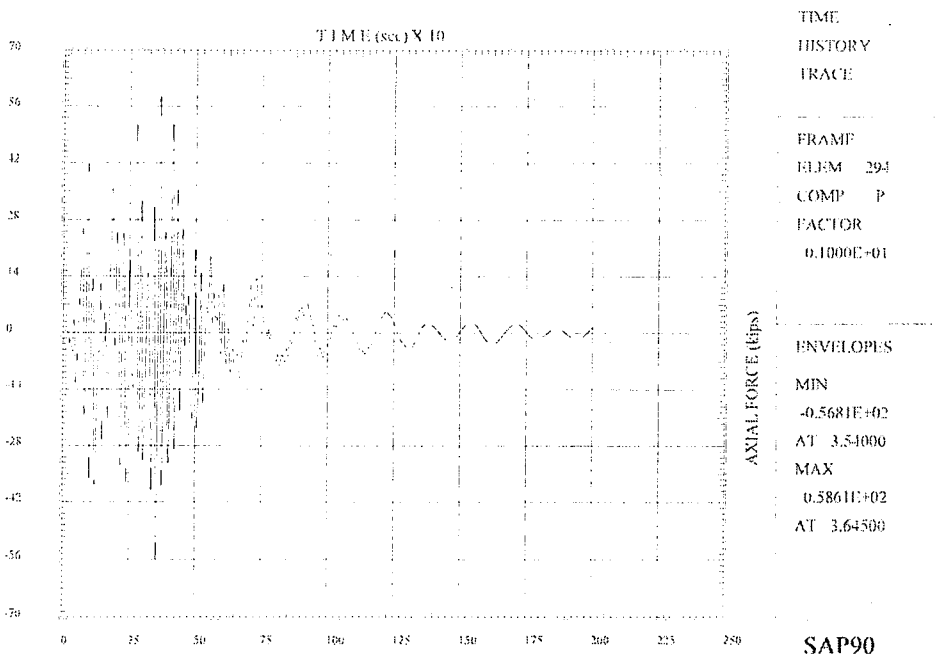
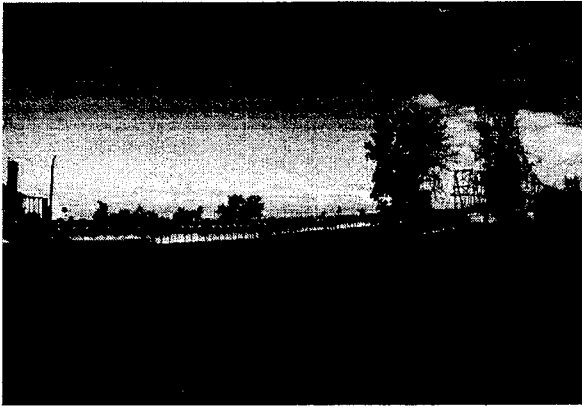
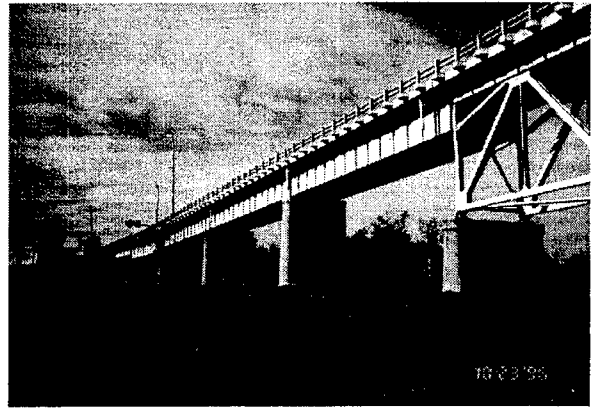


Figure 5.7 Axial Force-Time History for the Element 294 under L1T2V3 Excitation Case



(a)



(b)

Figures 6.1(a)-(b). Different Views of Illinois Approach



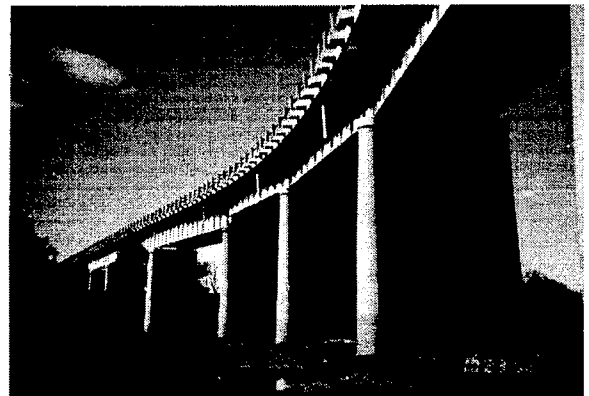
(a)



(b)



(c)



(d)

Figures 6.2(a)-(d). Different Views of Kentucky Approach

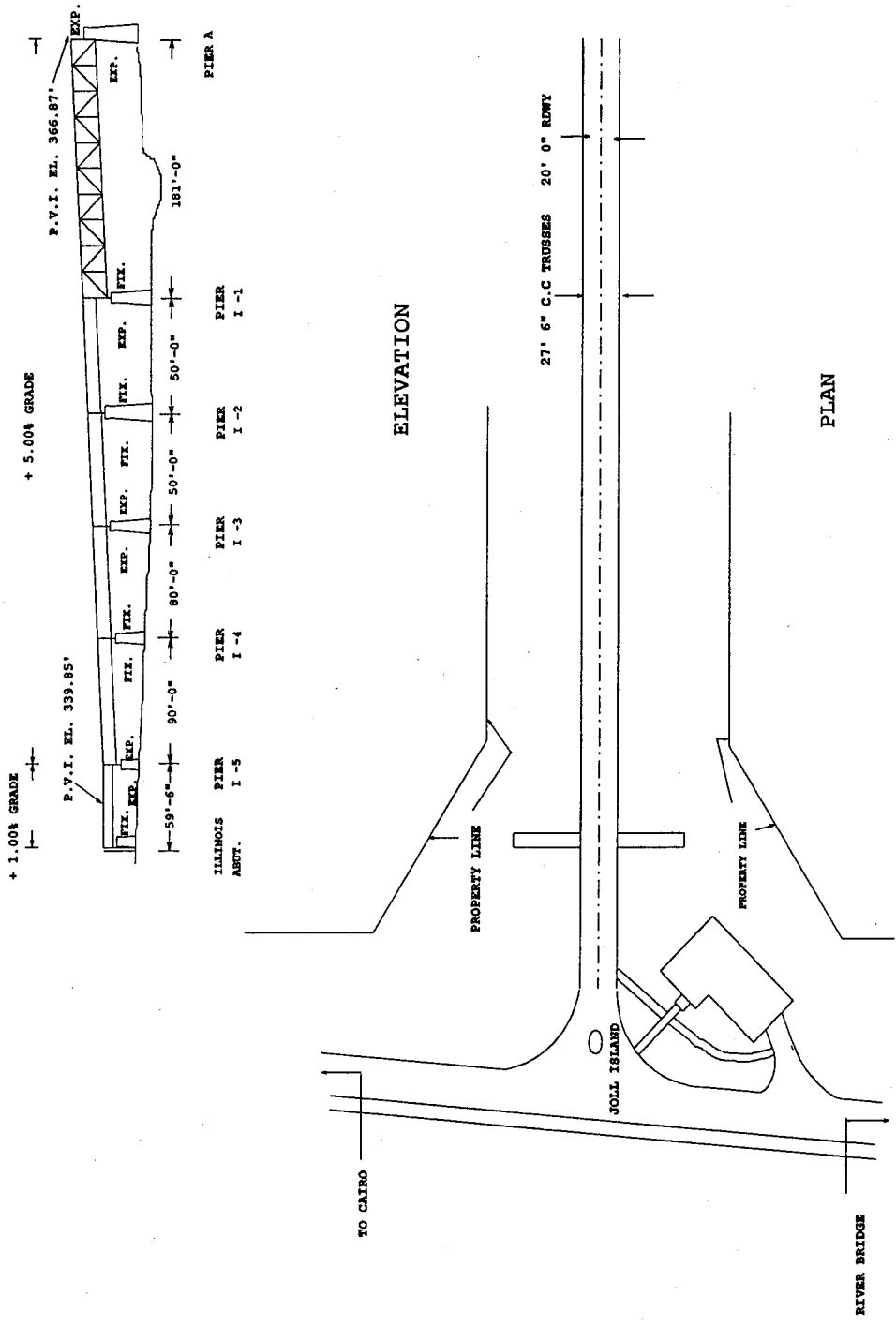


Figure 6.4 Elevation and Plan Views of the Illinois Approach

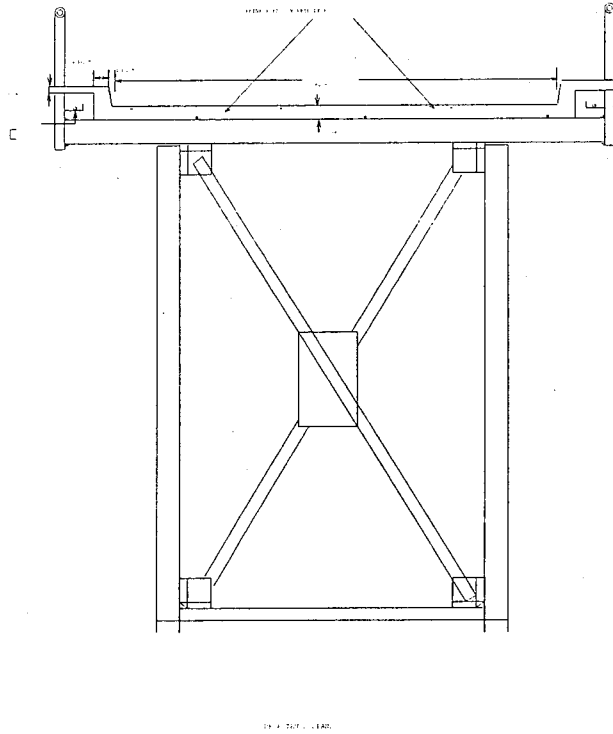


Figure 6.5 Cross Section of the Deck-Truss Type Approach Span

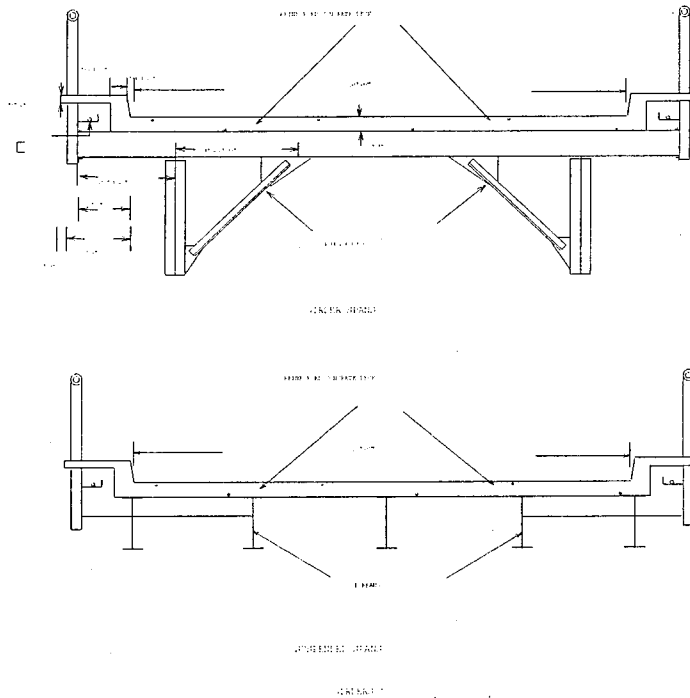


Figure 6.6 Cross Section of the Girder and Suspended Spans

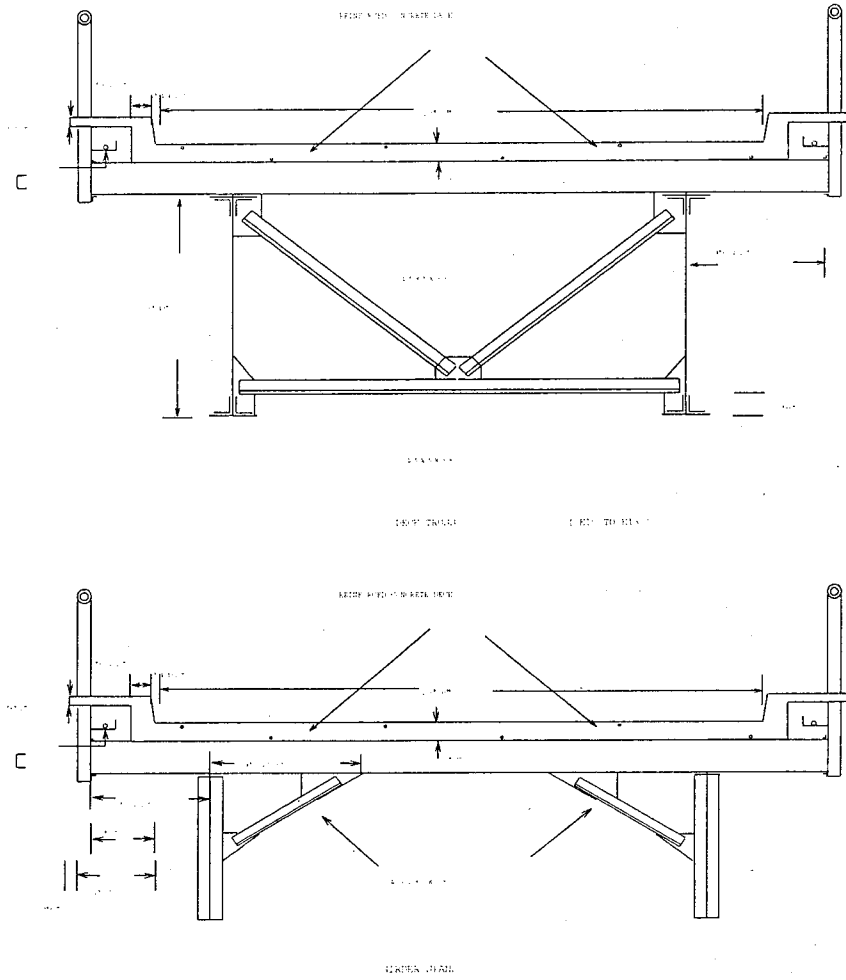


Figure 6.7 Details of the Deck-Truss Span (K10-K13)

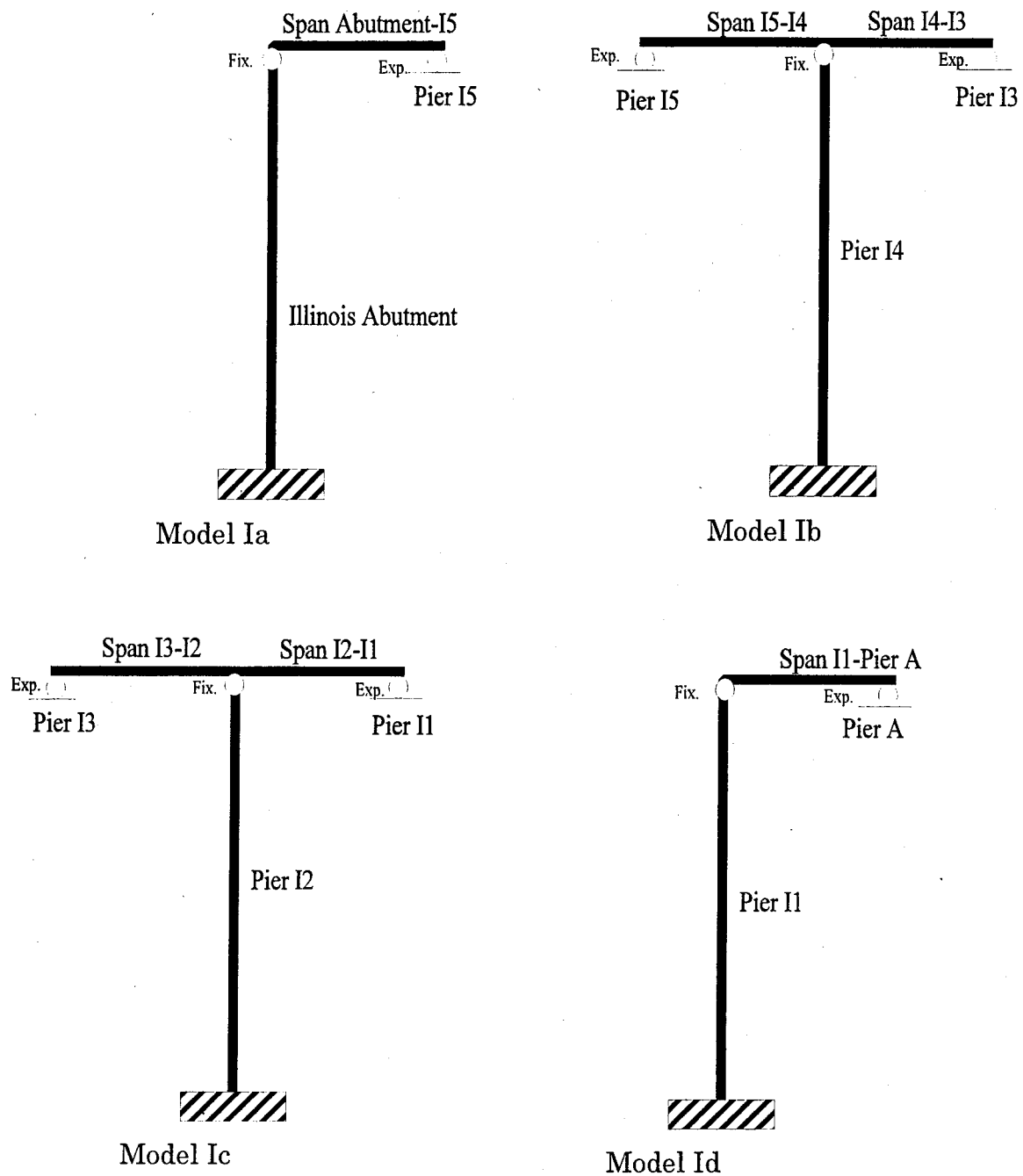


Figure 6.8 Structural Components for the SDOF Models of the Illinois Approach Spans

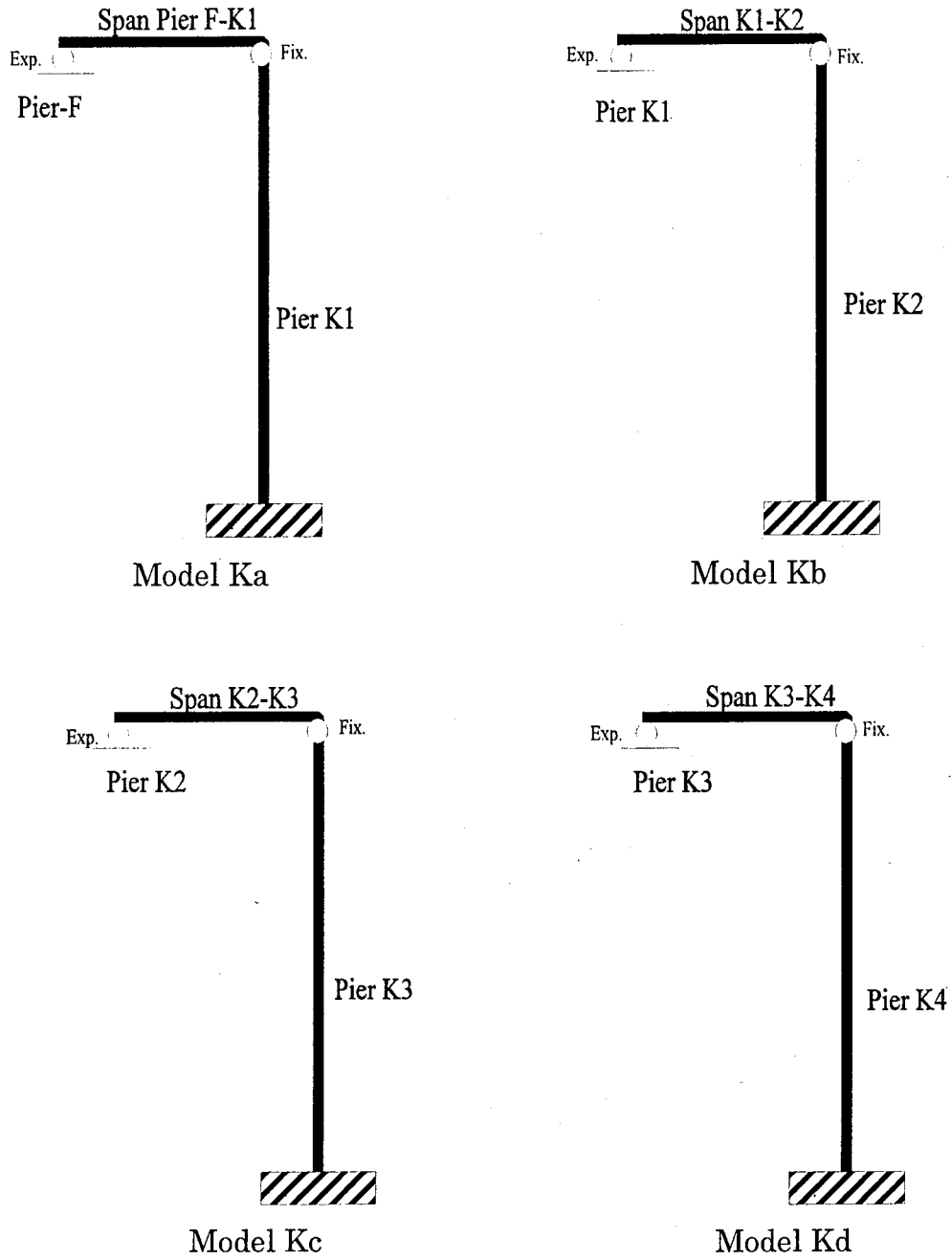


Figure 6.9 Structural Components for the SDOF models of the Kentucky Approach Spans

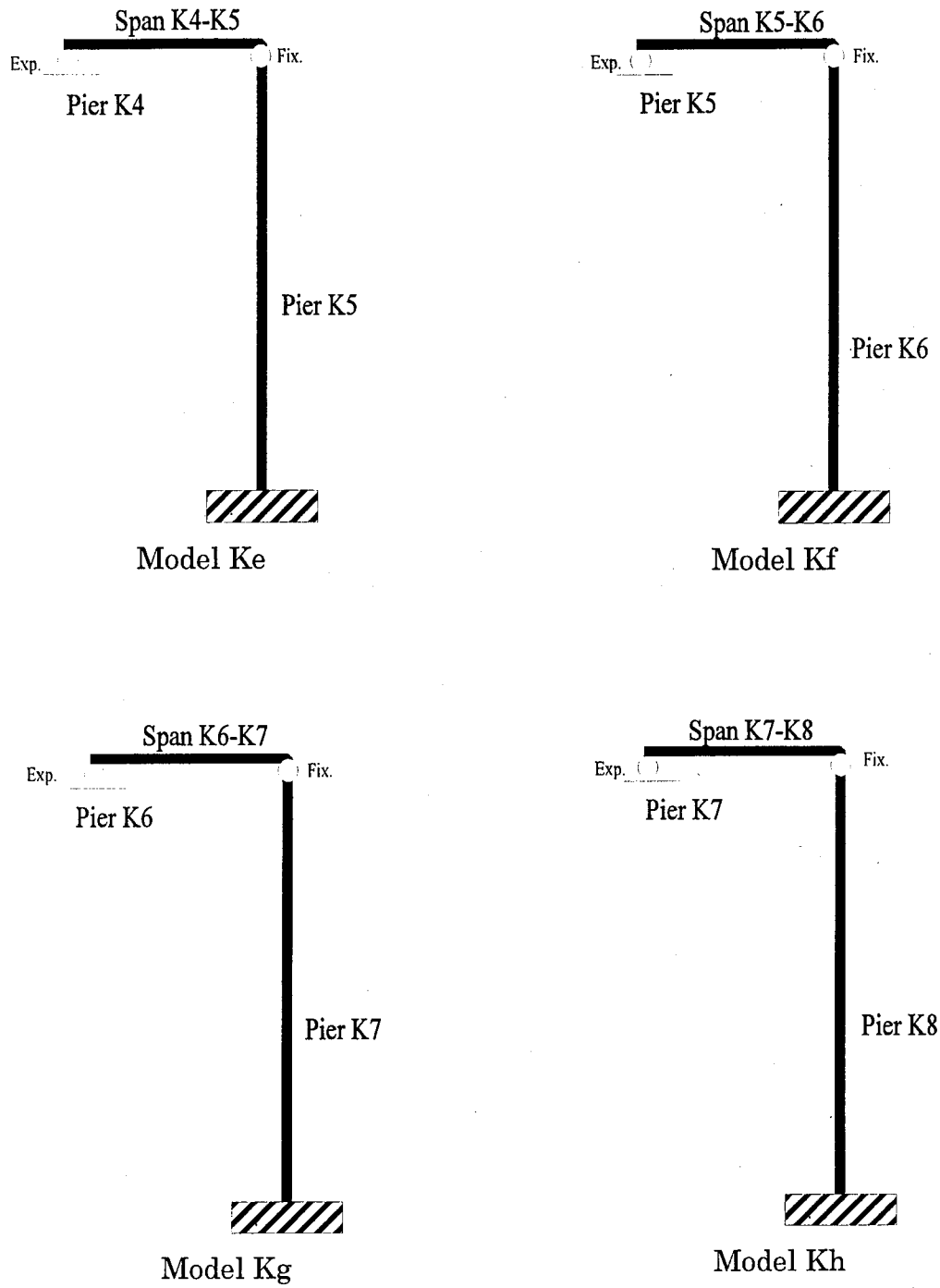


Figure 6.9 (cont'd). Structural Components for the SDOF models of the Kentucky Approach Spans

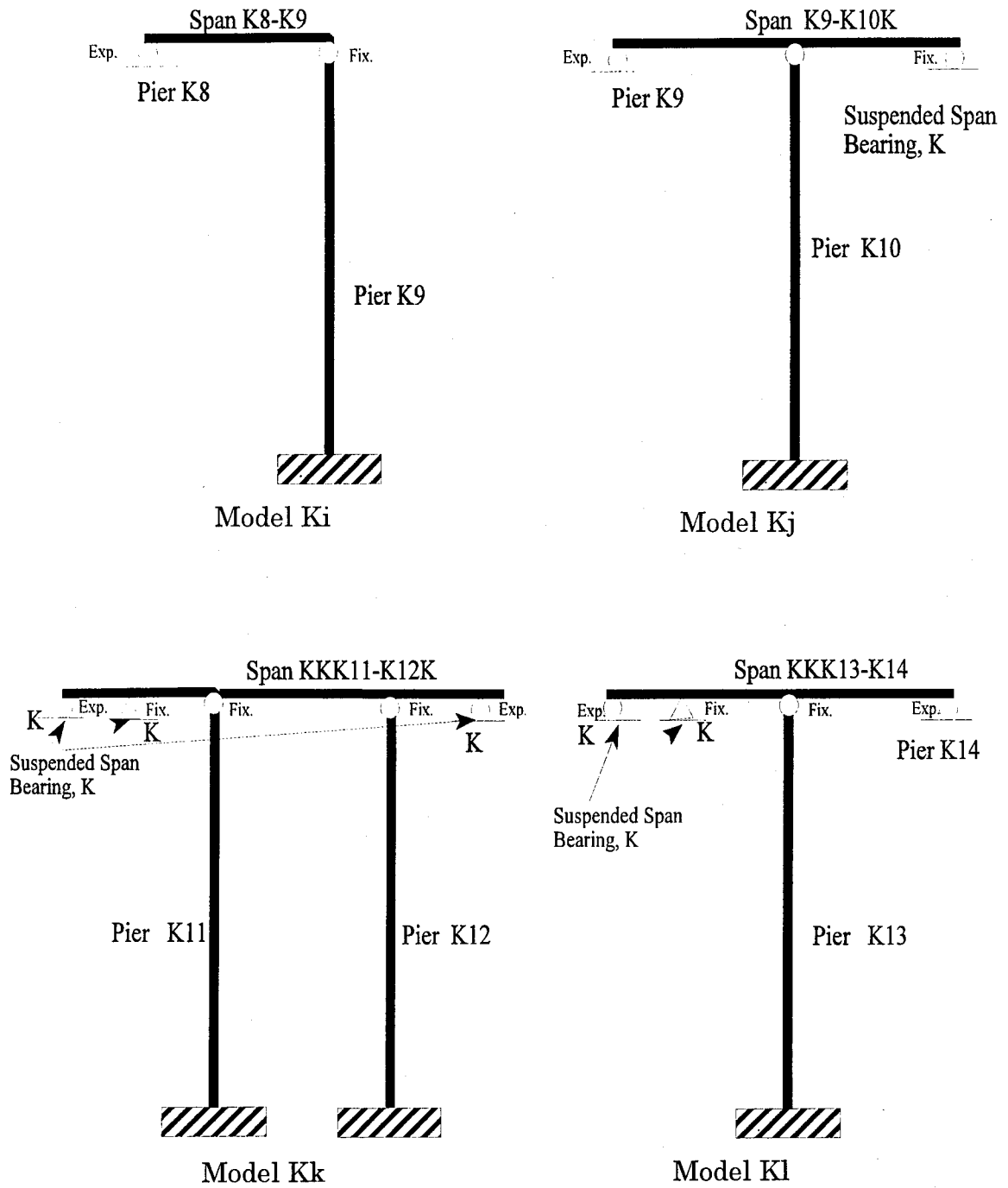


Figure 6.9 (cont'd). Structural Components for the SDOF models of the Kentucky Approach Spans

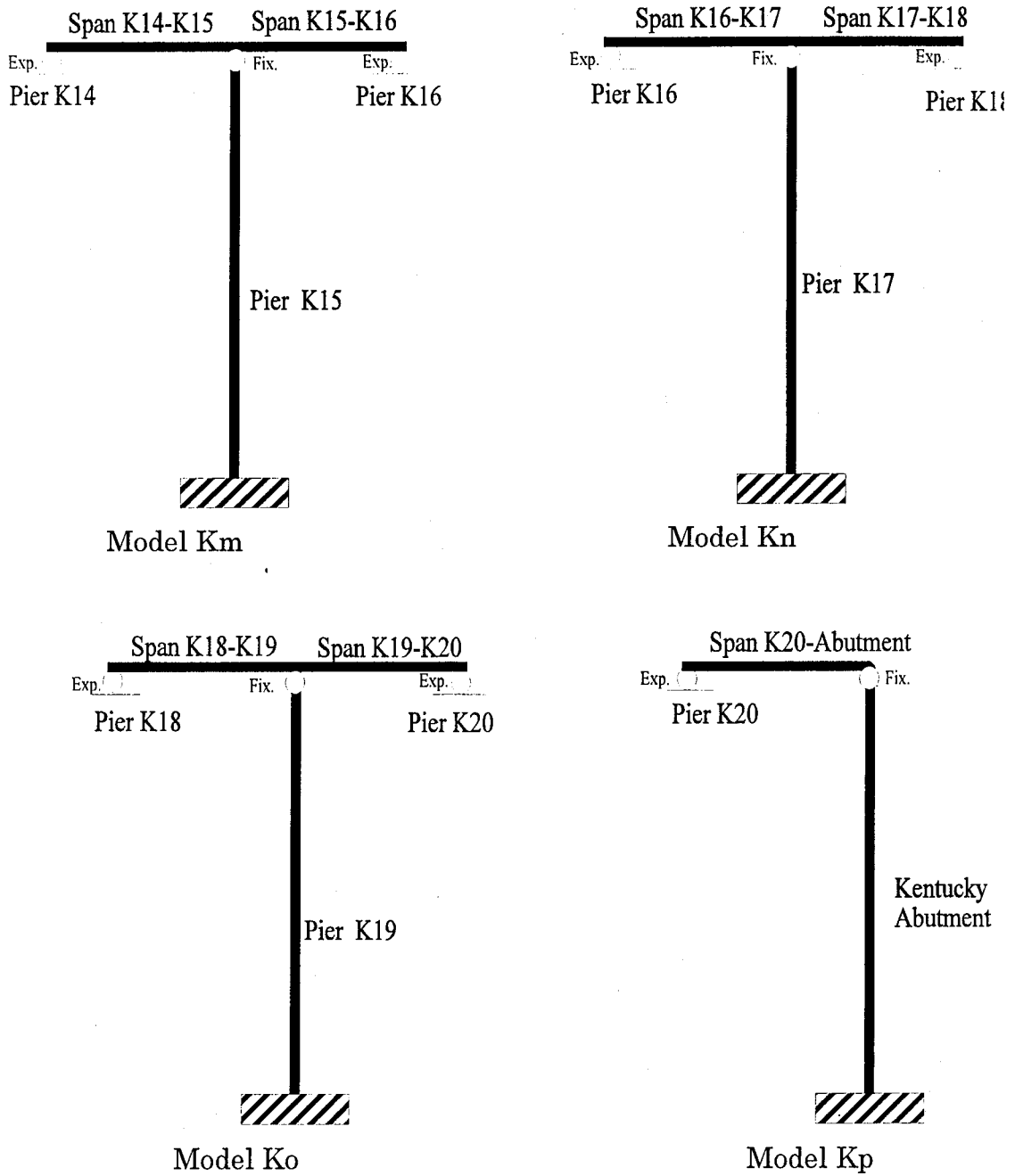


Figure 6.9 (cont'd). Structural Components for the SDOF models of the Kentucky Approach Spans

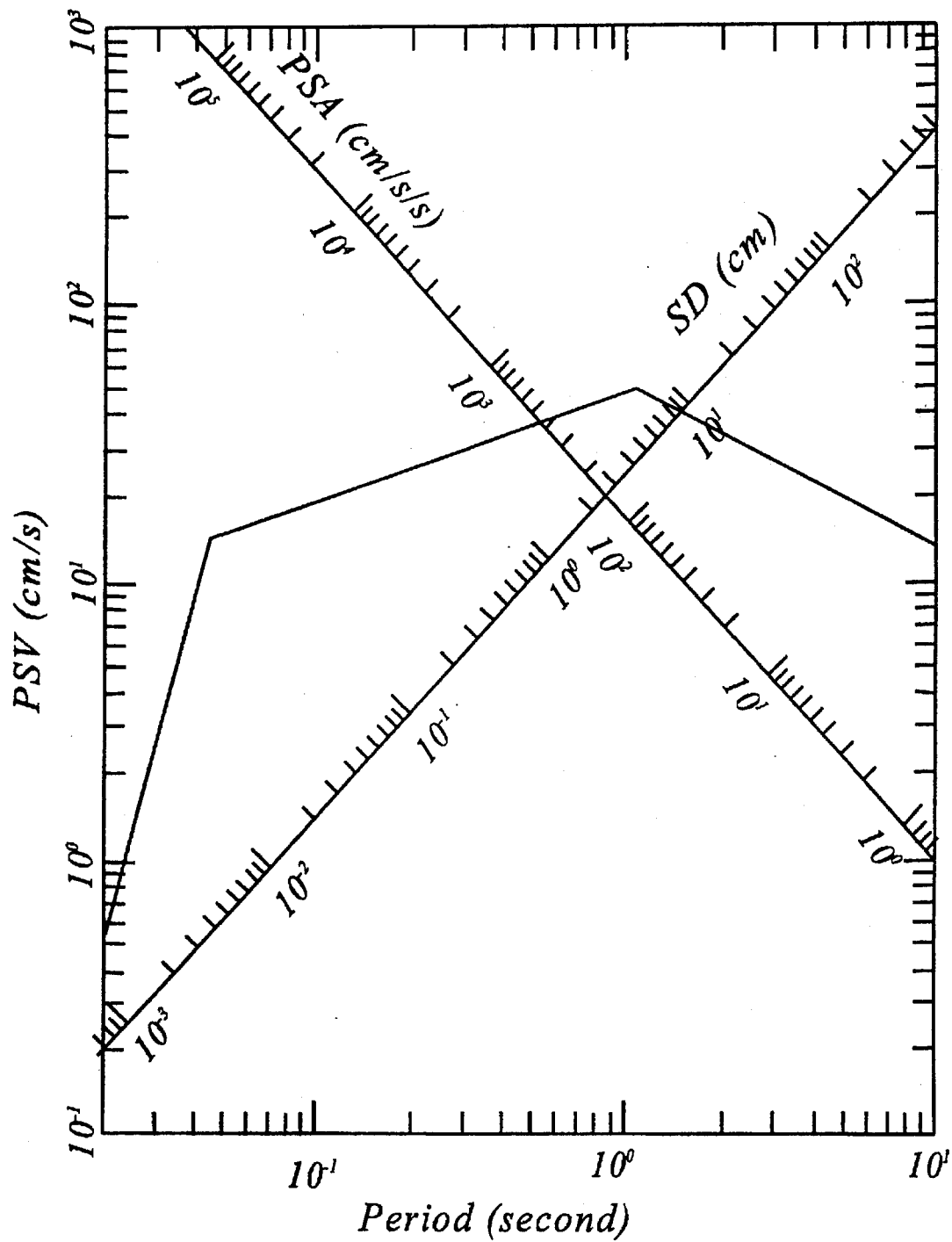


Figure 6.10 Response spectra for the 50-year event for Ballard Co. (0.30g-1 from fig. 5.1); Damping ratio = 0.05.

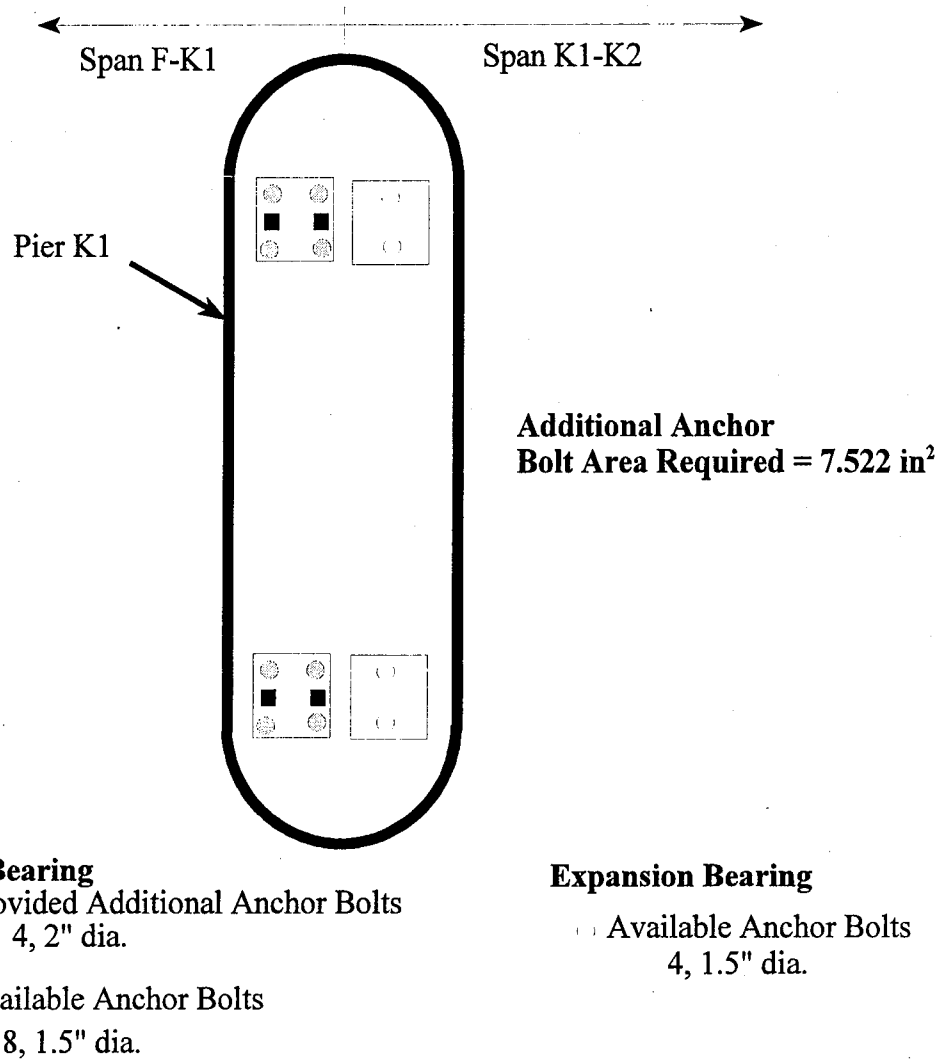
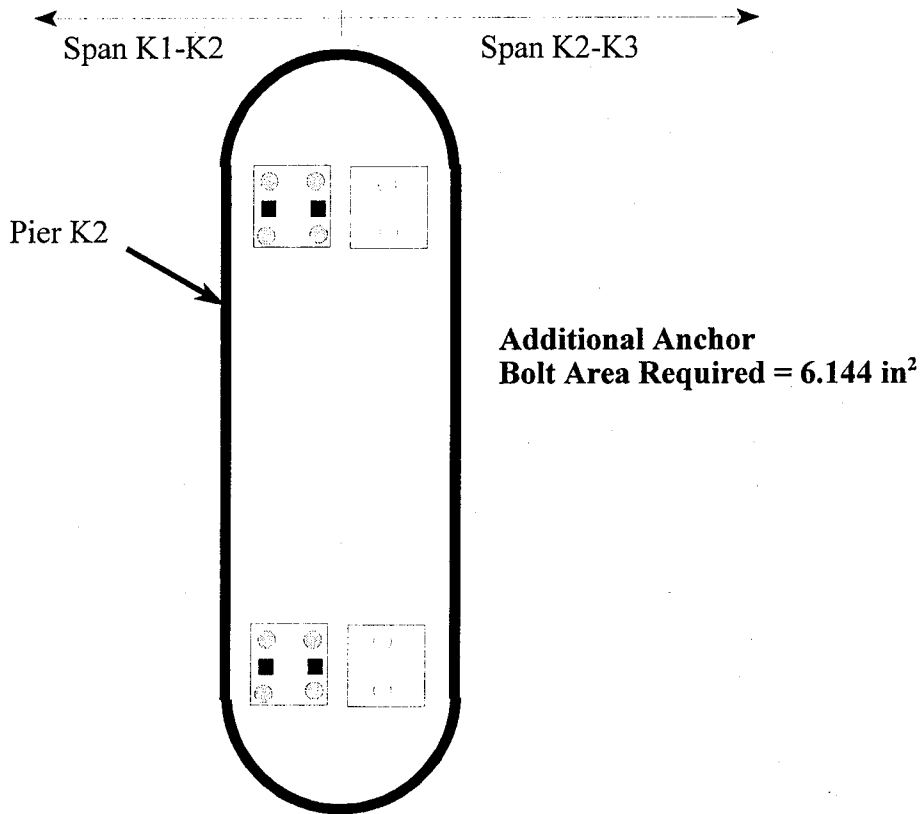


Figure 6.11 Arrangement of Additional Anchor Bolts on Pier K1



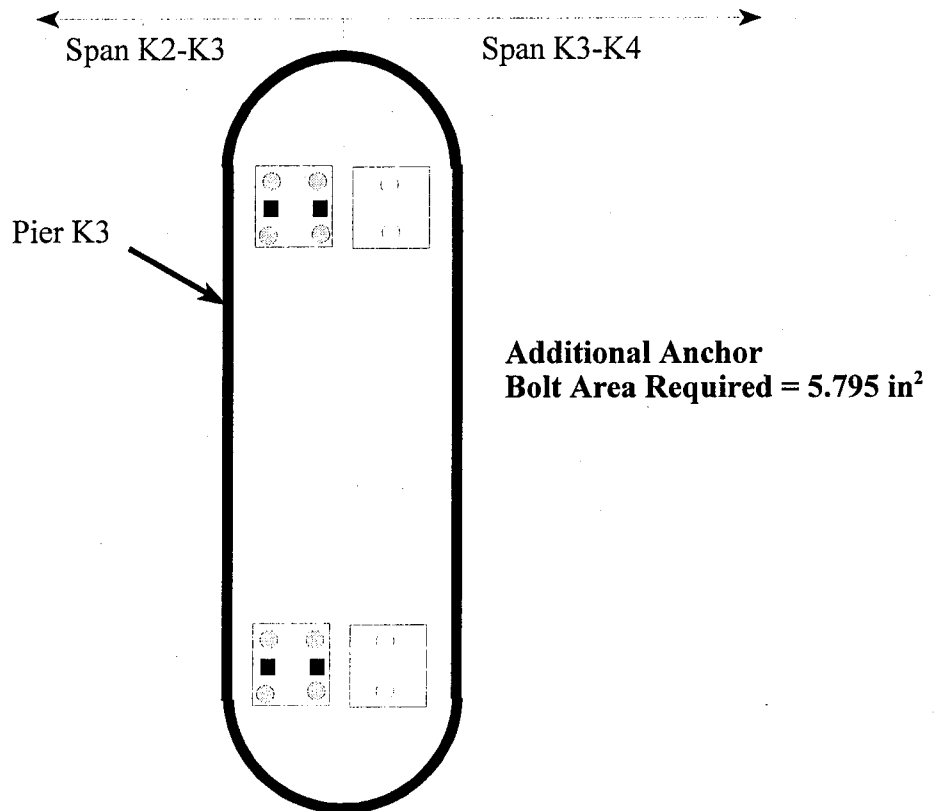
Fixed Bearing

- Provided Additional Anchor Bolts
4, 1.5" dia.
- Available Anchor Bolts
8, 1.5" dia.

Expansion Bearing

- Available Anchor Bolts
4, 1.5" dia.

Figure 6.12 Arrangement of Additional Anchor Bolts on Pier K2



Fixed Bearing

■ Provided Additional Anchor Bolts
4, 1.5" dia.

● Available Anchor Bolts
8, 1.5" dia.

Expansion Bearing

○ Available Anchor Bolts
4, 1.5" dia.

Figure 6.13 Arrangement of Additional Anchor Bolts on Pier K3

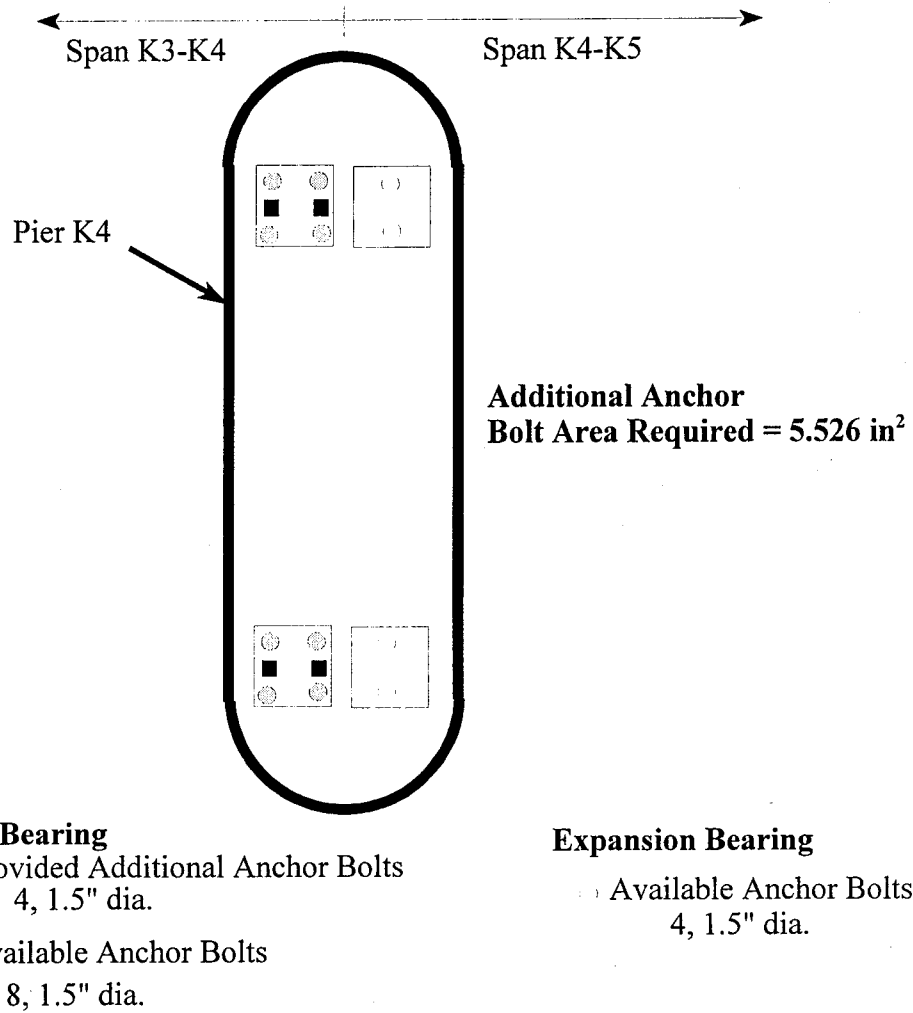


Figure 6.14 Arrangement of Additional Anchor Bolts on Pier K4

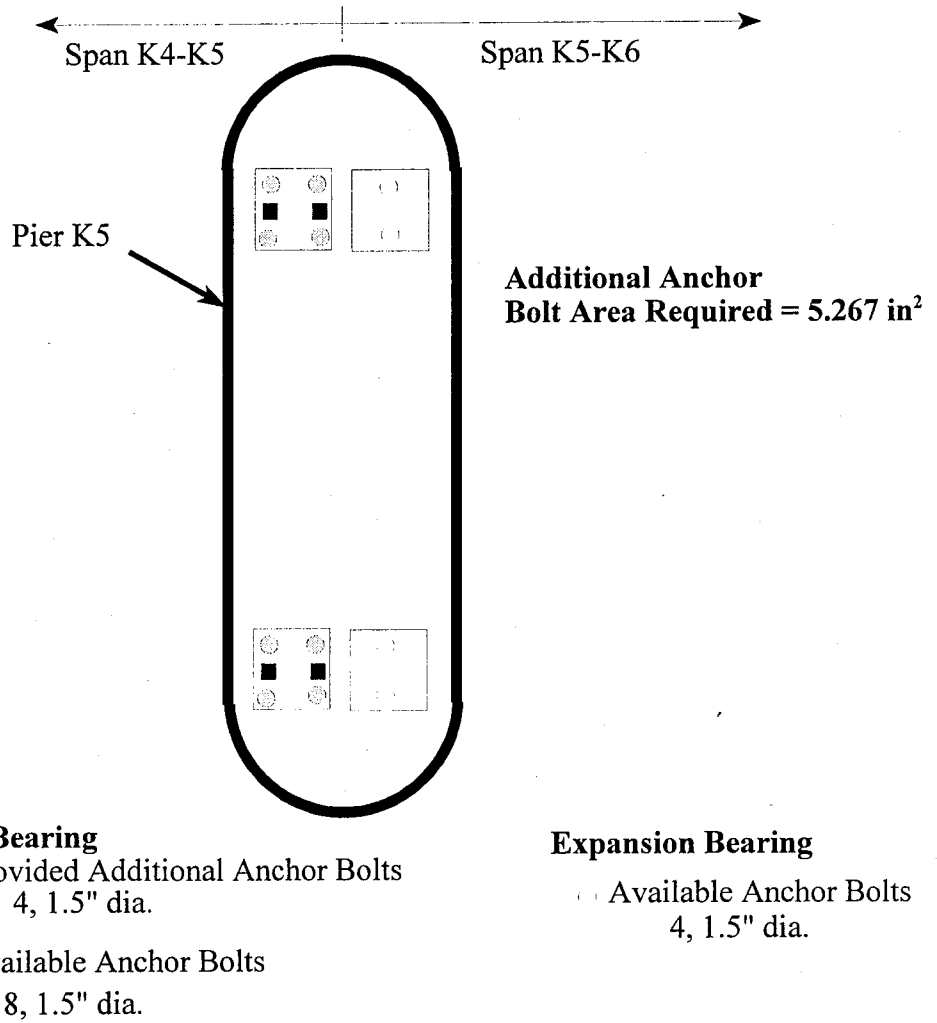
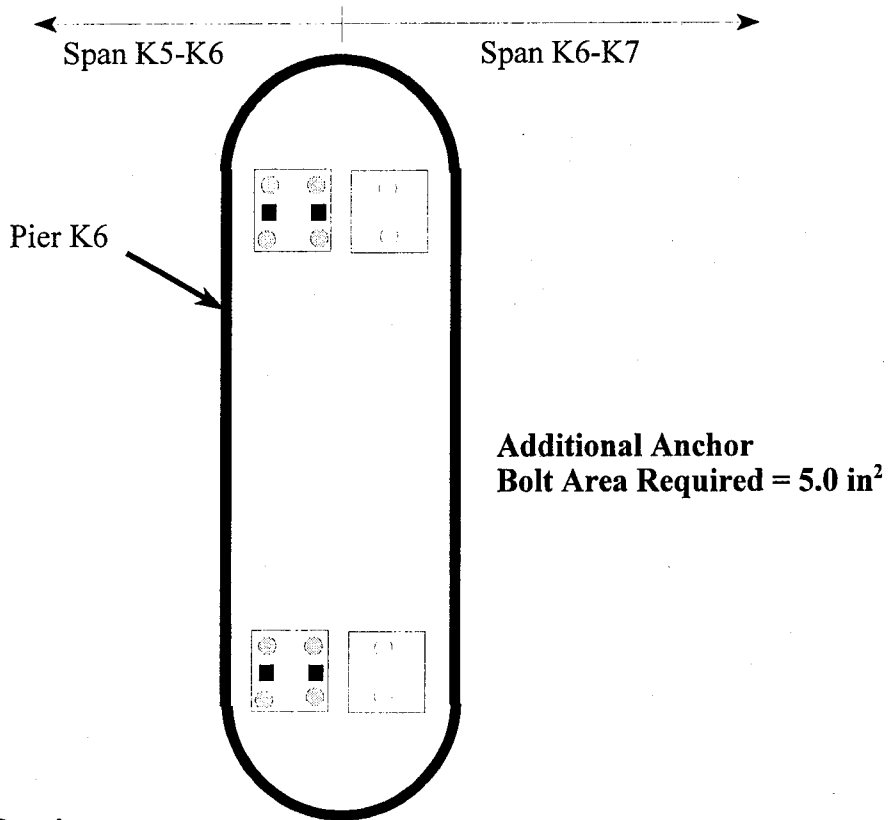


Figure 6.15 Arrangement of Additional Anchor Bolts on Pier K5



Fixed Bearing

- Provided Additional Anchor Bolts
4, 1.5" dia.
- Available Anchor Bolts
8, 1.5" dia.

Expansion Bearing

- Available Anchor Bolts
4, 1.5" dia.

Figure 6.16 Arrangement of Additional Bolts Anchor on Pier K6

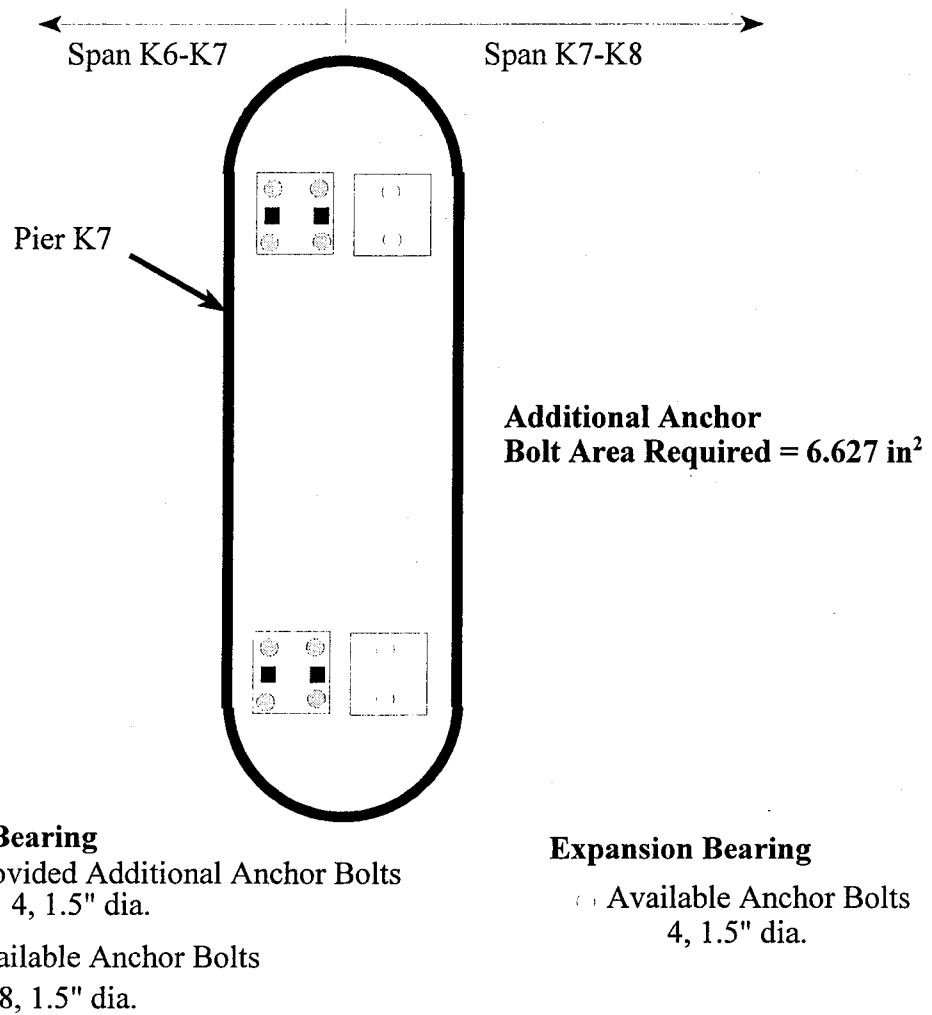


Figure 6.17 Arrangement of Additional Anchor Bolts on Pier K7

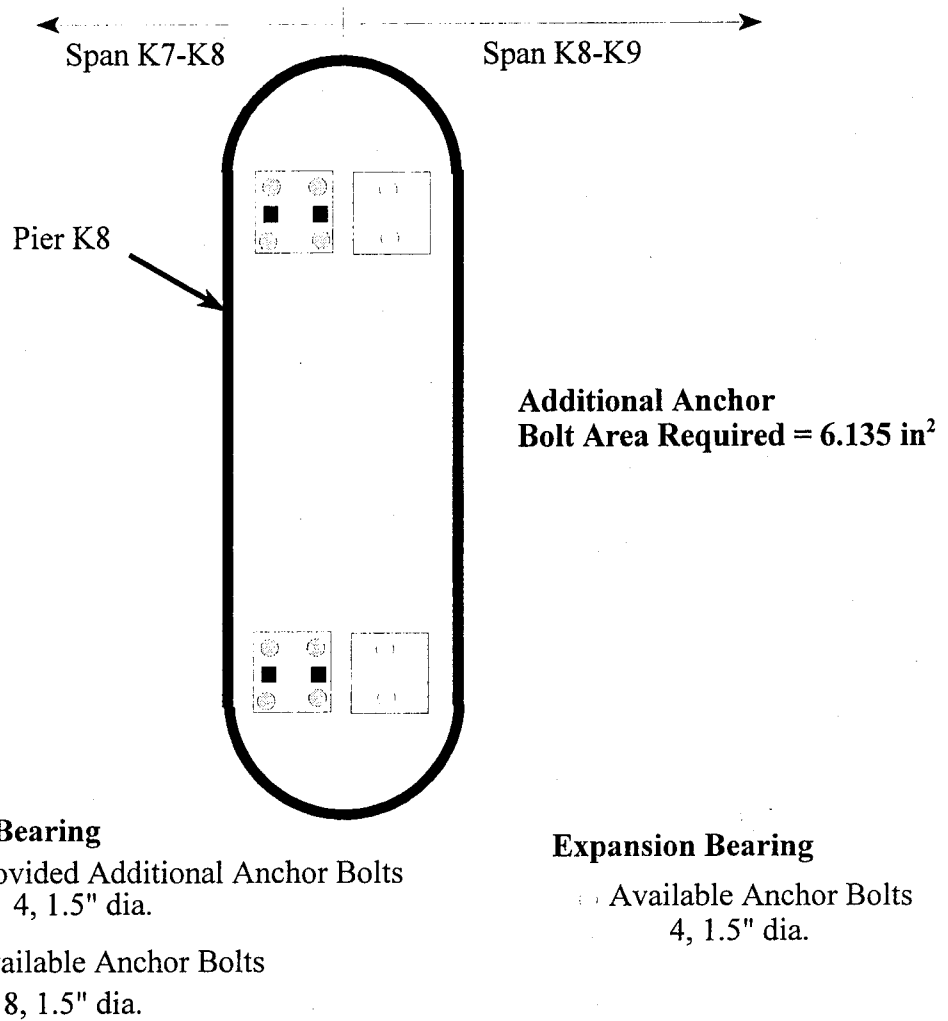


Figure 6.18 Arrangement of Additional Anchor Bolts on Pier K8

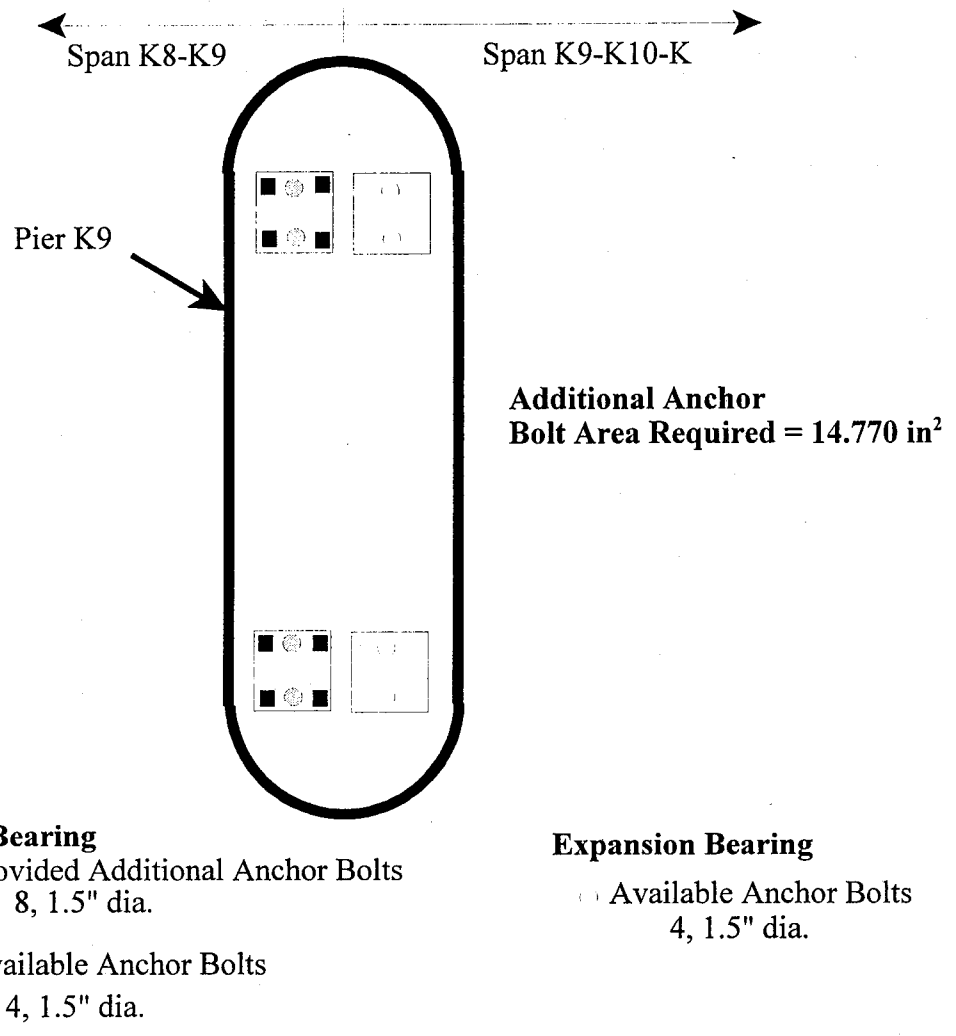
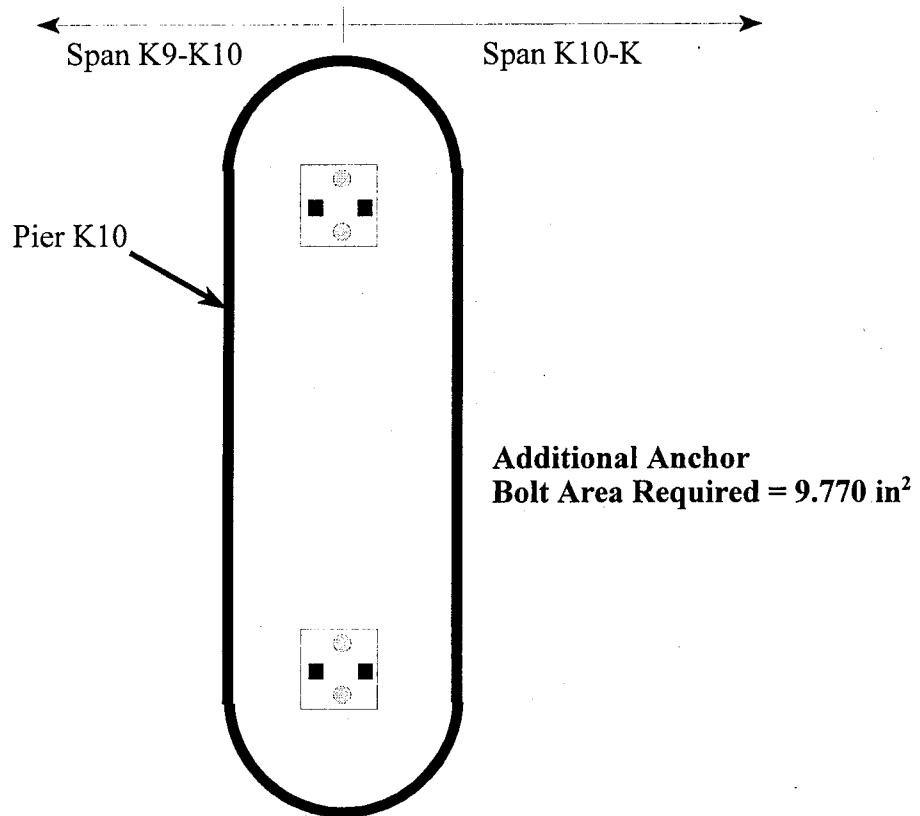


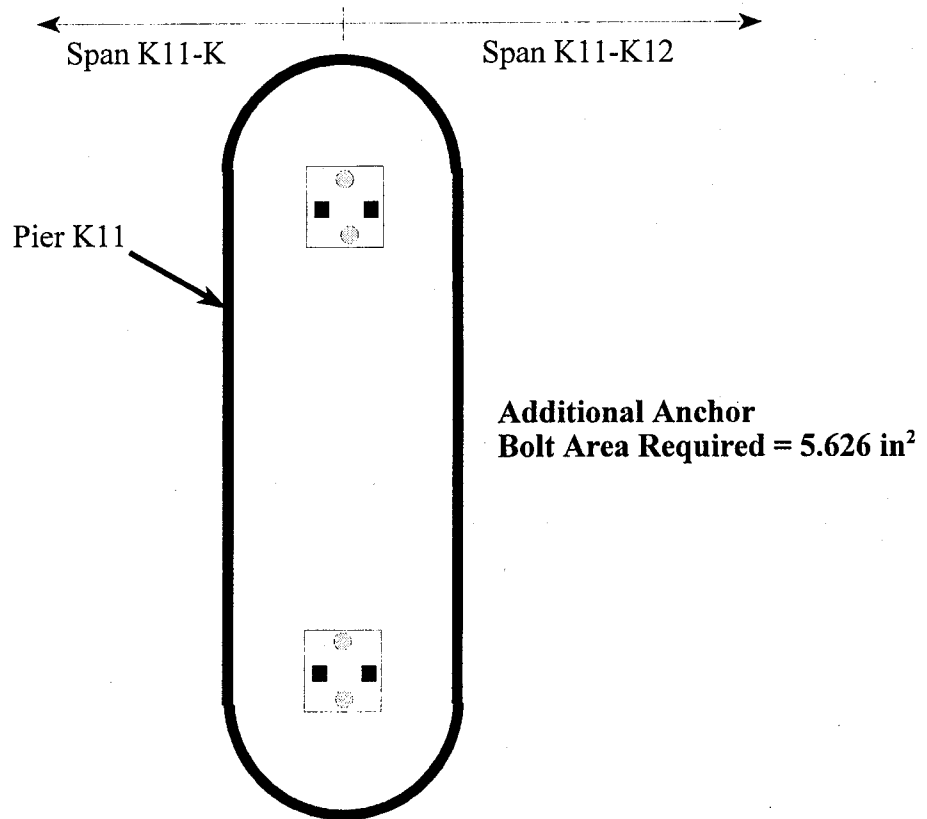
Figure 6.19 Arrangement of Additional Anchor Bolts on Pier K9



Fixed Bearing

- Provided Additional Anchor Bolts
4, 2" dia.
- Available Anchor Bolts
4, 1.25" dia.

Figure 6.20 Arrangement of Additional Anchor Bolts on Pier K10

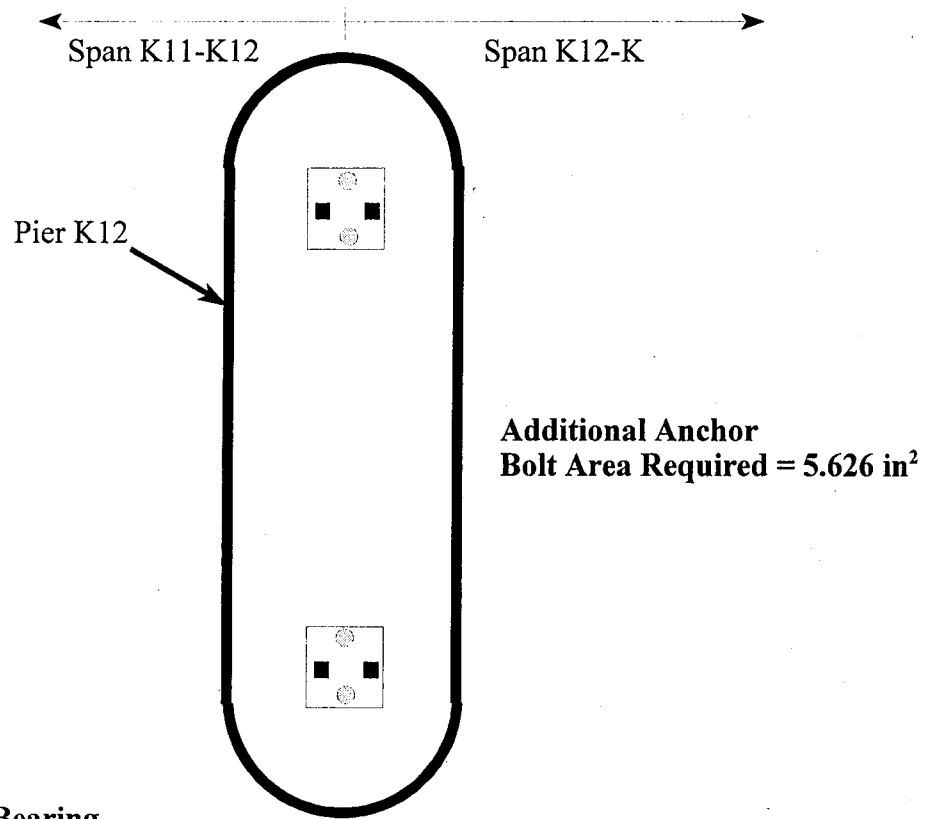


Fixed Bearing

■ Provided Additional Anchor Bolts
4, 1.5" dia.

⊙ Available Anchor Bolts
4, 1.25" dia.

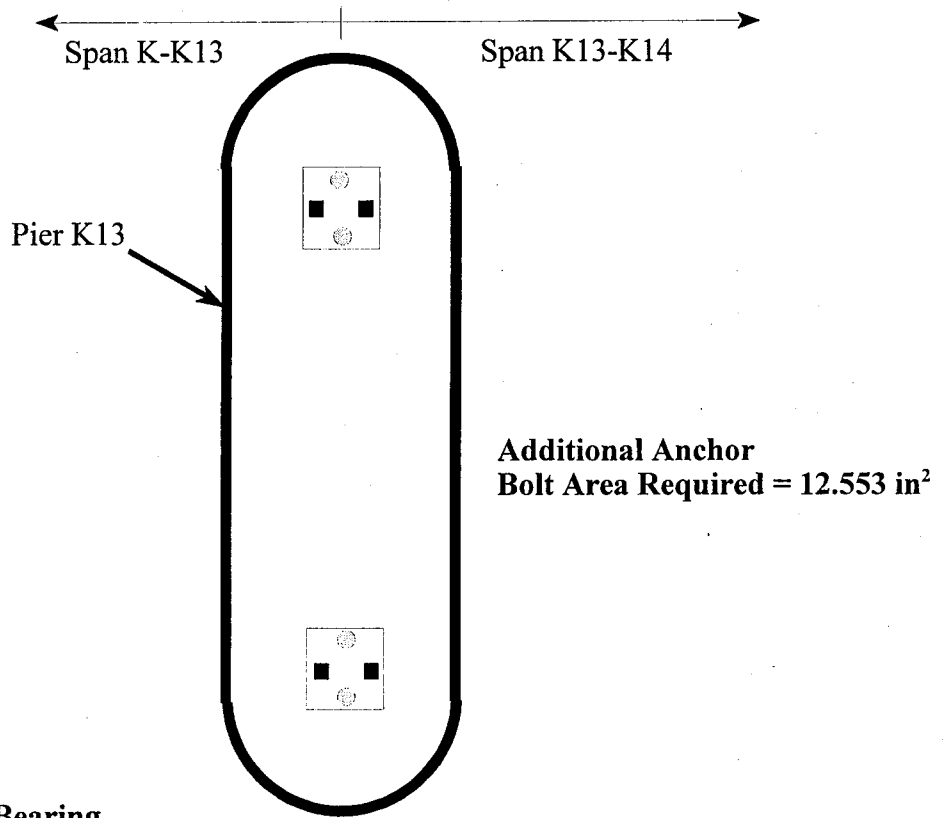
Figure 6.21 Arrangement of Additional Anchor Bolts on Pier K11



Fixed Bearing

- Provided Additional Anchor Bolts
4, 1.5" dia.
- Available Anchor Bolts
4, 1.25" dia.

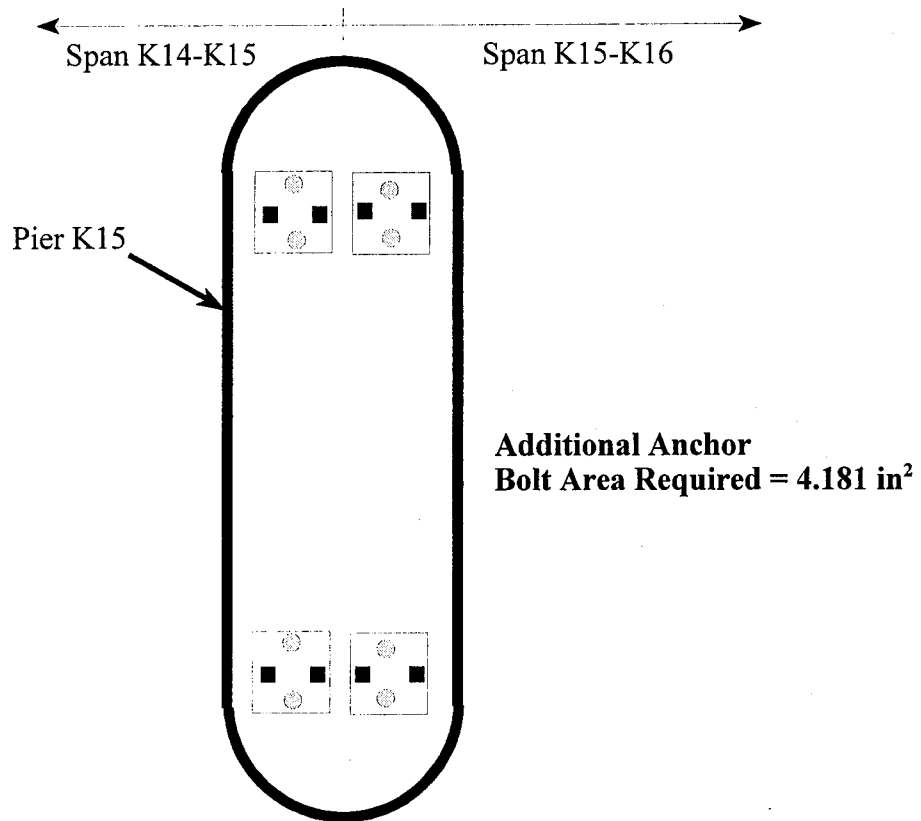
Figure 6.22 Arrangement of Additional Anchor Bolts on Pier K12



Fixed Bearing

- Provided Additional Anchor Bolts
8, 1.5" dia.
- Available Anchor Bolts
4, 1.25" dia.

Figure 6.23 Arrangement of Additional Anchor Bolts on Pier K13

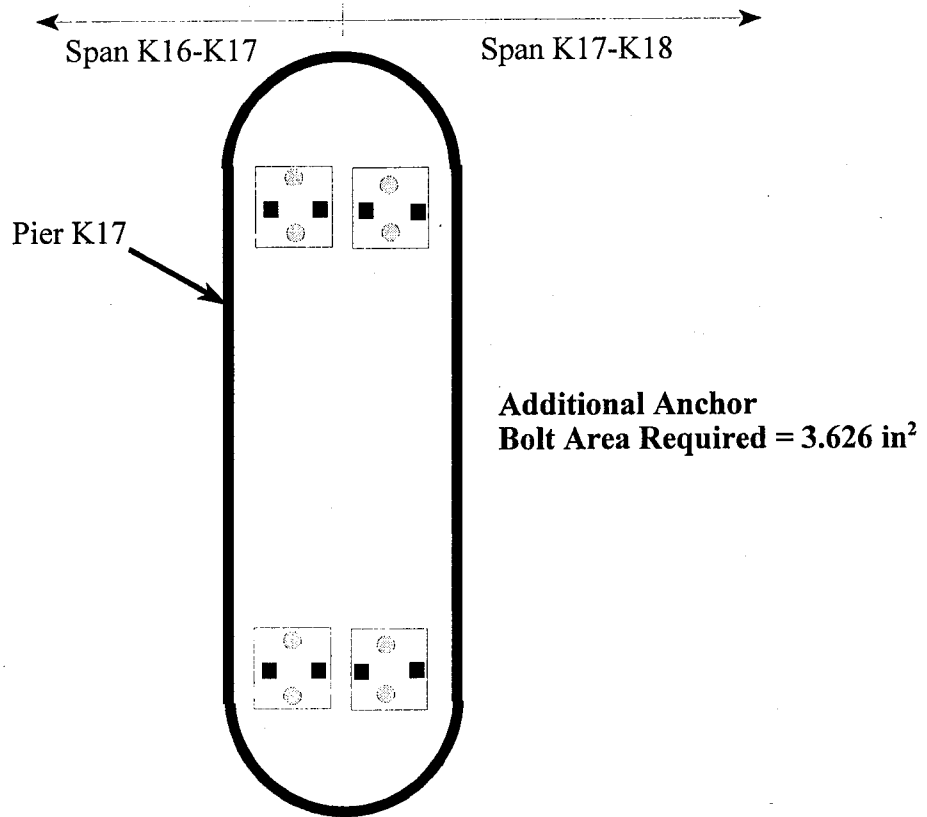


Fixed Bearing

■ Provided Additional Anchor Bolts
8, 1.5" dia.

⊙ Available Anchor Bolts
8, 1.25" dia.

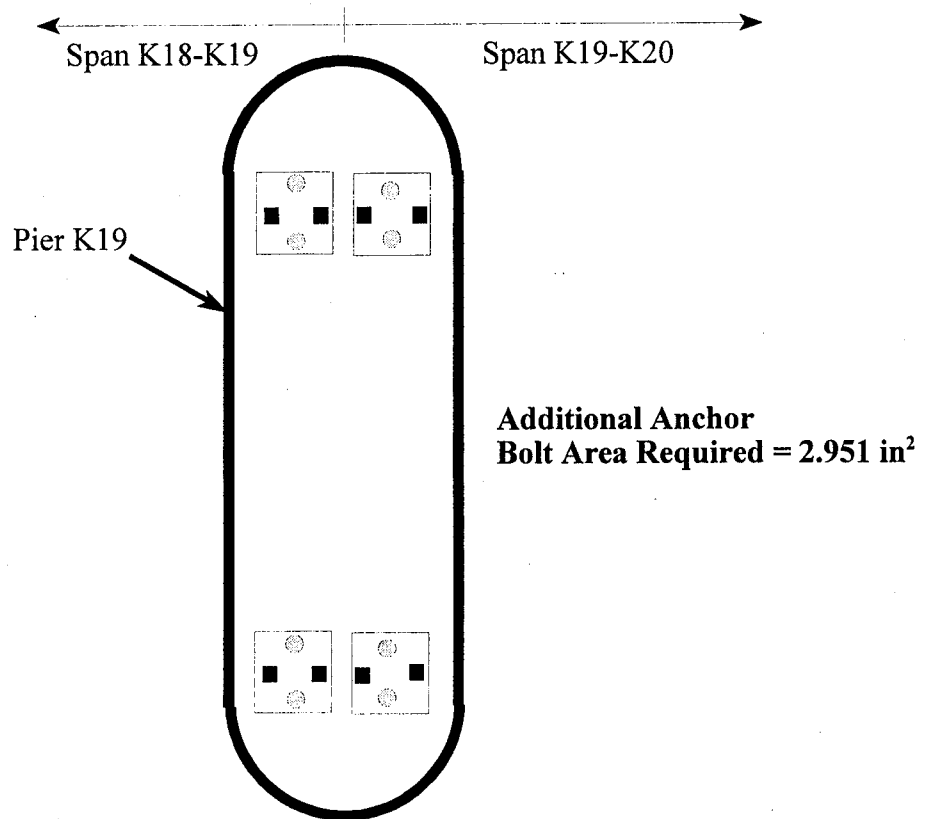
Figure 6.24 Arrangement of Additional Anchor Bolts on Pier K15



Fixed Bearing

- Provided Additional Anchor Bolts
8, 1.5" dia.
- Available Anchor Bolts
8, 1.25" dia.

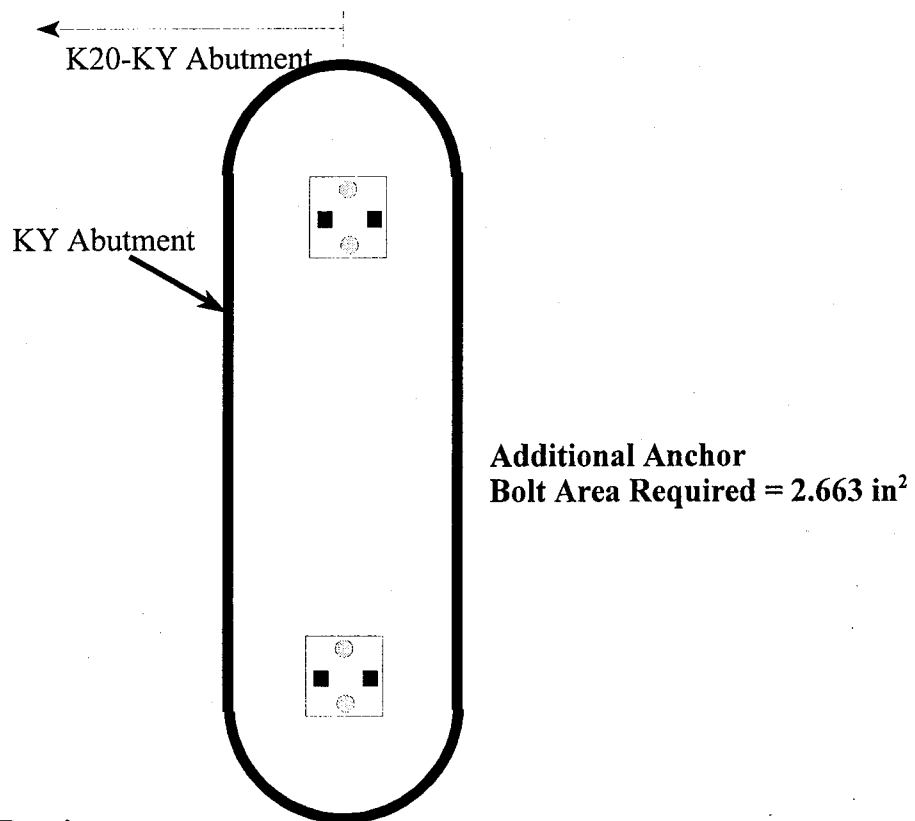
Figure 6.25 Arrangement of Additional Anchor Bolts on Pier K17



Fixed Bearing

- Provided Additional Anchor Bolts
8, 1.5" dia.
- ⊗ Available Anchor Bolts
8, 1.25" dia.

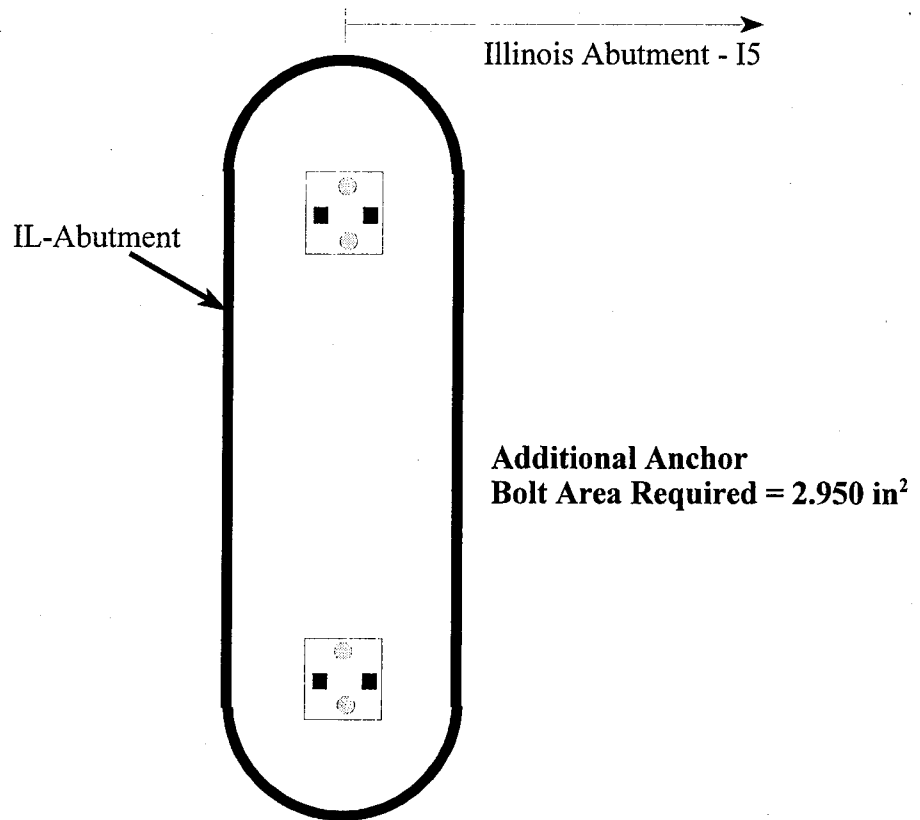
Figure 6.26 Arrangement of Additional Anchor Bolts on Pier K19



Fixed Bearing

- Provided Additional Anchor Bolts
4, 1.5" dia.
- Available Anchor Bolts
4, 1.25" dia.

Figure 6.27 Arrangement of Additional Anchor Bolts on KY-Abutment

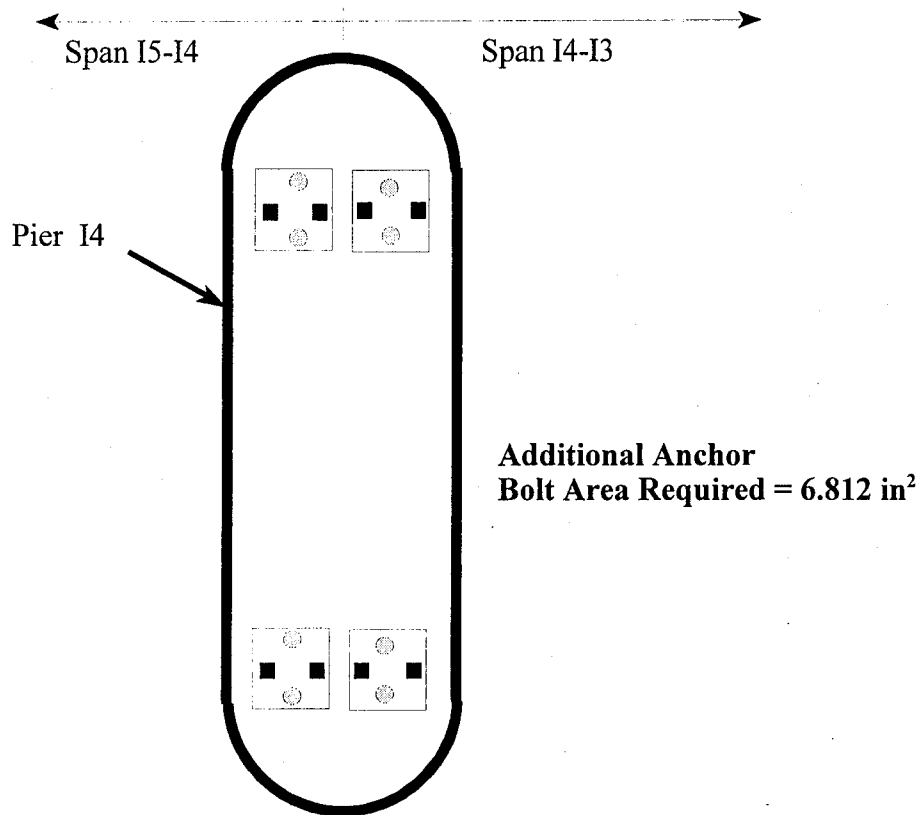


Fixed Bearing

■ Provided Additional Anchor Bolts
4, 1.5" dia.

⊙ Available Anchor Bolts
4, 1.25" dia.

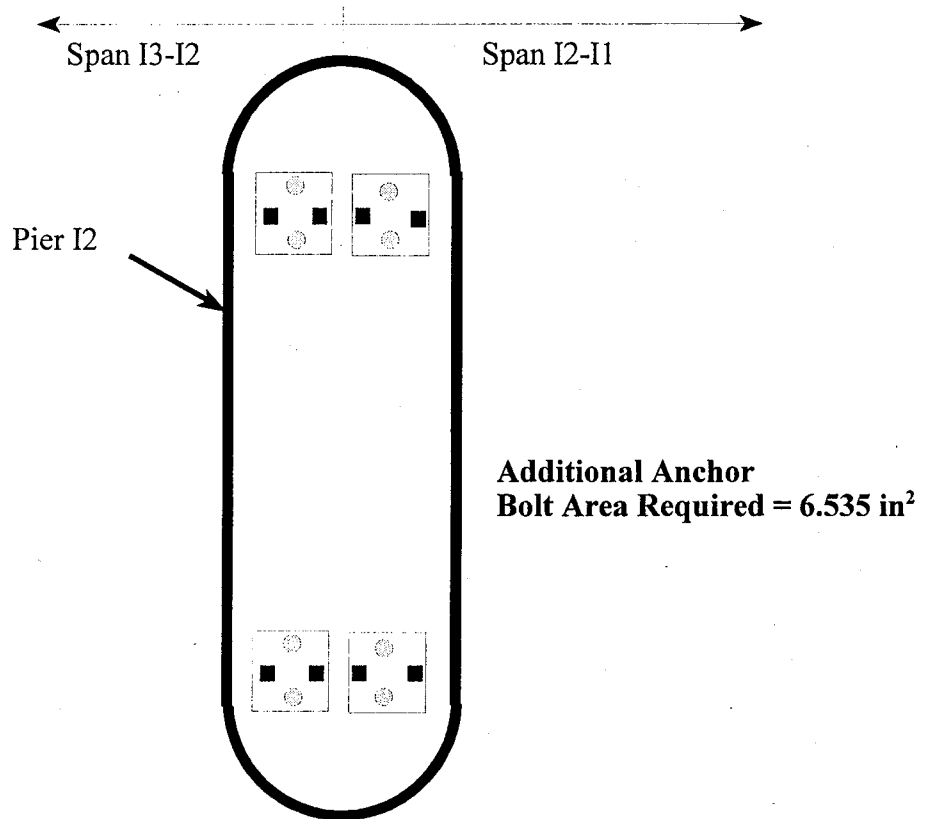
Figure 6.28 Arrangement of Additional Anchor Bolts on IL-Abutment



Fixed Bearing

- Provided Additional Anchor Bolts
8, 1.5" dia.
- ⊙ Available Anchor Bolts
8, 1.25" dia.

Figure 6.29 Arrangement of Additional Anchor Bolts on Pier I4



Fixed Bearing

- Provided Additional Anchor Bolts
8, 1.5" dia.
- Available Anchor Bolts
8, 1.25" dia.

Figure 6.30 Arrangement of Additional Anchor Bolts on Pier I2

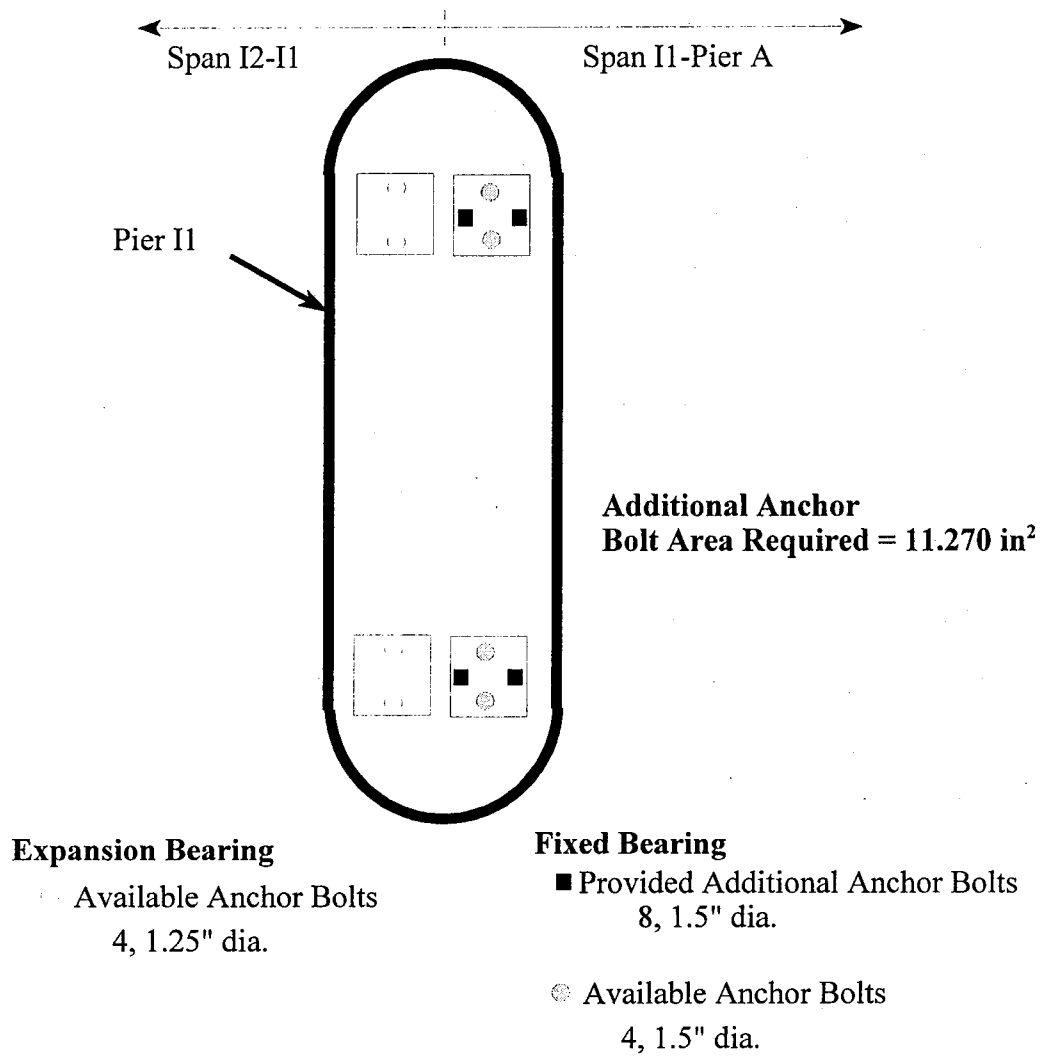


Figure 6.31 Arrangement of Additional Anchor Bolts on Pier I1